CORA Cork Open Research Archive
Cartlann Taighde Oscailte Chorcaí

Title	Characterisation of the effect of electroporation and electrochemotherapy on cancer cells and immune cells in the tumour microenvironment
Authors	Bendix, Maura
Publication date	2022-10
Original Citation	Bendix, M. B. S. 2022. Characterisation of the effect of electroporation and electrochemotherapy on cancer cells and immune cells in the tumour microenvironment. PhD Thesis, University College Cork.
Type of publication	Doctoral thesis
Rights	© 2022, Maura Bettina Susanne Bendix. - https://creativecommons.org/licenses/by-nc-nd/4.0/
Download date	2026-11-03 20:34:45
Item downloaded from	https://hdl.handle.net/10468/14518


UCC
University College Cork, Ireland
Coláiste na hOllscoile Corcaigh

Ollscoil na hÉireann, Corcaigh

National University of Ireland, Cork



Characterisation of the effect of electroporation and electrochemotherapy on cancer cells and immune cells in the tumour microenvironment

Thesis presented by

Maura Bettina Susanne Bendix, BSc., MSc.

https://orcid.org/0000-0001-8883-2677

for the degree of

Doctor of Philosophy

University College Cork

Departments of Pathology and Medicine
CancerResearch@UCC
School of Medicine

Supervisors: Dr. Elizabeth Brint, Dr. Aileen Houston, Dr. Sylvie Amu and Dr. Patrick Forde

October 2022

Table of Contents

Declaration 7

Abstract 8

Acknowledgments 10

Abbreviations 11

Publications and Presentations 15

Publications included as part of this thesis: 15

Oral Presentations 15

Poster Presentations 15

Chapter 1 Literature Review and Introduction 17

1.1 Abstract 18

1.2 Cancer 19

1.3 Lung Cancer 23

1.3.1 Different types of lung cancer 23

1.3.2 Lung Cancer Therapies 25

1.4 The Tumour Microenvironment 29

1.4.1 T cells 31

1.4.2 Dendritic cells 32

1.4.3 Macrophages 33

1.5 Electrochemotherapy for the treatment of cancer 35

1.5.1 Principles of Electroporation 35

1.5.2 Fundamental principles of Electrochemotherapy 38

1.5.3 Other electroporation-based treatment options for cancer treatment 41

1.5.4 Current status of ECT treatment in a clinical scenario 43

1.5.5 Cell death following ECT 45

1.5.6 Interactions between ECT and the Immune System 49

1.5.7 Developing immune co-treatments with ECT in cancer patients 52

1.6 Conclusion 55

1.7 Aim of my thesis 57

1.8 Bibliography 58

Chapter 2 Materials and Methods 71

2.1 Cell Lines and Maintenance 72

2.1.1 Lung cancer cell lines 73

2.2 Ethical Statement 73

2.3 Mice 74
2.4 Murine T cell isolation 74
2.5 Murine Dendritic cell and macrophage generation 76
2.6 Cell Counting 79
2.7 Reversible Electroporation in vitro 80
2.8 Development of LLC conditioned media 81
2.9 Viability assay with flow cytometry 81
2.10 Efficacy measurement by flow cytometry 83
2.11 MTT assay 84
2.12 Cell Recovery assay 85
2.13 Flow Cytometry 85
2.14 Enzyme-Linked Immunosorbent Assays (ELISA) 88
2.14.1 Stimulation protocol for ELISA 88
2.15 Immune Cell morphology analysis 89
2.16 qRT-PCR 89
2.16.1 RNA extraction 89
2.16.2 cDNA preparation 90
2.16.3 qRT-PCR 90
2.17 Cell Death Analysis 92
2.18 RNA Sequencing by Qiagen 92
2.19 Analysis of differentially expressed genes 94
2.20 *In vivo* murine lung cancer model 94
2.21 *In vivo* EP and ECT 95
2.22 Tissue preparation for flow cytometry 96
2.23 Statistical analysis 96
2.24 References 98
Chapter 3 Electroporation of cancer cell lines in suspension – a proposed assay set for optimizations of electric field strength 99
3.1 Abstract 100
3.2 Introduction 101
3.3 Materials and Methods 103
3.3.1 Cell Culturing 103
3.3.2 *In vitro* electroporation parameters 103
3.3.3 Efficacy Assay 104

3.3.4 Viability Assay 104
3.3.5 MTT Assay 104
3.3.6 Cell Recovery Assay 104
3.3.7 Statistical analysis 105
3.4 Results 106
3.4.1 Cell line dependent 95% efficacy threshold is reached between 800-1000V/cm 106
3.4.2 Viability is barely impacted by tested electric field strengths 108
3.4.3 Metabolic activity is impacted in a cell-line and electric field strength dependent manner 111
3.4.4 Recovery is impacted in a cell-line and electric field strength dependent manner 113
3.4.5 With the exception of the LLC cell line all other tested cell lines have optimal electric field strength below the typically used ESOPE-based 1300V/cm 115
3.5 Discussion and Conclusions 118
3.6 References 122
Chapter 4 Defining optimal parameters to maximize the effect of electrochemotherapy on lung cancer cells whilst preserving integrity of immune cells. 125
4.1 Abstract 126
4.2 Introduction 127
4.3 Materials & Methods: 130
4.3.1 Cell Culturing Cancer Cell Lines 130
4.3.2 Human Monocyte-derived Dendritic Cells 130
4.3.3 Murine Bone marrow-derived Dendritic and Macrophage cell derivation 130
4.3.4 Murine T cell isolation 131
4.3.5 *In vitro* electroporation parameters 131
4.3.6 *In vitro* ECT and CaEP parameters 132
4.3.7 Efficacy Assay 132
4.3.8 Viability Assay 132
4.3.9 MTT Assay 133
4.3.10 Cell Recovery Assay 133
4.3.11 *In Vivo* LLC subcutaneous cancer model 134
4.3.12 *In Vivo* ECT parameters 134
4.3.13 Processing tissue for flow cytometry 134
4.3.14 Flow cytometry 135

4.3.15 Statistical analysis 135
4.4 Results 137
4.4.1 Establishment of optimal chemotherapy drug combination for treatment of lung cancer cell lines by ECT. 137
4.4.2 Investigation of optimal calcium concentration for CaEP for treatment of lung cancer cell lines. 140
4.4.3 Deriving Human Dendritic cells to elucidate the impact of EP and ECT 143
4.4.4 Both EP and ECT effect viability, efficacy and metabolic activity of murine dendritic cells and macrophages but have no effect on T cells 145
4.4.5 Various treated LLC conditioned media have no discernible impact on DC viability or activation status 151
4.4.6 Comparison of 800V/cm and 1300V/cm ECT with 11µM cisplatin in LLC cells 152
4.4.7 Evaluating impact of ECT at 800V/cm versus ECT at 1300V/cm in a murine lung cancer model 155
4.5 Discussion & Conclusion 168
4.6 Bibliography 176
Chapter 5 An investigation into the effect of ECT on dendritic cell phenotype and function 182
5.1 Abstract 183
5.2 Introduction 184
5.3 Materials & Methods 187
5.3.1 Murine Bone marrow-derived Dendritic cell derivation 187
5.3.2 In vitro ECT parameters 187
5.3.3 Flow cytometry 187
5.3.4 RNA Sequencing by Qiagen 188
5.3.5 Morphology analysis 189
5.3.6 Cell Death Analysis 189
5.3.7 Enzyme-Linked Immunosorbent Assays (ELISA) 189
5.3.8 qRT-PCR 189
5.3.9 Statistical analysis 190
5.4 Results 191
5.4.1 DCs display a diffuse morphology post EP and ECT 191
5.4.2 Flow cytometry reveals that Dendritic cells undergo necrotic cell death post EP and ECT treatment 194

5.4.3 1000ECT and 1300ECT induces maturation and activation of surviving DCs 195
5.4.4 EP and ECT upregulate TLRs in a voltage dependent manner 198
5.4.5 Analysis of gene transcription in DCs post ECT treatment 201
5.4.6 DCs remain in part functionally active after EP and ECT treatment 217
5.5 Discussion & Conclusion 223
5.6 Bibliography 233
Chapter 6 Final Discussion and Future Directions 240
6.1 Final Discussion and future directions 241
6.2 ESOPE equivalent parameters for treatment of internal organ tumours 241
6.3 Optimizing ECT parameters for abscopal effects 243
6.4 Understanding molecular mechanisms of actions of ECT in a cell-type dependent manner 244
6.5 Considerations of use of ECT in the context of affordable cancer care 246
6.6 References 249
Appendix 255

Declaration

This is to certify that the work I am submitting is my own and has not been submitted for another degree, either at University College Cork or elsewhere. All external references and sources are clearly acknowledged and identified within the contents. I have read and understood the regulations of University College Cork concerning plagiarism and intellectual property.



Maura Bendix

Abstract

Lung cancer is the leading cause of cancer-related death worldwide, with the lung cancer incidence rate expected to rise further. Despite recently developed novel therapy options, 5-year survival rates for lung cancer patients remains below 20% generally and below 5% for late-stage diagnosis, thus additional therapy options are still needed. Electrochemotherapy (ECT), the application of an electric pulse to deliver chemotherapy drugs into cells, could be a new treatment option for lung cancer patients. ECT is a locally very effective treatment, with local tumour reduction of up to 85%, while the systemic effects are more varied. For clinical application ECT treatment modalities have been standardized since 2006, after the ESOPE study, which optimized ECT parameters to 8 pulses at 1000V/cm with 100µs pulse length at 1Hz frequency and either bleomycin or cisplatin as the drug of choice.

To evaluate whether ECT could be a potential treatment option for lung cancer patients' ECT parameters, the needed electric field strength and the needed drug and drug concentration, were optimized for *in vitro* lung cancer research. In our study, we initially developed a standard operating protocol (SOP) to determine the optimal electric field strength for a given cancer cell line *in vitro*, while keeping the other ESOPE parameters constant. The developed SOP combined short-, medium-, and long-term assays to fully visualize the impact treatment, at a given field strength, has on the tested cancer cell line. This evaluation showed that human lung cancer cell lines (A549, H460 and SK-MES 1) and the human pancreatic Pan02 cell line have an optimal electric field strength of 800V/cm, the melanoma A375 (human) and B16F10 (murine) cell lines as well as the murine pancreatic Mia-PACA2 cell line have an optimal electric field strength of 700V/cm, while the murine Lewis Lung carcinoma (LLC) cell line has an optimal electric field strength of 1300V/cm. In addition, our study findings demonstrate that cisplatin at 11µM would be the drug of choice when using ECT for lung cancer treatments.

In recent years while the importance of the immune system in lung cancer development and treatment results has become increasingly clear, little is known

about how ECT treatments impact immune cells. Therefore, the impact of ECT on murine T cells, dendritic cells (DCs) and macrophages was evaluated *in vitro*. Our data indicates that while T cells are able to tolerate electric field strengths of up to 1400V/cm, DCs and macrophages are significantly negatively impacted by electric field strengths exceeding 800V/cm. Further investigation on the impact of ECT on dendritic cells demonstrated that DCs die via necrosis following ECT treatment, while ECT at electric field strength exceeding 1000V/cm leads to DC maturation and activation of the surviving cells. In addition, DCs remain partially functional following ECT treatment in a stimuli and treatment dependent manner with distinctively different sets of genes upregulated 4-hours post treatment at 800V/cm compared to treatment at 1000V/cm and 1300V/cm.

Taken together, our data indicates that it is worthwhile to further investigate ECT as a potential therapy option for lung cancer patients, while more attention needs to be paid to the impact ECT has on immune cells in order to maximize treatment results.

Acknowledgments

First, I would like to thank Dr. Patrick Forde and Dr. Elizabeth Brint for giving me the opportunity to conduct this PhD research project. A big thank you to Beth and Dr. Aileen Houston for really improving my writing and challenging my conclusions and research ideas. Without them this thesis would not be what it is and I would not be the scientist I am today. I would like to also give a big thank you to Dr. Sylvie Amu for her continuous support throughout my PhD.

I would not be the person I am today without my family and friends, so thank you! The biggest thank you goes to Mama and Papa, and Florian. They supported me throughout my entire education, through the ups and downs and the moves to three foreign countries. Despite living in different countries and time zones, they were always there when I needed them. Ohne Euch wäre es nicht so möglich gewesen! Thank you to Anja, Kim, Kevin. Anja, thank you for making sure that I was able to really enjoy and the see the beautiful Irish countryside and for the great company. Kim, I really enjoyed our talks and walks, and without you my time in Cork would not have been the same. Kevin, it was a great pleasure to work with you on our PhD projects.

To all the staff and students in CancerReserach@UCC and the Department of Pathology, thank you for making my time in Cork enjoyable and for all the support I got from you! A special thanks goes to Dr. Garrett Casey for smilingly accepting the long lists of wishes, requests and orders I left on his desk or in his email inbox. Thank you to the SkillsCenter in UCC to welcome me with open arms when I started to work there and thank you for all the amazing times I had with the team along the way and the countless positive student encounters. Finally, I would like to give a special thank you to Jay, Noelle and Aine from the BSU for always being willing to help me and sending, on several occasions, mice out to me after a last-minute request.

Abbreviations

2ME	2-Mercaptoethanol
AEEC	Animal Experimentation Ethics Committee
AF488	Alexa Fluor 488 (flow cytometry)
AO	Acridine Orange
APC	Antigen-presenting Cell
APC	Allophycocyanin (flow cytometry)
APC-Cy7	APC- cyanine 7 (flow cytometry)
ATCC	American Type Culture Collection
ATP	Adenosine triphosphate
bp	Basepair
BV605	Brilliant Violet 605 (flow cytometry)
CaEP	Calcium electroporation
CD	Cluster of differentiation
cDC	Conventional dendritic cells
CpG	DNA where a cytosine nucleotide is followed by a guanine nucleotide; TLR9 agonist
CPI	Checkpoint inhibitor therapy
CRT	Calreticulin
CTLA4	Cytotoxic T-lymphocyte antigen 4
DAMP	Damage associated molecular pattern
DAPI	4’,6-Diamidin-2-phenylindol
DC	Dendritic cell
dDC	dermal dendritic cell
DEG	Differentially expressed gene
diH20	Deionized water
DMEM	Dulbecco's Modified Eagle Medium
DMSO	Dimethylsulfoxid
DSB	Double-Strand break
DUSP	Dual specific protein phosphatase
ECM	Extracellular Matrix

800 ECT	ECT at 800V/cm with 11µM Cisplatin
1000ECT	ECT at 1000V/cm with 11µM Cisplatin
1300 ECT	ECT at 1300V/cm with 11µM Cisplatin
EDTA	Ethylenediaminetetraacetic acid
ELISA	Enzyme-Linked-Immunosorbent assay
800EP	EP at 800V/cm
1000EP	EP at 1000V/cm
1300EP	EP at 1300V/cm
EPB	Electroporation buffer
ESOPE	European standard operating procedures for electrochemotherapy
FACS	Fluorescence-activated cell sorting
FBS	Foetal bovine serum
FSC	Forward scatter
GET	Gene electroporation
GM-CSF	Granulocyte-macrophage colony-stimulating factor
GO	Gene Ontology
HEPES	4-(2-hydroxyethyl)-1-piperazineethanesulfonic acid
HMGB1	High-mobility group box 1
HPRA	Irish Health Products Regulatory Authority
ICD	Immunogenic cell death
ICOS	Inducible T-cell costimulator
IFN	Interferon
IFN-γ	Interferon gamma
IL-17	Interleukin- 17
IRE	Irreversible electroporation
KEGG	Kyoto Encyclopedia of Genes and Genomes
L/D	Live/Dead Marker (FACS)
LLC	Lewis Lung Carcinoma
LP	Long Pass
LPS	Lipopolysaccharide; TLR4 agonist
MAPK	Mitogen-activated protein kinase

MCODE	Molecular complex detection
MDSC	Myeloid-derived suppressor cells
MHC II	Major histocompatibility complex class II
mRNA	Messenger RNA
MTT	3-(4,5-dimethylthiazol-2-yl)-2,5-diphenyltetrazolium bromide
NF-κB	Nuclear factor kappa-light-chain-enhancer of activated B cells
NIR	Near-Infrared
NK	Natural killer cell
NKT	Natural killer T cell
NLR	NOD-like receptor
NSCLC	Non-small cell lung cancer
ORR	Objective response rate
PAMP	Pathogen associated molecular pattern
PBMC	Peripheral blood mononuclear cell
PBS	Phosphate buffered saline
PCR	Polymerase chain reaction
PD-1	Programmed cell death protein 1
pDC	Plasmacytoid dendritic cells
PD-L1	Programmed cell death protein 1- ligand 1
PE	phycoerythrin (flow cytometry)
PEF	Pulsed-electric field
PerCP-Cy5.5	Peridinin-chlorophyll protein complex cyanine 5 (flow cytometry)
PI	Propidium iodide
polyI:C	Polyinosinic:polycytidylic acid; TLR3 agonists
PPI	Protein-protein interactions
PS	Performance Status
qRT-PCR	Quantitative Real Time polymerase chain reaction
R848	Resiquimod; TLR7/8 agonist
RBC	Red blood cell
PCR	Polymerase chain reaction
RIN	RNA integrity number

RNA	Ribonucleic acid
rpm	Rounds per minute (centrifuge)
RPMI	Roswell Park Memorial Institute -1640 media
RT	Room temperature
SABR	Stereotactic ablative body radiotherapy
SBRT	Stereotactic body radio- therapy
SCLC	Small-cell lung cancer
SOP	Standard operating protocol
SSB	Single-strand break
SSC	Side scatter
STRING	Search Tool for the Retrieval of Interacting Genes/Proteins
TAA	Tumour-associated antigens
TAM	Tumour-associated macrophages
TLR	Toll-like receptor
TMB	3,3’,5,5’-Tetramethylbenzidine
TME	Tumour microenvironment
TNF	Tumour necrosis factor
TNF-α	Tumour necrosis factor alpha
Treg	Regulatory T cell
UMI	Unique molecular identifier
WHO	World Health Organisation

Publications and Presentations

Publications included as part of this thesis:

1. Bendix, M. B., Brint, E., & Forde, P. F. (2021). Electroporation of suspension cell lines – A proposed assay set for optimizations. Bioelectrochemistry, 142. https://doi.org/10.1016/j.bioelechem.2021.107891

2. Bendix, M. B., Houston, A., Forde, P. F., & Brint, E. (2022b). Electrochemotherapy and immune interactions; A boost to the system? European Journal of Surgical Oncology, 48. https://doi.org/10.1016/j.ejso.2022.05.023

3. Bendix, M. B., Houston, A., Forde, P. F., & Brint, E. (2022). Defining optimal parameters to maximize the effect of electrochemotherapy on lung cancer cells whilst preserving the integrity of immune cells. Bioelectrochemistry, 148. https://doi.org/10.1016/j.bioelechem.2022.108257

Oral Presentations

3rd World Congress on electroporation-based therapies and treatments, 2-6 September 2019, Toulouse, France, Effect of EP and ECT on immune cells- *In vitro* study

4th World Congress on electroporation-based therapies and treatments, 9-13 October 2022, Copenhagen, Denmark, Impact of electrochemotherapy on immune cells in the context of cancer – *In vitro* study

Poster Presentations

Breaking Through: Research to Transform Cancer Treatment, 5- 6 September 2019, Cork, Ireland, Optimizing of ECT parameters for human lung cancer cell lines and their influence on TLR expression patterns

ISI Meeting 2019, 19 and 20 September 2019, Dublin, Ireland, Optimizing of ECT parameters for human lung cancer cell lines and their influence on TLR expression patterns

The 58th Annual IACR conference, March 30 – April 1 2022, Cork, Ireland, Differential responses of immune cells and lung cancer cells to electroporation and electrochemotherapy in vitro

Chapter 1

Literature Review and Introduction

Sections from this chapter have been published in European Journal of Surgical Oncology as:

Bendix, M. B., Houston, A., Forde, P. F., & Brint, E. (2022). Electrochemotherapy and immune interactions; A boost to the system? European Journal of Surgical Oncology, 48. https://doi.org/10.1016/j.ejso.2022.05.023

1.1 Abstract

Cancer is a complex disease which can impact any part of the body. Lung cancer is the leading cause of cancer-related deaths worldwide and current 5-year survival rates are generally below 20% and about 5% for diagnosis at a late disease stage. As current treatments seem not to be able to adequately treat lung cancer, new treatment options are needed. Electrochemotherapy (ECT), the application of an electric pulse to deliver chemotherapy drugs into cells, could be a new modality for lung cancer treatment. ECT has been in clinical trials since the early 1990s and has been used for a variety of different malignancies including melanoma and sarcoma. A standard operating procedure for the use of ECT in clinical settings has been established since 2006. ECT is very effective in reducing the local tumour burden via the increased concentration of the cytotoxic drug in the tumour cells and T-cell dependent killing of the cancer cells, however abscopal effects, the regression of distant disease after localized treatment, are not consistently observed. Currently little is known or understood about how ECT effects the immune cell population within the treated tumour and how these changes could impact the immune response. In this chapter, the current knowledge on ECT in the context of its interactions with the immune system will be reviewed and discussed how the gained knowledge could be harnessed to develop a potent ECT-immune co-treatment combination (Electroimmunotherapy). In addition, the potential advantages and drawbacks of employing ECT for lung cancer treatment will be evaluated.

1.2 Cancer

The World Health Organisation (WHO) describes cancer as a large group of diseases that can affect any part of the body and is also referred to as malignant tumours and neoplasms. Currently over 600 different types of cancer are recognized in the International Classification of Diseases[1], each with unique challenges in regard to diagnosis, treatment and survivorship. According to the WHO a defining feature of cancer is the rapid growth of abnormal cells beyond any boundaries and their potential spread to other organs and tissues in a process called metastasis[1]. Cancer itself is not just a modern-day disease, but the earliest known neoplastic case was noted in a fossil fish from about 300 million years ago, while the earliest possible human cancer case dates back about 1.5 million years[2]. Partially due to the very few remaining human fossils barely anything is known about the prevalence of cancer during human evolution, but evidence suggests that neoplastic diseases increased in accordance with the rise of terrestrial vertebrates and increased from there with the development of humans. Overall it is still assumed that cancer prevalence was significantly lower in the human population until very recently and that the higher level of malignancies seems to be correlated with the level of civilization within a given population in the same era[2].

In their seminal paper Hanahan and Weinberg defined 6 features as hallmarks of cancer which neoplastic cells acquire during their progression from normal, healthy cells to abnormal, malignant cells. The original 6 hallmarks of cancer were: Self-sufficiency in growth signals, Insensitivity to anti-growth signals, Tissue invasion & metastasis, Limitless replicative potential, Sustained angiogenesis and Evading apoptosis[3]. Eleven years later, Hanahan and Weinberg published their follow up paper on newly emerged hallmarks of cancer, which included 10 hallmarks of cancer: Evading growth suppressors, Avoiding immune destruction, Enabling replicative immortality, Tumour-promoting inflammation, Activating invasion & metastasis, Inducing angiogenesis, Genome instability & mutation, Resisting cell death, Deregulating cellular energetics, and Sustained proliferative signaling[4] (Figure 1.1). Together with a paper published by Cavallo *et al.* on the immune hallmarks of cancer in the same year, it increased the understanding of cancer from a disease involving

just abnormal cells to a disease involving abnormal cells that are in a complex interaction with their surroundings and having the ability to evade the immune system, thus making the growth of large tumours possible[4,5]. Furthermore, this understanding defines cancer as an inflammatory disease, to which the immune system would typically react effectively, but as cancer has the ability to change the immune environment in which it exists, the so called tumour-microenvironment, many normal immune system reactions are changed and thus either unable to limit the growth of neoplasm or even co-opted to support tumour growth[6].

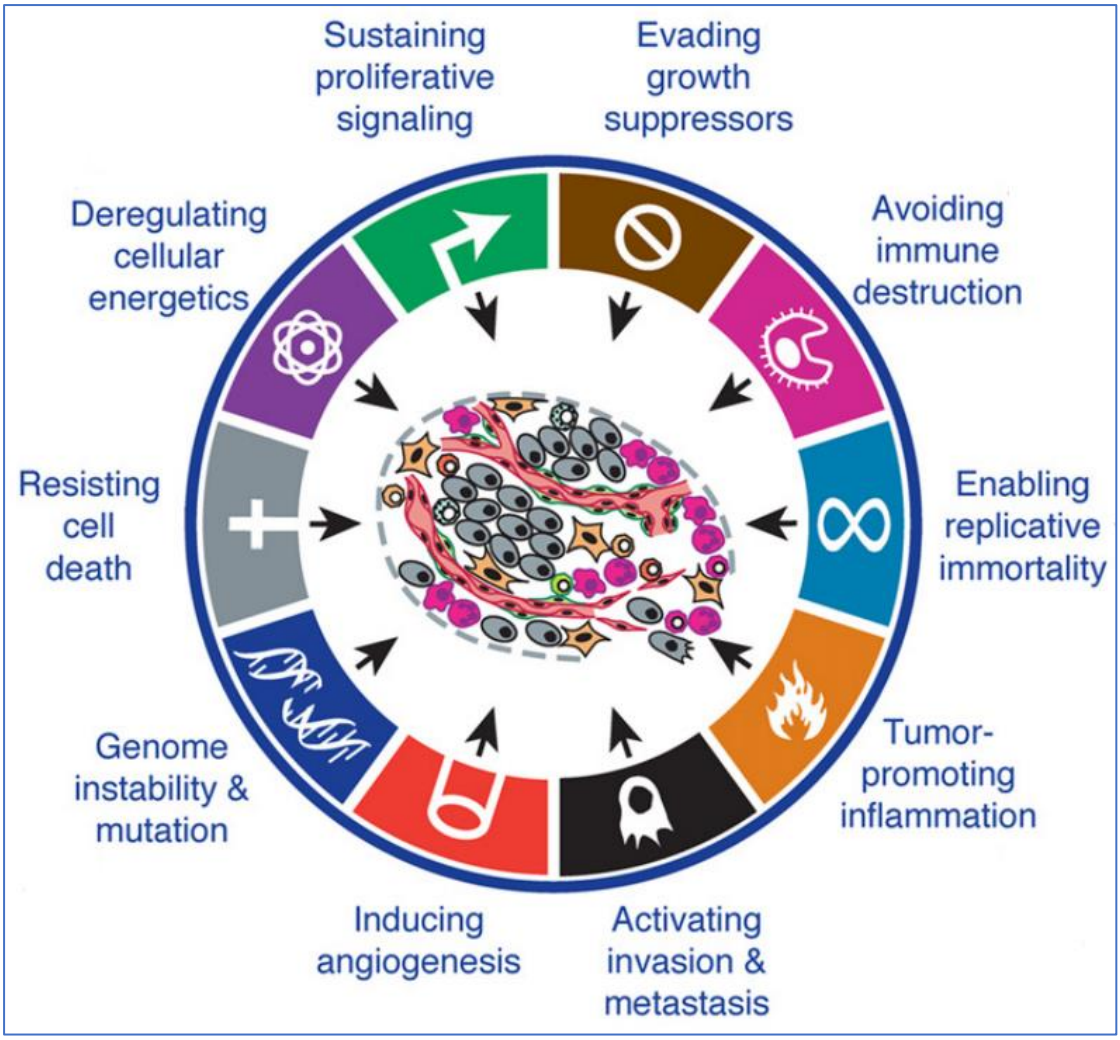


Figure 2.1: Hallmarks of Cancer. Currently there are 10 cellular characteristics assumed to be hallmarks of cancer cells: Evading growth suppressors, Avoiding immune destruction, Enabling replicative immortality, Tumour-promoting inflammation, Activating invasion & metastasis, Inducing angiogenesis, Genome instability & mutation, Resisting cell death, deregulating cellular energetics, and sustaining proliferative signalling. Adopted from Hanahan et al. 2011[4].

Cancer is a serious concern for healthcare systems worldwide with cancer being the leading cause of death globally as one in six death is caused by cancer. It is expected that globally 20% of humanity will face a cancer diagnosis at one point in their lifetime[1]. In addition, while one of the major reasons for an increase in the incidence of cancer diagnosis is the increase in adult life expectancy, about 400.000 children also get diagnosed annually with cancer[1]. Thus, targeted therapies are needed to increase the survival chance of cancer patients with the highest possible quality of

life for the longest possible amount of time. The targeted therapies need to consider the specific circumstances of each cancer type, its genesis and development to exploit any potential weaknesses. 5- year survival rates differ dramatically between cancer types, but also between countries, with lower income countries reporting lower 5-year survival rates than high-income countries. Prostate cancer and early-stage breast cancer have among the highest survival rate with surpassing a 5-year survival rate of 90% in some countries, while lung cancer generally has a very low 5-year survival rate of less than 20% across the world according to the CONCORD-2 study that covered 25.7 million patients with a primary tumour between 1996 and 2009[7].

1.3 Lung Cancer

Lung cancer is the most common cancer diagnosis in men and the third most common cancer diagnosis in women, being responsible for a total of over 2 million cancer diagnoses in 2018, which makes it the most common cancer diagnosis overall. While lung cancer is only responsible for about 12% of the overall cancer incidence, it is responsible for more than 18% of the cancer-related deaths (Figure 1.2)[1,8]. Despite already high lung cancer case numbers, the lung cancer incidence rate is still expected to rise, and while tobacco smoking is still the most common risk factor for developing lung cancer, non-tobacco risk factors are becoming more important as smoking becomes less common in the United States and other developed nations. Indeed, 25% of all lung cancer cases are now being diagnosed in people who have smoked less than 100 cigarettes in their life or never smoked. Next to environmental carcinogens, genetics, chronic lung diseases and infections are connected to the development of lung cancer and are becoming increasingly relevant[8].

1.3.1 Different types of lung cancer

According to the 2021 WHO Classification of Lung Tumours, lung cancer is the overarching diagnosis for 81 different types of cancer that are either present in the lung or originate in the lung. These can be further subdivided by morphological characteristics supported by immunohistochemistry and molecular factors[9]. Furthermore, lung cancer is typically broadly subdivided into two categories, Non-Small Cell Lung cancer (NSCLC) and Small Cell Lung Cancer (SCLC), with 85% of all lung cancer diagnosis accounting for NSCLC and 15% for SCLC[10] (Figure 1.2). Both subtypes differ from each other in their aetiology as well as clinical behaviour[11]. NSCLS is divided into adenocarcinoma, squamous cell carcinoma and large cell cancer, according to the WHO[12], with adenocarcinomas being the most common subtype of NSCLC[10]. SCLC is characterized by its tendency to metastasise, rapid growth and poor survival rates. It is subdivided into limited-stage SCLC and extensive-stage SCLC[10].

In addition to be classified according to morphology, cancer can also be classified according to the stage of the disease. The stage classification is used to describe the

anatomical extent of the disease and has impact on treatment modalities and 5-year survival rate. The stage classification for lung cancer is subdivided into T (Primary Tumour), N (Regional Lymph Nodes) and M (Distant metastasis) descriptors and each can be subdivided into up to 5 different stages within each descriptor. Depending on the stages within each descriptor overall stages from IA1 (early lung cancer with just a small primary tumour) to IVB (late stage lung cancer with multiple extra thoracic metastases) will be assigned to a patient[13]. The prevalence of a stage can vary dramatically between countries[11]. While the 5-year survival rate has improved from 15.6% in 2011 to 19.4% in 2019 across all lung cancer stages, it still remains quite low, and the averaged 5-year survival rate is skewed by the relatively high 5-year survival rate of 57.4% for early-stage lung cancer diagnosis. Late stage lung cancer, which accounts for 58% of all lung cancer diagnoses, reduces the 5-year survival rate to 5.2%[8] (Figure 1.2).

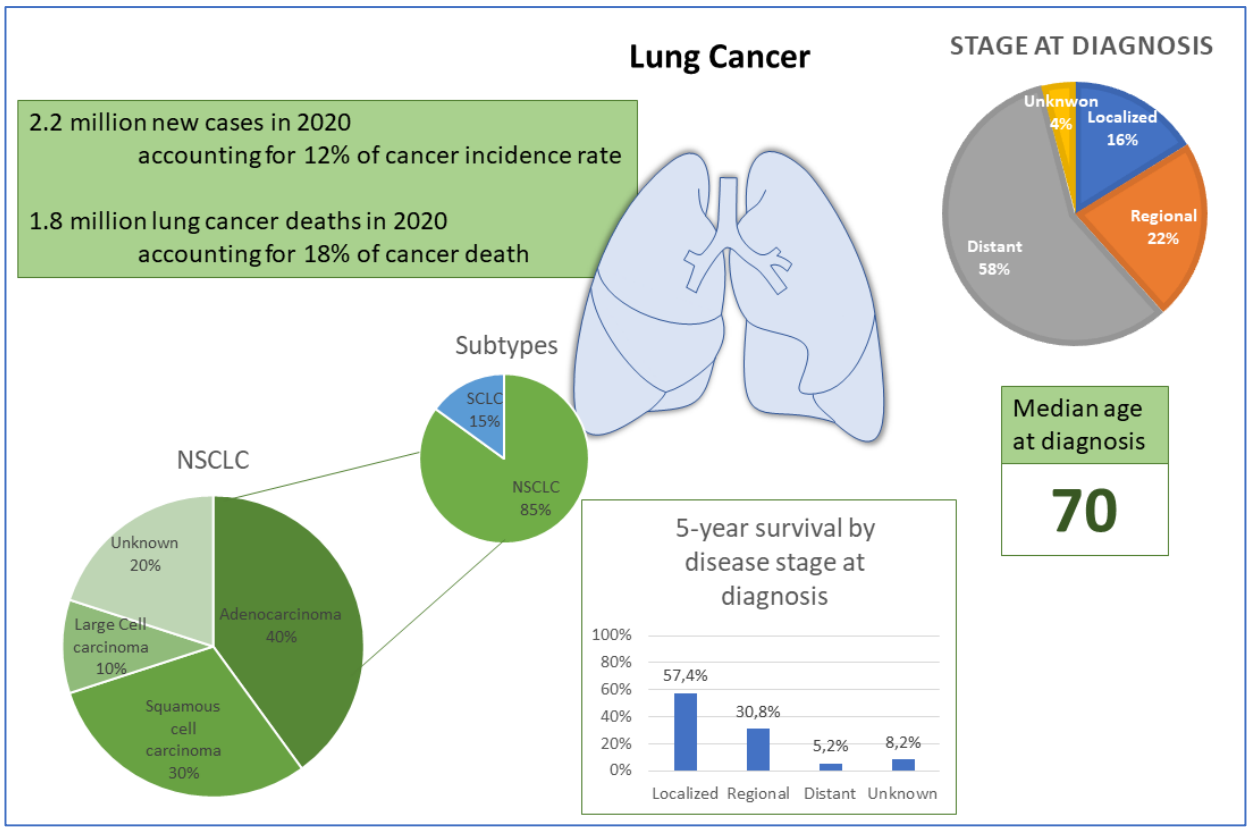


Figure 2.2: Lung cancer statistics. The median age at diagnosis is 70 years of age for a lung cancer patient and most commonly patients are diagnosed at an advanced disease stage (distant disease) which greatly reduces their 5-year survival rate. The most common subtype of lung cancer is the Non-Small Cell Lung cancer (NSCLC). In 2020 lung cancer was responsible for 2.2 million new cancer cases and 1.8 million cancer deaths[8–10,12,14]. Figure created with PowerPoint.

1.3.2 Lung Cancer Therapies

The stage at which lung cancer gets diagnosed predicts which therapy is the best to employ. Surgery, chemotherapy, radiation therapy, targeted therapy as well as immunotherapy, or a combination thereof, are all possible treatment options for lung cancer patients[15].

Surgical resurrection of the tumour is recommended for NSCLC patients with operable stage I and II disease and rarely stage IIIA disease[10,15,16]. Additionally, for a small subset SCLC patients without mediastinal lymph node involvement surgery is also the first line treatment[17]. While 5-year survival rate for early stage NSCLC patients post-surgery is between 30-80%, this drops to below 5% if the lung tumour has already metastazied[15]. Surgery is typically followed by either radiotherapy for

stage III patients, although post-surgery radiotherapy is not necessarily recommended for stage I and II patients, or adjuvant platinum-based chemotherapy[15,18,19]. However, a clear benefit of adjuvant chemotherapy has not yet been proven for stage I NSCLC patients, but adjuvant chemotherapy significantly prolonged overall survival of stage II and III NSCLC patients[15].

Chemotherapy is recommended for NSCLC patients with a performance status (PS; description of functional status of cancer patients) of 0 or 1[15], meaning the cancer patients are still full ambulatory[20]. Chemotherapy is less effective in patients with PS score above 3 and palliative care is more important for these patients. Chemotherapy for NSCLC patients with a PS score of 2, accounting for 40% of advantaged staged patients, is controversial and depends on the individual[15]. Chemotherapy can increase the 1-year survival of NSCLC patients with metastatic disease to up to 50%[15], which still means that half of these patients do not survive even 1 year post diagnosis. The chosen cytotoxic drug and drug combinations, if applicable, are PS-status dependent as the increased effectiveness of two cytotoxic drugs for the chemotherapy needs to be balanced with the increased toxicity of the drugs and the health status of the patient. Chemotherapy with platinum-based drugs (like cisplatin or oxaliplatin) is superior to non-platinum based chemotherapy and leads to higher response and overall survival rates[15].

Radiotherapy, is the first-line treatment for patients with inoperable tumours or for patients refusing surgery[10]. There are three different types of radiotherapy, stereotactic body radio- therapy (SBRT), stereotactic ablative body radiotherapy (SABR), and fractionated radiotherapy[10]. Either SBRT or SABR is recommended for patients with medically inoperable stage I NSCLC, with SBRT potentially also being applied for stage II NSCLC patients, while fractional radiotherapy has become less favoured in the past few years[10,19].

Lung cancer, like a variety of other cancer types, shows high somatic mutation rates[15]. Changes in the kinase expression level and activity are also commonly found in the different lung cancer types[15].The proto-oncogenes KRAS, EGFR, BRAF, PI3K, MEK and HER2 frequently show activation mutations[21]. EGFR- and ALK-targeted

therapies as well as angiogenesis inhibitors are currently under investigation for targeted lung cancer therapy[15]. So far targeted therapies against these mutations have had little impact on the overall survival of lung cancer patients and severe side effects have been observed[15].

Since the 1970s immunotherapy for lung cancer treatment has been under investigation, with initially no improved therapy outcome compared to standard of care treatment observable as only non-specific targets were chosen[22]. The use of immune checkpoint inhibitors (CPIs) like CTLA4 (cytotoxic T-lymphocyte antigen 4), PD-1 (programmed cell death protein 1) and PD-L1 (programmed cell death protein 1 ligand 1) are currently the most common forms of neo-adjuvant immunotherapy for lung cancer treatment[22,23]. In contrast to cytotoxic drugs, that directly target the cancer cells, CPIs block the immunosuppressive mechanism of cancer cells by preventing the cancer cells from interacting with their target immune cells. Thus, CPIs are able to employ the host's immune system for their anticancer effects[22]. Anti-PD-1 or anti-PD-L1 therapy is preferentially given to lung cancer patients whose cancer cells express PD-L1 on the cell surface, even though these therapies are also still effective in some patients without PD-L1 expression[10,24]. Treatment effectiveness can vary between 14-45% for neo-adjuvant CPIs therapy depending on the health status of the patient as well as the stage of the cancer[10]. Currently studies are underway that are exploring the combination of chemotherapy with adjuvant CPI treatments, with first promising results showing up to 80% response rate for the combination treatment in patients[10]. If these promising results will translate into improved 5-year survival rates will need to be observed in the next few years.

Despite the wide range of possible treatment options and the development of newer treatment modalities as well as new treatment combinations in the recent years, lung cancer survival rates remain the lowest across all cancer diagnosis[25]. In order to improve therapy outcomes for lung cancer patients, the immune environment in which any therapy takes place needs to be better understood and emerging cancer therapies for other malignancies need to be investigated to see if they could be

applied for lung cancer treatment. For example, the possibility of employing electrochemotherapy for the treatment of lung cancer patients.

1.4 The Tumour Microenvironment

Tumours are increasingly understood as organ-like tissues with complex structures and interactions occurring between the cells within the tumour[4]. The tumour microenvironment (TME) refers to the collection of cancer and immune cells, blood vessels, fibroblasts, stromal cells, signalling molecules and extracellular matrix (ECM) that make up not only the tumour itself, but also the direct surroundings of the tumour[4,15,26–28] (Figure 1.3). The presence of the TME is also now considered a hallmark of cancer[4] and is rearranged as needed by a mutual crosstalk of all participants[29]. The TME is able to foster tumour growth by supressing the local immune response and supporting the tumour in evading immune surveillance, via a process called cancer immunoediting, though physical alterations like changes in oxygen and pH levels[26,30,31].

The physical properties of the TME itself can promote tumour progression and malignancy via the increased stiffness of the TME caused by the ECM[32]. Next to the stiffness alone driving a malignant phenotype, the ECM can also influence cell migration behaviour[31]. Hypoxia is a common feature of TME and again can impact cell migratory behaviour[33] as well as influence the phenotype of cells in the TME[26]. Cancer cells metabolize glucose to lactate in the presence of oxygen, when in non-malignant cells this metabolic process only happens in oxygen-poor environments, in a process termed the Warburg effect[34]. As lactic acid is the final product of this metabolic process, the TME becomes increasingly acidic, which exerts a selection pressure on the cells within the TME towards cells that can survive in this hostile environment[28]. Taken together these physical changes, in addition with the TME being also relatively nutrient poor[35], prevents the infiltration of competent immune cells into the tumour and induces pro-tumorigenic changes in the immune cells present in the TME[26].

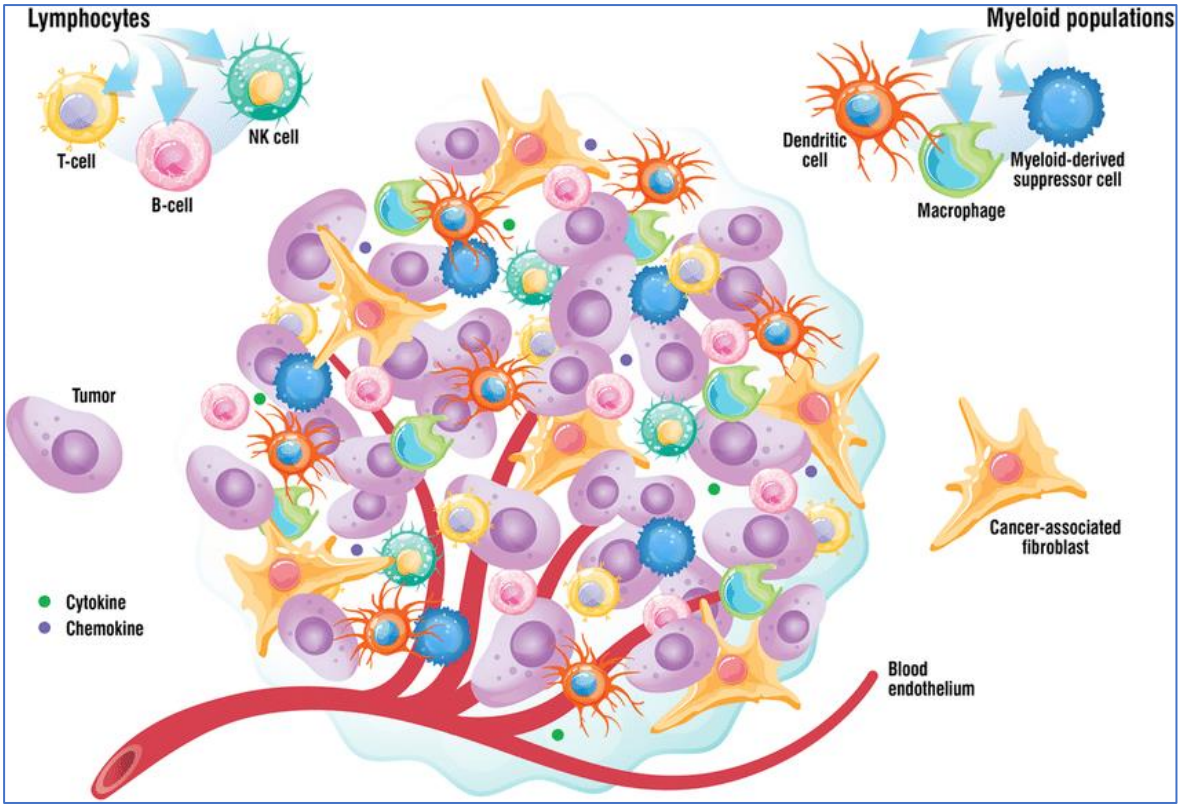


Figure 2.3: Main components of the TME are the tumour cells, various immune cell types as well as cancer-associated fibroblasts. Adopted from Zhang et al.[36].

T cells, dendritic cells (DCs), tumour-associated macrophages (TAM), natural killer cells and myeloid-derived suppressor cells (MDSCs) are among the immune cells present in the TME. Immune cells such as T cells and DCs are paramount to the eradication of malignant cells and to prevent tumour formation, yet at the same time other immune cells, among which are TAMs, are promoting tumour growth and metastasis[37]. Through physical changes as well as an inflammatory environment the TME can alter the functionality of the exposed cells, employing immune cells to facilitate tumour growth and angiogenesis as well as immune invasion[15]. The immune cell composition in the TME can be impacted by various anti-cancer treatments and impact the treatment itself, for example the TME can be responsible for multi-drug resistance[29]. A basic differentiation of the TME is subdividing tumours into hot and cold tumours, with lung cancers typically counted towards the immunogenic cold tumours[38,39]. The TME of hot tumours is characterized by infiltration of cytotoxic T cells, while in cold tumours very few immune cells are present in the TME with the tumour overall showing low levels of immunogenicity. Moreover, cold tumours

usually have a higher percentage of tumour promoting immune cells, while hot tumours have a bigger tumour suppression immune cell population. Both states exist on a continuum, so the same tumour might display features of both hot and cold tumours as well as the same tumour type showing different levels of immunogenicity between various patients[40].

The immune composition of the TME is vastly variable between patients, yet also highly predictive for tumour progression and patient outcome[24,38,41–43]. Not only is the presence or absence of immune cells relevant for the tumour growth, but also how these cells are able to physically interact. For example, $CD8^+$ T cells need physical interactions with their target cells, in this case the cancer cells, for their cell activity[24,27].

In the following section a closer look at T cells, dendritic cells and macrophages will be taken, as they play a central role in the immune function of the lung[38] and are also central to the immune response to cancer.

1.4.1 T cells

T cells are one type of lymphocyte and play a central role in the adaptive immune response[44,45]. There are several subtypes of T cells each with its own functionality. $CD4^+$ T cells, also referred to as T helper cells[44], and $CD8^+$ T cells, also referred to as cytotoxic T cell, are the two main groups of T cells[45]. $CD8^+$ T cells are able to directly kill cells infected with intracellular pathogens as well as cancer cells[45]. $CD4^+$ T cells generally support $CD8^+$ T cells as well as B cells[44]. There are several subtypes of T helper cells, among which are the T helper 1, T helper 2, T helper 17 and regulatory T (Treg) cell populations[44]. The Treg cells deserve special attention in the context of cancer as they are able to suppress anti-tumour responses and are able to create and support the immunosuppressive TME[46]. Chemotherapy generally leads to a decrease in $CD8^+$ T cells, while proliferation of $CD8^+$ T cells following treatment is a positive prognostic marker for effectiveness of CPI treatment in melanoma patients[47]. Reuben *et al.* found that T cell density itself is not a predictive marker for overall survival of lung cancer patients, but the more unique mutations the T cell had in the

tumour, compared to the unaffected lung, the higher the median survival of lung cancer patients[48].

1.4.2 Dendritic cells

Dendritic cells (DCs) are a group of heterogeneous cells and the most potent professional antigen-presenting cells (APCs) that are central to the immune system[49,50]. They are the only cells able to activate both the innate and adaptive immune systems. DCs are present in the form of resting DCs with a high phagocytic capacity in virtually all mammalian tissues[49,51]. There are two main subsets of DCs; myeloid DCs, also referred to as conventional DCs (cDCs) and plasmacytoid DCs (pDCs). cDCs are key players in immune responses against pathogens while pDCs are the main producers of interferons in response to microbial and viral infections[52]. DCs are the sentinels of the immune system recognizing pathogens via evolutionarily ancient family of pattern-recognition receptors, like the Toll-like receptor (TLR) family and instigate immune cascades targeted against the specific pathogen leading to the elimination of the pathogen[50]. DCs can prime both $CD4^+$ and $CD8^+$ T cells through tightly controlled antigen presentation via major histocompatibility complexes (MHC) I and II[53,54]. They can stimulate natural killer cells though cytokine secretion and also present antigens to B cells[49,50]. Next to their centrality to antigen-specific immunity and tolerance against pathogens, DCs are also vital for the anti-tumour response of the immune system[55]. To induce an anti-tumour response, activated DCs migrate to the draining lymph nodes of the tumours where they cross-present the tumour-associated antigens to cytotoxic T cells[56]. Whilst DCs generally have this antitumorigenic capacity, the suppressive environment of the tumour reduces the capacity of the activated DCs to elicit a potent immune response[52,56]. In the TME activation of DCs is inhibited, thus these vital cells remain in an immature state, which means they fail to prime T cells efficiently due to low expression of co-stimulatory molecules like CD40, CD80 and CD86[50–52,55]. cDCs have a key role in the immune response against malignancies, but the role of pDCs is not yet fully illuminated[56]. pDCs infiltrate various tumours, but some studies suggest they have a pro-tumorigenic function by supporting tumour growth[50].

1.4.3 Macrophages

Macrophages are tissue-based phagocytic cells that play an important role in the innate and adaptive immune system. In addition, they also play an important role in maintaining tissue-homeostasis[57]. Tumour-associated macrophages (TAMs) are the resident macrophages found across different solid tumour types and TAMs can comprise up to 50% of the tumour volume[58]. In contrast to normal macrophages, which are derived from embryonic progenitors[59,60], TAMs are more commonly derived from circulating populations of monocytes[61]. In order to better understand the duality of macrophages responses to pathogens and cancer they are typically categorized as M1 or M2 macrophages. M1 macrophages refers to classically activated macrophages, which mediate resistance against intracellular pathogens and are generally considered to be anti-tumorigenic. M2 macrophages are alternative activated macrophages and their functionality is oriented towards tissue remodelling and angiogenesis; they are generally considered to be pro-tumorigenic[62,63].

Generally, a high level of macrophage infiltration in solid tumours is connected with a poor clinical outcome, even though the data is not completely clear for all cancer types and the prognostic value might be dependent on the exact cancer type or also in which stage the cancer was analysed[37,59]. Macrophages have the capability to kill tumour cells and activate a leukocyte-dependent anti-tumour resistance, thus a high macrophage infiltration in the early stages of cancer development can lead to tumour destruction[64]. In established cancer their tissue-homeostasis capacities are co-opted by the tumour and thus TAMs can contribute to cancer progression and metastasis[65,66]. As such TAMs are a key component of the TME[66] and tumours secrete a range of chemoattractant to recruit macrophages to the TME and polarize the TAMs into M2-like phenotypes[67].

The role of TAMs remains controversial in the context of lung cancer. Approximately 70% of the TAMs in lung cancer are of the M2-like phenotype, thus presenting pro-tumorigenic features, and 30% are of the M1-like phenotype, thus presenting anti-tumorigenic features. Simultaneously, the density of the M2 TAMs in the lung cancer is being reported as not having an impact on the overall survival of lung cancer patients[68]. Other reports indicated that the density of the M1 and M2 TAMs was

markedly increased in the tumour islets in longer surviving lung cancer patients than in lung cancer patients with reduced survival[69]. Along the same lines, Jackute *et al.* found that a low level infiltration of M2 TAMs as well high level of M1 TAMs in lung tumour islets was associated with improved NSCLC patient's survival[70]. The islet density of both M1 and M2 macrophages was markedly increased in extended, compared with poor, survival patients.

1.5 Electrochemotherapy for the treatment of cancer

Despite recent advances in cancer treatments overall and lung cancer treatment in particular, cancer is still one of the leading causes of death worldwide, accounting for 17% of all death in 2019. New treatment modalities are needed that are also able to deliver the greatest quality of life to the patient post-treatment. To this end electroporation-based electrochemotherapy (ECT) is undergoing significant exploration as an alternative treatment modality for cancer in general and lung cancer in particular.

1.5.1 Principles of Electroporation

The cell membrane protects the inside of the cell from outside influences and, among other functions, prevents the free entrance of pathogens, molecules and drugs into the cell. Application of short (microseconds to milliseconds) externally applied electric pulsed fields increases the cell membrane permeability due to an increased transmembrane potential leading to pore formation. This effect is called electroporation (EP). While initially different theories existed as to how electroporation causes pore formation[71], the currently accepted description is the formation of aqueous pores in the cell lipid bilayer[72–74] (Figure 1.4).

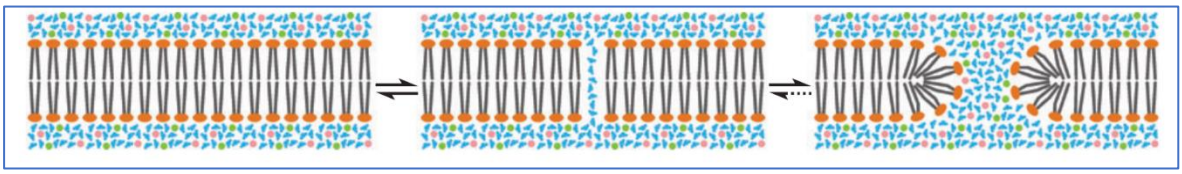


Figure 2.4: An idealized molecular scheme of the pore formation following electroporation in the cell lipid bilayer. Adopted from Yarmush et al. [72].

The speed with which the pores are formed depends on the applied electric field parameters (intensity, pulse duration, and number of pulses) and also impacts the size and duration (microseconds to minutes) of the formed pores. In addition, the electrical pulse parameters also influence whether the pores can either reseal (termed reversible electroporation) or if the pores remain permanently open (termed irreversible electroporation (IRE))[72]. Reversible electroporation uses lower

electric field strengths (below 10kV/cm for reversible electroporation; figure 1.5B) as well as lower exposure time (below 10 ms for reversible electroporation; Figure 1.5A) than irreversible electroporation[73].

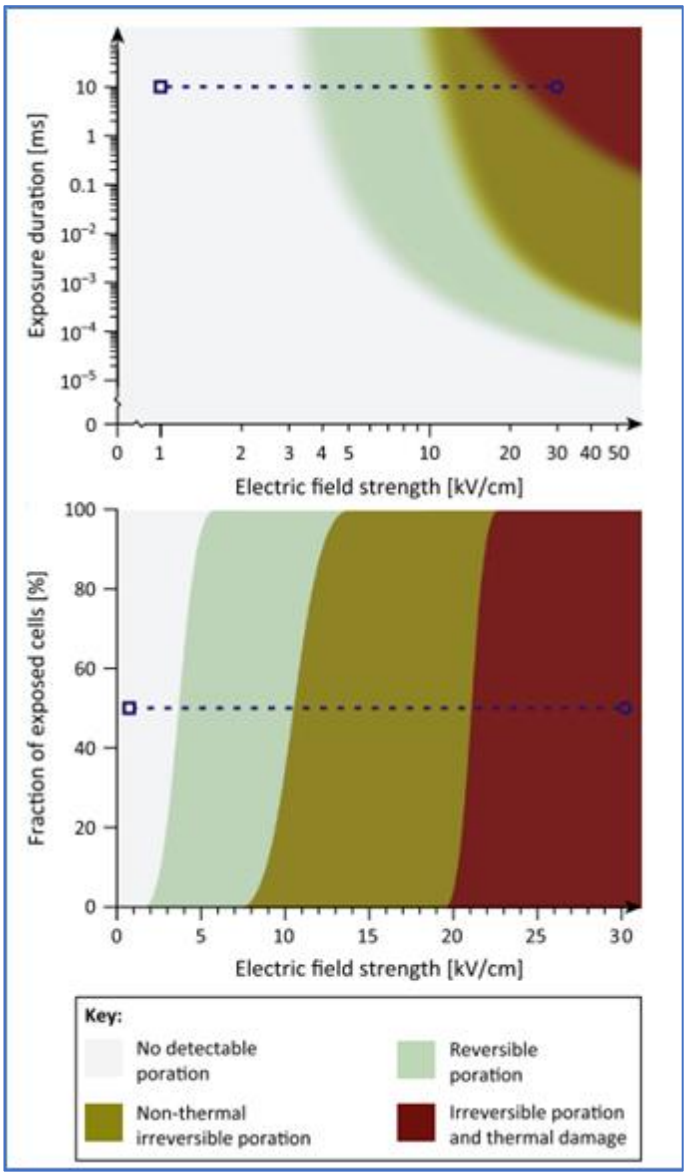


Figure 2.5 Membrane pore formation by electroporation depends on electric field strength and exposure time. Adopted from Kotnik et al. [73].

Electroporation at different electric field strengths with varying pulse duration can be used to induce different biological effects (Figure 1.6). The different biological effects result in different electric parameters being used for the application of electroporation in different treatments[75]. In the case of ECT and Calcium

electroporation (CaEP), electroporation is used to create transient pores in the cell membrane facilitating the uptake of the cytostatic drug or calcium respectively, but a high degree of cell survival is also a required for ECT and CaEP to be effectiv[76]. A high cell survival following treatment is also required for gene electroporation, whilst the cell death following IRE caused purely by the applied electric field is the designed-for treatment outcome[72].

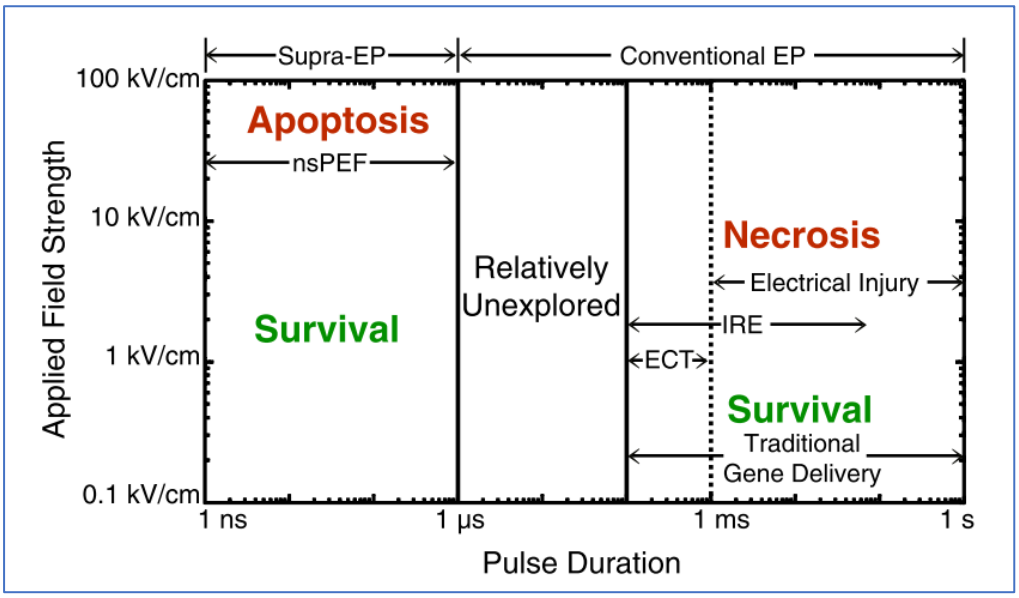


Figure 2.6: Impact on cell survival and cell death following electroporation is dependent on the applied electric field strength and the pulse duration. Weaker electric field and shorter pulse durations typically allow for more survival of the cells, while higher electric field strengths and short pulse durations induce apoptotic cell death and longer pulse durations induce necrotic cell death. Adopted from Weaver et al.[75].

Whilst the phenomenon of EP has been known since the middle of the 18th century[72,77], the medical application of EP started in 1982 with the seminal work by Neumann and colleagues, who also coined the term electroporation[78]. Neumann *et al.* authored the first paper on gene transfer into murine cells by electroporation, showing that the method was simply and easy to apply and that it showed higher treatment efficacy compared to the existing comparable biochemical techniques for gene transfer[78]. Electroporation is thus a non-viral gene delivery method. Initially EP was used mainly for the delivery of DNA into cells, often bacterial cells[79–81], whilst in

more recent years introduction of cytotoxic molecules, like bleomycin, has become also a standard use for electroporation-based medical application, particularly in the form of tissue electroporation. An additional emerging application option for EP is the treatment of Cardiac Arrythmias by using pulsed electric field ablation, a method that employs IRE[82]. Outside the medical application, EP has also become a sought-after method for food processing, in the form of pulsed electric field (PEF) application and wastewater treatment[73,83]. PEF is a non-thermal method that allows the targeted destruction of microbes while preserving the sensory and physical properties of the treated food items[83].

The development of different medical applications of electroporation occurred in unison with the development of different electric pulse generators for research and clinical applications. The first electric pulse generators were developed in the 1980s[77]. The commercially available CLINIPORATOR™, built by IGEA S.r.l. (Carpi, Italy), was developed in Europe for clinical applications during the process of standardizing ECT for clinical applications and the new generation of the Cliniporator devices has been designed to treat increasingly large volumes of tissue[84–86]. Most recently EP-based applications have become available for internal administration, with the development of EndoVE, an endoscopic EP device, as well as with the development of expandable probes for other EP devices[86].

1.5.2 Fundamental principles of Electrochemotherapy

ECT is the combination of electroporation and the administration of a chemotherapeutic agent, initially also called electroporation therapy[87]. Traditionally, cytotoxic drugs are poorly taken up by cancer cells as they cannot penetrate the membrane or only penetrate the membrane with low efficacy, therefore limiting their effectiveness. ECT, through the pore formation caused by the electroporation portion of the treatment, increases the uptake of the hydrophilic anticancer drugs into the cells and thus potentiates their cytotoxic capacity[85]. The resealing of the cell membrane in the minutes following the ECT treatment captures the cytotoxic drugs inside the cells leading to sufficient drug accumulation inside the cells for treatment impact, while using lower drug dosages then typically used in standard chemotherapy[88] (Figure 1.7).

Many different drugs were initially tested for *in vitro* potentiation of their effectiveness in ECT compared to drug only treatment. Bleomycin was the drug that showed the greatest increase in potentiation *in vitro*, with ECT increasing bleomycin's potency by up to 5000-fold[89]. Cisplatin showed an increased potency of up to 12-fold *in vitro*[89,90] and calcium, a non-cytotoxic alternative for ECT treatments, demonstrated a several hundred-fold increase in potency[91,92]. The greater increase in potency for bleomycin compared to cisplatin is most likely based on the higher effectiveness cisplatin has, compared to bleomycin, already by itself[89]. Of interest in the lung cancer context is that carboplatin and oxaliplatin also showed an increase in potency *in vitro* in combination with ECT compared to the drug alone[89,90].

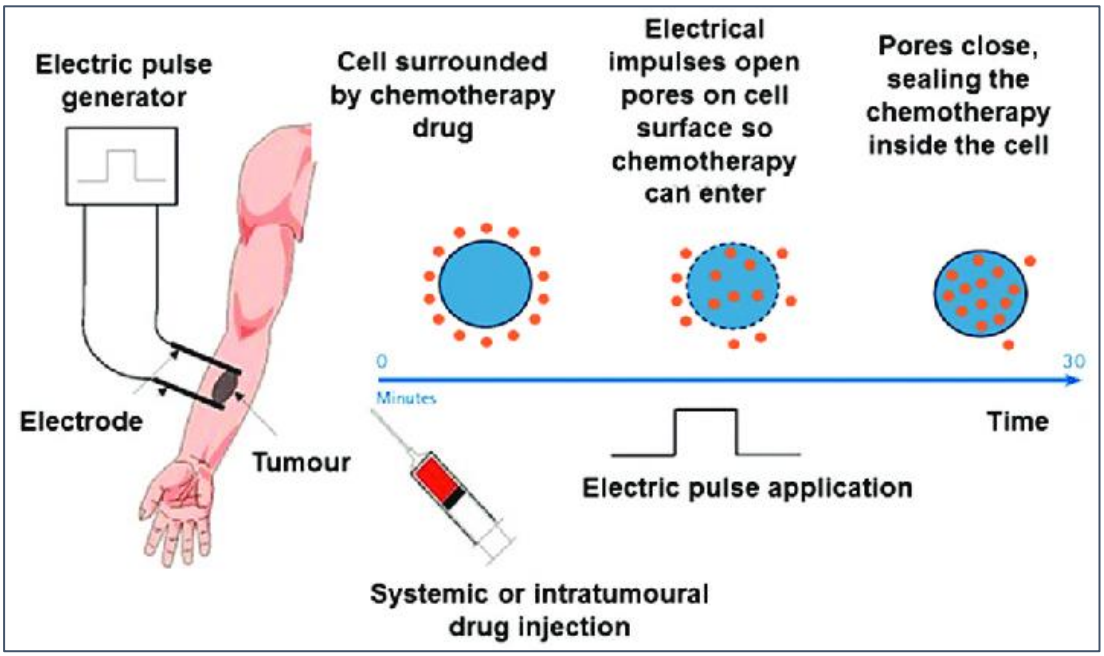


Figure 2.7 Fundamental principle of ECT. Prior to the application of the electric pulse, the cytotoxic drug, commonly used are bleomycin and cisplatin, is injected either systemically or intratumorally. The application of the electric pulse creates pores in the cell membrane allowing uninhibited efflux of the locally present drug into the cancer cells. Shortly after the electric pulse the cell membrane will re-seal and the drug is trapped inside the cancer cell allowing it to exert its cytotoxic function. Adopted from Deore et al.[85].

Under clinically approved settings, ECT *in vivo* has also exhibited an improved effectiveness compared to the drug only treatment. The efficacy of bleomycin was observed to be increased by up to 800-fold and up to 80-fold for cisplatin. In contrast,

reversible EP alone did not show any significant improvement in cancer patient outcome[84]. With drug uptake following ECT, and thus increased potency of the used drug, the local drug availability prior to the application of the electric pulse determines the increased effectiveness as well. Therefore, to optimize the treatment efficacy, the timing, the route of administration and the electrical pulse strength need to be determined prior to treatment[72,86].

There are two main routes in which drugs used during ECT are administered to patients (i) intravenous administration or (ii) intratumoral administration, wherein the drug is injected directly into the tumour[72,86]. Based on clinical evidence, smaller and single tumours can be treated well with intratumoral drug administration while for the treatment of numerous and bigger tumours intravenous drug administration leads to better results[93].

In addition to impacting the cell membrane, ECT also has an impact on the blood vessels in the treated tumour. Stromal cells are predisposed to take up the cytotoxic drugs used in ECT treatment. This drug uptake results in endothelial apoptotic cell death. This cell death leads to abrogation of the tumour blood flow[94], making the TME following ECT treatment even more hypoxic. The second effect ECT causes in blood vessels is named the vascular lock effect and describes the vasoconstricting effect ECT has on normal and tumour blood vessels following treatment. This effect can last anywhere from 12 hours to 5 days, and it leads to prolonged entrapment of the used cytotoxic drugs in the treatment area, as they are unable to leave, increasing their impact. However, the vascular lock also prevents the entry of other drugs, or molecules in general, into the tumour following ECT treatment[85,95,96].

Local immune system involvement has been shown to be necessary for the treatment effect of ECT[97–100]. With current ECT protocols, a systemic immune response is rarely observed, despite the potential of ECT to evoke such a response. Abscopal effects, such as the regression of distant disease after localized treatment, are sometimes observed[93,99,101], but the mechanism of action is unclear. Hence, one of the major drawbacks of ECT is that it seems to be effective only as a local treatment. Therefore, while ECT is used in more than 130 cancer centres across Europe[72], its current

therapeutic use is limited and is most often utilised in a palliative care setting in many European countries.

1.5.3 Other electroporation-based treatment options for cancer treatment

As well as ECT, other electroporation-based treatment options exist for cancer treatments. Namely, calcium electroporation (CaEP), gene electroporation (GET) and irreversible electroporation (IRE).

CaEP is the closest relative to ECT with respect to the underlying fundamental principles. In CaEP, electroporation is used to facilitate the uptake of calcium instead of a cytotoxic drug, with the increase in intracellular calcium concentration inducing tumour cell death. Calcium is an intracellular second messenger, that is tightly regulated at low cytoplasmic levels. It is involved in many different cellular processes including cell cycle, gene transcription, cell signalling, cell death and proliferation[102–104]. The excessive influx of calcium caused by CaEP overwhelms the homeostatic capacity of the cells to maintain the needed low intracellular calcium levels. This leads to increased storage of calcium in the endoplasmic reticulum and the mitochondria, leading to mitochondrial dysfunction, which in turns leads to apoptotic cell death caused by energy production failure just when the cells need more energy to return to homeostasis[102,104]. Similar to ECT, CaEP has a transient vascular lock effect on vasculature, but no long-term vascular responses have been observed[102]. In contrast to chemotherapeutic drugs, calcium has some distinctive advantages. Calcium is a non-toxic, non-mutagenic molecule, which means it can be administered by a non-oncologist, making CaEP a more accessible treatment than ECT, and calcium administration should have fewer side-effects than chemotherapeutic drugs[105,106]. Moreover, calcium is cheaper than chemotherapeutic drugs, and calcium also does not lead to the immunosuppressive effects of chemotherapy[105,106]. This makes CaEP a potentially better treatment option for cancer patients in middle- and low-income countries[106]countries which account for 80% of all cancer diagnosis currently.

GET facilitates the uptake of gene constructs into the cells via the application of electric pulses similar to the electric pulses used in ECT (8 pulses, 1Hz frequency,

100µs long, 400V/cm for the delivery of small molecules into tumour tissue *in vivo*). The exact electric field strength needed is dependent of the target tissue as GET is also used to deliver DNA plasmid into muscles for the systemic expression of the target gene[72,107,108]. The effectiveness of GET is, similar to ECT, influenced by the immune status of the treated animal/patient as well as the immune status of the tumour. Treated animals need to be immunocompetent for GET to work well and more immunogenic tumours lead to a higher cure rate than less immunogenic tumours[100,109]. One challenge in bringing GET into widespread use for human application is the low efficacy of the electroporation-based delivery of the gene construct into human tumours[109]. In addition to being used as a single-treatment, GET of plasmid DNA coding for IL-12 is under investigation as an adjuvant treatment modality to improve ECT effectiveness[100].

ECT, CaEP and GET are all considered reversible electroporation treatments. Treatment effects of IRE on the other hand are based on the irreversible electroporation of the tumour cell membrane leading to the formation of permanent pores in the cell membrane. Through these permanently formed pores, the cells are unable to maintain and restore cell homeostasis leading to cell death[110]. IRE can kill the treated tumour cells without the addition of a drug, molecule or by introducing foreign DNA into the cells[111]. The used electric field strength for IRE is several magnitudes higher than for ECT or CaEP, typically needing voltages of 1000V-3000V, compared to ECT who typically needs only a few hundred volts[77,112]. Also between 80-100 pulses are used with IRE[109], compared to the typically 8 pulses used for ECT[84]. Similarly, to ECT, IRE also preserves the tissue surrounding the treatment area making it a potentially treatment option for tumour eradication near vital structures like large blood vessels[109]. In contrast to ECT which is the mainly used form of electroporation-based cancer treatments in Europe, IRE is the more typically used form of electroporation-based cancer treatments in North America[77,86].

In the rest of this introduction, I will focus on ECT as an anti-cancer treatment, how it impacts the immune system and how it can potentially be improved by combining ECT with adjuvant immunotherapy.

1.5.4 Current status of ECT treatment in a clinical scenario

The first clinical phase I and II trial for ECT was performed with head and neck cancer patients in 1990 and 1991[113]. Since then, this treatment has extended to other cancer types, including, but not limited to, melanoma[114], colon cancer[115], prostate cancer[116] as well as veterinary cancers[117]. These early clinical studies were performed with different protocols in regard to the electric field properties as well as used drugs[84], causing a certain degree of difficulty in comparing effectiveness and overall treatment responses between studies and tumour types.

Several Phase I and II trials were setup to determine the use and safety of ECT for cancer treatment, using different drugs, drug concentration and pulse settings[84]. The seminal European Standard Operating procedure for ECT (ESOPE) study was the first clinical trial that used an agreed standard operating protocol (SOP) for the treatment of melanoma, thus, making treatment outcomes across various cancer centres comparable[84]. ESOPE was performed by 4 cancer centres throughout Europe, all contributing their experience for effective treatment and pain management. No significant differences in overall treatment results (complete or partial response), as well as pain management, were observed between the participating centres, showing that the use of a SOP can lead to safe and comparable treatment outcomes across various countries and health care systems. ESOPE was identified as a step forward to unifying the treatment protocols for ECT for malignancies, notwithstanding the study itself having certain drawbacks. Despite high initial enrolment numbers, only 41 patients for treatment response and 61 patients for toxicity studies could be finally analysed (other patients withdrew, did not have follow-up visits or died)[84]. Additionally, only cutaneous tumours of less than 3cm[84] were treated in the trial. While the ESOPE showed that ECT, when conducted properly, is a reliable and effective treatment with minimal adverse effects (only 5 adverse effects; all mild), it also led to standardised parameters (8 pulses, 1Hz frequency, 100µs pulse length at 1000V/cm and bleomycin being used as the standard ECT drug) being agreed upon for most follow-up trials. Subsequent trials did not vary from these pulse parameters, nor use different drugs or modifications to the protocol when applied to different malignancies or tumour locations.

An updated ESOPE was established in 2018[93], extending the original protocol to also include larger tumours (>3cm)[84] and subcutaneous tumours[93]. The updated ESOPE study concluded that intratumoral drug administration is best for small (<3cm³) and fewer (less than 7) tumours, whereas intravenous drug administration is better used for larger and more tumours. Furthermore, the updated ESOPE confirmed the results of the original ESOPE that, if needed, patients can be retreated with ECT utilizing the same drug should the original treatment not be sufficient or if reoccurrence appeared anywhere else. Several contraindications were established for ECT and for a second ECT treatment. If the patients are lactating or are pregnant, they should not be treated with ECT. Also, the lung function (for intravenous bleomycin administration), together with the liver and kidney function should be sufficient to be able to clear the drugs from the patient's system. In case of a decreased lung capacity after the first ECT treatment with bleomycin, any follow-up treatment should be substituted with cisplatin[93].

Following the ESOPE study, in 2017 InspECT was published, detailing further analysis of side effects and limitations of ECT[114]. InspECT used the ESOPE protocol with bleomycin, administered either intravenous or intratumorally, and correlated several factors via multivariant analysis, other than tumour size, with a favourable treatment outcome. They found that coverage of deep tumour margins, presence of lymph oedema, absence of visceral metastasis and faster healing time (mostly due to smaller tumour size) were all related to a favourable treatment response. Additionally, InspECT confirmed the results from both previously published ESOPE studies, i.e. treatment-related pain is well manageable and serious adverse events are not present[114]. Interestingly, lymph oedema was one of the positive biomarkers for a favourable ECT outcome, highlighting the potential importance of the immune response in ECT[114].

Currently, there are also various reversible electroporation-based treatment trials recruiting patients for clinical testing for cancer treatment, among which are ECT, GET and CaEP (Table 1.1). These trials are mostly extending the treatment modalities either to deep-seated tumours, like colorectal tumours, or are testing co-treatments with ECT. CaEP also has the potential to be combined with immune co-treatment as

calcium uptake is hypothesized to have immunogenic effects[99], potentially being able to increase the effectiveness of the immune co-treatment.

NCT Number	Cancer Type	Treatment Type	Trial type
NCT03448666	Malignant Melanoma	Bleomycin ECT with Pembrolizumab co-treatment	Phase II Trial
NCT04929912	Skin Cancer Gastrointestinal Cancer	ECT/ CaEP	Safety Study
NCT05395962	Vulvar Cancer	Carboplatin + Bleomycin ECT Bleomycin ECT	Phase II Trial
NCT04760327	Gynaecological Cancers	Bleomycin ECT Cisplatin ECT	Phase II Trial
NCT04816045	Colorectal Cancer	ECT	Phase I+II Trial
NCT04605419	Barrett's Oesophagus with High Grade Dysplasia	CaEP	Phase I Trial
NCT05046262	Basal Cell Carcinoma	CaEP	Phase II Trial
NCT04259658	Skin Cancers	CaEP	Phase II Trial
NCT04958044	Oesophageal Cancer	CaEP	Phase I Trial
NCT05077033	Basal Cell Carcinoma	phIL12 GET	Phase I Trial

Table 2.1: List of clinical trials testing ECT, CaEP and GET for cancer treatment that are currently recruiting patients (August 2022).

1.5.5 Cell death following ECT

The type of cell death cancer cells, and other cells in the treatment area, are undergoing following ECT is still not fully elucidated, even though several hypotheses exist. Understanding the cell death induced by ECT is a critical aspect of the therapeutic effectiveness as this could impact the systemic immune responses[118]. Controversial findings currently exist describing ECT-induced cell death varying from apoptosis to necrosis to immunogenic cell death. There are indications that the type of cell death might be more cell line than pulse parameter dependent[118,119].

Initially investigations into the type of cell death caused by electroporation revealed, in an *in vitro* model, that cells die in equal measures by necrosis as well as apoptosis[120]. The human HL60 (promyeloid leukaemia) cell line was electroporated at 750V/cm and the cell viability, morphology, apoptotic index and chromosomal DNA fragmentation was investigated. Pinero *et al.* concluded that from the cells dying following the treatment, about half of these cells die immediately after the EP treatment via necrosis, while the initially surviving cells die in the following days via apoptosis induced by the lipid peroxidation caused by the EP treatment[120]. While apoptosis is considered a "quiet" cell death, that does not lead to immune system activation, necrosis on the other hand can lead to the secretion of damage-associated molecular patterns (DAMPs) potentially inducing an immune response[118].

ECT with bleomycin, cisplatin or oxaliplatin induced a caspase-independent necrotic like cell death in pancreatic cancer cells *in vitro*[121]. The pancreatic cancer cell lines were treated with cisplatin, oxaliplatin or bleomycin at 8 pulses of 99 µs at a frequency of 1 Hz with 600V/cm for PANC-1 cells or 1000V/cm for Pan02 cells and their survival, morphology and Caspase-3 activity was analysed following ECT treatment. Fernandes *et al.* found that all tested ECT treatments induced necroptosis in the pancreatic cancer cells based on biochemical and morphological changes. Necroptosis is counted towards the immunogenic cell death types[121]. Earlier research into the mechanisms of cell death after bleomycin treatment indicated that the absolute and relative induced levels of single-strand breaks (SSB) and double-strand breaks (DSB) in the DNA following bleomycin treatment determine the type of cell death[119]. Low levels of DSBs together with high levels of SSBs following treatment induced a mitotic cell death, while high level of DSBs independent of the level of SSBs induced pseudoapoptosis, while moderate levels of DSBs in combination with high levels of SSBs induce apoptosis[122,123]. As ECT increase the effects of the chosen cytotoxic drug, the bleomycin data would indicate that cells die via apoptosis following bleomycin ECT.

Special attention has been paid over the last several years of the ability of ECT to potentially induce immunogenic cell death. Immunogenic cell death (ICD) is any form of regulated cell death (cell death regulated by signal transduction molecule(s)) that can cause activation of the adaptive immune system specific to the antigens expressed by dying cells[124]. Several different stimuli including, but not limited to, viral infection, some chemotherapies, radiotherapy and ECT can induce ICD[115,124,125]. ICD stimulates the immune system via timed release of DAMPs, which act like a danger signal to the immune system by activating various pattern recognition receptors, including Toll-like receptors (TLRs) and NOD-like receptors (NLRs)[124,125]. The elicited immune response is generally linked to the formation of immunogenic memory[124]. ICD causes the release of several DAMPs including calreticulin (CRT), heat shock proteins, high-mobility group box 1 (HMGB1), type I interferon (IFN) and adenosine triphosphate (ATP)[124,125]. The cell surface exposed CRT acts like an "eat me" signal for phagocytes, mostly DCs and macrophages, and is needed for antigen cross-presentation by these cells[124] (Figure 1.8). According to Dudek *et al.*, while induction of ICD has been shown in many *in vitro* and rodent data, ICD associated anti-tumour immunity is seldom observed in cancer patients. They conclude that the dosage at which ICD inducers are needed to induce ICD in patients is simply too toxic for clinical use[125]. Based on this conclusion and knowing that ECT is able to lower the dose of chemotherapeutics (compared to chemotherapy), there might be an opportunity to use ICD inducers in systemically non-toxic yet locally effective concentrations by delivering them straight into the tumour by EP or even in combination with ECT.

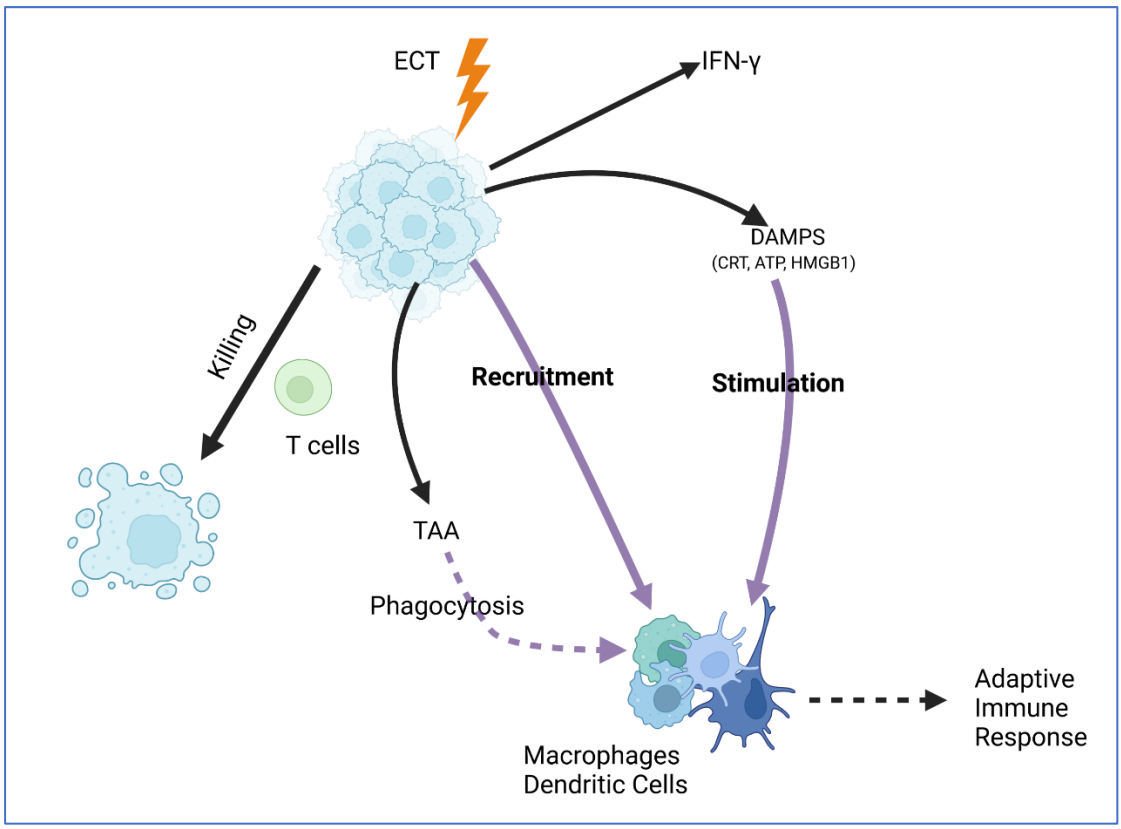


Figure 2.8: Possible mechanism through which ECT leads to local tumour reduction. T cells are necessary for the local tumour reduction observed after ECT. ECT also leads to the recruitment of antigen-presenting cells (Dendritic cells and macrophages) and causes the release of DAMPS and TAA from the treated tumour cells. CRT induces phagocytosis and cross-presentation when present on the cell surface and while this should lead to an adaptive immune response this is not consistently observed. (DAMPs: damage-associated molecular patterns; CRT: calreticulin; ATP: adenosine triphosphate; TAA: tumour-associated antigens). Figure created with Biorender.com.

Supporting this hypothesis, Calvet *et al.* showed that *in vitro* reversible EP (8 pulses 100 microsecond long at 1200V/cm) alone was able to induce CRT exposure and ATP release from CT26 murine colon cancer cells. In contrast, HMGB1 was only released when the cancer cells were treated with bleomycin ECT[115]. Additionally, Ursic *et al.* showed that not only can bleomycin ECT induce ICD, but that ECT with cisplatin and oxaliplatin elicits ICD to a similar degree to bleomycin ECT[126]. Interestingly, even though Oxaliplatin is a known inducer of ICD[125], there was no increase in ICD induction with oxaliplatin ECT compared to cisplatin ECT. These above findings could

indicate that induction of ICD after ECT is due to the electric properties of the treatment rather than the drugs used.

1.5.6 Interactions between ECT and the Immune System

Early in the development of ECT as a therapeutic approach, it was shown that in order for ECT to have local or systemic effects, the treatment needed to be administered to immunocompetent mice. While a range of models of ECT treatments, (ECT, CaEP alone or ECT combination treatments) significantly delayed tumour growth and have been observed to be potentially curative in various murine cancer models, including colon[115,127] and melanoma[98] when immunocompetent mice were treated, this treatment effect was either greatly diminished or absent in immunodeficient mice[97,98,100,115,127]. To reach the same level of anti-tumour effectiveness post ECT with cisplatin, a double dose of cisplatin needed to be administered to nude mice compared to immunocompetent mice in a fibrosarcoma model[97]. T cells have been shown to be a key mediator of the immune response for the local as well as the systemic effects of the ECT treatment[98,115,128], as no systemic effect was observed in T cell deficient mice.

Despite ECT inducing the release of DAMPs such as CRT, ATP and HMGB1, as well as indications that ECT leads to ICD, systemic immune responses have not been observed consistently in patients. Therefore, the immune response to ECT does not seem to be robust enough to trigger a systemic response and promote abscopal effects. The robustness of the immune response could therefore potentially be amplified by combining ECT with immune co-treatments, with several murine studies focusing on this approach. One such potential group of adjuvants comprises Toll-like receptor (TLR) agonists. A combination of ECT with the TLR9 agonist CpG ODN (administered at days 2 and 9 post ECT) was seen to potentiate the local treatment response and induce a systemic immune response in three murine tumour models (murine fibrosarcoma [LPB cell line] and murine melanoma [B16OVA and B16F10 cell lines]). In this study, the TLR9 agonist was selected as expression of TLR9 was observed to be strongly upregulated 48 hours post ECT treatment in fibrosarcoma bearing mice (no changes were observed in TLR3 and TLR4 and no further TLRs were

investigated). This 'electroimmunotherapy' combination led to a specific memory immunity insofar as the treatment induced a T-cell dependant systemic protection against tumour metastasis and cancer reoccurrence. Additionally, ECT in combination with CpG ODN showed a synergistic increase in the level of IFN-γ secretion, which may subsequently lead to further immune activation[98]. Similar to the findings concerning co-administration of CpG ODN, combining cisplatin ECT with administration of ICOS (inducible T-cell costimulator) three times post ECT in murine colon and lung cancer models led to all cured mice being immune to a rechallenge by the same tumour cells. The combination of ECT and ICOS led to a cure rate of 50% in CT26 colon cancer model compared to no cure after either monotherapy[128], highlighting the potential associated with administration of an adjuvant in combination with ECT treatment.

Similar to adjuvant administration of CpG oligonucleotides, adjuvant IL-12 GET prior to ECT treatment improved the outcome of ECT[100,129]. IL-12 GET involved injecting an IL-12 encoding gene plasmid into skeletal muscle prior to the application of the electric pulse, leading to robust IL-12 gene expression. The intramuscular IL-12 GET was either performed one day prior to ECT treatment[100,129] or performed both one day prior to and one and three days post ECT treatment[100]. IL-12 GET was shown to increase the specific tumour kill rate in SA-1 sarcoma and TS/A carcinoma *in vitro*[100] and potentiated the tumour cure rate in B16F10 melanoma *in vivo*[129] compared to ECT alone. IL-12 GET prior to ECT appeared to act as a primer for the immune system, augmenting immune responses to DAMPs and tumour-associated antigens (TAA) secretion post ECT treatment, with the possibility that such adjuvant therapy may turn immunological 'cold' tumours into immunological 'hot' tumours. This is also reflected in the observation that administration of IL-12 GET prior to ECT significantly augmented the effect of any ECT treatment only in the B16F10 tumour model (considered an immunogenic cold tumour) with no potentiation observed in either CT26 and 4T1 tumour models. The best result was observed for the combination of IL-12 GET with cisplatin ECT in the B16F10 model. Taken together, Ursic *et al.* concluded, that the immune status of the treated tumour should be the primary denominator of the adjuvant treatment[129]. Based on these reports and others, Sersa

et al. propose that ECT boosted with IL-12 GET can act like an in situ vaccination leading to successful tumour treatments[108].

It has also been observed that ECT can also directly influence the composition of the immune populations within a tumour. Bleomycin ECT treatment alters the make-up of both DC[130] and T cell[131] subpopulations in the treated lesions of melanoma patients. Before ECT treatment, epidermal Langerhans cells (a specialized subset of DC residing in the skin) comprise the majority of the DC population in these patients, but this population is not detectable at any level 14 days following treatment. In contrast, while plasmacytoid DCs (pDCs) and dermal $CD1c^+$ DCs (dDCs) were completely absent prior to treatment, they significantly increased in the 14 days following ECT treatment. These authors conclude that ECT induces activation of Langerhans cells and their migration to the draining lymph nodes as well as subsequent recruitment of pDCs and dDCs to the treatment site[130]. ECT also significantly reduced the percentage of $CD4^+FOXP3^+$ T regulatory (Treg) cells in the perilisonal dermis in the 14 days following ECT treatment in melanoma patients, whilst the percentage of $CD8^+$ T cells was significantly increased and the percentage of $CD4^+$ T cells was unchanged[131] (Table 1.2). Not only has ECT been observed to directly impact the immune cell composition in murine tumour models within the tumour itself, but alterations have also been identified in sites distant to the treatment site, for example the spleen. Increased infiltration of CD11b and CD11c positive, as well as CD80 and CD86 positive immune cells, into the tumour was observed in a murine fibrosarcoma tumour model between 48 and 96 hours post ECT-treatment[98]. In contrast, 3 days post ECT treatment, no change was observed in the infiltration of $CD8^+$ T cells and $CD11c^+$ DCs into a primary melanoma tumour, although ECT alone and ECT with ICOS was observed to increase the percentage of $CD19^+CD138^+$ B cells in the same tumour model[128]. Furthermore, ECT changed the immune cell composition, both within the spleen and the tumour, in a murine colorectal tumour at three days post treatment with the percentage of B cells, natural killer (NK) cells, NKT cells, DCs, macrophages and neutrophils significantly increased in both the tumour and spleen[132] (Table 1.2). Additionally, ECT with either cisplatin or oxaliplatin led to a 4-fold increase of infiltration of granzyme B-positive

immune cells in melanoma tumours. Granzyme B-positive immune cells were higher at the tumour edge and in the tissue surrounding the tumour in either treatment group compared to untreated animals[126]. Granzyme B is most commonly found in NK cells and in cytotoxic T cells[133]. Taken together, these findings indicate that ECT itself can change the composition of immune cells in the treated lesions. However, the exact changes might be dependent on the tumour type, treatment modalities and/or species treated.

3 days post ECT (mice)	14 days post ECT (human)
B cells ↑	**Langerhans cells ↓**
NK cells ↑	**pDCs ↑**
NKT cells ↑	**dDCs ↑**
Dendritic cells ↑	**$CD4^+FOXP3^+$ Tregs ↓**
Macrophages ↑	**$CD8^+$ T cells ↑**
Neutrophils ↑	**$CD4^+$ T cells ↔**

Table 2.2: Changes in Immune populations observed post-ECT in both murine models and patients.Observed changes in the immune cell population in tumours treated with ECT, either 3 days post ECT in mice or 14 days post ECT in humans. (NK: natural killer; DCs: dendritic cells; pDCs: plasmacytoid DCs; dDCs: dermal DCs; Tregs: regulatory T cells)

1.5.7 Developing immune co-treatments with ECT in cancer patients

Despite the promising findings of the above murine trials, to date, there are no completed prospective studies combing ECT with immunotherapy in patients. Several retrospective analyses and case reports have been published however, examining patient outcome subsequent to combinations of immune checkpoint inhibitor (CPI) therapy and ECT.

The two reports examining a combination of ECT with ipilimumab (CTLA-4 inhibitor) for advanced melanoma patients have been somewhat conflicting in their outcomes. It was initially shown that 15 patients who underwent ipilimumab treatment, followed by ECT, showed robust treatment responses (objective response rate (ORR) of 67% (ORR: tumours either reduced in size or were completely gone after

treatment) and 60% overall survival) with no notable toxicity reported[134]. In contrast, out of 28 patients who underwent an initial round of ECT followed by ipilimumab treatment, 7 patients reported severe systemic adverse effects (25%)[135]. In this cohort, the local ORR was also 67%, while the systemic ORR only reached 19%. The same study also retrospectively analysed the combination of ECT followed by PD-1 inhibitor treatment (pembrolizumab or nivolumab) in 5 patients. The local ORR was also 67%, but the systemic ORR increased to 40% in this combination of treatments. Additionally, no severe side effects were observed in the PD-1 treatment group[135]. Furthermore, a retrospective analysis by Campana *et al.* showed that pembrolizumab therapy with ECT performed after, but within 3 months of starting therapy can significantly increase the ORR, 1-year progression free survival and the 1-year overall survival compared to pembrolizumab treatment alone for cutaneous metastases therapy[136]. In addition, the anti PD-1 CPI and ECT combination can still be effective in heavily pre-treated patients, as a case study by Karaca *et al.* showed. A 39- year old patient with stage II metastatic melanoma was treated with anti PD-1 CPI and ECT as a 5th line treatment and the patient did not show any sign of disease reoccurrence 4 years after the treatment[137]. A further case report indicated that repeat ECT treatments are still effective for local tumour burden reduction when being used before anti PD-1 CPI and also after anti PD-1 CPI[138]. Quaresmini *et al.* concluded that their case report highlights the possibility of ECT to increase tumour immunogenicity, thus leading to an increase response to CPI. Finally, the combination of ECT and CPI was seen to lead to a complete clinical response in multiple cutaneous melanoma metastases[139].

In addition to combining ECT with CPI, combining IFN-α adjuvant therapy with ECT for melanoma patients (1- 80 lesions per patient) was also retrospectively analysed. Analysis of 5 patients, who received IFN-α therapy anytime between 6 months and almost 13 years prior to the ECT treatment, showed a good safety profile for this combination treatment and a ORR of 85% across all lesions[140]. This response rate is very similar to the response rate previously reported for ECT alone in primary tumours (74%[84]), but in this study the combination treatment reached that level with multiple metastases being present.

Combining these retrospective analyses and case reports, it seems likely that ECT treatment may be effectively combined with CPI treatment to improve patient outcome in certain tumour types and while attention has been primarily focused on melanoma patients, Trotovsek *et al.* argues that a combination ECT immunotherapy treatment could also be applied to liver tumours and other deep-seated tumours[107]. It is clear that combining ECT with immune co-treatments needs to be thoroughly investigated in prospective studies with the appropriate controls (ECT only treatment groups as well as immunotherapy only treatment groups) to elucidate the gain in efficacy, when combing ECT with immunotherapy. Additionally, similar to the ESOPE protocol, the best treatment parameters (timing of ECT and immunotherapy, type of immunotherapy, route of drug administration) should be determined to optimize any synergistic gains in combining the two treatment options with each other across a range of different cancer types.

1.6 Conclusion

Cancer is an ever-increasing burden on the health care systems worldwide, accounting for one in six deaths, and cancer incidence is increasing across the world. Lung cancer is the deadliest cancer, accounting for 20% of all cancer-related death. As 5-year survival rates for lung cancer patients remains very low despite the treatment advances made in the past few years, new treatment modalities are needed. Given how the lung cancer incidences are consistently rising in middle- and low- income countries, ideally new treatment options would also be as affordable as possible[10]. Also, only between 14-22% of NSCLC patients are undergoing resurrection of their tumours[141], which is considered the standard of care for lung cancer patients, thus new treatment modalities should be able to work well with lung cancers which are unsuitable for resurrection.

Electrochemotherapy (ECT) could potentially be a new treatment modality for lung cancer. ECT is effective after a single treatment even though repeated treatments are an option, if needed. The increased effectiveness when combining a cytotoxic drug with ECT means that a lower drug concentration is sufficient to induce tumour cell killing, thus leading to a decreased systemic toxicity of the chosen drug. Finally, case reports from other cancer patients have shown that ECT can be used on combination with other anti-cancer treatments, including surgical resection and immunotherapy, and can also be applied before and after various treatments without marked reduction in the effectiveness of the ECT treatment[137,138,140].

There are currently no clinical trials or even case reports published about the application of ECT for lung cancer treatment, but two pre-clinical models reported effectiveness of ECT in the lung cancer application. In 1998, Orlowski *et al.* showed that bleomycin ECT can reduce the tumours size and the number of lung metastases in a murine lung cancer model in which Lewis lung carcinoma cells (LLCs) were subcutaneously injected into immunocompetent mice[142]. Subsequently, in 2019, Tremble *et al.* showed that cisplatin ECT in the same murine lung cancer model was not only able to reduce the size of the primary tumour but also reduced the number of lung metastasis as well, leading to significantly longer survival of the treated mice

compared to the untreated mice. Furthermore this study showed that the ECT induce significant intratumoral recruitment of myeloid and humoral immune cells into the treated tumors[132]. This indicates that the ECT in the lung cancer context potentially would be able to also impact untreated metastatic tumours.

Further research would be needed to make ECT a viable therapeutic option for lung cancer treatment. The recent development of the EndoVE electroporator[86], allowing endoscopic delivery of electric pulses, has delivered the technical ability to treat lung tumours that are reachable endoscopically. Accessibility to lung tumours unreachable by an endoscopic device is a challenge that would need to be solved in the future to increase the number of lung cancer patients that could be treated with ECT. Cisplatin is only one of the standardly used platinum-based drugs for lung cancer therapy and thus it might be beneficial to test the other platinum-based drugs in combination for their impact on lung cancer, as at least carboplatin and oxaliplatin have also shown an increased effectiveness when combined with ECT *in vitro*. Whether these increases translate into *in vivo* application will need to be evaluated.

It has become clearer over the past few years that the TME of a given tumour has great implications, not only for the long-term overall survival of a lung cancer patient, but also that any anti-cancer treatment has an impact on the TME. In turn, the composition of the TME can have an impact on the effectiveness of the treatment itself. Thus, further research is needed into the TME of lung cancer patients as well as the impact ECT has on the TME of tumours in general, and of lung tumours in particular. Whilst there is an ever-accruing evidence base highlighting the importance of the immune response in ECT treatment, much work remains to be done in this developing field. There is a paucity of murine studies examining co-treatment of ECT with immunotherapy, and the data that has been published is somewhat confounded by the breath of different models, different cancer types and different forms of ECT used. As highlighted above, whilst combining ECT and immunotherapy in several murine studies has generated improved outcomes, these findings have not yet been translated into the clinic. In addition, currently little is

known concerning the direct effect of ECT on immune populations within the tumour.

Whilst several approaches to altering the TME prior to ECT treatment or augmenting ECT treatment by adjuvant immunotherapy have been examined, identifying the best strategy appears to be tumour-type dependent or even immune status of a specific tumour dependent. It is possible that more than one additional treatment regime might be needed to be combined to create a true systemic immune response that can withstand rechallenges (metastasis, disease reoccurrence) in humans. Finally, it is critical to consider the broader context when examining administration of immunotherapy with ECT. Immunotherapy and adjuvant treatment can potently modulate the systemic immune response, with patients experiencing severe autoimmune and/or autoinflammatory side effects. When combining strategies to boost the effectiveness and longevity of the ECT treatment special attention needs to be paid towards such adverse reactions.

1.7 Aim of my thesis

Work presented in this thesis had three specific aims:

1. Design a standard operating protocol to determine optimal EP voltages for ESOPE-based cell suspension *in vitro* work
2. To determine if ECT is a suitable treatment option for lung cancer treatment.
3. To determine the effect of EP and ECT on primary immune cells.

1.8 Bibliography

1. *WHO report on cancer: setting priorities, investing wisely and providing care for all.* (2020). doi:10.1007/978-3-662-11496-4_24.
2. Capasso, L. L. Antiquity of cancer. *Int. J. Cancer* **113**, 2–13 (2005).
3. Douglas Hanahan and Robert A. Weinberg. The Hallmarks of Cancer. *Cell* **100**, 57–70 (2000).
4. Hanahan, D. & Weinberg, R. A. Hallmarks of cancer: the next generation. *Cell* **144**, 646–74 (2011).
5. Cavallo, F., De Giovanni, C., Nanni, P., Forni, G. & Lollini, P.-L. 2011: the immune hallmarks of cancer. *Cancer Immunol. Immunother.* **60**, 319–26 (2011).
6. Disis, M. L. Immune regulation of cancer. *J. Clin. Oncol.* **28**, 4531–4538 (2010).
7. Allemani, C. *et al.* Global surveillance of cancer survival 1995-2009: Analysis of individual data for 25 676 887 patients from 279 population-based registries in 67 countries (CONCORD-2). *Lancet* **385**, 977–1010 (2015).
8. Bade, B. C. & Dela Cruz, C. S. Lung Cancer 2020: Epidemiology, Etiology, and Prevention. *Clin. Chest Med.* **41**, 1–24 (2020).
9. Nicholson, A. G. *et al.* The 2021 WHO Classification of Lung Tumors: Impact of Advances Since 2015. *J. Thorac. Oncol.* **17**, 362–387 (2022).
10. Thai, A. A., Solomon, B. J., Sequist, L. V., Gainor, J. F. & Heist, R. S. Lung cancer. *Lancet* **398**, 535–554 (2021).
11. Walters, S. *et al.* Lung cancer survival and stage at diagnosis in Australia, Canada, Denmark, Norway, Sweden and the UK: A population-based study, 2004-2007. *Thorax* **68**, 551–564 (2013).
12. Duma, N., Santana-Davila, R. & Molina, J. R. Non–Small Cell Lung Cancer: Epidemiology, Screening, Diagnosis, and Treatment. *Mayo Clin. Proc.* **94**, 1623–1640 (2019).
13. Detterbeck, F. C., Boffa, D. J., Kim, A. W. & Tanoue, L. T. The Eighth Edition Lung Cancer Stage Classification. *Chest* **151**, 193–203 (2017).
14. Zhou, B. *et al.* Worldwide burden and epidemiological trends of tracheal, bronchus, and lung cancer: A population-based study. *eBioMedicine* **78**,

103951 (2022).

15. Hassan Lemjabbar-Alaoui, Omer UI Hassan, Yi-Wei Yang, P. B. Lung cancer: Biology and treatment options. *Biochim. Biophys. Acta* **1856**, 189–210 (2015).
16. Gil-Torregrosa, B. C. *et al.* Control of cross-presentation during dendritic cell maturation. *Eur. J. Immunol.* **34**, 398–407 (2004).
17. Farago, A. F. & Keane, F. K. Current standards for clinical management of small cell lung cancer. *Transl. Lung Cancer Res.* **7**, 69–79 (2018).
18. Burdett, S. *et al.* Postoperative radiotherapy for non-small cell lung cancer. *Cochrane Database Syst. Rev.* **2016**, (2016).
19. Howington, J. A., Blum, M. G., Chang, A. C., Balekian, A. A. & Murthy, S. C. Treatment of stage I and II non-small cell lung cancer: Diagnosis and management of lung cancer, 3rd ed: American college of chest physicians evidence-based clinical practice guidelines. *Chest* **143**, e278S-e313S (2013).
20. Sørensen, J. B., Klee, M., Palshof, T. & Hansen, H. H. Performance status assessment in cancer patients. an inter-observer variability study. *Br. J. Cancer* **67**, 773–775 (1993).
21. E. Shtivelman, T. Hensing, G.R. Simon, P.A. Dennis, G.A. Otterson, R. Bueno, R. S. Molecular pathways and therapeutic targets in lung cancer. *Oncotarget* **5**, (2014).
22. Onoi, K. *et al.* Immune checkpoint inhibitors for lung cancer treatment: A review. *J. Clin. Med.* **9**, (2020).
23. Carbone, D. P. *et al.* First-Line Nivolumab in Stage IV or Recurrent Non–Small-Cell Lung Cancer. *N. Engl. J. Med.* **376**, 2415–2426 (2017).
24. Enfield, K. S. S. *et al.* Hyperspectral cell sociology reveals spatial tumor-immune cell interactions associated with lung cancer recurrence. *J. Immunother. Cancer* **7**, 13 (2019).
25. Zhao, S. *et al.* Low-dose apatinib optimizes tumor microenvironment and potentiates antitumor effect of PD-1/PD-L1 blockade in lung cancer. *Cancer Immunol. Res.* **7**, 630–643 (2019).
26. Anderson, N. M. & Simon, M. C. Tumor Microenvironment. *Curr. Biol.* **30**, (2020).
27. Joyce, Johanna A.; Fearon, D. T. T cell exclusion, immune privilege, and the

tumor microenvironment. *Science (80-.).* **348**, (2015).

28. Alfarouk, K. O., Muddathir, A. K. & Shayoub, M. E. A. Tumor acidity as evolutionary spite. *Cancers (Basel).* **3**, 408–414 (2011).
29. Baghban, R. *et al.* Tumor microenvironment complexity and therapeutic implications at a glance. *Cell Commun. Signal.* **18**, 1–19 (2020).
30. Gavin P. Dunn, Allen T. Bruce, Hiroaki Ikeda, Lloyd J. Old2, R. D. S. Cancer Immunoediting: From Surveillance to Escape. *Cancer Immunother. Immune Suppr. Tumor Growth Second Ed.* **3**, (2002).
31. Spill, Fabian; Reynolds, Daniel S; Kamm, Roger D.; Zaman, M. H. Impact of the Physical Microenvironment on Tumor Progression and Metastasis. *Curr Opin Biotechnol.* **40**, (2016).
32. Paszek, M. J. *et al.* Tensional homeostasis and the malignant phenotype. *Cancer Cell* **8**, 241–254 (2005).
33. Sahlgren, C., Gustafsson, M. V., Jin, S., Poellinger, L. & Lendahl, U. Notch signaling mediates hypoxia-induced tumor cell migration and invasion. *Proc. Natl. Acad. Sci. U. S. A.* **105**, 6392–6397 (2008).
34. Palsson-Mcdermott, E. M. & O'Neill, L. A. J. The Warburg effect then and now: From cancer to inflammatory diseases. *BioEssays* **35**, 965–973 (2013).
35. Parker, K. H., Beury, D. W. & Ostrand-rosenberg, S. Suppression in the Tumor Microenvironment. *Adv Cancer Res* **128**, 95–139 (2015).
36. Zhang, J. & Veeramachaneni, N. Targeting interleukin-1β and inflammation in lung cancer. *Biomark. Res.* **10**, 1–10 (2022).
37. Biswas, S. K., Allavena, P. & Mantovani, A. Tumor-associated macrophages: Functional diversity, clinical significance, and open questions. *Semin. Immunopathol.* **35**, 585–600 (2013).
38. Schoenhals, J. E. *et al.* Uncovering the immune tumor microenvironment in non-small cell lung cancer to understand response rates to checkpoint blockade and radiation. *Transl. Lung Cancer Res.* **6**, 148–158 (2017).
39. Duan, Q., Zhang, H., Zheng, J. & Zhang, L. Turning Cold into Hot: Firing up the Tumor Microenvironment. *Trends in Cancer* **6**, 605–618 (2020).
40. Duan, Q., Zhang, H., Zheng, J. & Zhang, L. Turning Cold into Hot: Firing up the Tumor Microenvironment. *Trends in Cancer* **6**, 605–618 (2020).

41. Sautès-Fridman, C. *et al.* Tumor microenvironment is multifaceted. *Cancer Metastasis Rev.* **30**, 13–25 (2011).
42. Pagès, F. *et al.* Effector Memory T Cells, Early Metastasis, and Survival in Colorectal Cancer. *N. Engl. J. Med.* **353**, 2654–2666 (2005).
43. Pagès, J. G. C. S.-C. K. M. L.-P. T. C. B. W. Z. B.-H. C. T.-H. F. F. Type, Density, and Location of Immune Cells Within Human Colorectal Tumors Predict Clinical Outcome. *Some Early Tools Am. Sci.* **313**, (2006).
44. Luckheeram, R. V., Zhou, R., Verma, A. D. & Xia, B. CD4 +T cells: Differentiation and functions. *Clin. Dev. Immunol.* **2012**, (2012).
45. Raskov, H., Orhan, A., Christensen, J. P. & Gögenur, I. Cytotoxic CD8+ T cells in cancer and cancer immunotherapy. *Br. J. Cancer* **124**, 359–367 (2021).
46. Chaudhary, B. & Elkord, E. Regulatory T cells in the tumor microenvironment and cancer progression: Role and therapeutic targeting. *Vaccines* **4**, 1–25 (2016).
47. Hiam-Galvez, K. J., Allen, B. M. & Spitzer, M. H. Systemic immunity in cancer. *Nat. Rev. Cancer* **21**, 345–359 (2021).
48. Reuben, A. *et al.* Comprehensive T cell repertoire characterization of non-small cell lung cancer. *Nat. Commun.* **11**, (2020).
49. Cabeza-Cabrerizo, M., Cardoso, A., Minutti, C. M., Pereira Da Costa, M. & Reis E Sousa, C. Dendritic Cells Revisited. *Annu. Rev. Immunol.* **39**, 131–166 (2021).
50. Gallois, A. & Bhardwaj, N. Dendritic cell-targeted approaches to modulate immune dysfunction in the tumor microenvironment. *Front. Immunol.* **4**, 1–8 (2013).
51. Bell, B. D. *et al.* In Breast Carcinoma Tissue, Immature Dendritic Cells Reside within the Tumor, whereas Mature Dendritic Cells Are Located in Peritumoral Areas. *J. Exp. Med.* **190**, (1999).
52. Veglia, F. & Gabrilovich, D. I. Dendritic cells in cancer: the role revisited. *Curr. Opin. Immunol.* **45**, 43–51 (2017).
53. Münz, C. Antigen processing via autophagy – not only for MHC class II. *Curr. Opin. Immunol.* **22 (1)**, 89–93 (2010).
54. Dingjan, I. *et al.* Lipid peroxidation causes endosomal antigen release for

cross-presentation. *Sci. Rep.* **6**, 22064 (2016).

55. Wculek, S. K. *et al.* Dendritic cells in cancer immunology and immunotherapy. *Nat. Rev. Immunol.* **20**, 7–24 (2020).
56. Gardner, A. & Ruffell, B. Dendritic Cells and Cancer Immunity. *Trends Immunol.* **37**, 855–865 (2016).
57. Ruffell, B., Affara, N. I. & Coussens, L. M. Differential macrophage programming in the tumor microenvironment. *Trends Immunol.* **33**, 119–126 (2012).
58. Solinas, G., Germano, G., Mantovani, A. & Allavena, P. Tumor-associated macrophages (TAM) as major players of the cancer-related inflammation. *J. Leukoc. Biol.* **86**, 1065–1073 (2009).
59. Ruffell, B. & Coussens, L. M. Perspective Macrophages and Therapeutic Resistance in Cancer. *Cancer Cell* **27**, 462–472 (2015).
60. Davies, L. C., Jenkins, S. J., Allen, J. E. & Taylor, P. R. Tissue-resident macrophages. *Nat. Immunol.* **14**, 986–995 (2013).
61. Noy, R. & Pollard, J. W. Review Tumor-Associated Macrophages : From Mechanisms to Therapy. *Immunity* **41**, 49–61 (2014).
62. Mantovani, A., Sica, A., Allavena, P., Garlanda, C. & Locati, M. Tumor-associated macrophages and the related myeloid-derived suppressor cells as a paradigm of the diversity of macrophage activation. *Hum. Immunol.* **70**, 325–330 (2009).
63. Shapouri-Moghaddam, A. *et al.* Macrophage plasticity, polarization, and function in health and disease. *J. Cell. Physiol.* **233**, 6425–6440 (2018).
64. König, S. *et al.* Depletion of cutaneous macrophages and dendritic cells promotes growth of basal cell carcinoma in mice. *PLoS One* **9**, (2014).
65. Mantovani, A., Allavena, P., Marchesi, F. & Garlanda, C. Macrophages as tools and targets in cancer therapy. *Nat. Rev. Drug Discov.* **0123456789**, (2022).
66. Alberto Mantovani, Federica Marchesi, Alberto Malesci, L. L. and P. A. Tumour-associated macrophages as treatment targets in oncology. *Nat. Rev.* (2017) doi:10.1038/nrclinonc.2016.217.
67. Dhabekar, G., Dandekar, R. & Kingaonkar, A. Role of macrophages in malignancy. *Ann. Maxillofac. Surg.* **1**, 150 (2011).

68. Ma, J. *et al.* The M1 form of tumor-associated macrophages in non-small cell lung cancer is positively associated with survival time. *BMC Cancer* **10**, 1–9 (2010).

69. Ohri, C. M., Shikotra, A., Green, R. H., Waller, D. A. & Bradding, P. Macrophages within NSCLC tumour islets are predominantly of a cytotoxic M1 phenotype associated with extended survival. *Eur. Respir. J.* **33**, 118–126 (2009).

70. Jackute, J. *et al.* Distribution of M1 and M2 macrophages in tumor islets and stroma in relation to prognosis of non-small cell lung cancer. *BMC Immunol.* **19**, 1–13 (2018).

71. Maccarrone, M., Bladergroen, M. R., Rosato, N. & Agrò, A. F. Role of lipid peroxidation in electroporation-induced cell permeability. *Biochemical and Biophysical Research Communications* vol. 209 417–425 (1995).

72. Yarmush, M. L., Golberg, A., Serša, G., Kotnik, T. & Miklavčič, D. Electroporation-Based Technologies for Medicine: Principles, Applications, and Challenges. *Annu. Rev. Biomed. Eng.* **16**, 295–320 (2014).

73. Kotnik, T. *et al.* Electroporation-based applications in biotechnology. *Trends Biotechnol.* **33**, 480–488 (2015).

74. Weaver, J. C. & Chizmadzhev, Y. A. Theory of electroporation: A review. *Bioelectrochemistry Bioenerg.* **41**, 135–160 (1996).

75. Weaver, J. C., Smith, K. C., Esser, A. T., Son, R. S. & Gowrishankar, T. R. A brief overview of electroporation pulse strength-duration space: A region where additional intracellular effects are expected. *Bioelectrochemistry* **87**, 236–243 (2012).

76. Bendix, M. B., Brint, E. & Forde, P. F. Electroporation of suspension cell lines – A proposed assay set for optimizations. *Bioelectrochemistry* **142**, 107891 (2021).

77. Lee, E. W., Gehl, J. & Kee, S. T. Clinical Aspects of Electroporation. *Clin. Asp. Electroporation* 3–7 (2011) doi:10.1007/978-1-4419-8363-3.

78. Neumann, E., Schaefer-Ridder, M., Wang, Y. & Hofschneider, P. H. Gene transfer into mouse lyoma cells by electroporation in high electric fields. *EMBO J.* **1**, 841–845 (1982).

79. Dower, W. J., Miller, J. F. & Ragsdale, C. W. High efficiency transformation of E.coli by high voltage electroporation. *Nucleic Acids Res.* **16**, 6127–6145 (1988).

80. Weaver, J. C. Electroporation: A general phenomenon for manipulating cells and tissues. *J. Cell. Biochem.* **51**, 426–435 (1993).

81. Prasanna, G. L. & Panda, T. Electroporation: Basic principles, practical considerations and applications in molecular biology. *Bioprocess Eng.* **16**, 261–264 (1997).

82. Lavee, J., Onik, G., Mikus, P. & Rubinsky, B. A novel nonthermal energy source for surgical epicardial atrial ablation: Irreversible electroporation. *Heart Surg. Forum* **10**, 96–101 (2007).

83. Mohamed, M. & Eissa, A. Pulsed Electric Fields for Food Processing Technology. *Struct. Funct. Food Eng.* 32 (2012).

84. Marty, M. *et al.* Electrochemotherapy - An easy, highly effective and safe treatment of cutaneous and subcutaneous metastases: Results of ESOPE (European Standard Operating Procedures of Electrochemotherapy) study. *Eur. J. Cancer, Suppl.* **4**, 3–13 (2006).

85. Deore, A. B., Sapakal, V. D. & Shikalgar, T. S. Electrochemotherapy : An enhancement of cytotoxicity of anticancer drugs. *In- nov Pharm Pharmacother* 147–153 (2019).

86. Miklavčič, D. *et al.* Electrochemotherapy: Technological advancements for efficient electroporation-based treatment of internal tumors. *Med. Biol. Eng. Comput.* **50**, 1213–1225 (2012).

87. Dev, S. B. *et al.* Effective electroporation therapy of human pancreatic tumors implanted in nude mice. *Drug Deliv. J. Deliv. Target. Ther. Agents* **4**, 293–299 (1997).

88. Čemažar, M., Miklavčič, D. & Serša, G. Intrinsic sensitivity of tumor cells to bleomycin as an indicator of tumor response to electrochemotherapy. *Japanese J. Cancer Res.* **89**, 328–333 (1998).

89. Miklavčič, D., Mali, B., Kos, B., Heller, R. & Serša, G. Electrochemotherapy: From the drawing board into medical practice. *Biomed. Eng. Online* **13**, 1–20 (2014).

90. Cemazar, M., Pipan, Z., Grabner, S., Bukovec, N. & Sersa, G. Cytotoxicity of Different Platinum (II) Analogues to Human Tumour Cell Lines In Vitro and Murine Tumour In Vivo Alone or Combined with Electroporation. (2006).
91. Frandsen, S. K. *et al.* Direct therapeutic applications of calcium electroporation to effectively induce tumor necrosis. *Cancer Res.* **72**, 1336–1341 (2012).
92. Frandsen, S. K., Gissel, H., Hojman, P., Eriksen, J. & Gehl, J. Calcium electroporation in three cell lines: A comparison of bleomycin and calcium, calcium compounds, and pulsing conditions. *Biochim. Biophys. Acta - Gen. Subj.* **1840**, 1204–1208 (2014).
93. Gehl, J. *et al.* Updated standard operating procedures for electrochemotherapy of cutaneous tumours and skin metastases. *Acta Oncol. (Madr).* **57**, 874–882 (2018).
94. Sersa, G. *et al.* Vascular disrupting action of electroporation and electrochemotherapy with bleomycin in murine sarcoma. *Br. J. Cancer* **98**, 388–398 (2008).
95. Jarm, T., Cemazar, M., Miklavcic, D. & Sersa, G. Antivascular effects of electrochemotherapy: Implications in treatment of bleeding metastases. *Expert Rev. Anticancer Ther.* **10**, 729–746 (2010).
96. Markelc, B., Sersa, G. & Cemazar, M. Differential Mechanisms Associated with Vascular Disrupting Action of Electrochemotherapy: Intravital Microscopy on the Level of Single Normal and Tumor Blood Vessels. *PLoS One* **8**, 1–11 (2013).
97. Serša, G. *et al.* Electrochemotherapy with CDDP on LPB sarcoma: Comparison of the anti- tumor effectiveness in immunocompetent and immunodeficient mice. *Bioelectrochemistry Bioenerg.* **43**, 279–283 (1997).
98. Roux, S. *et al.* Tumor destruction using electrochemotherapy followed by CpG oligodeoxynucleotide injection induces distant tumor responses. *Cancer Immunol. Immunother.* **57**, 1291–1300 (2008).
99. Falk, H. *et al.* Electrochemotherapy and calcium electroporation inducing a systemic immune response with local and distant remission of tumors in a patient with malignant melanoma–a case report. *Acta Oncol. (Madr).* **56**,

1126–1131 (2017).

100. Sedlar, A. *et al.* Potentiation of electrochemotherapy by intramuscular IL-12 gene electrotransfer in murine sarcoma and carcinoma with different immunogenicity. *Radiol. Oncol.* **46**, 302–311 (2012).
101. Snoj, M., Cemazar, M., Kolar, B. S. & Sersa, G. Effective Treatment of Multiple Unresectable Skin Melanoma Metastases by Electrochemotherapy. *Croat. Med. J.* 391–395 (2007).
102. Staresinic, B. *et al.* Effect of calcium electroporation on tumour vasculature. *Sci. Rep.* **8**, 1–14 (2018).
103. Frandsen, S. K., Vissing, M. & Gehl, J. A comprehensive review of calcium electroporation —A novel cancer treatment modality. *Cancers (Basel).* **12**, 1–21 (2020).
104. Szewczyk, A., Saczko, J. & Kulbacka, J. Apoptosis as the main type of cell death induced by calcium electroporation in rhabdomyosarcoma cells. *Bioelectrochemistry* **136**, 107592 (2020).
105. Tremble, L. F., Heffron, C. C. B. B. & Forde, P. F. The effect of calcium electroporation on viability, phenotype and function of melanoma conditioned macrophages. *Sci. Rep.* **10**, 1–12 (2020).
106. Hoejholt, K. L. *et al.* Calcium electroporation and electrochemotherapy for cancer treatment: Importance of cell membrane composition investigated by lipidomics, calorimetry and in vitro efficacy. *Sci. Rep.* **9**, 1–12 (2019).
107. Trotovšek, B., Djokić, M., Čemažar, M. & Serša, G. New era of electrochemotherapy in treatment of liver tumors in conjunction with immunotherapies. *World J. Gastroenterol.* **27**, 8216–8226 (2021).
108. Sersa, G. *et al.* Electrochemotherapy of tumors as in situ vaccination boosted by immunogene electrotransfer. *Cancer Immunol. Immunother.* **64**, 1315–1327 (2015).
109. Bart Geboers, MD • Hester J. Scheffer, MD, PhD • Philip M. Graybill, BSc • Alette H. Ruarus, MD • Sanne Nieuwenhuizen, MD • Robbert S. Puijk, MD • Petrousjka M. van den Tol, MD, PhD • Rafael V. Davalos, MSc, PhD • Boris Rubinsky, MSc, PhD • Tanja D. de Gr, P. High-Voltage Electrical Pulses in Oncology : Irreversible Electroporation, Electrochemotherapy, Gene

Electrotransfer, Electrofusion, and Electroimmunotherapy. *Radiology* (2020) doi:10.1148/radiol.2020192190.

110. Lee, E. W. *et al.* Advanced hepatic ablation technique for creating complete cell death: Irreversible electroporation. *Radiology* **255**, 426–433 (2010).
111. Rubinsky, B. Irreversible electroporation in medicine. *Technol. Cancer Res. Treat.* **6**, 255–259 (2007).
112. Bertacchini, C. *et al.* Design of an irreversible electroporation system for clinical use. *Technol. Cancer Res. Treat.* **6**, 313–320 (2007).
113. Belehradek, M. *et al.* Electrochemotherapy, a new antitumor treatment. First clinical phase I-II trial. *Cancer* **72**, 3694–3700 (1993).
114. Gehl, J. *et al.* Electrochemotherapy in the treatment of metastatic malignant melanoma : a prospective cohort study by InspECT. *Br. J. Dermatol.* **176**, 1475–1485 (2017).
115. Calvet, C. Y., Famin, D., André, F. M. & Mir, L. M. Electrochemotherapy with bleomycin induces hallmarks of immunogenic cell death in murine colon cancer cells. *Oncoimmunology* **3**, 2–11 (2014).
116. Calvet, C. Y. & Mir, L. M. The promising alliance of anti-cancer electrochemotherapy with immunotherapy. *Cancer Metastasis Rev.* **35**, 165–177 (2016).
117. Tellado, M. N., Maglietti, F. H., Michinski, S. D., Marshall, G. R. & Signori, E. Electrochemotherapy in treatment of canine oral malignant melanoma and factors influencing treatment outcome. *Radiol. Oncol.* **54**, 68–78 (2020).
118. Brock, R. M., Beitel-White, N., Davalos, R. V. & Allen, I. C. Starting a Fire Without Flame: The Induction of Cell Death and Inflammation in Electroporation-Based Tumor Ablation Strategies. *Front. Oncol.* **10**, 1–9 (2020).
119. Batista Napotnik, T., Polajžer, T. & Miklavčič, D. Cell death due to electroporation – A review. *Bioelectrochemistry* **141**, (2021).
120. Piñero, J., López-Baena, M., Ortiz, T. & Cortés, F. Apoptotic and necrotic cell death are both induced by electroporation in HL60 human promyeloid leukaemia cells. *Apoptosis* **2**, 330–336 (1997).
121. Fernandes, P., O'Donovan, T. R., McKenna, S. L. & Forde, P. F.

Electrochemotherapy causes caspase-independent necrotic-like death in pancreatic cancer cells. *Cancers (Basel).* **11**, (2019).

122. Tounekti, O., Kenani, A., Foray, N., Orlowski, S. & Mir, L. M. The ratio of single-to double-strand DNA breaks and their absolute values determine cell death pathway. *Br. J. Cancer* **84**, 1272–1279 (2001).
123. Mekid, H. *et al.* In vivo evolution of tumour cells after the generation of double-strand DNA breaks. *Br. J. Cancer* **88**, 1763–1771 (2003).
124. Galluzzi, L. *et al.* Molecular mechanisms of cell death: Recommendations of the Nomenclature Committee on Cell Death 2018. *Cell Death Differ.* **25**, 486–541 (2018).
125. Dudek, A. M., Garg, A. D., Krysko, D. V., De Ruysscher, D. & Agostinis, P. Inducers of immunogenic cancer cell death. *Cytokine Growth Factor Rev.* **24**, 319–333 (2013).
126. Ursic, K. *et al.* Comparable effectiveness and immunomodulatory actions of oxaliplatin and cisplatin in electrochemotherapy of murine melanoma. *Bioelectrochemistry* **119**, 161–171 (2018).
127. Falk, H. *et al.* Calcium electroporation induces tumor eradication, long-lasting immunity and cytokine responses in the CT26 colon cancer mouse model. *Oncoimmunology* **6**, 1–8 (2017).
128. Tremble, L. F., O'Brien, M. A., Forde, P. F. & Soden, D. M. ICOS activation in combination with electrochemotherapy generates effective anti-cancer immunological responses in murine models of primary, secondary and metastatic disease. *Cancer Lett.* **420**, 109–115 (2018).
129. Ursic, K. *et al.* Potentiation of electrochemotherapy effectiveness by immunostimulation with IL-12 gene electrotransfer in mice is dependent on tumor immune status. *J. Control. Release* **332**, 623–635 (2021).
130. Gerlini, G. *et al.* Dendritic cells recruitment in melanoma metastasis treated by electrochemotherapy. *Clin. Exp. Metastasis* **30**, 37–45 (2013).
131. Di Gennaro, P. *et al.* CD4+FOXP3+ T regulatory cells decrease and CD3+CD8+ T cells recruitment in TILs from melanoma metastases after electrochemotherapy. *Clin. Exp. Metastasis* **33**, 787–798 (2016).
132. Tremble, L. F., O'Brien, M. A., Soden, D. M. & Forde, P. F.

Electrochemotherapy with cisplatin increases survival and induces immunogenic responses in murine models of lung cancer and colorectal cancer. *Cancer Lett.* **442**, 475–482 (2019).

133. Afonina, I. S., Cullen, S. P. & Martin, S. J. Cytotoxic and non-cytotoxic roles of the CTL/NK protease granzyme B. *Immunol. Rev.* **235**, 105–116 (2010).
134. Mozzillo, N. *et al.* Assessing a novel immuno-oncology-based combination therapy: Ipilimumab plus electrochemotherapy. *Oncoimmunology* **4**, (2015).
135. Heppt, M. V. *et al.* Immune checkpoint blockade with concurrent electrochemotherapy in advanced melanoma: a retrospective multicenter analysis. *Cancer Immunol. Immunother.* **65**, 951–959 (2016).
136. Campana, L. G. *et al.* Combination of pembrolizumab with electrochemotherapy in cutaneous metastases from melanoma: A comparative retrospective study from the inspect and slovenian cancer registry. *Cancers (Basel).* **13**, (2021).
137. Karaca, B., Yayla, G., Erdem, M. & Gürler, T. Electrochemotherapy with anti-PD-1 treatment induced durable complete response in heavily pretreated Metastatic melanoma patient. *Anticancer. Drugs* **29**, 190–196 (2018).
138. Quaresmini, D. *et al.* Electrochemotherapy as a Trigger to Overcome Primary Resistance to Anti-PD-1 Treatment: A Case Report of Melanoma of the Scalp. *Front. Oncol.* **11**, 1–7 (2021).
139. Brizio, M., Fava, P., Astrua, C., Cavaliere, G. & Savoia, P. Complete regression of melanoma skin metastases after electrochemotherapy plus ipilimumab treatment: An unusual clinical presentation. *Eur. J. Dermatology* **25**, 271–272 (2015).
140. Hribernik, A., Cemazar, M., Sersa, G., Bosnjak, M. & Snoj, M. Effectiveness of electrochemotherapy after IFN-α adjuvant therapy of melanoma patients. *Radiol. Oncol.* **50**, 21–27 (2016).
141. Jahangeer, S., Forde, P., Soden, D. & Hinchion, J. Review of current thermal ablation treatment for lung cancer and the potential of electrochemotherapy as a means for treatment of lung tumours. *Cancer Treat. Rev.* **39**, 862–871 (2013).
142. Orlowski, S., An, D., Belehradek, J. & Mir, L. M. Antimetastatic effects of

electrochemotherapy and of histoincompatible interleukin-2-secreting cells in the murine Lewis lung tumor. *Anti-Cancer Drugs* vol. 9 551–556 (1998).

Chapter 2

Materials and Methods

2.1 Cell Lines and Maintenance

Lewis Lung Carcinoma (LLC; murine lung cancer), A549 (human lung cancer), H460 (human lung cancer), SK-MES-1 (human lung cancer) and A375 (human melanoma) cell lines were obtained from the American Type Culture Collection (ATCC; Maryland, USA). The B16F10 (murine melanoma) cell line was obtained from the European Collection of Authenticated Cell Cultures (Salisbury, UK). The Mia-PACA2 (human pancreatic cancer) cell line was obtained from the European Cell and Culture Collection. Pan-02 (murine pancreatic cancer) cell line was obtained from the National Cancer Institute at Frederick (Frederick, USA).

A549, H460, Pan-02 and B16F10 cell lines were maintained in Roswell Park Memorial Institute -1640 media (RMPI; Sigma-Aldrich, St. Louis, USA), supplemented with 10% foetal bovine serum (FBS; Sigma-Aldrich), 50 IU/mL penicillin (Sigma-Aldrich) and 50 µg/mL streptomycin (Sigma-Aldrich) (RPMI10). Mia-PACA2 and LLC cell lines were cultured in Dulbecco's Modified Eagle Medium (DMEM; Sigma-Aldrich), supplemented with 10% FBS, 50 IU/mL penicillin (Sigma-Aldrich) and 50 µg/mL streptomycin (Sigma-Aldrich) (DMEM10). A375 and SK-MES-1 cell lines were maintained in DMEM (Sigma-Aldrich) supplemented with 20% FBS (Sigma-Aldrich), 50 I.U/mL penicillin (Sigma-Aldrich) and 50 µg/mL streptomycin (Sigma-Aldrich) (DMEM20). Cell lines were incubated at 37°C in an incubator with 5% CO_2 and constant humidity. Cells were passaged upon reaching 70-90% confluency.

To passage cells, the medium was decanted, cells were rinsed with PBS (Sigma-Aldrich) and the trypsin-ethylenediaminetetraacetic acid (EDTA) solution (Sigma-Aldrich) was added to the flasks. The trypsin-EDTA solution was then quenched with at least double the volume of the medium the cells were cultured in. In the case of A549, H460, SK-MES-1, Pan02, B16F10, Mia-PACA2 and A375 cell lines, cells were incubated with the EDTA solution at 37 °C in an incubator with 5% CO_2 for 5 minutes prior to the quenching. LLC cells were incubated with the EDTA solution at room temperature for 2.5 minutes. Cells were centrifuged at 1000 revolutions-per minute (rpm; Eppendorf 5810 centrifuge) for 4 minutes at room temperature (RT). Cells were grown in tissue culture treated flasks (T25, T75 or T175 depending on needed cell

numbers) (Sarstedt, Nümbrecht, Germany) or tissue culture treated 6/12/24 or 96 well plates (Sarstedt).

2.1.1 Lung cancer cell lines

The Lewis-Lung carcinoma (LLC) cell line is a representative cell line of Non-small cell lung cancer (NSCLC) in mice. It is a mixed cell line containing a mixed population of adherent and suspension cells. The LLC cell line was established from the lung of a C57/BL mouse bearing a tumour resulting from an implantation of a primary Lewis Lung carcinoma. The cell line is highly tumorigenic when grown *in vivo*, but only weakly metastatic.

The A549 cell line is an adherent human cell line representative of NSCLC adenocarcinoma. The cell line was derived in 1972 through explant culture of lung carcinomatous tissue from a 58-year-old Caucasian male. The A549 cell line was cultured in RPMI10 after the cell line was progressively accustomed to transfer from the original growth medium of ATCC-formulated F-12K Medium (ATCC).

The SK-MES-1 cell line is an adherent human cell line representative of NSCLC squamous carcinoma. The cell line was derived from a 65-year-old Caucasian male. This cell line was cultured in DMEM with 20% FBS (DMEM20) instead of the recommended Eagle's Minimum Essential Medium with 10% FBS, as the SK-MES-1 cell line did grow very slowly with 10% FBS supplemented DMEM. Once the cell line was cultured with the DMEM20, cells grew as expected.

The H460 cell line is an adherent human cell line representative of a lung large cell carcinoma. The cell line was derived in 1982 from the pleural fluid of a male patient with large cell cancer of the lung.

2.2 Ethical Statement

Animal husbandry and handling was performed under the 2010/63/EU Directive and animals were culled under a euthanasia-only licence to derive T cells, dendritic cells

and macrophages, granted by the University College Cork's Animal Experimentation Ethics Committee (AEEC), under application ID 20/004.

All animal procedures were approved and licensed by the AEEC in University College Cork and the Irish Health Products Regulatory Authority (HPRA) under license AE19130/P148.

2.3 Mice

Eight-week-old plus female C57BL6J mice were obtained from Envigo UK (Bicester, UK) and housed in the animal facility of University College Cork (Biological Service Unit; Western Gateway Building) with standard housing and environmental conditions (21°C and 50% humidity with 12hrs light-dark cycles). Animals had free access to a standard pellet diet and water. For experiments, but not for euthanasia only use, the mice were allowed to acclimate for at least 7 days prior to the start of the experiments.

2.4 Murine T cell isolation

Spleen cells were obtained by passing the spleen of healthy 8–20-week-old female C57BL6J mice through a 0.45µM cell strainer (BD Falcon, Franklin Lakes, USA) with cold PBS (Sigma-Aldrich). Cells were centrifuged at RT for 5 minutes at 1500rpm (Eppendorf 5810 centrifuge). Individual cell pellets were resuspended in 5mL red cell lysis buffer (Biolegend) for 4 minutes on ice to lyse red blood cells. 10mL of RPMI10 was added to stop the lysis process and cells were centrifugated at RT for 5 minutes at 1500rpm. Cell pellets were resuspended in 1mL RMPI10 and cell suspension was transferred into a sterile, round 5mL FACS tube (Falcon™; FisherScientific, Waltham, USA). Cells were centrifuged at RT for 5 minutes at 1500rpm prior to T cells being isolated using the EasySep™ Mouse T Cell Isolation Kit (Stemcell Technologies, Vancouver, Canada). Spleen cells were resuspended at $1x10^8$ cells/mL in labelling buffer (PBS (Sigma-Aldrich) supplemented with 2% heat-inactivated FBS (Sigma-Aldrich) and 1mM EDTA (Sigma-Aldrich)). Normal rat serum (Stemcell) was added at 50µL/mL and also EasySep Mouse T cell isolation cocktail (Stemcell) was added at 50µL/ml to the cell suspension. Suspension was well mixed and incubated for 10

minutes at RT. EasySep Streptavidin RapidSpheres 5001 (Stemcell) were vortexed for 30 seconds to create a uniform suspension and 75µL/mL of the RapidSpheres solution was added to the cell mixture. The cell suspension was well mixed again and incubated for 5 minutes at RT. Following this, the cell suspension was brought up to a total volume of 2.5mL by adding T cell medium (RPMI (Sigma-Aldrich) supplemented with 10mM HEPES (4-(2-hydroxyethyl)-1-piperazineethanesulfonic acid; Sigma-Aldrich), $5.5x10^{-5}$ M 2-Mercaptoethanol (2ME) (Sigma-Aldrich), 5% heat-inactivated FBS (heated for 30 minutes at 60°C; Sigma-Aldrich), 50 I.U/mL penicillin (Sigma-Aldrich) and 50 µg/mL streptomycin (Sigma-Aldrich). The suspension was mixed gently and placed in the EasySep™ magnet at RT for 2.5 minutes. After the incubation, the cell suspension, only containing $CD3^+$ T cells, was decanted into a new tube and experiments were carried out. Figure 2.1 shows the purity of the isolated T cells as well as the percentage of $CD4^+$ and $CD8^+$ T cells.

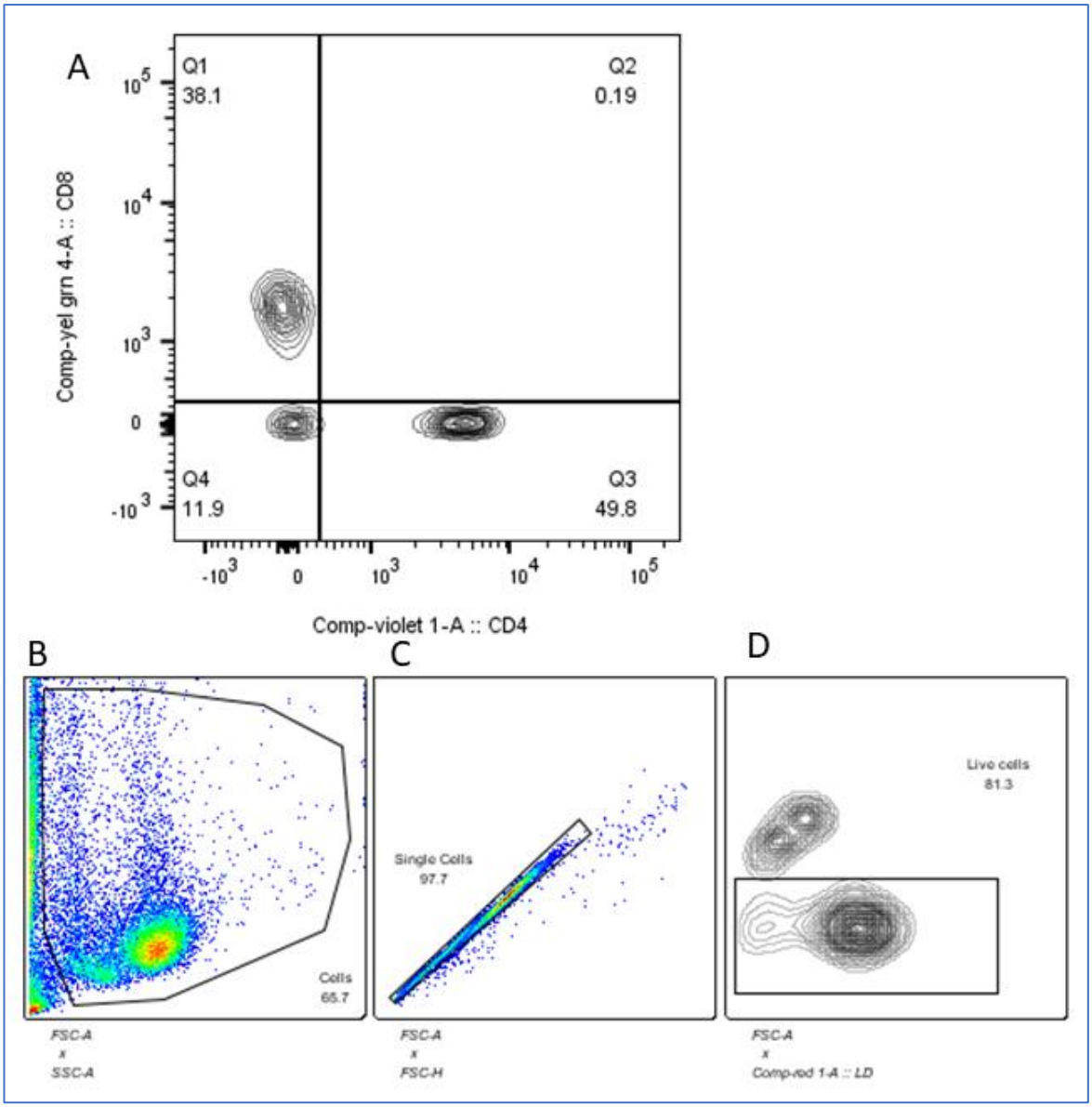


Figure 2.1: Gating of isolated T cells. Flow cytometry analysis shows that isolated T cells have a purity of about 90%, with approximately 38% of the isolated T cells being $CD8^+$ and approximately 50% being $CD4^+$ (A). B shows all collected events with selected events to go forward for the single cell analysis (C) and finally the single cells were analyzed for being viable cells (D). Numbers in A refer to the percentage of cell expressing either $CD4^+$, $CD8^+$, both or neither.

2.5 Murine Dendritic cell and macrophage generation

Murine bone marrow-derived cells were obtained from the tibia of healthy 8–20-week-old female C57BL6J mice (Envigo, Bicester, UK) by passing ice cold RPMI through the bones to obtain the bone marrow, which was then passed through

0.45µM cell strainer (BD, Falcon) to obtain the cells. Cells were centrifuged at RT for 5 minutes at 1500rpm (Eppendorf 5810 centrifuge). The cell pellet was resuspended in 5mL red cell lysis buffer (Biolegend) for 4 minutes on ice to lyse red blood cells. Bone marrow cells were diluted at $1x10^6$ cells/mL in immune cell medium (DMEM with 10% heat inactivated FBS, 50 IU/mL penicillin (Sigma-Aldrich) and 50 µg/mL streptomycin (Sigma-Aldrich) supplemented with 10ng/mL GM-CSF (Peprotech, London, UK) and 10ng/mL IL-4 (Peprotech)). Cells were cultured in 4mL/well in 6 well plates for a total of 6 days. On day 2, half of the medium in each well, containing suspension cells, was removed, centrifuged at RT for 5 minutes and 1500rpm, and the cell pellet was diluted in 8mL of immune cell medium and replated into fresh wells. Removed medium was replaced by supplying fresh immune cell medium. On day 4, cell density was halved by splitting each wells content into two new wells and resupplying 2 mL of immune cell medium. Non-adherent cells on day 6 were considered to be bone marrow-derived Dendritic cells (DCs; Figure 2.3) and adherent cells were considered bone marrow-derived macrophages (referred to as macrophages; Figure 2.4) (Figure 2.2).

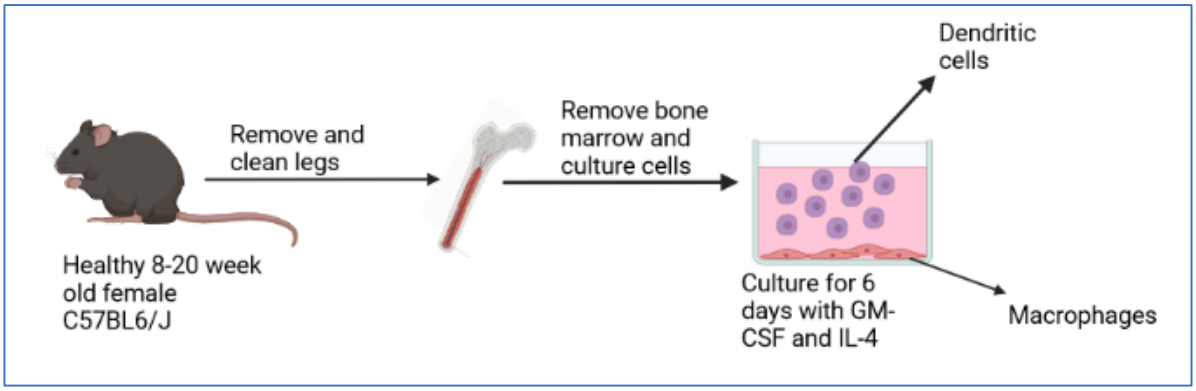


Figure 2.2: Schematic representation of the protocol to derive dendritic cells and macrophages from the bone-marrow of C57BL6/J mice. Both cell types were generated from the bone marrow of healthy 8–20-week-old female C57BL6/J mice by culturing the cells in growth medium with GM-CSF and IL-4 for 6 days. Adherent cells on day 6 were macrophage-like, referred to as macrophages, and non-adherent cells were DC-like, referred to as Dendritic cells. Graphic was created with Biorender.com.

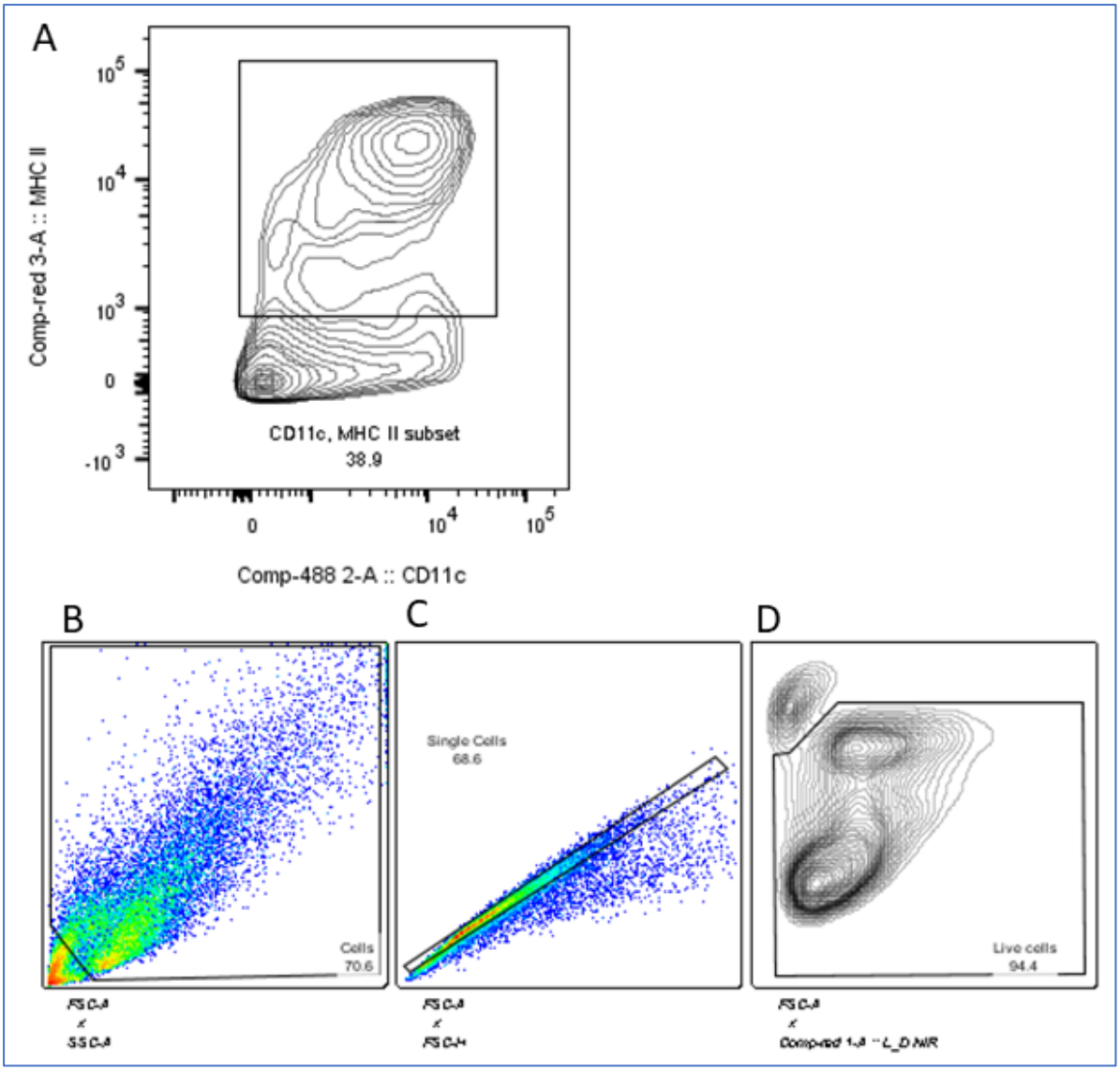


Figure 2.3: Gating of derived DCs. Flow cytometry analysis shows derived DCs express in 38% of the case CD11c and MHCII (A). B shows all collected events with selected events to go forward for the single cell analysis (C) and finally the single cells were analyzed for being viable cells (D).

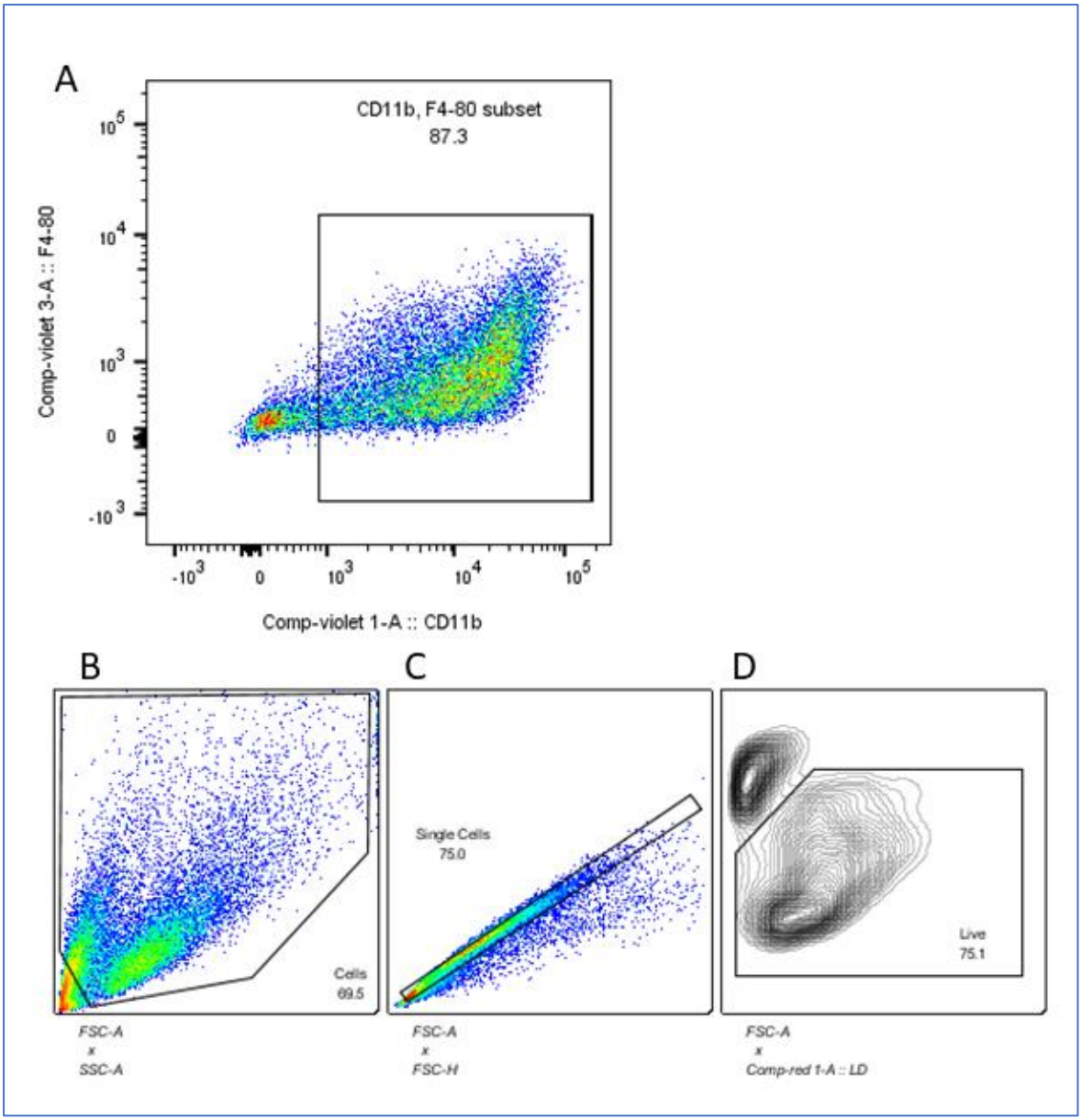


Figure 2.4: Gating of derived macrophages. Flow cytometry analysis shows that derived macrophages have a purity of about 87%, as indicated by CD11b and F4/80 expression (A). B shows all collected events with selected events to go forward for the single cell analysis (C) and finally the single cells were analyzed for being viable cells (D).

2.6 Cell Counting

Cancer cells were initially counted on NucleoCounter® NC-100™ (Chemometec, Allerod, Denmark) and later on a NucleoCounter® NC-200™ (Chemometec) employing the Viability and Cell Count Assay.

Cell counting in the NucleoCounter® NC-100™ was propidium iodine (PI) based with the PI staining provided by a specialized cassette (NucleoCassette™ (Chemometec)).

To lyse the cells for analysis, 200µL cell solution was first mixed with 200µL of solution A100 (Chemometec) for 30 seconds before and 200µl of solution B (Chemometec) was added and mixed for a further 30 seconds. NucleoCassette™ was then employed to take up the required amount of the lysed cell mixture and cells were counted using the NucleoCounter® NC-100™. Cell Counting in the NucleoCounter® NC-200™ was AO (Acridine Orange) and DAPI (4',6-diamidino-2-phenylindole) based, with both AO and DAPI staining provided by the specialized Via1-Cassette™ (Chemometec). For cell counting, 200µL of cell supernatant was directly taken up by the Via1-Cassette™, no lysis steps were required, as Chemometec had adapted the cell counter to work without the additional lysis step necessary for older machines.

Immune cells were initially counted by Trypan Blue (Sigma Aldrich, U.S.A.) staining and a haemocytometer and later counted also by employing the NucleoCounter® NC-200™ (Chemometec) using the White Blood Cell protocol.

2.7 Reversible Electroporation in vitro

Cells from the cell lines were trypsinized, counted and suspended at $2.5x10^6$cells/mL in 37°C warm electroporation buffer (EPB; 10mM 4-(2-hydroxyethyl)-1-piperazineethanesulfonic acid (HEPES; Merck), 250mM Sucrose (Merck) and 1mM $MgCl_2$ (Merck) in deionized water (diH_2O)). 400µL of cell suspension ($1×10^6$ cells) was aliquoted into sterile 4mm EP cuvettes (VWR, Pennsylvania, USA).

Cells were electroporated at RT with eight electric pulses, with pulse duration of 100 µs and 1 Hz frequency (ESOPE parameters) at electric field intensities of 600V/cm, 700V/cm, 800V/cm, 1000V/cm, 1200V/cm, 1300V/cm and 1400V/cm (indicated per experiment) using a BTX ECM 2001 square wave electroporator (BTX, San Diego, USA). After the electroporation, cells were rested for 20-30 minutes at 37°C and 5% CO_2 before various assays were carried out, except for efficacy testing which was performed immediately after the treatment.

To test the combined impact of electroporation, various drugs and calcium concentrations on the cell lines, EPB was supplemented with either 1µM, 5µM or 11µM respectively of cisplatin or oxaliplatin. Alternatively, EPB was supplemented

with 0.5mM, 1mM, 2.5mM or 5mM calcium ($CaCl_2$ stock solution, Merck). For calcium experiments, diH_2O used to prepare the EPB was Milli-Q® ultrapure water from a Milli-Q® Integral Water Purification System for Ultrapure Water (Merck). This ensured that buffer was not contaminated with calcium.

2.8 Development of LLC conditioned media

To generate different LLC conditioned media, $1x10^6$ cells were treated with electroporation at 800V/cm (EP-800 LLC media) respectively at 1300V/cm (EP-1300 LLC media) while maintaining the other ESOPE parameters (8 pulses; 100 µs; 1 Hz frequency). Cells were also treated with ECT with 11µM cisplatin and electroporation at 800V/cm (ECT-800 LLC media) respectively at 1300V/cm (ECT-1300 LLC media) while maintaining the other ESOPE parameters. For non-treatment controls, cells were left undisturbed. Following treatment, cells were plated in a total volume of 4mL DMEM10 in a 6-well plate and incubated for 48 hours. Supernatants were then isolated and centrifuged to remove cellular debris. Supernatants were then used immediately to condition dendritic cells.

2.9 Viability assay with flow cytometry

Viability of electroporated cells was evaluated within one hour of the treatment, and 4 and 24 hours post treatment depending on treatment and cell type. For the direct viability testing, 250,000 cells were transferred into FACS tubes, and immediately before being analysed by flow cytometry, PI was added to the tubes (final concentration 0.05mg/mL). For the 4 hour viability assays, 250,000 cells were incubated at 37°C and 5% CO_2 in constant humidity within sterile FACS tubes for 4 hours. For the 24 hours viability assay, 250,000 cells were plated and incubated for 24 hours at 37°C and 5% CO_2 in constant humidity. Adherent cancer cell lines were trypsinized prior to analysis and macrophages (primary cells) were mechanically detached. Prior to being analysed by flow cytometry, PI was added into the FACS tube (Falcon). Flow cytometry was conducted using an LSRII instrument with a 5-laser (355 /405 /488 /561 /640nm) configuration (Table 2.2) (BD Biosciences) and the results were analysed employing FlowJo V10 (BD Biosciences) (Figure 2.5).

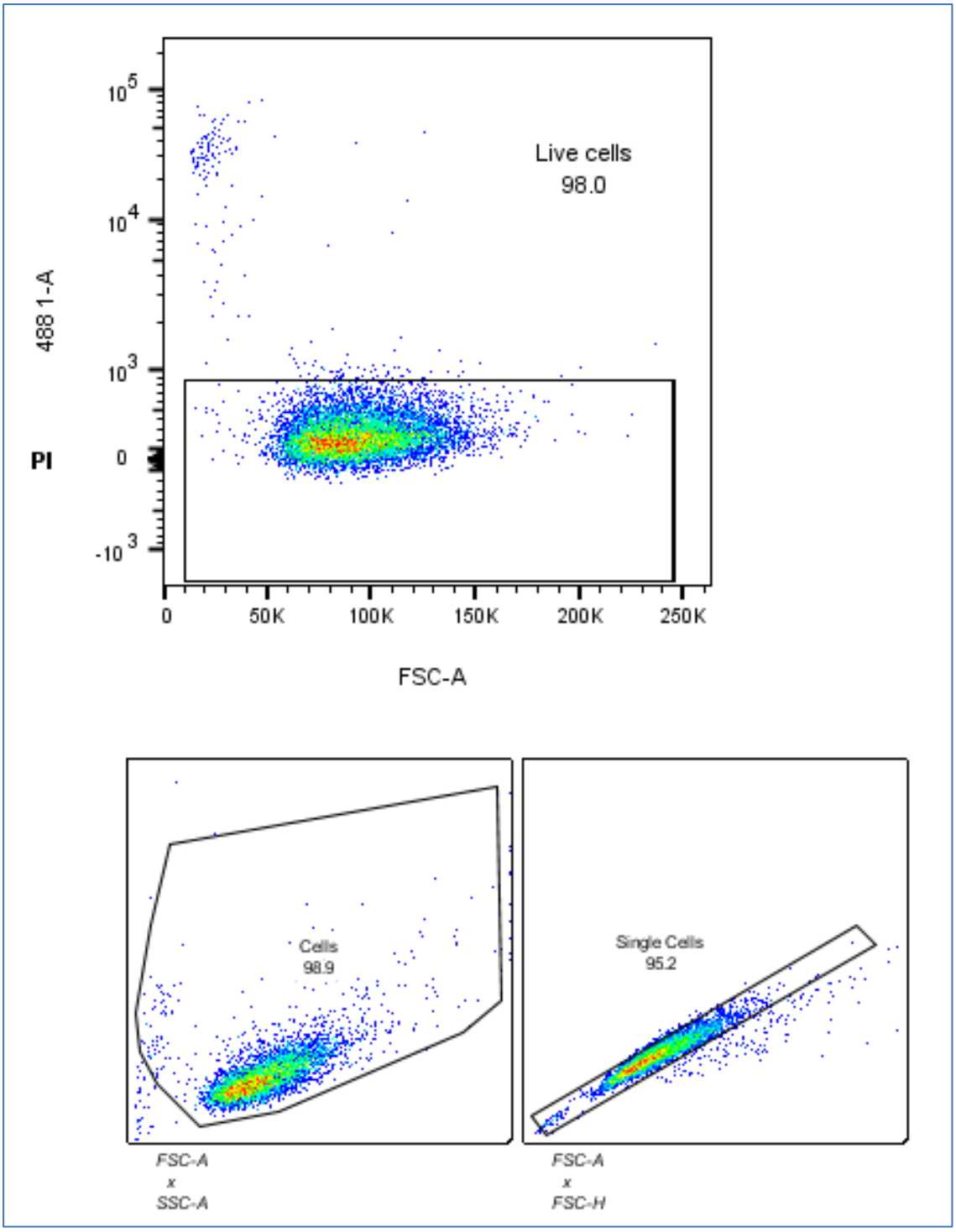


Figure 2.5: Gating for viable cells post EP treatment. After debris (lower left) was excluded and single cells were included (lower right), PI negative cells (top panel) were selected to determine the percentage of viable cells.

2.10 Efficacy measurement by flow cytometry

To test the efficacy of electroporation treatments, PI was added into the EP cuvettes, prior to the cells being electroporated, at a final concentration of 0.05mg/mL. Within 30 minutes of being electroporated, cells were analysed by flow cytometry. Flow cytometry was conducted using an LSRII instrument with a 5-laser (355 /405 /488 /561 /640nm) configuration (Table 2.2) (BD Biosciences) and the results analysed employing FlowJo V10 (BD Biosciences) (Figure 2.6).

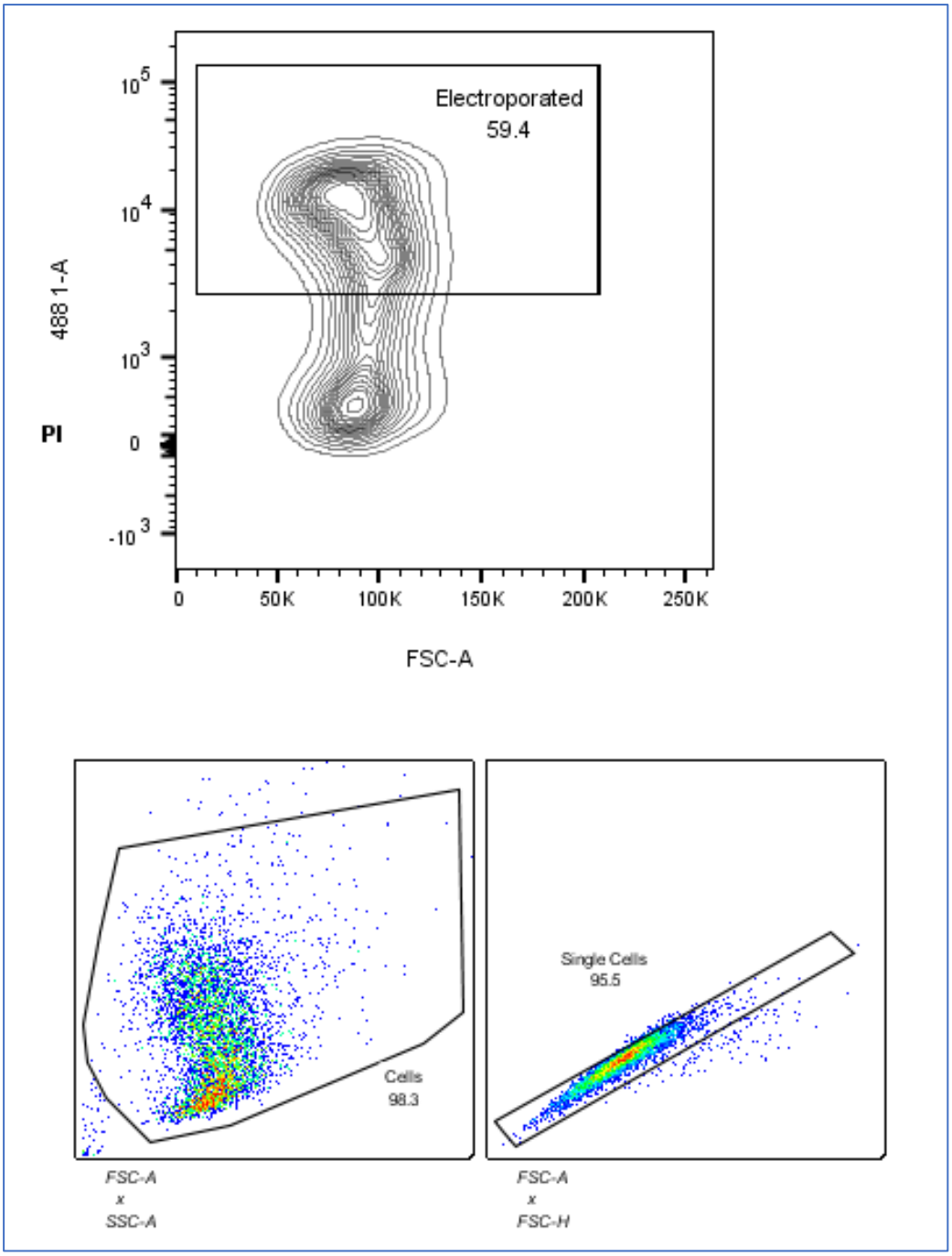


Figure 2.6: Gating for electroporated cells post EP treatment. After debris (lower left) was excluded and single cells were included (lower right), PI positive cells (top panel) were selected to determine the percentage of electroporated cells.

2.11 MTT assay

To determine how metabolic activity is impacted by EP and ECT treatments, metabolic activity of the cells post-treatment was analysed by 3-(4,5-dimethylthiazol-2-yl)-2,5-diphenyltetrazolium bromide (MTT) assay. For the MTT assay, 100,000 cells

were incubated for 4, 24, 72 and 120 hours, respectively depending on the experiment in either 12-well or 24-well plate wells depending on the cell type, at 37 °C in a humidified incubator with 5% CO_2. After incubation, the cells were incubated with the MTT reagent (5 µg/mL final concentration; Abcam, Cambridge, UK) at 37 °C in a humidified incubator with 5% CO_2 for up to one hour. Formed formazan, as an indicator of cell metabolic activity, was solubilized by adding 1000µL dimethyl sulfoxide (DMSO) into each well. The extent of formazan production was determined on a SpectraMax M2 (Molecular Devices, San Jose, USA) plate reader at 550nm, while 630nm served as the reference wavelength; each measurement was completed in triplicate.

2.12 Cell Recovery assay

Following treatment and resting, cells were seeded in triplicate in 6 well plates at a cell line specific concentration and incubated for 7-21 days, until the untreated control contained visible colonies. A549, H460, B16F10, Pan02 and A375 cell lines were plated at 400 cells/well, LLC cells were plated at 800 cells/well, Mia-PACA2 cells were plated at 2,400 cells/well and SK-MES-1 cells were plated at 6,000 cells/well.

For visualization of the colonies, the supernatant was discarded, cells were fixed in methanol for 10 minutes and then stained in Prodiff stain II for 10 minutes. Methanol fixation and Prodiff stain II staining were both completed over 20 minutes each for the SK-MES-1 cell line. Excess Prodiff stain II was removed by rinsing with water under a running tap. Once fully dry, the plates were analysed on an Odyssey® CLx system (Licor, Cambridge, UK) by determining the mean fluorescence intensity of each well.

2.13 Flow Cytometry

Single cell suspension from tissue (tumour, spleen, tumour-associated lymph nodes) or cell culture was prepared prior to the staining. 100,000 to 200,000 cells were diluted in 100µL FACS buffer (Phosphate buffered saline (PBS; Sigma-Aldrich) supplemented with 5% heat-inactivated FBS (Sigma-Aldrich) and 2mM EDTA (Sigma-Aldrich). To prevent non-specific binding of the flow cytometry antibodies, CD16/32 Fc-receptors were blocked by incubating 1µg of TruStain FcX™ Antibody (Biolegend)

per 1x10^6 cells for 10 minutes at 8°C in the dark. Following the blocking step, without washing, the cell suspensions were stained for 30 minutes at 8°C in the dark with Fixable live-dead Near-infrared marker (Thermofisher Scientific) for immune cell staining. Fixable live-dead Green marker (Thermofisher Scientific) was used for tissue samples. Both live-dead markers were used with appropriate fluorescently conjugated antibodies (Table 2.1) at a 1:50 dilution. Samples were washed twice with FACS buffer after the staining was completed and at least 10,000 events were collected per sample. Flow cytometry was conducted using an LSRII instrument with a 5-laser (355 /405 /488 /561 /640 nm) configuration (Table 2.2) (BD Biosciences) and the results were analysed employing FlowJo V10 (BD Biosciences). Exclusion of debris and selecting for single cells is shown in Figure 2.7.

Target (Clone)	Conjugate	Supplier	Flow Panel
CD45 (30-F11)	APC-Cy7	Biolegend	Murine Tissue
CD8α (53-6.7)	PE-Dazzle™ 594	Biolegend	Murine Tissue T cells
CD4 (RM4-5)	BV605	Biolegend	Murine Tissue T cells
MHC II (M5/114.15.2)	APC	Biolegend	Murine Tissue DCs
CD11c (N418)	AF488	Biolegend	DCs
CD80 (16-10A1)	PerCP-Cy5.5	Biolegend	DCs

Table 2.1: Antibody list for flow cytometry analysis. Conjugated, primary antibodies were used to identify specific cell surface proteins for phenotyping of murine immune cells and identification of immune cells in the tumour tissue by flow cytometry. Listed above are the targets of each antibody, the clone of the antibody, the fluorochrome to which the antibody was bound, the suppliers of each antibody and the flow panel in which the antibody was used. Allophycocyanin (APC), APC- cyanine 7 (APC-Cy7), phycoerythrin (PE), Brilliant violet 605 (BV605), Alexa Fluor 488 (AF488), Peridinin-chlorophyllprotein complex cyanine 5.5 (PerCP-Cy5.5).

Laser	Dichroic filter (nm)	Filter (nm)	Filter Range	Fluorophores detected
UV 355nm	505LP	525/50	500-550	
		450/50	425-475	
Violet 405nm	595LP	610/20	600-620	BV605
	505LP	525/50	500-550	
		450/50	425-475	
Blue 488nm	505LP	525/50	500-550	AlexaFluor488, L/D Green
	675LP	685/35	668-702	PerCP/Cy5.5, PI
Yellow/Green 561nm	755LP	780/60	750-810	
	685LP	710/50	685-735	
	635LP	660/20	650-670	
	600LP	610/20	600-620	PE-Dazzle 594
		582/15	574-589	PE
Red 640nm	735LP	780/60	750-810	APC-Cy7, L/D NIR
	685LP	710/50	685-735	
		670/14	663-677	APC

Table 2.2: Lasers, filters, channels and fluorophores detected on a custom BD 5 Laser LSR II flow cytometer used for all experiments. Long pass filters (LP).

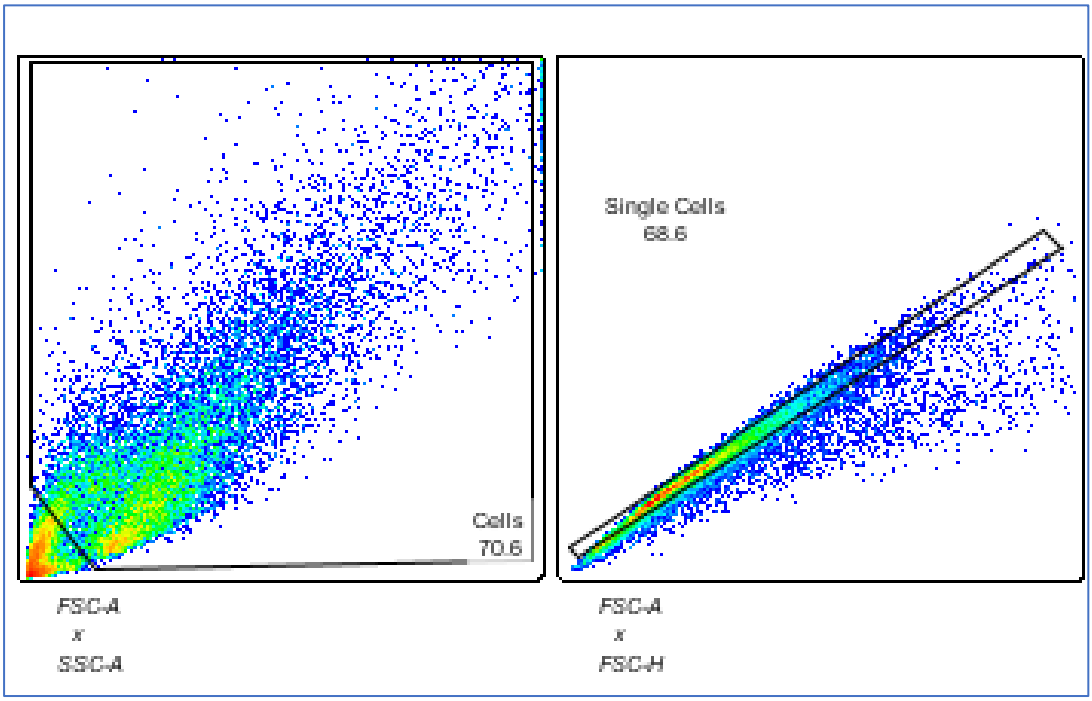


Figure 2.7: Exclusion of debris and inclusion of single cells from flow cytometry data. At the start of the flow cytometry analysis, debris (left) was excluded by gating all events except those with a near zero size on the Side-scatter (SSC) and the forward scatter (FSC). Single cells were included by comparing the FSC-area (FSC-A) with the FSC-height (FSC-H) (right).

2.14 Enzyme-Linked Immunosorbent Assays (ELISA)

Supernatants were either stored at -20°C or used directly to determine the concentration of murine IFN-γ and TNF-α cytokines using Biolegend ELISA MAX Deluxe Kits according to manufacturer's manual (Cat. Nr. 430804 for INF-γ and Cat. Nr. 430904 for TNF-α). Undiluted supernatants were used to determine the concentration for IFN-γ and TNF-α ELISAs. One day prior to the running the ELISAs, Nunc™ MaxiSorp™ flat-bottom 96 well plates (Cat. Nr. 423501) were coated with 100µL capture antibody per well and incubated overnight at 4°C. Prior to use on the day of the ELISA run, all reagents were brought to RT and the coated plates were washed 4 times with Wash Buffer (PBS with 0.05% Tween-20). The plates were then blocked for 1 hour at RT with shaking with 1X Assay Diluent A followed by 4 more washes. Then 100µL per well either standard (Top-standard 1000pg/mL for IFN-γ and Top standard of 500pg/mL for TNF-α; making six two-fold dilutions and including a 0 pg/mL standard) or supernatant was pipetted; all standards and supernatants were completed in technical duplicate and no less than three separate biological samples were analysed per cytokine. Standards and samples were incubated for 2 hours at RT with shaking followed by 4 more washes. Then plates were incubated with detection antibody per cytokine for 1 hour at RT while shaking followed by 4 more washes. Finally, plates were incubated with Avidin-HRP for 30 minutes at RT with shaking followed by 5 extensive wash steps before 3,3',5,5'-Tetramethylbenzidine (TMB) was added for 10-20 minutes (cytokine dependent; time was determined by development of standard curve) in the dark and reaction was stopped with 2M H_2SO_4 solution. Absorbance was directly read at 450nm with correction absorbance read at 570nmm on a FluoStar Omega (BMG Labtech; Aylesbury UK) machine. Difference between the 450nm and 570nm was calculated by the accompanying MARS software (BMG Labtech) and the standard curve and sample cytokine concentration was calculated using the Standard Curve analysis option in GraphPad Prism Version 9.

2.14.1 Stimulation protocol for ELISA

To further elucidate if dendritic cells are still functionally active post-treatment, dendritic cells were stimulated prior to ELISA analysis (2.14). DCs were left to rest for

30 minutes post-treatment before being stimulated for 24 hours by either 1µg/mL Lipopolysaccharides (LPS; Invivogen, San Diego, USA), 1µM CpG (ODN2395, Invivogen), 10µg/mL polyI:C (Invivogen) or 1µg/mL R848 (Invivogen). After the 24-hour stimulation period was over, supernatants were collected and analysed via ELISA (2.14).

2.15 Immune Cell morphology analysis

Morphology of treated cells was analysed 4 hours post-treatment by light microscopy. 50.000 cells per condition were cytospun onto glass slides (2 minutes spin at 400rpm on Shandon Cytospin 4 centrifuge) and left to air-dry at RT for 10 minutes. Slides were stained using Rapi-Diff (Braidwood Laboratories, London, UK). Slides were first left for 10 seconds in Solution A (fixative), excess fluids were then removed before slides were left for 20 seconds in Solution B. Excess fluids were removed from the slides by washing the back side of the slides with water. Slides were then left for 5 seconds in Solution C and slides were again washed with water, back and front. Slides were allowed to air dry overnight and then the slides were fixed by mounting cover slides with DPX mounting medium on them. DPX was allowed to dry before slides were analysed. Slides were analysed on Olympus BX51 microscope (10X eyepiece) with an Olympus DP74 camera (40X objective was used) mounted to take pictures.

2.16 qRT-PCR

2.16.1 RNA extraction

Ribonucleic acid (RNA) was isolated from treated cells 4 hours post-treatment utilizing the GenElute total mRNA kit (Sigma Aldrich), all materials are from this kit unless specified. Cells were lysed in 250µL RNA lysis buffer, lysate was transferred to filtration column and centrifuged at 14000rpm (Eppendorf Centrifuge 5424) for 2 minutes. 250µL of 70% ethanol was added and mixed thoroughly with the filtrate and transferred to the binding column. After subsequent 15 seconds 14000rpm centrifugation step, 500µL of Wash solution 1 was added to the column and centrifuged again for 15 seconds at 14000rpm. After the column was transferred to

a new tube, 500µL of Wash solution 2 was added to the column and spun down (15 seconds, 14000rpm) again. Another 500µL of Wash solution 2 was added to the column and spun down for 2 minutes at 14000rpm. Finally, the binding column was transferred to the collection tube and 25µL of elution solution was added to the column and centrifuged for 1 minute at 14000rpm. RNA concentration (ng/µL) and quality (260/280nm absorbance ratio) was determined by employing the Nanodrop 1000 spectrophotometer (Thermo Fisher Scientific). 260/280 ratio values above 1.8 were considered good enough to continue with the cDNA preparation.

2.16.2 cDNA preparation

cDNA synthesis was done by utilizing the Bioline cDNA synthesis kit (Bioline, London, UK). 8µl of standardised RNA template (100-200ng RNA; equal amount of RNA was used per experiment) was mixed with 1µl of random primers, and 1µl of 10Mm dNTP per sample. Mixture was heated to 65°C for 10 minutes, followed by cooling down with the mixture placed on ice for 5 minutes. Then, 2.75µL of nuclease-free water, 4µL of 5x Reverse Transcriptase Buffer, 0.25µl of Reverse Transcriptase and 1µl of RNase inhibitor was added to the mixture before the mixture was incubated at 37°C for 30 minutes, followed by 15 minutes of incubation at 70°C. Finally, cDNA solution was diluted 1:1 with nuclease-free water and stored at -20°C until the qRT-PCR was performed (2.17.3).

2.16.3 qRT-PCR

In 10µL total reaction volume was 2µL of prepared cDNA template (2.17.2) amplified on the LightCycler® 480 (Roche, Basel, Switzerland). Reaction mix was prepared by mixing 2µL of nuclease-free water, 0.5µL of each forward and reverse primer (final concentration of 400nM per primer; Roche respectively Integrated DNA Technologies (IDT), BV., Leuven; Table 2.3), 0.2µL of the appropriate Universal Probe Library probe (200nM final concentration; Roche) and 5µL of Sensifast Probe Lo-Rox kit (Bioline). Alternatively, pre-made primers from IDT (Integrated DNA Technologies, BV., Leuven, Belgium) were used. 8µL of reaction mix was added to 2µL of cDNA template and combined in a 96 well LightCycler plate (Roche). The plate was then

loaded into the LightCycler® 480 (Roche). Conditions for the LightCycler® 480 (Roche) were one cycle of 95°C for 10 minutes; 45 cycles of 95°C for 10 seconds, one cycle of 60°C for 30 seconds, followed by a final cooling cycle at 40°C for 30 seconds. All results were analysed using the $2^{-\Delta\Delta ct}$ method[1] and the gene of interest was normalized to the corresponding β-actin (housekeeping gene) gene results. Fold-change values over the untreated condition are represented. A minimum of three biological replicates were completed per condition.

Protein	Gene	Direction	Sequence (5'-3')	Company
β-actin	ACTB	Fwd	CTCCGCTGACTCTCTTGG	Roche
		Rev	AGGTGGTCGCAAAAACGA	
TLR1	Tlr1	Fwd	CCTGGAGAGGTTCCGTGAT	Roche
		Rev	TTCACCAACTGCATTCACAAA	
TLR2*	Tlr2	Fwd	GGGGCTTCACTTCTCTGCTT	Roche
		Rev	AGCATCCTCTGAGATTTGACG	
TLR3	Tlr3	Fwd	GATACAGGGATTGCACCCATA	Roche
		Rev	TCCCCCAAAGGAGTACATTAGA	
TLR4	Tlr4	Fwd	GGACTCTGATCATGGCACTG	Roche
		Rev	CTGATCCATGCATTGGTAGGT	
TLR5	Tlr5	Fwd	TCATGGATGGATGCTGAGTT	Roche
		Rev	TGGCCATGAAGATCACACC	
TLR6	Tlr6	Fwd	ACTATGCTGGTGCTGGCTGT	Roche
		Rev	CCAGGGCAGGTCAAAGTAGA	
TLR7	Tlr7	Fwd	TGATCCTGGCCTATCTCTGAC	Roche
		Rev	CGTGTCCACATCGAAAACAC	
TLR8	Tlr8	Fwd	CAAACGTTTTACCTTCCTTTGTCT	Roche
		Rev	ATGGAAGATGGCACTGGTTC	
TLR9	Tlr9	Fwd	GAATCCTCCATCTCCCAACA	Roche
		Rev	CAGCTCACAGGGTAGGAAGG	
Pre-made primers				
Protein	Gene	Primer Code		Company
CXCL10	Cxcl10	Mm.PT.58.28790444		Integrated DNA Technologies (IDT)
PTGS2	Ptgs2	Mm.PT.58.9154407		IDT
ISG15	Isg15	Mm.PT.58.41476392.g		IDT
DUSP14	Dusp14	Mm.PT.58.33092319		IDT
TLR2**	Tlr2	Mm.PT.58.45820113		IDT

Table 2.3: Primers used for qRT-PCR experiments

*Was used to determine the TLR2 expression following EP treatment.

**Was used to determine the TLR2 expression following ECT treatment.

2.17 Cell Death Analysis

To determine if treated cells die by apoptotic or necrotic cell death, cells were analysed with APC Annexin V Apoptosis Detection Kit and PI (Biolegend). After 4 hours incubation post-treatment, cells were washed once in FACS buffer and resuspend in 100µL Annexin V Binding buffer (2mM $CaCl_2$ in PBS). Cells were stained with 5µL of Annexin V and 5µL of PI per sample and incubated for 15 minutes at RT in the dark. An additional 150µL of Annexin V binding buffer was added after the 15 minutes and the cells were analysed using the BD LSRII machine and the results analysed employing FlowJo V10 (BD Biosciences).

2.18 RNA Sequencing by Qiagen

UPX 3' Transcriptome Sequencing, including all related processing of the cells from the cell pellet stage up until the full statistical analysis was performed by Qiagen (Qiagen, Hilden, Germany). In short, $1x10^6$ dendritic cells were untreated or treated with ECT at 800V/cm, 1000V/cm and respectively 1300V/cm, and left to rest for 4 hours prior to being pelleted (1500rpm (Eppendorf 5810 centrifuge), 10 minutes, RT) and frozen down (-80°C). Qiagen isolated the RNA using their RNeasy Plus Mini Universal (Qiagen) according to manufacturer's instructions with an elution volume of 30µL. RNA integrity level was measured for each RNA sample using the Agilent TapeStation (Agilent) in order to obtain the RINe (RNA integrity number) value per sample and only samples reaching a RINe value of at least 7.1 were used for further processing.

The library preparation was completed using the QIAseq UPX 3' Transcriptome Kit (Qiagen). A total of 5ng purified RNA was converted into cDNA Next-generation sequencing libraries. Internal quality control was executed at this stage and only once samples passed it, samples were sequenced on a NextSeq®500 sequencing instrument (Illumina® Inc., San Diego, USA) according to the manufacturer instructions with 100 base pair (bp) read length for read 1 and 27 bp for read 2. Raw data was demultiplexed and FASTQ files for each pool was generated using the

bcl2fastq Conversion Software (Illumina® Inc.). The "Demultiplex QIAseq UPX 3' reads" tool of the CLC Genomics Workbench 20.0.4 was used to demultiplex the raw sequencing reads according to the sample indices. The "Quantify QIAseq UPX 3' workflow" was used to process the demultiplexed sequencing reads with default settings. In short, the reads are annotated with their unique molecular identifier (UMI) and are then trimmed for poly(A) and adapter sequences, minimum reads length (15 nucleotides), read quality, and ambiguous nucleotides (maximum of 2). They are then deduplicated using their UMI. Reads are grouped into UMI groups when they (1) start at the same position based on the end of the read to which the UMI is ligated (i.e., Read2 for paired data), (2) are from the same strand, and (3) have identical UMIs. Groups that contain only one read (singletons) are merged into non-singleton groups if the singleton's UMI can be converted to a UMI of a non-singleton group by introducing an SNP (the biggest group is chosen). The reads were then mapped to the mMouse genome GRCm38 v. 80 and annotated using the ENSEMBL GRCm38 v. 86 mRNA annotation.

The 'Empirical analysis of DGE' algorithm of the CLC Genomics Workbench 21.0.4 was used for differential expression analysis with default settings. It is an implementation of the 'Exact Test' for two-group comparisons developed by Robinson and Smyth[2] and incorporated in the EdgeR Bioconductor package[3].

For all unsupervised analysis, only miRNAs were considered with at least 10 counts summed over all samples. A variance stabilizing transformation was performed on the raw count matrix using the function vst of the R package DESeq2 version 1.28.1. 500 genes with the highest variance were used for the principal component analysis. The variance was calculated agnostically to the pre-defined groups (blind=TRUE). 35 genes with the highest variance across samples were selected for hierarchical clustering.

Further analysis to gain a more in-depth understanding of the changes in the gene expression brought on by the different ECT treatments are described in 2.19.

2.19 Analysis of differentially expressed genes

Cytoscape software[4,5] was employed to execute STRING (*Search Tool for the Retrieval of Interacting Genes/Proteins*)[5,6] and Molecular complex detection (MCODE) analysis to explore the protein-protein interactions (PPI) of the differentially expressed genes (DEGs) per treatment condition. STRING analysis was executed for a full STRING network, with a confidence cut off of 0.40 and maximum additional interactions of 0. The resulting PPI networks were visualized using Cytoscape. STRING enrichment was performed with Gene Ontology (GO) and Kyoto Encyclopedia of Genes and Genomes (KEGG) annotations on the whole STRING network. The MCODE plug-in identifies the highly interconnected regions (called clusters) in a given network by Markov clustering[7]. Identified modules were then presented as separate networks and also analysed by STRING enrichment for KEGG and GO annotations.

2.20 *In vivo* murine lung cancer model

Prior to the start of any experiments, mice were randomly assigned to their treatment groups and housed with up to 5 mice per cage together. Their ears were clipped for identification purposes one day prior to the start of the experiment.

Subcutaneous tumours were generated by injecting LLC cells ($5x10^5$ or $1x10^6$; indicated per experiment) subcutaneously into the right flank of female C57BL6 mice (8-15 weeks of age; Envigo). Tumour formation was assessed three times a week by palpation on the right flank of the animals. Once tumours were established, tumour area was determined daily by measuring the longest and shortest diameter of the tumour using electrical callipers. In addition, the weight of the animals was monitored three times a week until they developed tumours and then daily. Animals were euthanized by cervical dislocation once animals reached either humane endpoint or study endpoint (tumour size reaching 2.5cmx2.5cm or animals surviving 45 days post tumour cell injection).

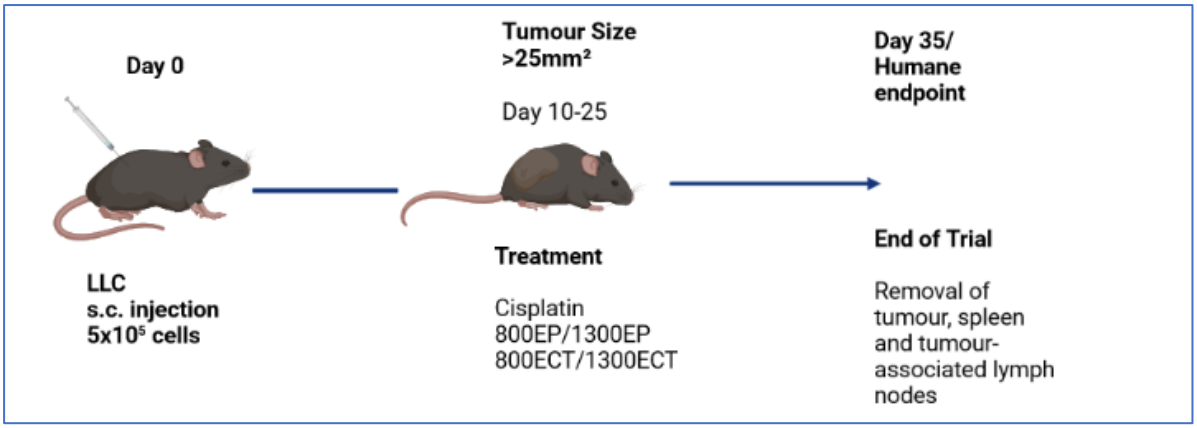


Figure 2.8: Timeline of murine lung cancer study to investigate the effectiveness of ECT at 800V/cm versus the effectiveness of ECT at 1300V/cm with respect to both tumour reduction and the impact on the immune cells present at the treatment side. Mice were treated with either cisplatin alone, or with EP at 800V/cm (800EP) respectively 1300V/cm (1300EP), or cisplatin ECT at 800V/cm (800ECT) respectively (1300ECT) once the tumour reached at least 25mm² in size. Graphic was created with Biorender.com.

2.21 *In vivo* EP and ECT

The tumours were treated once they reached an approximal area of 25mm² (treatment was done on different days for different animals as tumour size was the determining parameter for treatment). Cisplatin was made up at 1mg/kg in 20µL sterile PBS and injected intratumorally employing a fan pattern as the needle was removed to increase the distribution of the cisplatin within the tumour. Electrical parameters were applied at 8 pulses, 1Hz frequency, 100µs pulse length and electric field strength of 800V/cm or 1300V/cm respectively using a Cliniporator™ device (IGEA S.R.L, Carpi, Italy) and employing an in-house made 8-needle electrode. Parameters were applied as often as necessary to cover the entire tumour and the tumour margin surrounding it.

Prior to the application of the electric pulses, mice were anaesthetised using subcutaneous anaesthetics (Ketamine 75mg/kg at and Medetomidine at 0.5mg/kg) and post-treatment analgesia (meloxicam at 5mg/kg) was applied straight after the EP/ECT treatments. Anaesthesia was reversed by subcutaneous injection of Atipamezole (5mg/kg). Mice were placed in individual cages and monitored after the

anaesthesia was reversed until they were conscious again and placed back with their group.

2.22 Tissue preparation for flow cytometry

Tumours, spleen and tumour-associated lymph nodes were recovered once the tumours reached a size of 2.5x2.5cm² or the animal had reached the humane endpoint (weight loss, ulcerations). Tumour tissues were washed twice in ice-cold PBS before tumours were minced, washed once more, and incubated for 1 hour at 60°C with collagenase II (Merck Millipore, U.S.A.) and DNase I (Merck Millipore) at a final concentration of 1mg/mL and 100 Kunitz/mL, respectively, in warm DMEM. The resulting sample was run through a 0.7µM cell strainer (Corning, New York, USA). Spleens and lymph nodes were run through 0.45µM cell strainer (BD, Falcon). The resulting cell suspension were washed once more with PBS and red cells were removed from the cell suspensions by incubating the samples with Red Cell lysis buffer (Biolegend) for 3 minutes on ice. Resulting sample was washed once more and stained according to the protocol in 2.13.

2.23 Statistical analysis

Values of $p \leq 0.05$ are indicated by one asterisk (*). Values of $p \leq 0.01$ are indicated by two asterisks (**). Values of $p \leq 0.001$ are indicated by three asterisks (***). Values of $p \leq 0.0001$ are indicated by four asterisks (****). Performed tests are indicated below on a per chapter basis.

Chapter 3

In vitro experiments were repeated at least three times on different days and with different cell passage numbers.

All treatment conditions were normalized to the untreated condition for viability, metabolic activity and recovery assays. First a one-way ANOVA, assuming Gaussian distribution and equal standard deviations, was performed to determine overall significant changes followed by Dunnett's post-hoc test to determine difference between treatment conditions and untreated control groups. GraphPad Prism

Version 9.0 software was used for all statistical analysis. P-values of p≤ 0.05 were considered significant.

Chapter 4

In vitro experiments were repeated at least three times on different days and with different passage numbers. All treatment conditions were normalized to the untreated condition for viability, metabolic activity and recovery assays. First a one-way ANOVA, with Gaussian distribution and equal standard deviations, was performed to determine overall significant changes followed by Tukey's post-hoc test to determine difference between all treatment conditions and untreated control groups, EP control group and ECT treatment conditions as well as between ECT treatments with the two different drugs at the same drug concentration. The D'Agostino-Pearson normality test was used to test for Gaussian distribution. GraphPad Prism Version 9.0 software was used for all statistical analysis. P-values of p≤ 0.05 were considered significant.

Chapter 5

In vitro experiments were repeated at least three times on different days and with different passage numbers. All treatment conditions were normalized to the untreated condition for viability, metabolic activity and recovery assays. First a one-way ANOVA, assuming Gaussian distribution and equal standard deviations, was performed to determine overall significant changes followed by Dunnett's post-hoc test to determine difference between treatment conditions and untreated control groups. Grubb's Test was employed to identify outliers. GraphPad Prism Version 9.0 software was used for all statistical analysis. P-values of p≤ 0.05 were considered significant.

2.24 References

1. Livak, K. J. & Schmittgen, T. D. Analysis of relative gene expression data using real-time quantitative PCR and the 2-ΔΔCT method. *Methods* **25**, 402–408 (2001).
2. Robinson, M. D. & Smyth, G. K. Small-sample estimation of negative binomial dispersion, with applications to SAGE data. *Biostatistics* **9**, 321–332 (2008).
3. Robinson, M. D., McCarthy, D. J. & Smyth, G. K. edgeR: A Bioconductor package for differential expression analysis of digital gene expression data. *Bioinformatics* **26**, 139–140 (2009).
4. Paul Shannon, 1 *et al.* Cytoscape: A Software Environment for Integrated Models. *Genome Res.* **13**, 426 (1971).
5. Doncheva, N. T., Morris, J. H., Gorodkin, J. & Jensen, L. J. Cytoscape StringApp: Network Analysis and Visualization of Proteomics Data. *J. Proteome Res.* **18**, 623–632 (2019).
6. Szklarczyk, D. *et al.* The STRING database in 2021: Customizable protein-protein networks, and functional characterization of user-uploaded gene/measurement sets. *Nucleic Acids Res.* **49**, D605–D612 (2021).
7. Hogue, C. W. & Groll, M. An automated method for finding molecular complexes in large protein interaction networks. *BMC Bioinformatics* **29**, 137–140 (2001).

Chapter 3

Electroporation of cancer cell lines in suspension – a proposed assay set for optimizations of electric field strength

Results from this chapter have been published in part as:

> Bendix, M. B., Brint, E., & Forde, P. F. (2021). Electroporation of suspension cell lines – A proposed assay set for optimizations. Bioelectrochemistry, 142. https://doi.org/10.1016/j.bioelechem.2021.1078913.11.

3.1 Abstract

To make *in vitro* single cell electroporation protocols more comparable between various cancer cell types and research groups, here we propose a set of assays to test a range of electric field strengths at the start of any new project to determine the optimal electric field strength for a given cell line. While testing a range of electric field strengths, we kept the other ESOPE parameters (8 pulses, 100µs pulse duration, 1Hz pulse frequency) constant. Basic assays were employed to measure short-term viability, effectiveness of treatment, metabolic activity, and recovery potential post-treatment to determine the optimal field strength for a particular cell line. Eight adherent cancer cell lines were tested, five human cell lines (A549, H460, SK-MES 1, A375 and Pan02) and three murine cell lines (LLC, B16F10 and MIA-PACA2). Our findings demonstrate that the optimal electroporation setting, while keeping with all other ESOPE parameters, are 800V/cm for A549, H460, SK-MES 1 and Pan02 cells, 700V/cm for A375, Mia-PACA2, and B16F10 cells, and 1300V/cm for LLC cells. Having an agreed upon set of assays to determine each cancer cell line's optimal electric field strength should allow for improved translation of findings between cancer cell lines for *in vitro* work from various research groups and potentially improve translation into the clinic.

3.2 Introduction

Electrochemotherapy (ECT) is a novel anti-cancer treatment that has been explored for anti-cancer therapy for over 30 years across a range of malignancies[1]. ECT combines the application of an electric pulse (electroporation (EP)) to open cell pores in the treated areas with the injection of a cytotoxic drug, like bleomycin or cisplatin, or calcium (then called CaEP), to increase the uptake of the drug or calcium, while preserving as much healthy tissue as possible and reducing side-effects[2–5]. ECT leads to an increased drug uptake of up to 700-fold for bleomycin[6] and can delay tumour growth, as well as in some cases prevent re-emergence of the tumour altogether[7–9]. ECT also impacts healthy tissue significantly less than tumour tissue, while there is no long-term impact on blood vessels once the initial vascular lock has resolved[4,10,11].

The seminal ESOPE (European standard operating procedures for electrochemotherapy) study standardized the clinically used ECT parameters, making it easier to compare study results across centers and cancer types[6,12]. Unfortunately, those parameters were also translated into bench side research, without considering that cells in single-cell suspension may react quite differently than those in tissue and that the use of various buffers may increase the effectiveness of any applied charges. To render comparing *in vitro* results possible and more reliable, there is a need to establish a consensus of agreed upon EP parameters for ESOPE related ECT in a cell-line depended manner[6]. Also, as ECT has now advanced to internal organs[3,13–15], there is a need to consider that different cell types may react differently to these parameters (8 pulses, 100µs pulse duration, 1Hz pulse frequency and electric field strength of 1000V/cm) and therefore we cannot assume that the adopted ESOPE parameters that work well for skin based cells *in vitro* hold true for colon, lung or other cell types. Thus, similar to the ESOPE protocol, we need a guideline to evaluate the impact of electroporation on cells in single cell suspension.

It was shown in a case of CaEP for macrophages that lower electric field strengths are beneficial for the effectiveness of the treatment[16]. Therefore, testing if cancer cell lines are sufficiently impacted by lower electric field strength than the currently used ESOPE-based parameters could increase the treatment efficacy overall. Furthermore,

lowering the electric field strength has the potential to protect non-malignant cells and structures better than the currently used higher voltages, thus potentially making the treatment even safer and possibly also allowing the effective application of ECT in ever more sensitive areas such as the lung. This will make designing co-treatments, like adjuvant immunotherapy, easier and potentially even more effective.

Thus, in this chapter, we compare the impact of a range of electric field strengths (600- 1400V/cm) to each other while keeping the number of pulses (8), pulse duration (100µs), pulse frequency (1Hz) (ESOPE protocol) and buffer constant for various human and murine cancer cell lines, and define the optimal voltage setting for each cell line. Keeping the majority of the ESOPE parameters has the potential to make the translation into *in vivo* work easier rather than having to design completely new parameters. In this chapter, optimal electric field strength/optimal voltage, will refer to the minimum needed electric field strength that has the highest possible efficacy (≥95%) with the lowest possible detrimental effect on cell viability, metabolic activity, and recovery of the cancer cell line in *in vitro* cell-suspension research while keeping with the ESOPE parameters for the prescribed number of pulses, pulse duration and pulse frequency.

The overall aim of this chapter, therefore, is to design a standardizable protocol to determine optimal electric field strengths for a wide range of cancer cell lines *in vitro*, both murine and human cell lines. Therefore, the protocol was tested on Lewis-Lung carcinoma (LLC; murine lung cancer), A549 (human lung cancer), H460 (human lung cancer), SK-MES-1 (human lung cancer), B16F10 (murine melanoma), A375 (human melanoma), Pan02 (murine pancreatic cancer) and Mia-PACA2 (human pancreatic cancer) cell lines. Having a comparable approach to define *in vitro* EP settings will make future studies more comparable, similar to having the ESOPE protocol which makes clinical studies more comparable. This should increase the capacity to transfer knowledge between cancer cell lines and cancer types.

3.3 Materials and Methods

3.3.1 Cell Culturing

Lewis Lungs Carcinoma (LLC; murine lung cancer), A549 (human lung cancer), H460 (human lung cancer), SK-MES 1 (human lung cancer) and A375 (human melanoma) cell lines were obtained from the American Type Culture Collection (ATCC). B16F10 (murine melanoma) cell line was obtained from the European Collection of Authenticated Cell Cultures. Mia-PACA2 (human pancreatic cancer) cell line was obtained from European Cell and Culture Collection. Pan-02 (murine pancreatic cancer) cell line was obtained from the National Cancer Institute at Frederick. A549, H460, Pan02 and B16F10 cell lines were maintained in RMPI 1640 medium, supplemented with 10% foetal bovine serum (FBS), 2mM L-glutamine, 50 IU/mL penicillin and 50 µg/mL streptomycin. LLC and Mia-PACA2 cell lines were maintained in Dulbecco's Modified Eagle Medium (DMEM), supplemented with 10% FBS, 2mM L-glutamine, 50 IU/mL penicillin and 50 µg/mL streptomycin. A375 and SK-MES 1 cell lines were maintained in DMEM supplemented with 20% FBS, 2mM L-glutamine, 50 I.U/mL penicillin and 50 µg/mL streptomycin. Cell lines were incubated at 37 °C in constant humidity with 5% CO_2. Cells were split at 70-90% confluency. All tested cell lines are adherent cells, which were detached prior to the experiments using a trypsin-ethylenediaminetetraacetic acid (EDTA) solution (Merck).

3.3.2 *In vitro* electroporation parameters

To test the impact of electroporation alone on several cell properties, 1×10^6 cells were suspended in 400 µL of electroporation buffer (EPB; 10mM HEPES, 250mM Sucrose and 1mM MgCl2 in ddH20) and aliquoted into sterile 4mm EP cuvettes (VWR, USA). Cuvettes were exposed to eight electric pulses at electric field intensities of 600V/cm, 700V/cm, 800V/cm, 1000V/cm, 1200V/cm, 1300V/cm and 1400V/cm, with pulse duration of 100 µs and 1 Hz frequency using a BTX ECM 2001 square wave electroporator (BTX, San Diego, USA). After the electroporation cells were rested for 20-30 minutes at 37°C and 5% CO_2 before various assays were set-up.

3.3.3 Efficacy Assay

To test efficacy of electroporation with various electric field strength, propidium iodide (PI; Sigma-Aldrich or Fisher) was added into the EP cuvettes before electroporation with a final concentration of 0,05mg/mL. Within 30 minutes of being electroporated cells were analysed by flow cytometry.

3.3.4 Viability Assay

Viability of electroporated cells were tested within one hour of the treatment and 24 hours post treatment. For the direct viability testing, 250.000 cells were transferred into FACS (Falcon™ Round-Bottom Polystyrene 5mL tubes) tubes and immediately before being analysed by flow cytometry PI (final concentration 0,08mg/mL) was added into the tubes. For the 24 hours viability, 250.000 cells were plated into 6-well plates and incubated at 37°C 5% CO_2 for 24 hours. Prior to being analysed by flow cytometry, PI was added into the FACS tube.

3.3.5 MTT Assay

For the MTT assay, 100.000 cells were incubated for 24 hours at 37˚C at constant humidity with 5% CO_2. After incubation, the cells were left with MTT (3-(4,5-dimethylthiazol-2-yl)-2,5-diphenyltetrazolium bromide) reagent (5 µg/mL final concentration) at 37°C for up to one hour. Formazan was used as an indicator of cell viability and then solubilised by adding 100µl of DMSO (Sigma-Aldrich) in to each well. The extent of formazan production was determined by a plate reader at 550 nm, while 630 nm served as the reference wavelength; each measurement was carried out in triplicate.

3.3.6 Cell Recovery Assay

Following treatment and resting, cells were seeded in triplicate in 6 well plates at a cell line specific concentration and incubated for 7-21 days until the untreated control contained visible colonies at 37 °C under 5% CO_2. A549, H460, B16F10, Pan02 and A375 cell lines were plated at 400 cells/well, LLC cell line was plated at 800

cells/well, Mia-PACA2 cell line was plated at 2400 cells/well and SK-MES-1 cell line was plated at 6000 cells/well.

For visualization of the colonies the supernatant was discarded, cells were fixed in methanol for 10min and then stained in Prodiff stain II for 10min; 20 minutes each in the case of SK-MES-1 cell line. Excess Prodiff stain II was removed by rinsing with water under a running tap. Once fully dry the plates were analysed on an Odyssey® CLx system.

3.3.7 Statistical analysis

In vitro experiments were repeated at least three times on different days and with different cell passage numbers.

All treatment conditions were normalized to the untreated condition for viability, metabolic activity and recovery assays. First a one-way ANOVA, assuming Gaussian distribution and equal standard deviations, was performed to determine overall significant changes followed by Dunnett's post-hoc test to determine difference between treatment conditions and untreated control groups. GraphPad Prism Version 9.0 software was used for all statistical analysis. P-values of $p \leq 0.05$ were considered significant.

3.4 Results

3.4.1 Cell line dependent 95% efficacy threshold is reached between 800-1000V/cm

Initially, the efficacy of electroporation, as assessed by propidium iodide (PI) uptake, with various electric field strengths based on the ESOPE parameters, was tested in order to determine the minimum electric field strength needed which had an efficacy of 95% or higher. Application of an electric field results in opening of the cell pores, which in turn allows the present PI to enter the cells, and traps the PI within the cells once the pores close. Thus, PI intensity illustrates perforation of cells by electroporation. All tested cell lines showed an initial linear increase in treatment efficacy with increasing electric field strength (Figure 3.1), with electric field strengths between 800- 1000V/cm reaching the 95% cell-line specific efficacy threshold. 95% efficacy was reached at 800V/cm for A375 and B16F10 cells whilst A549, H460, SK-MES-1, Mia-PACA2, LLC and Pan02 cells reached 95% efficacy at 1000V/cm (Figure 3.1). Furthermore, we also tested whether there was any efficacy benefit to increasing the field strength above the 95% cell-line specific efficacy level or if 100% efficacy was only reached by using 1400V/cm. After 95% efficacy was reached, an efficacy plateau persisted for all tested cell lines. It was observed that even with the highest tested electric field strength (1400V/cm) there was a residual percentage of cells in all tested cell lines that did not form electropores (Figure 3.1).

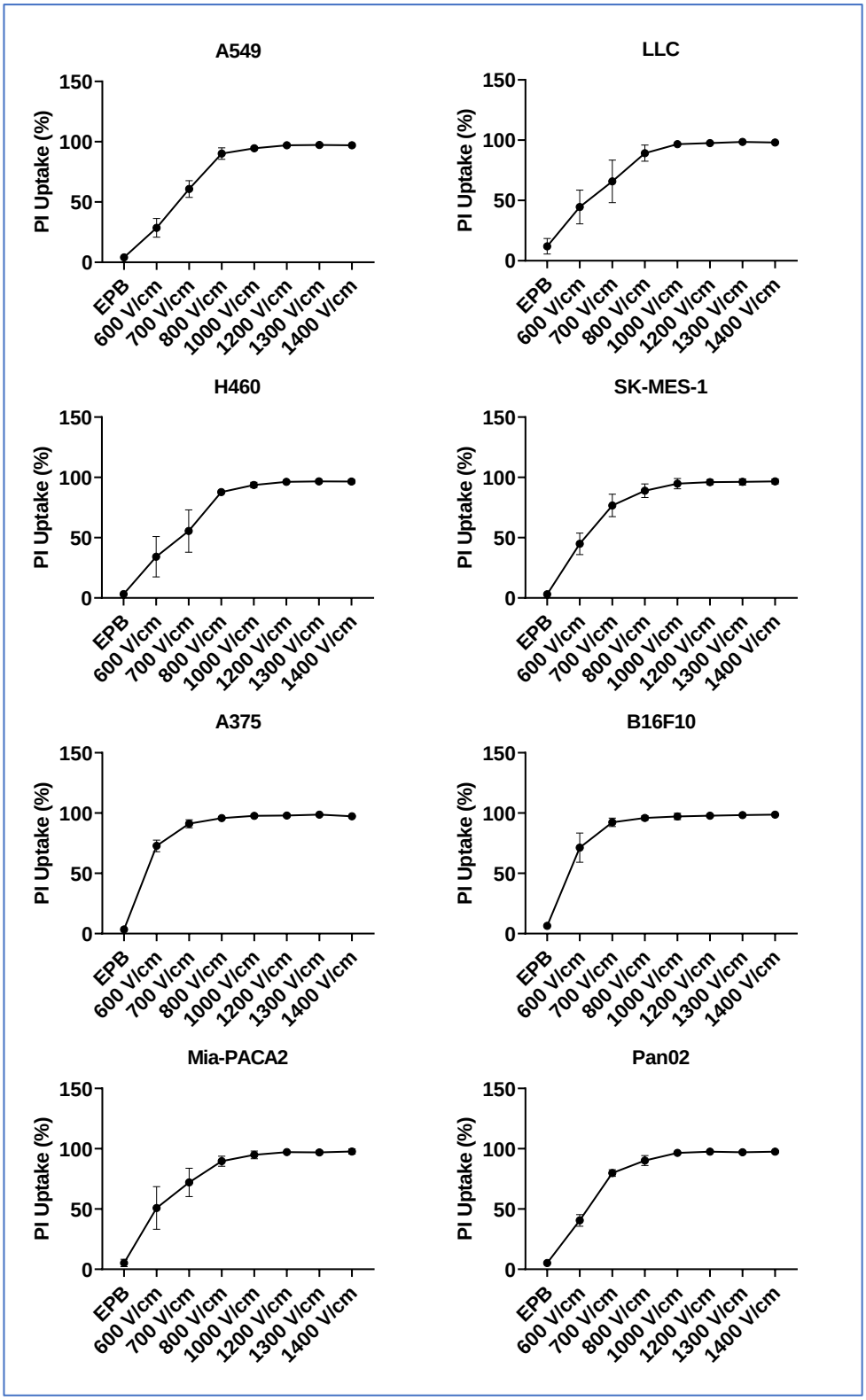


Figure 3.1: Efficacy of electroporation with various electric field strengths (600- 1400V/cm) in 8 different cancer cell lines (A549, LLC, H460, SK-MES 1, A375, B16F10, Mia-PACA2 and Pan02). PI was added into the EP cuvette prior to cells exposure to electroporation. Cells were analysed within 60 minutes of treatment by flow cytometry and gated appropriately for single cells and being PI positive.

3.4.2 Viability is barely impacted by tested electric field strengths

Having established optimal efficacy in terms of PI uptake, we next examined the viability of the cells within both one hour after the EP treatment (Direct Viability; Figure 3.2) and 24 hours post-treatment (Figure 3.3). A high level of viable cells (viability more than 85%) after EP treatment alone is required when determining the optimal EP parameter for ECT treatment, as the effectiveness of ECT is not based on the electric portion of the treatment, but rather on the pharmaceutical reactions of the cells to the chosen chemotherapeutic drug. Electroporation is only applied to facilitate the maximum possible uptake of the drug, preventing or circumventing any uptake related drug resistance. If a lower electric field strength results in the same treatment efficacy, adopting *in vivo* ESOPE-based ECT settings to account for this might lead to an even better safety profile of ECT. Overall, the impact of electroporation was observed to be more cell-line specific than voltage-dependant (Figures 3.2 and 3.3). The direct viability of some cell lines seems to be completely unaffected (A549, H460, SK-MES 1, A375, and Pan02), while other cell lines (LLC, Mia-PACA2 and B16F10) show some loss of direct viability (Figure 3.2). Only the B16F10 cell line shows a clear downward trend in viability with increased electric field strength, starting at 1200V/cm in the direct viability measurement, while all other cell lines stay at a constantly high level of viability. Overall, all cell lines, in all tested conditions, are reasonably viable; generally, viability was greater than 90%. 24 hours post-treatment viability seems to reflect the same trends as direct viability, with overall a slightly lower percentage of viable cells (Figure 3.3).

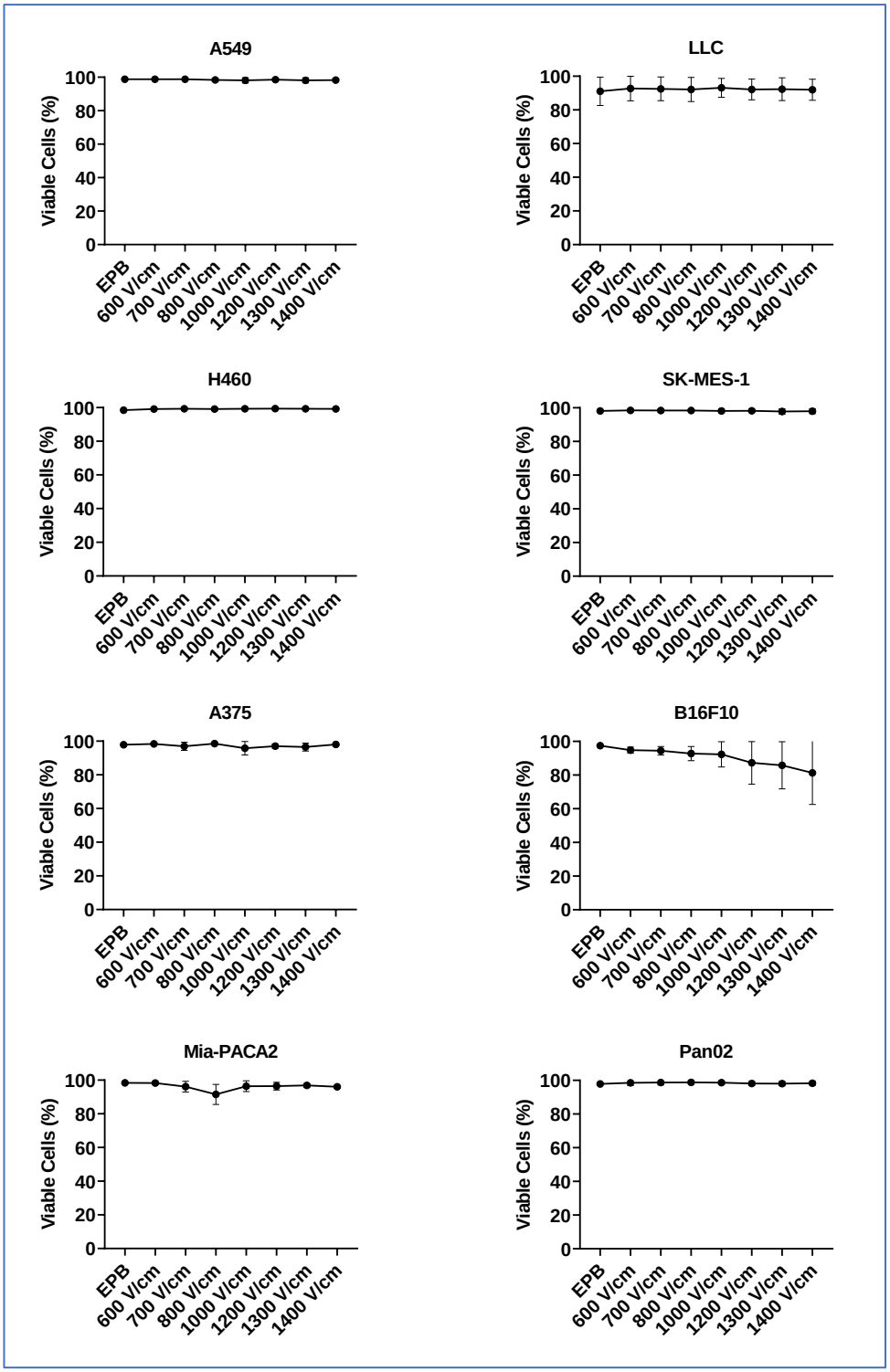


Figure 3.2: Viability within 60 minutes of treatment is largely unaffected by all tested field strengths for all cell lines. Direct Viability (within 60 minutes of treatment) was assessed for A549, LLC, H460, SK-MES 1, A375, B16F10, Mia-PACA2 and Pan02 following EP treatment. Following electroporation with various electric field strengths (600- 1400V/cm), cells were rested for 30 minutes at 37°C and analysed by flow cytometry, PI was added into the cell supernatants prior to analysis. Cells were gated appropriately for single cells and PI negativity.

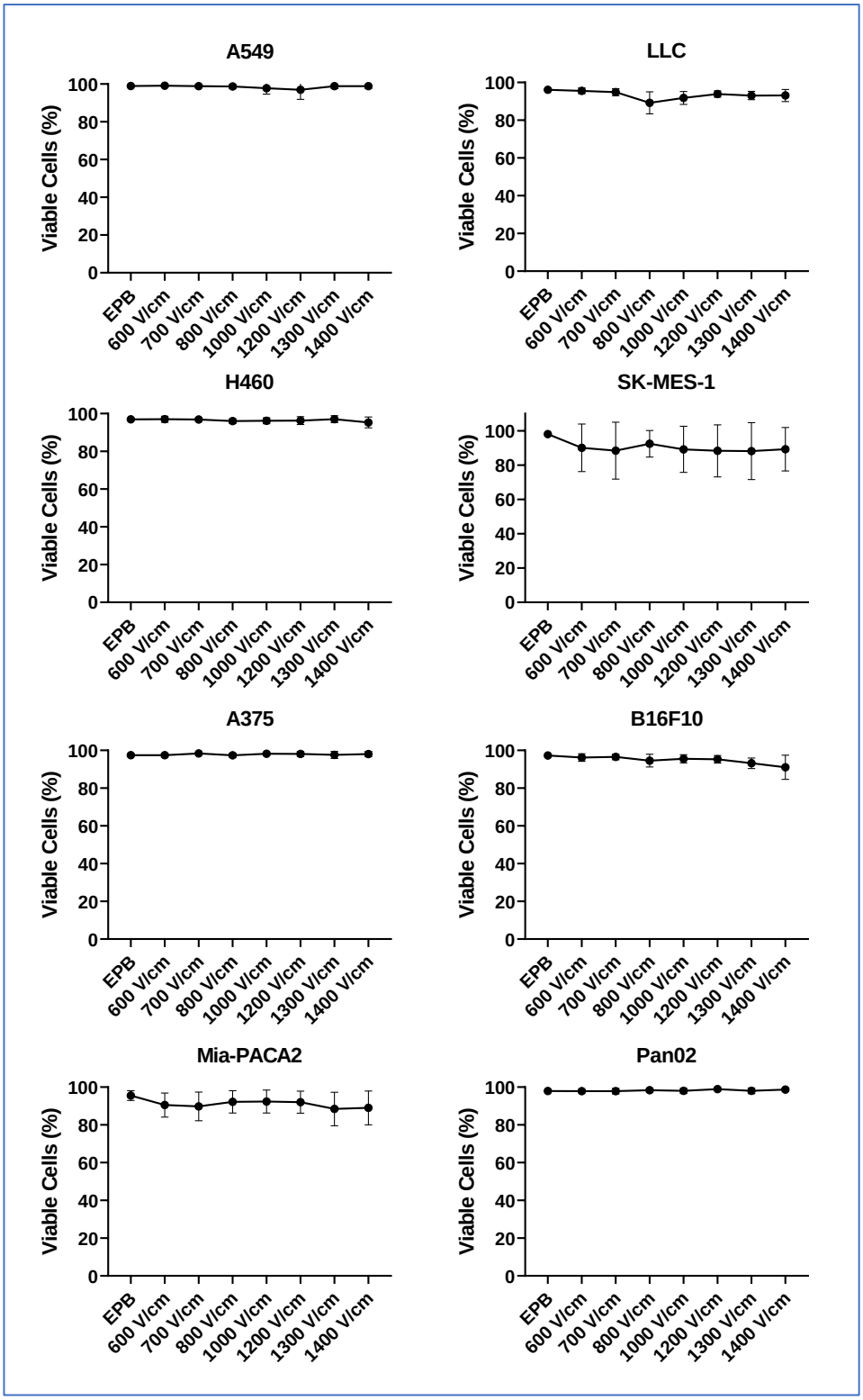


Figure 3.3: Viability 24 hours post treatment is largely unaffected by all tested field strengths. 24 hours viability was assessed for A549, LLC, H460, SK-MES 1, A375, B16F10, Mia-PACA2 and Pan02 following EP treatment. Following electroporation with various electric field strengths (600- 1400V/cm), cells were incubated overnight at 37°C and analysed by flow cytometry, PI was added into the cell supernatants prior to analysis. Cells were gated appropriately for single cells and PI negativity.

3.4.3 Metabolic activity is impacted in a cell-line and electric field strength dependent manner

In addition to assessing efficacy and viability, the metabolic activity of the cell lines 24 hours post-treatment was tested to determine what percentage of viable cells remained metabolically active after EP treatment and therefore able to continue to grow. Only actively growing cells can be impacted by the commonly used ECT drugs bleomycin and cisplatin, as both drugs interact with the cell cycle. In addition, senescence cells will show up as viable cells in the previous assays, while they are unable to continue to grow, thus determining the metabolic activity of the cells post-treatment will give a more precise picture of their future growth potential.

Metabolic activity, as determined by MTT assay, was significantly decreased in the A549, H460, A375, SK-MES 1 and B16F10 cell lines at various electric field strengths (Figure 3.4). While the viability of both the Mia-PACA2 and B16F10 cell lines was most impacted by EP treatment (Figure 3.3), only treatment with the highest tested electric field strengths (1400V/cm) significantly decreased the metabolic activity of the B16F10 cell line ($p \leq 0.05$) and had no impact on the Mia-PACA2 cell line. In contrast, while the viability of H460 had not been observed to be impacted by any tested electric field strength, the metabolic activity of this cell line was significantly reduced for all tested field strength above 800V/cm ($p \leq 0.05$) (Figure 3.4). Similarly, the metabolic activity of the SK-MES 1 cell line was significantly impacted above 1200V/cm ($p \leq 0.05$) (Figure 3.4). Electric field strengths of equal or higher than 800V/cm for both A375 and A549 cell lines also significantly decreased metabolic cell activity ($p \leq 0.05$). Neither LLC nor Pan02 cells' metabolic activity was significantly impacted at any tested electric field strength (Figure 3.4). Once a plateau of significantly decreased metabolic activity was reached, increases in the electric field strength did not decrease the metabolic activity further.

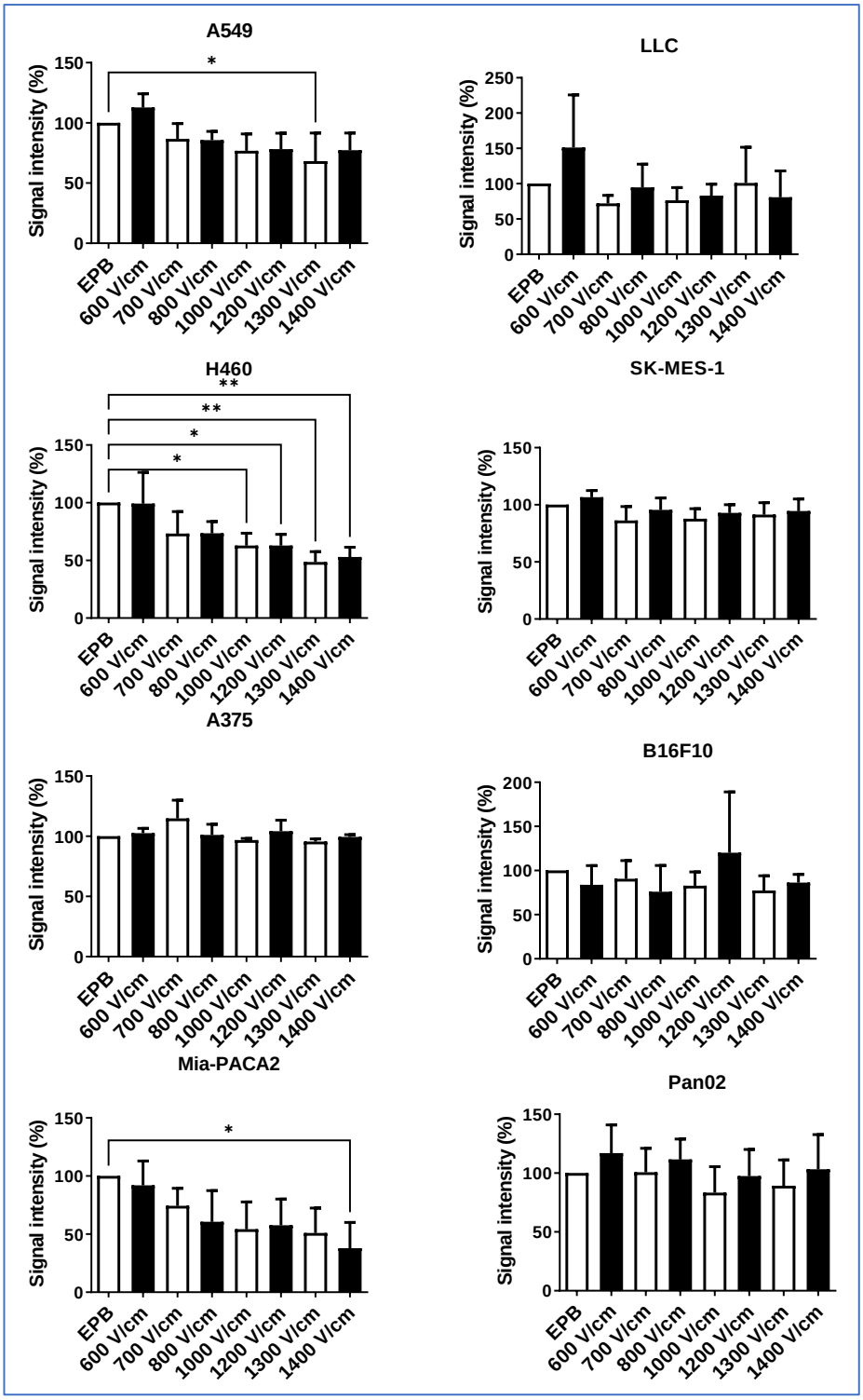


*Figure 3.4: Metabolic activity of A549, LLC, H460, SK-MES 1, A375, B16F10, Mia-PACA2 and Pan02 24 hours post EP treatment. Cells were subjected to electroporation with various electric field strengths (600- 1400V/cm) and plated in 12-well plates. 24 hours post-treatment metabolic activity was determined by MTT assay. Graphs show signal intensity of the wells reflecting metabolic activity normalized to the control group (EPB), an equal number of cells were plated in the wells. Data represents the mean ± SD. *p≤0.05, **p≤0.01, and ***p≤0.001 compared to untreated.*

3.4.4 Recovery is impacted in a cell-line and electric field strength dependent manner

Cell recovery assays were also performed to ascertain the effects of EP treatment on cancer cell line survival and the ability of surviving cells to recover following treatment (Figure 3.5). Cell recovery was only significantly impacted in the A549, H460 and Mia-PACA2 cell lines. Recovery was significantly reduced in A549 cell line for electric field strength at 1300V/cm ($p \leq 0.05$). For Mia-PACA2 cell lines recovery was significantly impacted only at the highest used electric field strength of 1400V/cm ($p \leq 0.05$), in contrast to their metabolic activity which was not impacted by any tested condition (Figure 3.4). Recovery for H460 cell line was significantly ($p \leq 0.05$) reduced above 1000V/cm (Figure 3.5).

Of note, across all tested cell lines, one or more tested electric field strength seems to slightly increase the recovery potential of the treated cell lines, for example B16F10 at 1200V/cm or LLC at 600V/cm.

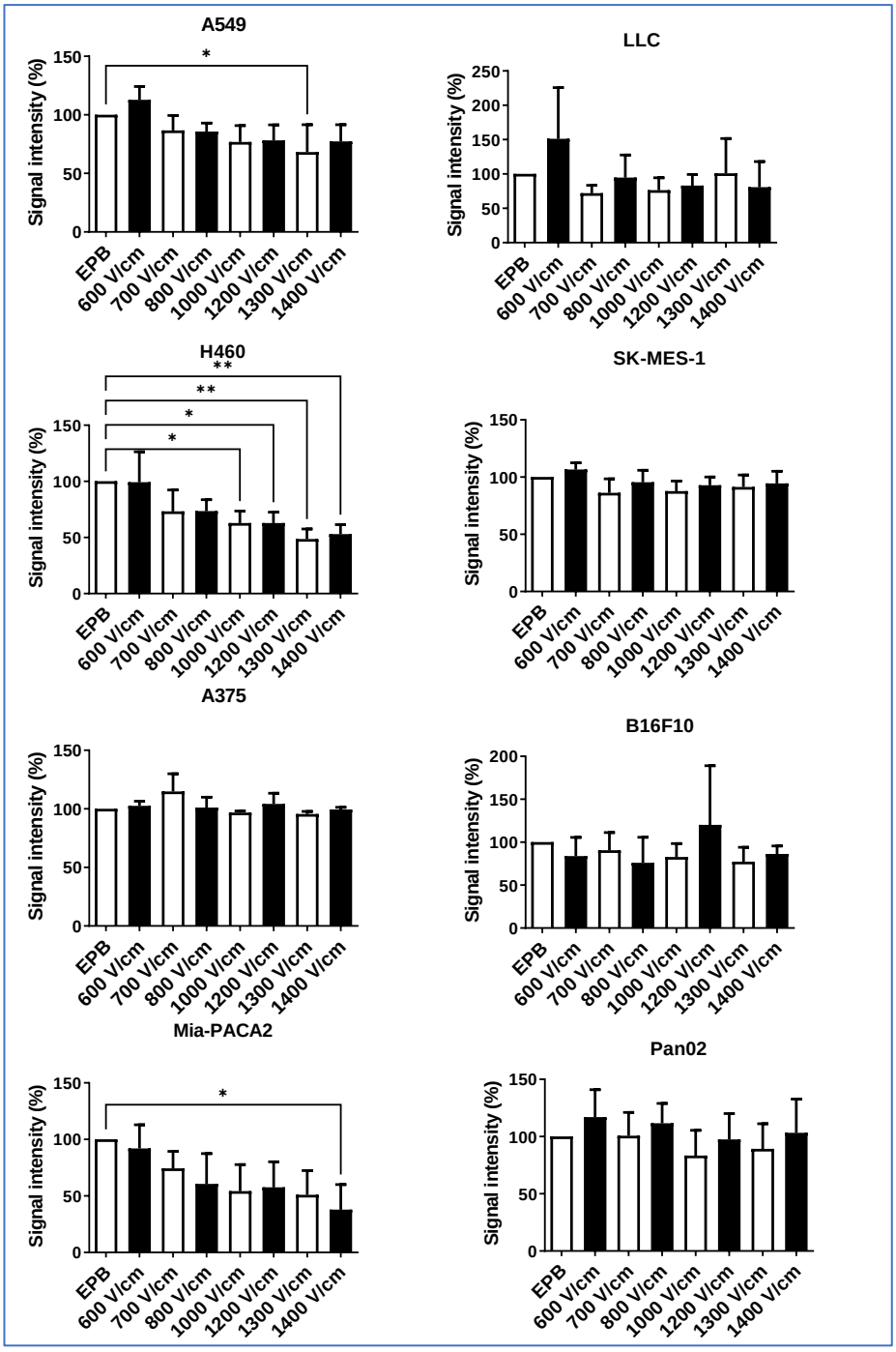


*Figure 3.5. Recovery of A549, LLC, H460, SK-MES 1, A375, B16F10, Mia-PACA2 and Pan02 following EP treatment as assessed by colony-formation assay. Cells were subjected to electroporation with various electric field strengths (600- 1400V/cm). After resting for 20-30 minutes a standardized number of cells per cell line were seeded in complete media specific to each cell line for 7-21 days. Formed colonies were fixed and stained, and the staining intensity was measured by the CLx imaging system. The signal intensities of the wells reflect the number and size of the formed colonies normalized to the control group (EPB). The graph shows signalling intensity normalized per cell line to the control treatment (EPB). Data represents the mean ± SD. *p≤0.05 and **p≤0.01 compared to untreated.*

3.4.5 With the exception of the LLC cell line all other tested cell lines have optimal electric field strength below the typically used ESOPE-based 1300V/cm

After determining the cell-line specific 95% efficacy threshold (Figure 3.1) post EP treatment as well as the impact of the different electric field strengths on direct (Figure 3.2) and 24 hours (Figure 3.3) viability, metabolic activity (Figure 3.4) and recovery potential (Figure 3.5), we next combined these 5 different outcomes to determine the optimal electric field strength per tested cell line (Figure 3.6). The optimal electric field strength as designed to be the minimum needed electric field strength that has at least 95% efficacy with the lowest possible detrimental effect on cell viability, metabolic activity, and recovery for *in vitro* research while keeping with the ESOPE parameters for the prescribed number of pulses, pulse duration and pulse frequency is as follows for the tested cell lines: 800V/cm is the optimal electric field strength for A549, H460, SK-MES 1, and Pan02 cell lines, while 700V/cm is optimal for A375, Mia-PACA2 and B16F10 cell lines, and 1300V/cm is optimal for the LLC cell line (Figure 3.6). With the exception of the LLC cell line, the optimal EP settings for *in vitro* experiments was determined to be lower than is customary in current research for ESOPE related parameters.

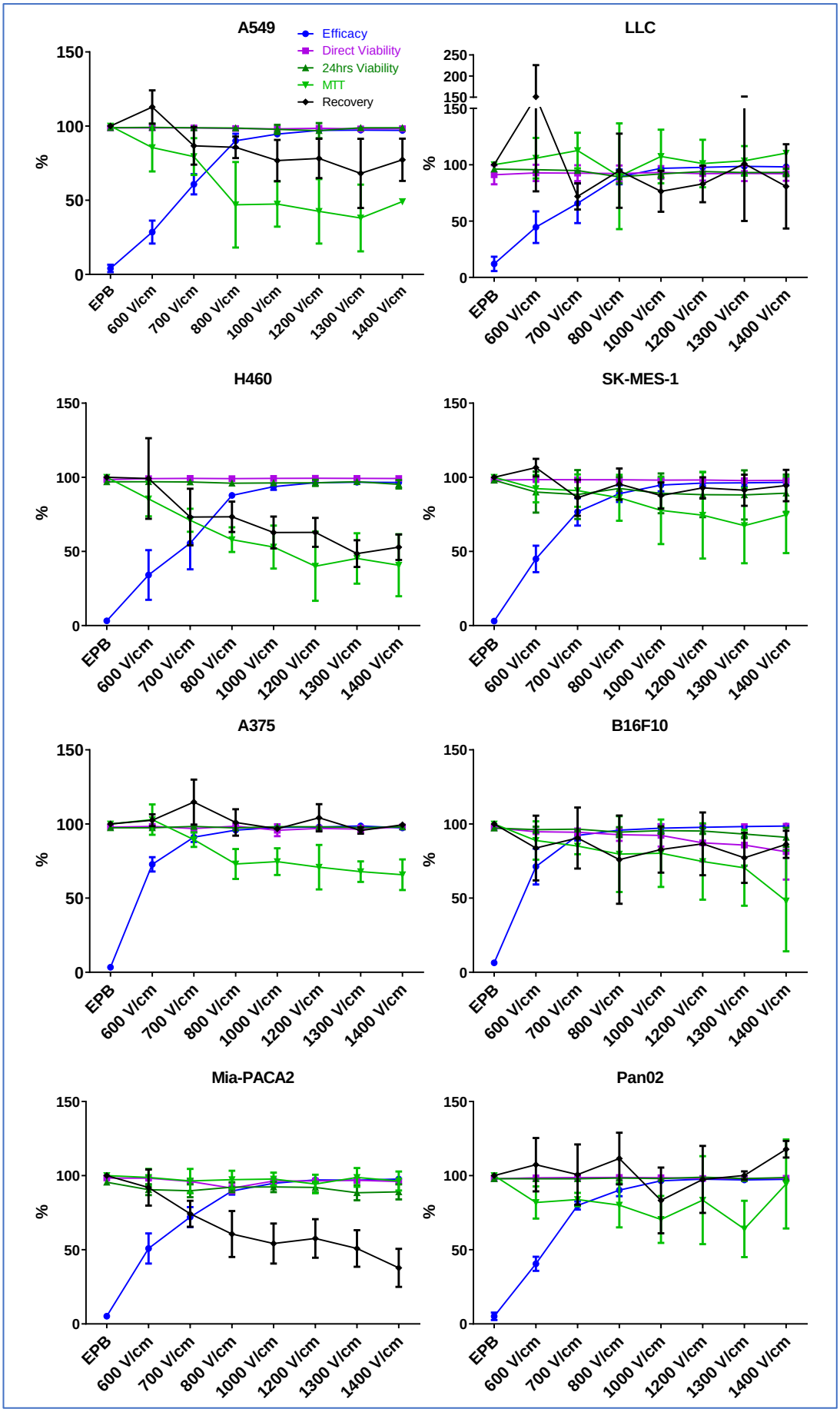

A549
Efficacy
Direct Viability
24hrs Viability
MTT
Recovery
LLC
H460
SK-MES-1
A375
B16F10
Mia-PACA2
Pan02
%
150
100
50
0
250
200
EPB
600 V/cm
700 V/cm
800 V/cm
1000 V/cm
1200 V/cm
1300 V/cm
1400 V/cm

Figure 3.6: Efficacy, Viability, metabolic activity and recovery measurements of A549, LLC, H460, SK-MES 1, A375, B16F10, Mia-PACA2 and Pan02 following EP treatment between 600V/cm and 1400V/cm were combined to determine optimal cell-line specific electric field strength. Based on the tested parameters, optimal EP settings are as followed: 800V/cm for A549, H460, SK-MES-1, Pan02, 700V/cm for A375, MiaPACA2 and B16F10, and 1300V/cm for LLC.

3.5 Discussion and Conclusions

In this chapter, we determined the effect of various electric field strengths on cell viability, metabolic activity, and recovery for various adherent cancer cell lines in *in vitro* single cell suspensions, while keeping all other ESOPE parameters constant. The overarching aim of these experiments was to determine the optimal electric field strength for *in vitro* ECT-related experiments. Our findings shown here demonstrate that the optimal EP settings are 800V/cm for A549, H460, SK-MES 1 and Pan02 cell lines, 700V/cm for A375, Mia-PACA2 and B16F10 cell lines, and 1300V/cm for LLC cell line. This indicates that different cell lines have lower optimal electric field strength requirements than the typically used 1300V/cm within the ESOPE cell-based protocols[17–19].

Likewise, Vera-Tizatl *et al.*[20] showed for three breast-cancer cell lines (BT-20, MCF-7 and HCC1419), that these cell lines would be reversibly permeabilized between 250V/cm and 625V/cm when in suspension and between 228V/cm and 415V/cm when adherent. The BT-20 and HCC1419 cells were observed to have very similar parameters, for being reversibly electroporated both when in suspension as well as adherent, whilst the MCF-7 cells required a higher electric field strength when in suspension (625V/cm) compared to when the cells were adherent (415V/cm)[20]. These data indicate that the suspension status alone can alter the needed electric field strength, in addition to cell-line specific electroporation parameters.

Data shown in this chapter clearly indicate that there are clear cell line specific responses for all parameters examined. As such, there does not seem to be a rationale to use a sole electroporation setting for all bench-side research independent of cell type, “suspension status”, cell density or buffers used. Depending on the above variables, the same electroporation setting might have very different effects per cell line or type in regard to cell viability, metabolic activity or recovery potential. Previously, our group has shown that most cell lines electroporated at 1300V/cm had their viability too significantly decreased to be useful for further experiments, and therefore our laboratory group undertook the task of optimizing electroporation parameters for reversible electroporation treatments and used

those settings to evaluate the effectiveness of these treatments[7,16]. Thus, we recommend that any *in vitro* EP-based experiments start with the optimization of the EP parameter before undertaking any further exploration.

Various other groups have published bench-side research with varying electroporation parameters for electroporation-based treatments. The electroporation parameters were optimized by the authors in these reports, but not all papers stated how they were optimized, with none of these manuscripts explicitly outlining which assays were used to determine the optimized electroporation parameter[17,21]. In contrast, other reports have chosen electroporation parameters that were either based on the clinically used 1000V/cm[4] for spheroid models or based on the adapted ESOPE parameter of 1300V/cm for cell work[18], with these studies not performing in-depth analyses on the effect of the parameters on cell viability, metabolic activity or recovery. Frandsen *et al.* optimized DC-3F (transformed Chinese hamster lung fibroblast cell line) and K562 (human leukaemia cell line) to 1200V/cm and LLCs to 1400V/cm, while keeping the other ESOPE parameters, and stated that these electric field strength were optimized for high permeabilization and low cellular death[17]. Their optimized parameter for LLC cells is just slightly higher than what we optimized, with this difference possibly being due to the higher cell density used ($6.1x10^6$ cells/mL) and the lowered temperature (8°C) at which the experiments were performed at. Overall, their optimized parameters do not differ remarkably from the ESOPE adapted 1300V/cm to be used for *in vitro* work. In contrast, Griseti *et al.* optimized 600V/cm while keeping the other ESOPE parameters for Human multicellular tumour spheroids at room temperature[21] as 800V/cm was observed to decrease the spheroid growth rate slightly, thereby lowering the needed electric field strength notably compared to the 1000V/cm ESOPE parameter. These results showcase the importance of examining all parameters, as in addition to suspension status, cell density, or potentially spheroid size, and the experimental temperature impacts the optimal electric field strength as well.

It is important that *in vitro* experiments from different groups within the pre-clinical ESOPE community become more comparable, as such alignment will allow for a fast-

moving translation of *in vitro* findings into the clinic. By providing a framework on how to judge the impact of ESOPE electroporation on a given cancer cell line, it may be possible to extrapolate findings at different parameters for comparable cancer cell lines. This would allow for a more comprehensive understanding of electroporation-based effects on cancer cell lines. Also, by utilizing a universal approach in determining optimal electroporation parameters, it will be easier to compare cell-based work and transfer results between various cell lines as this field progresses, as well as test emerging concepts more efficiently.

Overall, our results show that a lower electric field strength, while keeping all other ESOPE parameters, is as effective as a higher electric field strength, with a cell-line specific minimum required field strength, while also assuring cell viability and recovery. Future work could focus on determining whether there are different molecular or metabolic changes when cancer cells are electroporated at lower field strengths and if there are some possible advantageous changes similar to the one observed for immune cells with CaEP[16]. In addition, the proposed protocol could be tested and, as needed, adapted to be also able to determine optimal electric field strength for adherent cells, immune cells or cells inside a spheroid, allowing for a comprehensive understanding of the impact of the electric field on various cells in different set-ups. Adapting the proposed standardized protocol for adherent cell lines electroporated in cell culture plate wells would have the benefit of observing adherent cell lines in their more natural state of being stretched out and connected to each other rather than being trypsinized, becoming rounded and being in suspension, as they are here in our proposed protocol. Furthermore, it would also be interesting to determine whether there are any underlying cell properties that make cells more or less susceptible to electroporation. For example, for the same cancer type, human cell lines seem to be more susceptible to electroporation than murine cell lines. The human A549 lung cancer cell line has an optimal electric field strength of 800V/cm while the murine LLC lung cancer cell line as an optimal electric field strength of 1300V/cm, according to our results. Moreover, the differential impact of electroporation between the short- and long-term is currently unclear and understanding the mechanism behind this difference could allow further fine-tuning

of ECT treatments. Krysztofiak *et al.* showed in a mathematical model that cancer cell irradiation leads to a mitochondrial shutdown in parallel with a rapid downregulation of glycolytic activity, but these initial responses were reconstituted in a time-dependent manner[22]. Potentially, EP might lead to similar changes as irradiation in the cancer cells, explaining the difference between metabolic activity one day post-treatment and recovery potential in the following 10-21 days.

Finally, here we have introduced a comprehensive standardizable protocol to test the optimal electric field strengths for adherent cancer cell lines. The protocol has the potential for adaptation to test optimal field strength for non-adherent cell lines by changing some of the read-out assays. By using a standardized approach, we eliminate differences in results based on cell density, buffers used, temperature and utilized assays including their timing. This should allow future studies to be compared more easily with each other and reduce potential issues for translating research findings between different cancer cell lines. Accepted standardization of these protocols could allow for bench research to be easily translated into pre-clinical and clinical studies, hopefully reducing negative or ambiguous study results. It should make the translation pipeline work faster as a wider range of studies can be utilized to inform study design decisions. Furthermore, as our proposed assays combine two short-term (<2 hours and 24 hours) and long-term (7-21 days) effects to define the optimal voltage to be used for a cell-line, we should gain a clearer picture of how cancer cells will react in clinical situations. For example, metabolic activity was in part significantly decreased compared to the control situation 24 hours post-electroporation, but that decrease was not necessarily echoed in the ability of the cancer cells to recover. Therefore, by just observing short-term effects to determine the optimal electroporation settings we might overestimate its effectiveness.

3.6 References

1. Mir LM, Belehradek M, Domenge C, Orlowski S, Poddevin B, Belehradek J Jr, Schwaab G, Luboinski B, P. C. L. Electrochemotherapy, a novel antitumor treatment - 1st clinical-trial. *COMPTES RENDUS L Acad. DES Sci. Ser. III-SCIENCES LA VIE-LIFE Sci.* **313**, 613–618 (1991).
2. Yarmush, M. L., Golberg, A., Serša, G., Kotnik, T. & Miklavčič, D. Electroporation-Based Technologies for Medicine: Principles, Applications, and Challenges. *Annu. Rev. Biomed. Eng.* **16**, 295–320 (2014).
3. Miklavčič, D. *et al.* Electrochemotherapy: Technological advancements for efficient electroporation-based treatment of internal tumors. *Med. Biol. Eng. Comput.* **50**, 1213–1225 (2012).
4. Frandsen, S. K., Gibot, L., Madi, M., Gehl, J. & Rols, M. P. Calcium electroporation: Evidence for differential effects in normal and malignant cell lines, evaluated in a 3D spheroid model. *PLoS One* **10**, 1–11 (2015).
5. Szewczyk, A. *et al.* Calcium electroporation for treatment of sarcoma in preclinical studies. *Oncotarget* **9**, 11604–11618 (2018).
6. Marty, M. *et al.* Electrochemotherapy - An easy, highly effective and safe treatment of cutaneous and subcutaneous metastases: Results of ESOPE (European Standard Operating Procedures of Electrochemotherapy) study. *Eur. J. Cancer, Suppl.* **4**, 3–13 (2006).
7. Tremble, L. F., O'Brien, M. A., Soden, D. M. & Forde, P. F. Electrochemotherapy with cisplatin increases survival and induces immunogenic responses in murine models of lung cancer and colorectal cancer. *Cancer Lett.* **442**, 475–482 (2019).
8. Gehl, J. *et al.* Electrochemotherapy in the treatment of metastatic malignant melanoma : a prospective cohort study by InspECT. *Br. J. Dermatol.* **176**, 1475–1485 (2017).
9. Falk, H. *et al.* Calcium electroporation induces tumor eradication, long-lasting immunity and cytokine responses in the CT26 colon cancer mouse model. *Oncoimmunology* **6**, 1–8 (2017).
10. Staresinic, B. *et al.* Effect of calcium electroporation on tumour vasculature. *Sci. Rep.* **8**, 1–14 (2018).

11. Gehl, J., Skovsgaard, T. & Mir, L. M. Vascular reactions to in vivo electroporation: Characterization and consequences for drug and gene delivery. *Biochim. Biophys. Acta - Gen. Subj.* **1569**, 51–58 (2002).
12. Gehl, J. *et al.* Updated standard operating procedures for electrochemotherapy of cutaneous tumours and skin metastases. *Acta Oncol. (Madr).* **57**, 874–882 (2018).
13. Mali, B., Jarm, T., Snoj, M., Sersa, G. & Miklavcic, D. Antitumor effectiveness of electrochemotherapy: A systematic review and meta-analysis. *Eur. J. Surg. Oncol.* **39**, 4–16 (2013).
14. Kiełbik, A., Szlasa, W., Saczko, J. & Kulbacka, J. Electroporation-based treatments in urology. *Cancers (Basel).* **12**, 1–26 (2020).
15. Plaschke, C. C. *et al.* European Research on Electrochemotherapy in Head and Neck Cancer (EURECA) project: Results from the treatment of mucosal cancers. *Eur. J. Cancer* **87**, 172–181 (2017).
16. Tremble, L. F., Heffron, C. C. B. B. & Forde, P. F. The effect of calcium electroporation on viability, phenotype and function of melanoma conditioned macrophages. *Sci. Rep.* **10**, 1–12 (2020).
17. Frandsen, S. K., Gissel, H., Hojman, P., Eriksen, J. & Gehl, J. Calcium electroporation in three cell lines: A comparison of bleomycin and calcium, calcium compounds, and pulsing conditions. *Biochim. Biophys. Acta - Gen. Subj.* **1840**, 1204–1208 (2014).
18. Ursic, K. *et al.* Comparable effectiveness and immunomodulatory actions of oxaliplatin and cisplatin in electrochemotherapy of murine melanoma. *Bioelectrochemistry* **119**, 161–171 (2018).
19. Mlakar, V., Todorovic, V., Cemazar, M., Glavac, D. & Sersa, G. Electric pulses used in electrochemotherapy and electrogene therapy do not significantly change the expression profile of genes involved in the development of cancer in malignant melanoma cells. *BMC Cancer* **9**, 299 (2009).
20. Vera-Tizatl, C. E. *et al.* Cell morphology impact on the set-up of electroporation protocols for in-suspension and adhered breast cancer cells. *Electromagn. Biol. Med.* **39**, 323–339 (2020).
21. Griseti, E. *et al.* Pulsed Electric Field Treatment Enhances the Cytotoxicity of

Plasma-Activated Liquids in a Three-Dimensional Human Colorectal Cancer Cell Model. *Sci. Rep.* **9**, 1–15 (2019).

22. Krysztofiak, A. *et al.* Metabolism of cancer cells commonly responds to irradiation by a transient early mitochondrial shutdown. *iScience* **24**, 103366 (2021).

Chapter 4

Defining optimal parameters to maximize the effect of electrochemotherapy on lung cancer cells whilst preserving integrity of immune cells.

Sections from this chapter have been published in Bioelectrochemistry as:

Bendix, M. B., Houston, A., Forde, P. F., & Brint, E. (2022). Defining optimal parameters to maximize the effect of electrochemotherapy on lung cancer cells whilst preserving the integrity of immune cells. Bioelectrochemistry, *148*. https://doi.org/10.1016/j.bioelechem.2022.108257

4.1 Abstract

Electrochemotherapy (ECT) is becoming an established therapy for melanoma and is under investigation for application in additional cancer types. One potential cancer type that may benefit from ECT is lung cancer, as current lung cancer treatments are still not able to deliver long-lasting positive outcomes for the patients.

The impact of ECT on three human lung cancer cell lines (A549, H460, SK-MES-1), one murine cell line (Lewis lung carcinoma; LLC) and the impact of electroporation and ECT on three murine primary immune cell types (T cells, dendritic cells and macrophages) was examined. The viability, metabolic activity and recovery potential post-treatment of all cell types was determined to evaluate the potential utility of ECT as a lung cancer treatment. Our findings demonstrate that cisplatin at 11µM would be the suggested drug of choice when using ECT for lung cancer treatment. Additionally, the effectiveness of calcium electroporation (the use of calcium instead of a chemotherapeutic drug) was tested in the A549 and LLC cell lines. However, calcium concentrations up to 5mM was not observed to have any significant impact on the metabolic activity and recovery potential of A549 and LLC cell lines.

Given the increasingly understood importance of the immune system in lung cancer, within this context, we have also examined the impact of ECT on immune cell populations that may facilitate the anti-cancer immune response. Our study shows that T cells are not impacted by any tested condition, whilst dendritic cells and macrophages are significantly negatively impacted by electric field strength surpassing 800V/cm *in vitro*. Our attempt at testing the effectiveness of ECT at 800V/cm failed in an *in vivo* murine lung cancer model. Therefore, current ECT protocols (using 1000V/cm *in vivo*) still need to be further investigated regarding their impact on the immune cells and potentially protocols need to be adapted to improve viability of the immune cell population, thus improving therapy outcomes.

4.2 Introduction

Lung cancer is the fourth most common cancer worldwide and is the leading cause of cancer-related death. The two major forms of lung cancer are non–small cell lung cancer (NSCLC), predominantly comprising squamous cell carcinoma and adenocarcinoma, which account for about 85% of all lung cancers, and small cell lung cancer (SCLC), which accounts for about 15% of cases. Whilst treatment options include surgery, chemotherapy, radiotherapy and targeted therapy, the majority of cases are diagnosed at an advanced stage and have a very poor prognosis, with a 5-year survival rate of just 15%[1]. Lung cancer shows marked resistance to conventional forms of chemotherapy[2]. Moreover, despite advances in the field of cancer immunotherapy, in particular immune checkpoint inhibitors such as PD-1/PD-L1 inhibitors, beneficial disease prognosis remains low[3], highlighting the need for novel therapies for lung cancer patients. New treatment options for lung cancer should ideally have low side-effects, preserve as much healthy tissue as possible and should not induce treatment-resistance in the cancer cells, allowing for re-treatment if needed.

Electrochemotherapy (ECT) has been investigated for the treatment of solid tumour cancers over the past three decades[4], and could potentially also be applied to lung cancer. ECT combines the local delivery of non-ablative electrical pulses to the tumour tissue, called electroporation (EP), in combination with administration of a chemotherapy drug [5,6]. While cell membranes, being a physical barrier, prevent the entry of molecules including anti-cancer drugs, the application of several, brief electric pulses facilitate the formation of pores in the cell membrane, allowing the free influx of molecules, including locally present chemotherapy drugs. As the pore formation is electro-mechanical based, ECT can overcome the resistance to drug entry and re-treatment[7–9]. When exploring ECT for novel use in different tumour types, it is important to consider which chemotherapy drug would be optimal. Bleomycin is the most commonly administered chemotherapy drug combined with ECT, as ECT increases the cellular uptake by up to 300-fold for bleomycin[8]. However, bleomycin is not the ideal drug for lung cancer treatments as bleomycin is known to reduce lung capacity[10]. Therefore, an alternative chemotherapeutic drug is needed

for ECT-based lung cancer treatment. Platinum based chemotherapy drugs (for example cisplatin and oxaliplatin) are the standard drugs used in traditional chemotherapy for lung cancer treatment[11], and as such, these chemotherapy drugs be optimal for dosing with ECT in the context of lung cancer. Additionally, while bleomycin is typically administered systemically for ECT treatment, cisplatin is administered intratumorally, which makes the therapy more targeted to the tumour area. Intratumoral administration of the chosen drugs allows for a better determination and fine-tuning of the local drug concentration than with systemic drug administration[5,6]. Next to the targeted cancer cells, ECT can also impact any other cells present within the treatment area, of which the immune cells are the most relevant for any local and systemic immune response post treatment.

Whilst the effect of ECT on tumour cells has been thoroughly interrogated, the effect of EP and ECT on immune cells is largely uncharacterised. As the role of the immune system in lung cancer rejection and/or progression is now well established[12], it is of significant interest to understand the interplay between ECT and the immune system when investigating optimal conditions for use of ECT in the context of lung cancer. Additionally, while ECT leads to immunogenic cell death[13,14], which in turn should activate an immune reaction, enhancing systemic and abscopal effects post-treatment, this has not been observed consistently in either human or murine studies[14]. Thus far it is known that a single ECT treatment is only effective in immune competent mice and, in particular, that T cells are responsible for the local effect of the ECT treatment[13,15–18]. Furthermore, the immune cell population changes its composition following ECT treatment[16,19–22] (Table 1.1), but the direct effects of ECT on immune cells regarding their viability and functionality is still unknown. Considering that lung cancer is typically diagnosed after the disease has already spread[1], it is of particular importance for the application of ECT in the lung cancer context to create and sustain an immune response that is capable of responding to metastatic cells.

The aim of this chapter is to evaluate the effect of ECT on lung cancer cell lines in suspension, with platinum-based drugs. We measured tumour cell recovery and

metabolic activity post-treatment in a range of human and murine cell lines to determine the efficacy of ECT as a lung cancer treatment. Additionally, we determined the impact of electroporation and ECT on different primary immune cells *in vitro* in order to establish potential parameters to improve ECT treatment protocols to optimize abscopal effects post-treatment. Finally, we also tested ECT at 800V/cm against ECT at 1300V/cm in an *in vivo* murine lung cancer model to attempt to further investigate our *in vitro* findings.

4.3 Materials & Methods:

4.3.1 Cell Culturing Cancer Cell Lines

Lewis-Lung Carcinoma (LLC), H460, A549 and SK-MES-1 were obtained from the American Type Culture Collection (ATCC). A549 and H460 cell lines were maintained in RMPI 1640 medium, supplemented with 10% foetal bovine serum (FBS) (Sigma-Aldrich, St. Louis, USA), 50 I.U/mL penicillin and 50 µg/mL streptomycin (Sigma-Aldrich). LLC cell line was maintained in Dulbecco's Modified Eagle Medium (DMEM), supplemented with 10% FBS, 50 IU/mL penicillin and 50 µg/mL streptomycin. SK-MES-1 cell line was maintained in DMEM supplemented with 20% FBS, 50 IU/mL penicillin and 50 µg/mL streptomycin. Cell lines were incubated at 37 °C in a humidified incubator with 5% CO_2 and were split at 70-90% confluency. All tested cell lines are adherent cells, which were detached prior to the experiments using a trypsin-ethylenediaminetetraacetic acid (EDTA) solution (Sigma).

4.3.2 Human Monocyte-derived Dendritic Cells

Peripheral blood mononuclear cells (PBMCs) were isolated from buffy coats of healthy individuals and differentiated into monocyte-derived dendritic cells (DCs) in 6 days. PBMCs were purified on a Lymphoprep (Stemcell Technologies, Vancouver, canada) -gradient by centrifugation and culturing for one hour at 37 °C in a humidified incubator with 5% CO_2 to kill any remaining red blood cells. The adherent cells after this step were then cultured for 6 days at 37 °C in a humidified incubator with 5% CO_2 in the presence of 450 U/ml GM-CSF (granulocyte macrophage colony-stimulating factor; Peprotech, London, UK) and 300 U/ml IL-4 (Peprotech) in complete RPMI-1640 medium supplemented with 10% heat-inactivated FBS (heated for 30 minutes at 60°C), 50 IU/mL penicillin and 50 µg/mL streptomycin. Adherent cells at 6 days of culturing are DCs like in phenotype and will be used for the human DC experiments.

4.3.3 Murine Bone marrow-derived Dendritic and Macrophage cell derivation

All mice were obtained from Envigo (Bicester, UK) and housed in the Bioscience Unit at University College Cork. Animals were 8-weeks old on arrival and only female

animals were used for any experiment. All animal husbandry and experimental procedures were approved and licensed by the Irish Health Products Regulatory Authority (HPRA).

Murine Bone marrow-derived cells were obtained from the back legs of healthy 8–20-week-old female C57BL6J mice (Envigo, Bicester, UK) by passing ice cold RPMI through the bones to obtain the bone marrow cells, which was then passed through 0.45µM cell strainer (BD, Falcon, Franklin Lakes, USA) to obtain the pure cells. Red blood cells were lysed with red blood cell lysis buffer (Biolegend, San Diego, USA) for 3 minutes on ice. Bone marrow cells were diluted at $1x10^6$ cells/mL in RPMI with 10% heat inactivated FBS, 50 IU/mL penicillin and 50 µg/mL streptomycin supplemented with 10ng/mL GM-CSF (Peprotech, London, UK) and 10ng/mL IL-4 (Peprotech). Cells were cultured at 4mL/well in 6 well plates for a total of 6 days 37 °C in a humidified incubator with 5% CO_2. Cells were split in half on day 2 and day 4. Non-adherent cells on day 6 were considered to be bone marrow-derived Dendritic cells (DCs) and adherent cells were considered bone marrow-derived macrophages (referred to as macrophages).

4.3.4 Murine T cell isolation

Spleen cells were obtained by passing the spleen of healthy 8–20-week-old female C57BL6J mice through a 0.45µM cell strainer (BD, Falcon) with cold PBS. For red blood cell lysis, all cell suspensions were treated with red blood cell lysis buffer (Biolegend) for 3 minutes on ice. T cells were isolated using the EasySep™ Mouse T Cell Isolation Kit (Stemcell Technologies, Vancouver, Canada) according to manufacturer's instructions (purity above 90% for whole CD3 T cells).

4.3.5 *In vitro* electroporation parameters

To test the impact of electroporation alone on several cell properties, $1×10^6$ cells (cell line and primary immune cells) were suspended in 400 µL of electroporation buffer (EPB; 10mM HEPES, 250mM Sucrose and 1mM $MgCl_2$ in ddH20) and aliquoted into sterile 4mm EP cuvettes (VWR, Pennsylvania, USA). Cuvettes were exposed to eight electric pulses with pulse duration of 100µs and 1Hz frequency (ESOPE parameters)

at electric field intensities of 600V/cm, 700V/cm, 800V/cm, 1000V/cm, 1200V/cm, 1300V/cm and 1400V/cm using a BTX ECM 2001 square wave electroporator (BTX, San Diego, USA). After the electroporation, cells were rested for 20-30 minutes at 37°C and 5% CO_2 before various assays were set-up, except for efficacy testing which was performed straight after the treatment.

4.3.6 *In vitro* ECT and CaEP parameters

To test the combined impact of electroporation and various drugs and calcium concentrations on the cell lines, 1×10^6 cells (cell line and primary immune cells) were suspended in 400 µL of either EPB alone or in EPB with 1µM, 5µM or 11µM respectively of cisplatin or oxaliplatin or alternatively in EPB with 0.5mM, 1mM, 2.5mM or 5mM calcium ($CaCl_2$ stock solution, Merck) respectively. Cell suspensions were aliquoted into sterile EP cuvettes (VWR). Cuvettes were exposed to eight electric pulses at cell line specific electric field intensities (A549, H460 and SK-MES-1: 800V/cm; LLC: 1300V/cm; Immune cells: 800V/cm, 1000V/cm and 1300V/cm), with pulse duration of 100 µs and 1 Hz frequency using a BTX ECM 2001 square wave electroporator (BTX, San Diego, USA). After the electroporation cells were rested for 20-30 minutes at 37°C and 5% CO_2 before various assays were set-up.

4.3.7 Efficacy Assay

To test the efficacy of electroporation with various electric field strength, propidium iodine (PI; Sigma) was added into the EP cuvettes before electroporation at a final concentration of 0.05mg/mL. Within 30 minutes of being electroporated, cells were analysed by flow cytometry. Flow cytometry was conducted using an LSRII machine with a 5-laser (355 /405 /488 /561 /640nm) configuration (Table 2.2) (BD Biosciences) and the results analysed employing FlowJo V10 (BD Biosciences).

4.3.8 Viability Assay

Viability of electroporated cells was tested within one hour of the treatment, and 4 and 24 hours post treatment depending on treatment and cell type. For the direct viability testing, 250,000 cells were transferred into FACS tubes, and immediately

before being analysed by flow cytometry, PI was added to the tubes. For the 4 hours viability assays, 250,000 cells were incubated at 37 °C in a humidified incubator with 5% CO_2 in sterile FACS tubes for 4 hours and for the 24 hours viability assay, 250,000 cells were plated and incubated for 24 hours at 37 °C in a humidified incubator with 5% CO_2. Adherent cell lines were trypsinized prior to analysis and macrophages were mechanically detached. Prior to being analysed by flow cytometry, PI was added into the FACS tube (Falcon).

4.3.9 MTT Assay

For the MTT assay, 100,000 cells were incubated for 4, 24, 72 and 120 hours, respectively depending on the treatment and cell type at 37 °C in a humidified incubator with 5% CO_2. After incubation, the cells were incubated with the MTT reagent (5 µg/mL final concentration; Abcam, Cambridge, UK) at 37 °C in a humidified incubator with 5% CO_2 for up to one hour. Formed formazan as an indicator of cell viability was solubilized by adding 1000µL DMSO into each well. The extent of formazan production was determined by a plate reader at 550nm, while 630nm served as the reference wavelength; each measurement was done in triplicate.

4.3.10 Cell Recovery Assay

Following treatment and resting, cells were seeded in triplicate in 6 well plates at a cell line specific concentration and incubated for 7-21 days at 37 °C in a humidified incubator with 5% CO_2 until the untreated control contained visible colonies. H460 and A549 cell lines were plated at 400 cells/well, LLC cell line was plated at 800 cells/well and SK-MES-1 cell line was plated at 6.000 cells/well.

For visualization of the colonies, the supernatant was discarded, cells were fixed in methanol for 10 minutes and then stained in Prodiff stain II for 10; 20 minutes each in the case of SK-MES-1 cell line. Excess Prodiff stain II was removed by rinsing with water under a running tap. Once fully dry, the plates were analysed on an Odyssey® CLx system (Licor, Cambridge, UK).

4.3.11 *In Vivo* LLC subcutaneous cancer model

Subcutaneous tumours were generated by injecting $0.5x10^6$ or $1x10^6$ LLC cells respectively subcutaneously into the right flank of female C57BL6 mice (8-15 weeks of age; Envigo). Tumour area was determined by measuring the longest and shortest diameter of the tumour using electrical callipers. In addition, the weight of the animals was monitored. All animal husbandry and experimental procedures were approved and licensed by the Irish Health Products Regulatory Authority (HPRA).

4.3.12 *In Vivo* ECT parameters

The tumours were treated once they reached an approximal area of $25mm^2$ (treatment was done on different days for different animals as tumour size was the determining parameter for treatment). Cisplatin was made up at 1mg/kg in 20µL sterile PBS and injected intratumorally employing a fan pattern as the needle was removed to increase the distribution of the cisplatin within the tumour. Electrical parameters were applied at 8 pulses, 1Hz frequency, 100µs pulse length and electric field strength of 800V/cm or 1300V/cm respectively using a Cliniporator™ device (IGEA S.R.L, Carpi, Italy) and employing an in-house made 8-needle electrode. Parameters were applied as often as necessary to cover the entire tumour and the tumour margin surrounding it.

Prior to the application of the electric pulses, mice were anaesthesia using injectable anaesthetics and post-treatment analgesia was also supplied.

4.3.13 Processing tissue for flow cytometry

Tumours, spleen and lymph nodes were recovered once the tumours reached a size of 2.5cmx2.5cm or the animal had reached the humane endpoint (weight loss, ulcerations). Tumour tissues were washed twice in ice-cold PBS before being minced, washed once more, and incubated for 1 hour at 60°C with collagenase II (Merck Millipore, U.S.A.) and DNase I (Merck Millipore) at a final concentration of 1mg/mL and 100 Kunitz/mL, respectively, in warm DMEM. The resulting sample was run through a 0.7µM cell strainer (Corning) while the spleens and lymph nodes were run through 0.45µM cell strainer (BD, Falcon). The resulting cell suspension were washed

once more with PBS and red cells were removed from the cell suspensions by incubating the samples with Red Cell lysis buffer (Biolegend) for 3 minutes on ice. Resulting sample was washed once more and stained according to the protocol in 4.3.14.

4.3.14 Flow cytometry

Single cell suspension from tissue or cell culture was prepared prior to the staining. 100,000 to 200,000 cells were diluted in 100µL FACS buffer (PBS supplemented with 5% heat-inactivated FBS and 2mM EDTA), CD16/32 were blocked by incubating 1µg/1x10^6 cells of TruStain FcX^{TM} Antibody (Biolegend) for 10 minutes at 8°C in the dark. Following the blocking, without washing, the tissue samples were stained for 30 minutes at 8°C in the dark with Fiaxable live-death marker Near-infrared (Thermofisher Scientific), APC-Cy7 Anti-CD45 (Biolegend), PE-Dazzle Anti-CD8α (Biolegend), BV605 Anti-CD4 (Biolegend) and APC Anti-MCH II (Biolegend). DC cell culture samples were stained for 30 minutes at 8°C in the dark with Fiaxable live-death marker Near-infrared (Thermofisher Scientific), AF488 Anti-CD11c (Biolegend), PerCP-Cy5.5 Anti-CD80 (Biolegend) and APC Anti-MCH II (Biolegend). Samples were washed twice after the staining was completed and at least 10,000 events were collected per sample. Flow cytometry was conducted using an LSRII machine with a 5-laser (355 /405 /488 /561 /640nm) configuration (Table 2.2) (BD Biosciences) and the results analysed employing FlowJo V10 (BD Biosciences).

4.3.15 Statistical analysis

In vitro experiments were repeated at least three times on different days and with different passage numbers. All treatment conditions were normalized to the untreated condition for viability, metabolic activity and recovery assays. First a one-way ANOVA, with Gaussian distribution and equal standard deviations, was performed to determine overall significant changes followed by Tukey's post-hoc test to determine difference between all treatment conditions and untreated control groups, EP control group and ECT treatment conditions as well as between ECT treatments with the two different drugs at the same drug concentration. The

D'Agostino-Pearson normality test was used to test for Gaussian distribution. GraphPad Prism Version 9.0 software was used for all statistical analysis. P-values of $p \leq 0.05$ were considered significant.

4.4 Results

4.4.1 Establishment of optimal chemotherapy drug combination for treatment of lung cancer cell lines by ECT.

We have previously reported that the optimal electric field strength in terms of viability, effectiveness of treatment and recovery for four lung cancer cell lines are 800V/cm for the human A549, H460 and SK-MES-1 cell lines and 1300V/cm for the murine LLC cell line[23]. Subsequently the optimal choice of chemotherapy drug and drug concentration was determined to complete the ECT parameters for all four lung cancer cell lines in suspension set-up. As bleomycin is known to cause a reduction in lung capacity[7], cisplatin and oxaliplatin, both platinum-based drugs commonly used in lung cancer chemotherapy treatments, were tested across a range of concentrations.

Metabolic activity was determined at 24 hours, 72 hours and 120 hours post ECT (800V/cm for the human cell lines and 1300V/cm for the murine LLC cells) treatment to determine the effect of the drug at both the short- and medium-term timeframes (Figure 4.1). Determination of metabolic activity not only estimates what percentage of cells are viable post ECT treatment, but also those that are metabolically active and therefore able to continue to grow. Neither electroporation, nor drug exposure by itself significantly impacted the metabolic activity of any cell line at any time point. Moreover, a reduction in metabolic activity in the LLC cells was not observed with any of the tested conditions (Figure 4.1). In the H460 and A549 cell lines, both oxaliplatin and cisplatin show a trend of decreasing metabolic activity with increased drug concentrations, with the decrease more prominent when combined with electrochemotherapy than with either of the drugs alone (Figure 4.1; Table 4.1). This was also observed in the SK-MES-1 cell line following cisplatin, but not oxaliplatin, administration. Therefore, at equimolar concentrations, cisplatin administration, in combination with ECT, resulted in a more significant decrease in metabolic activity than oxaliplatin, similar to findings shown in other cancer types[21]. The most significant effect was observed 120 hours post ECT treatment with cisplatin at a concentration of 11µM in the three human lung cancer cell lines. All treatments which reached statistical significance are highlighted in Table 4.1.

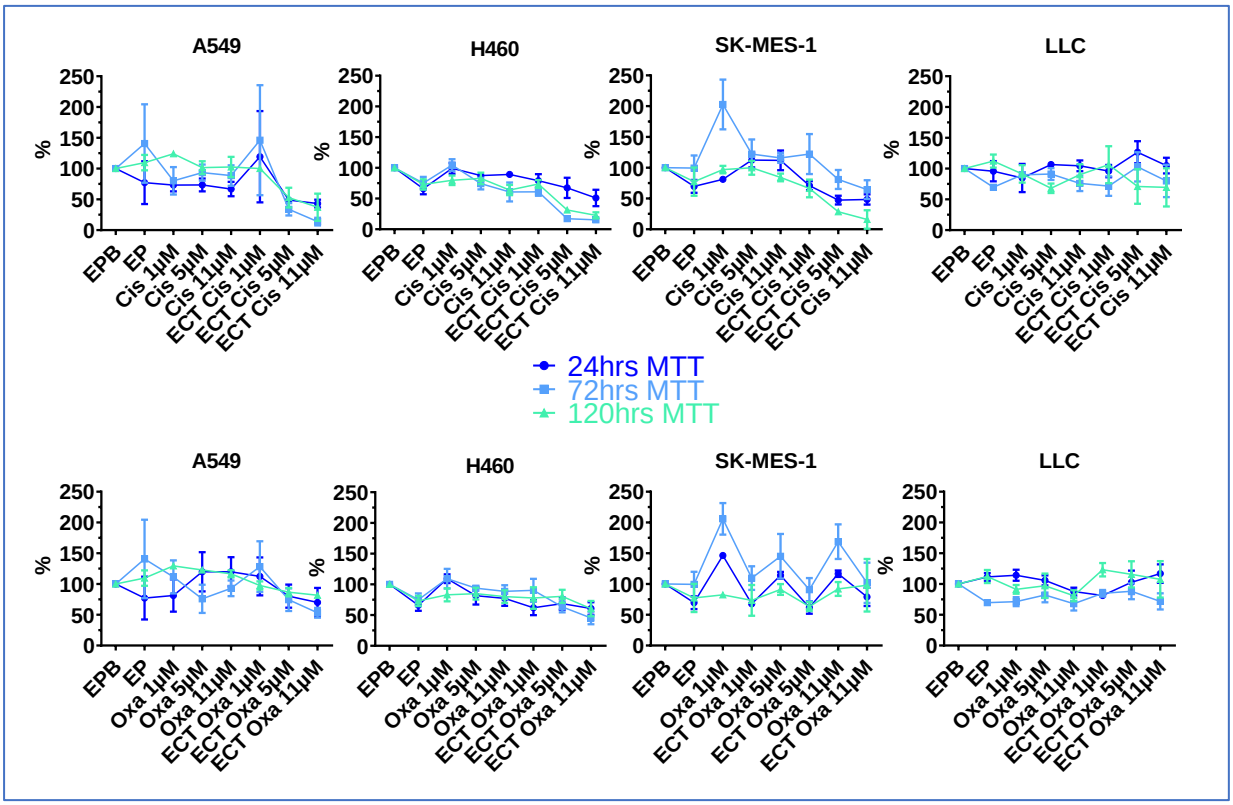


Figure 4.1: Metabolic activity of A549, H460, SK-MES-1 and LLC 24, 72 and 120 hours post ECT treatment. Cells were subjected to electroporation at 800V/cm electric field strength for A549, H460 and SK-MES-1 and 1300V/cm electric field strength for LLC in the presence of cisplatin or oxaliplatin. Graphs show signal intensity of the wells normalized to the control treatment (EPB) in % reflecting metabolic activity, an equal number of cells were plated in the wells. Data represents the mean ± SD from at least 3 separate experiments.

Cell line	Assay	Comparison	Significance level
A549	120hrs MTT	EPB vs. ECT Cis 11µM	*
		EP vs. ECT Cis 11µM	**
H460	72hrs MTT	EPB vs. ECT Cis 5µM	****
		EPB vs. ECT Cis 11µM	****
		EPB vs. ECT Oxa 11µM	*
		EP vs. ECT Cis 5µM	**
		EP vs ECT 11µM	**
	120hrs MTT	EPB vs ECT Cis 5µM	**
		EPB vs ECT Cis 11µM	**
SK-MES-1	24hrs MTT	EPB vs ECT Cis 5µM	*
		EPB vs ECT Cis 11µM	*

*Table 4.1: ECT with Cisplatin at 11µM most consistently impacts the metabolic activity of human lung cancer cell lines in vitro significantly. Different lung cancer cell lines (A549, H460, SK-MES-1 and LLC) were treated with EP at increasing electric field strength (600- 1400V/cm) and the impact on the and metabolic activity (MTT) was determined. Results were analysed by One-way ANOVA with Tukey's post-hoc test; only comparisons showing significant differences are presented. *p ≤ 0.05, ** ≤0.01, ****p ≤ 0.0001; compared to untreated (EPB).*

As metabolic activity is an indirect measure of predicting future growth of cells (post treatment), we next determined the recovery potential of the treated cells. Cell recovery was not impacted for any cell line with either drugs or electroporation alone (Figure 4.2). Similar to the trend observed for metabolic activity, increasing drug concentrations decreased the recovery potential of the cell lines, both with, and without, the combination ECT treatment, with the exception of oxaliplatin treatment of the A549 cell line. Indeed, recovery of all cell lines was more affected following administration of cisplatin than oxaliplatin. Recovery was most affected following ECT administration in combination with 11µM cisplatin across all four cell lines. Taken together, these results indicate that the optimal conditions for ESOPE-based *in vitro* ECT of human lung cancer cell lines tested is 800V/cm with cisplatin at 11µM and for the murine LLC cell line is 1300V/cm with 11µM cisplatin.

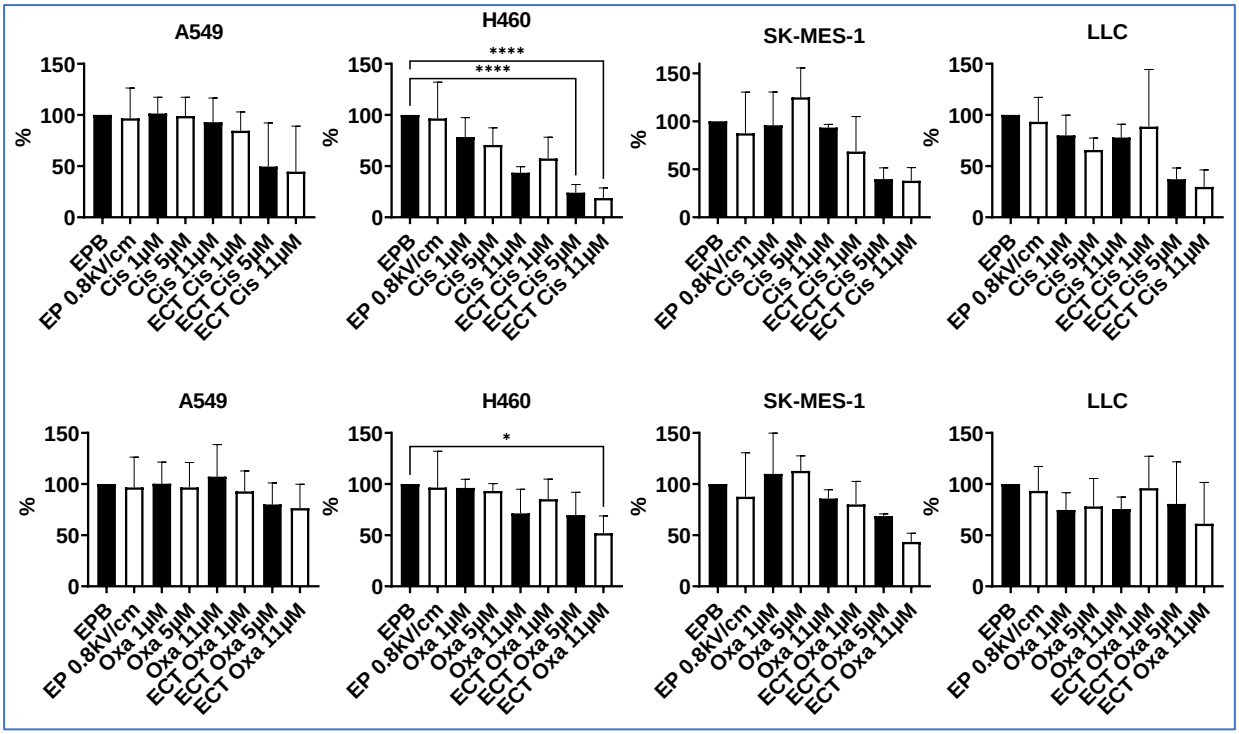


*Figure 4.2: Recovery of A549, H460, SK-MES-1 and LLC post treatment. Cells were subjected to electroporation at 800V/cm electric field strength for A549, H460 and SK-MES-1 and 1300V/cm electric field strength for LLC in the presence of cisplatin or oxaliplatin. 400 cells for A549, H460 and LLC cell lines as well as 6000 cells for SK-MES-1 cell line were seeded in complete media for 7-21 days. Formed colonies were fixed and stained, and the staining intensity was measured by the CLx imaging system. The signal intensities of the wells reflect the number and size of the formed colonies. The graph shows signal intensity normalized per cell line to the control treatment (EPB) and represents at least 3 unique experiments. Data represents the mean ± SD from at least 3 separate experiments. *p ≤ 0.05, ****p ≤ 0.0001; compared to untreated (EPB).*

4.4.2 Investigation of optimal calcium concentration for CaEP for treatment of lung cancer cell lines.

In addition to chemotherapeutic drugs, calcium can also be used in combination with electroporation (CaEP) to treat malignancies. Currently CaEP is under investigation for a range of malignancies such as colon cancer[18] and Rhabdomyosarcoma[24]. Therefore, we also investigated the effect of CaEP on lung cancer cell lines *in vitro* by exploring the impact of CaEP with increasing calcium concentrations used (0.5-5mM) on the metabolic activity and recovery potential of lung cancer cells to determine if

CaEP could be a suitable treatment for lung cancer patients. We examined the effect on a subset of our lung cancer cell lines, namely both the A549 and LLC cell lines. The A549 cell line was chosen as a representative human lung cancer cell line as it is an adenocarcinoma cell line and adenocarcinoma represent the biggest subgroup of lung cancer diagnosis[25]. The LLC cell line was chosen as it is the most commonly used murine lung cancer cell line for *in vitro* and *in vivo* experiments. Calcium concentrations between 0.5 and 5mM are the typical range tested for use in CaEP for *in vitro* cell work[24,26,27], with higher calcium concentrations (9mM-168mM)[24,28] used for 3D spheroid and *in vivo* models.

Metabolic activity was determined at 24 hours, 72 hours and 120 hours post CaEP (800V/cm for the A549 cell line and 1300V/cm for the murine LLC cells) treatment to determine the effect of increasing calcium concentrations at both the short- and medium-term timeframes (Figure 4.3), similar to how the impact of increasing drug concentrations of cisplatin and oxaliplatin was evaluated. CaEP was only seen to significantly ($p \leq 0.05$) reduce the metabolic activity of A549 cells at the highest concentration (5mM) at 24 and 72 hours post-treatment (Figure 4.3A). At 24 hours calcium alone seemed to slightly increase the metabolic activity of A549 cells (Figure 4.3A). The metabolic activity of A549 cells 120 hours post-treatment across all treatment conditions was completely unchanged compared to untreated cells (Figure 4.3A), indicating that cells that survived the initial treatment continue to be active. In contrast, the metabolic activity of LLC cells was unchanged at both 24 and 72 hours across all tested treatment conditions (Figure 4.3B), whilst 120 hours post-treatment the metabolic activity of these cells increased with all tested CaEP treatments compared to untreated or EP alone (Figure 4.3B). As metabolic activity is just an indirect measure in regard to future cell growth post-treatment, we next evaluated the recovery potential of the A549 and LLC cells post CaEP.

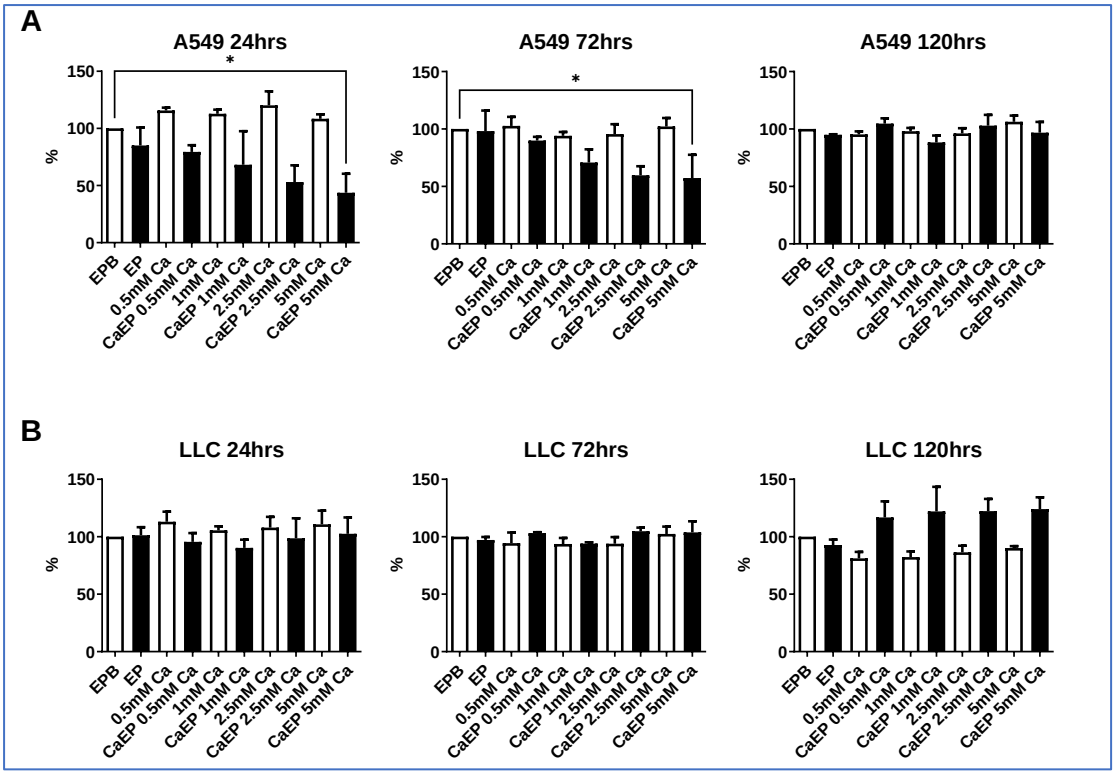


*Figure 4.3: Metabolic activity of A549 (A) and LLC (B) 24, 72 and 120 hours post CaEP treatment. Cells were subjected to electroporation at 800V/cm electric field strength for A549 and 1300V/cm electric field strength for LLC in the presence of calcium. Graphs show signal intensity of the wells normalized to the control treatment (EPB) reflecting metabolic activity, an equal number of cells were plated in the wells. Data represents the mean ± SD rom at least 3 separate experiments. *p ≤ 0.05; compared to untreated (EPB).*

Similar to the trend observed for the metabolic activity of A549 cells, there was a slight increase in the recovery potential of calcium treated cells above 1mM calcium concentration, for both calcium alone and CaEP treatment (Figure 4.4A). In contrast to the effect seen on metabolic impact, CaEP did not impact the recovery potential of A549 cells (Figure 4.4A). The observed recovery potential of LLC cells, however, was in contrast to the effect seen on the metabolic activity of these cells impacted, as an increase in calcium concentration for CaEP did decrease the recovery potential of LLCs slightly (Figure 4.4B). Recovery of LLC cells also increased with all tested calcium concentrations alone (Figure 4.4B). Combined, these results indicate that calcium concentration above 5mM could be tested to improve the reduction of metabolic activity and recovery post CaEP treatment. Furthermore, the tested

conditions for CaEP impact A549 and LLC cells less than the optimized cisplatin ECT does in terms of both metabolic activity and recovery potential, thereby indicating that CaEP may be a less effective than Cisplatin-ECT treatment for lung cancer.

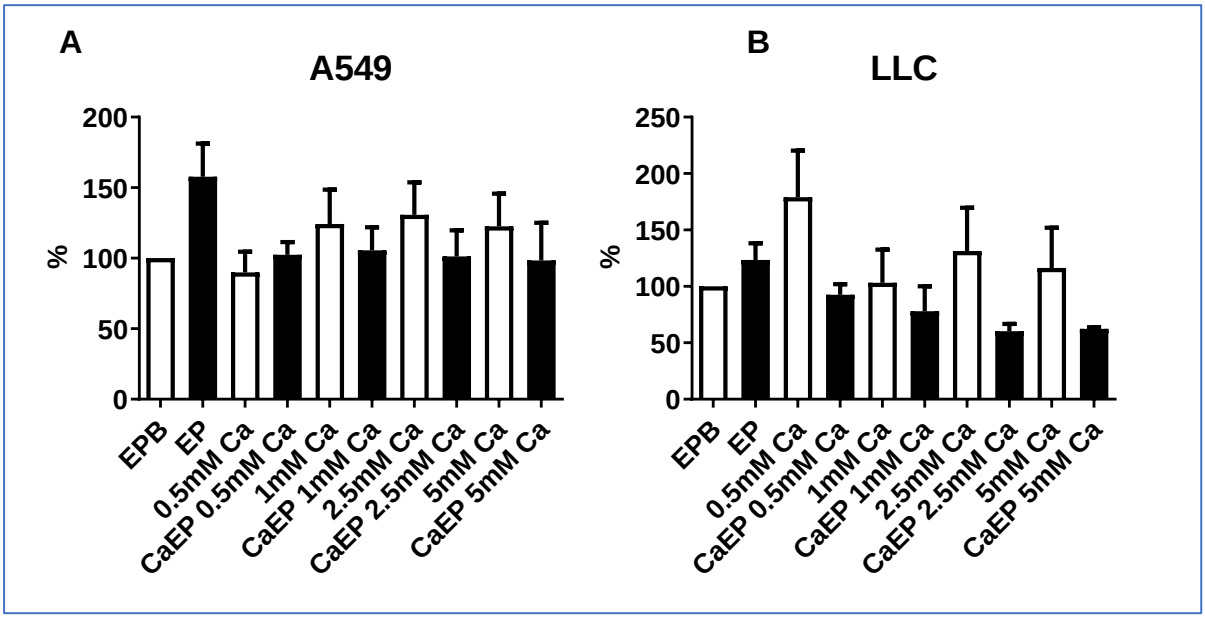


Figure 4.4: Recovery of A549 (A) and LLC (B) post CaEP treatment. Cells were subjected to electroporation at 800V/cm electric field strength for A549 and 1300V/cm electric field strength for LLC in the presence of increasing concentrations of calcium. 400 cells for A549 and LLC cell were seeded in complete media for 7-14 days. Formed colonies were fixed and stained, and the staining intensity was measured by the CLx imaging system. The signal intensities of the wells reflect the number and size of the formed colonies. The graph shows signal intensity normalized per cell line to the control treatment (EPB) and represents at least 3 unique experiments. Data represents the mean ± SD from at least 3 separate experiments.

4.4.3 Deriving Human Dendritic cells to elucidate the impact of EP and ECT

In order to fully understand the impact of EP and ECT on the tumour microenvironment, we next wished to investigate the impact of EP and ECT on human immune cells, with a focus on antigen presenting cells such as macrophages and dendritic cells (DCs). To undertake this component, I initially aimed to generate human DCs derived from Buffy Coats using a protocol I had previously optimised during my MSc studies in the Netherlands[29]. Buffy Coats are by-products of processing whole blood for use in patients and contain mostly white blood cells and

platelets. Since Ireland has a centrally organized blood-processing system, with all Buffy Coats being processed in Dublin, the Buffy Coats in Cork were standardly 3 days old. Despite multiple modifications to the protocol to maximize the number of DCs, only 0.5-1.5x10^6 DCs per Buffy Coat could be derived (previously a minimum of 20x10^6 DCs per Buffy Coat could be derived in the Netherlands using 24 hours old Buffy Coats). Neither further initial dilution of the Buffy Coats nor repeating the lympho prep centrifugation step reduced the total amount of red blood cells present or improved the overall yield of DCs. Additionally, the provided Buffy Coats differed significantly in volume, leading to concerns about the quality of the Buffy Coats themselves.

As there was no possibility to improve either the quality or the age of the provided Buffy Coat, alternatives were subsequently investigated. The high costs associated with ordering in whole blood, Buffy Coats, or already derived DCs from companies prevented me from gaining access to better-quality Buffy Coats via this acquisition route. Another option that was explored was getting whole blood from local patients with hemochromatosis. DCs derived from patients with hemochromatosis are phenotypically and functionally identical to DCs derived from healthy volunteers[30]. Ethical approval was obtained to use blood derived from therapeutic phlebotomy at Cork University Hospital for further academic research. As the blood provided under this ethical approval was whole blood, in contrast to the earlier used Buffy Coats, the protocols to derive DCs from Buffy Coats needed to be adopted to derive DCs from whole blood. Just as processing of the whole blood and the amount of DCs derived was optimized, the COVID19 pandemic began, with not only a full country-wide shutdown of all teaching institutions but also a local restriction on access to hospitals/patients and clinical samples that then remained in place for the next 18 months. As a result of these restrictions, the challenging decision was made to switch the focus of this component of the project to murine bone-marrow derived DCs to explore the impact of EP and ECT on immune cells. Additionally, with the use of mice for the derivation of DCs, it was also possible to derive T cells and macrophages at the same time and thus investigate the impact of EP and ECT on three distinct immune cell subsets.

4.4.4 Both EP and ECT effect viability, efficacy and metabolic activity of murine dendritic cells and macrophages but have no effect on T cells

As the immune compartment is critical in determining the lung cancer anti-tumour response and could potentially be impacted by EP/ECT treatment, which could in turn influence both local and systemic immune responses to the tumour, we next investigated what effect a range of EP and ECT parameters would have on different immune populations. As unstimulated immune cells have a shorter life span than cancer cells *in vitro* and immune cells are not adherent, we adapted our protocol by eliminating the recovery potential assay and instead included a second MTT assay 72 hours post-treatment (based on Bendix *et al*[23]) to take these different cell properties into account.

We initially investigated the effect of a range of electric field strengths on the efficacy, viability and metabolic activity of $CD3^+$ whole T cells. Effectiveness of electroporation for murine T cells reached a maximum of 57% at 1400V/cm while keeping with the other ESOPE parameters (8 pulses, 100µs pulse duration, 1Hz pulse frequency; Figure 4.5A). The direct viability of the T cells was only slightly impacted at all electric field strengths, with a maximum of a 10% decrease in viability observed at 1400V/cm. Interestingly, 24 hours post treatment, the viability at all tested conditions was slightly increased compared to the untreated condition (Figure 4.5A), with the increase between 700V/m to 1000V/cm being significant ($p \leq 0.05$) compared to untreated (Table 4.2). Similarly, at 24 hours post-treatment, little impact of any tested condition on the metabolic activity of T cells was observed, whereas at 72 hours post-treatment the metabolic activity increased slightly with increasing electric field strengths (Figure 4.5A). Therefore, T cells are not negatively impacted by being electroporated *in vitro* at standard ESOPE parameters.

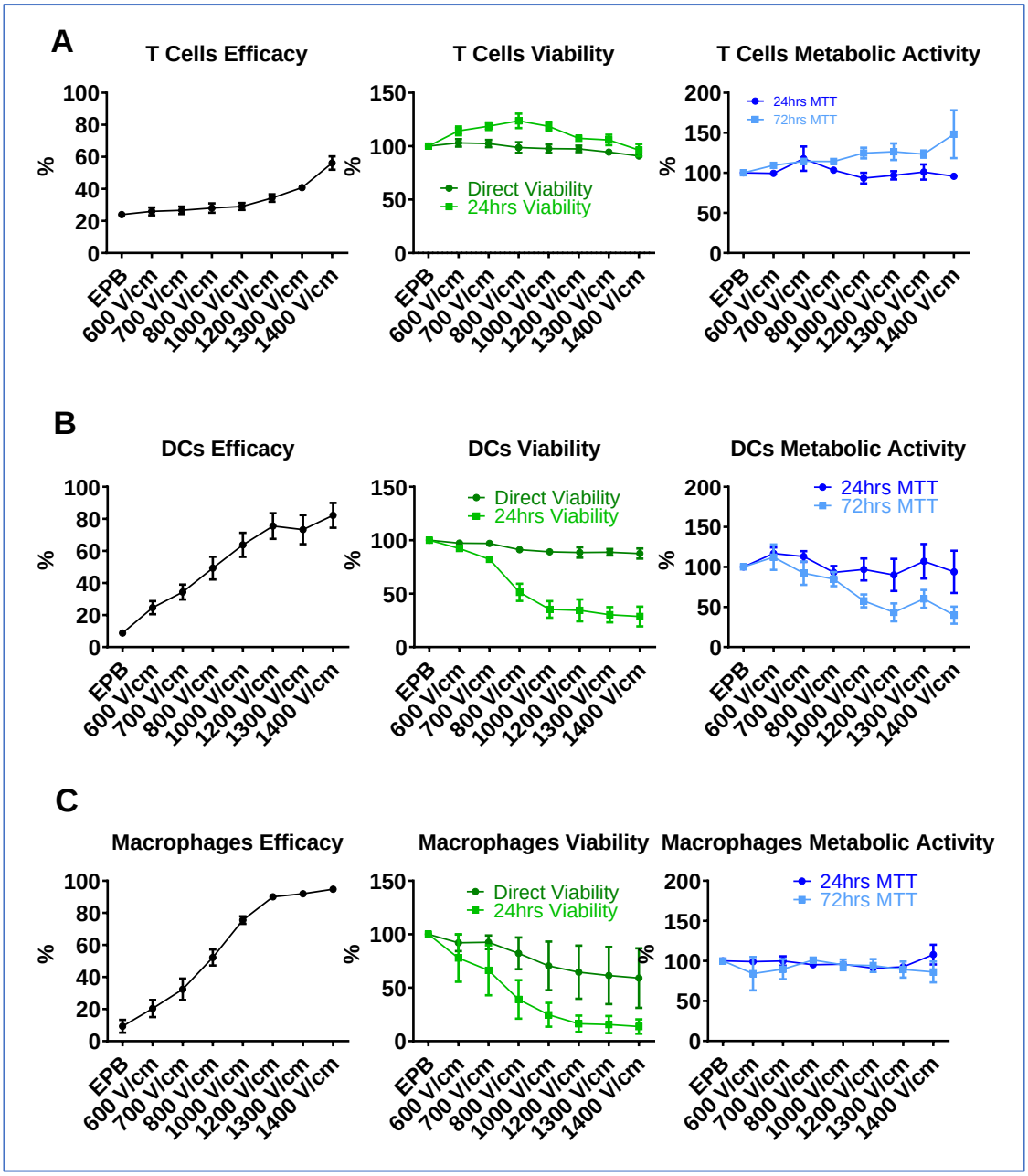


Figure 4.5: Efficacy, viability and metabolic activity of immune cells following EP treatment to determine optimal electric field strength per tested cell type. For efficacy measurement, PI was added into EP cuvette prior to cells exposure to electroporation. PI intensity illustrates perforation of cells by electroporation. Cells were analysed within 60 minutes of treatment by flow cytometry. For viability, PI was added into the cell supernatant directly before cells were analysed via flow cytometry, viable cells have an intact cell membrane and therefore do not take up PI. Metabolic activity was determined by MTT assay 24 and 48 hours post-treatment. Data represents the mean ± SD from at least 3 separate experiments. Based on the tested parameters, T cells (A) are barely impacted by any tested EP treatment whereas the antigen-presenting cells (DCs (B) and macrophages(C)) are significantly impacted by EP treatments above 800V/cm.

Next, we investigated the impact of electroporation on two murine antigen-presenting cells (APCs), dendritic cells (DCs) and macrophages. In contrast to T cells, both DCs (Figure 4.5B) and macrophages (Figure 4.5C) showed a linear increase in electroporation efficacy with increasing electric field strength. Additionally, cell viability directly after treatment decreased significantly ($p \leq 0.05$) for DCs above 1000V/cm (Figure 4.5B). While viability 24 hours post EP, significantly decreased with increasing electric field strengths above 800V/cm for both DCs ($p \leq 0.0001$) (Figure 4.5B) and macrophages ($p \leq 0.05$) (Figure 4.5C). Metabolic activity was almost unchanged for DCs at 24 hours post-treatment but did decrease with increased electric field strength 72 hours post-treatment, with the decrease being significant above 1000V/cm ($p \leq 0.05$) (Figure 4.5B). Metabolic activity in macrophages was unchanged at both 24 and 72 hours post-treatment (Figure 4.5C). All treatments which reached statistical significance are highlighted in Table 4.2. Taken together these findings could indicate that a sizable percentage of DCs and macrophages present in the tumour microenvironment are killed during ECT with standard ESOPE parameters in the tumour, and those that are not killed may not function optimally post ECT. Based on this, it seems that the maximum tolerable electric field strength for both DCs and macrophages is 800V/cm, at least for *in vitro* research.

Cell type	Assay	Comparison	Significance level
T cells	24 hours Viability	EPB vs. 700V/cm	*
		EPB vs. 800V/cm	**
		EPB vs. 1000V/cm	*
DCs	Direct Viability	EPB vs. 1000V/cm	*
		EPB vs. 1200V/cm	*
		EPB vs. 1300V/cm	*
		EPB vs. 1400V/cm	*
	24 hours Viability	EPB vs. 800V/cm	****
		EPB vs. 1000V/cm	****
		EPB vs. 1200V/cm	****
		EPB vs. 1300V/cm	****
		EPB vs. 1400V/cm	****
	72 hours MTT	EPB vs. 1000V/cm	*
		EPB vs. 1200V/cm	**
		EPB vs. 1300V/cm	*
		EPB vs. 1400V/cm	**
Macrophages	24 hours Viability	EPB vs. 800V/cm	*
		EPB vs. 1000V/cm	*
		EPB vs. 1200V/cm	**
		EPB vs. 1300V/cm	**
		EPB vs. 140 V/cm	**

*Table 4.2: Electroporation between 800V/cm and 1000V/cm most consistently impacts the 24 hours viability of murine immune cells in vitro significantly. T cells, DCs and macrophages were treated with EP at increasing electric field strength (600V/cm-1400V/cm) and the impact on their viability and metabolic activity (MTT) was determined. Results were analysed by One-way ANOVA with Tukey's post-hoc test. *p ≤ 0.05, ** ≤0.01, ****p ≤ 0.0001; compared to untreated (EPB).*

The impact of ECT on the immune cells with 11µM cisplatin, based on the optimal drug dosage identified for the lung cancer cell lines, at 800V/cm, 1000V/cm and 1300V/cm was also determined. Similar to the findings in Figure 4.5, the viability of the T cells was unchanged at both 4 and 24 hours post-treatment except for ECT at 1300V/cm which significantly ($p \leq 0.05$) decreased the viability of the treated T cells 24 hours post-treatment (Figure 4.6A). In contrast, the viability of both DCs (Figure 4.6B) and macrophages (Figure 4.6C) was significantly impacted compared to untreated cells at all tested treatment conditions ($p \leq 0.01$) both at 4 hours and 24

hours post ECT treatment, apart from macrophages treated with ECT at 800V/cm 4 hours post treatment. These results indicate that ECT at standard ESOPE parameters (1000V/cm *in vivo* and 1300V/cm *in vitro*) do negatively impact immune cells, at least *in vitro*, which could indicate that this may also reduce local and systemic immune effects.

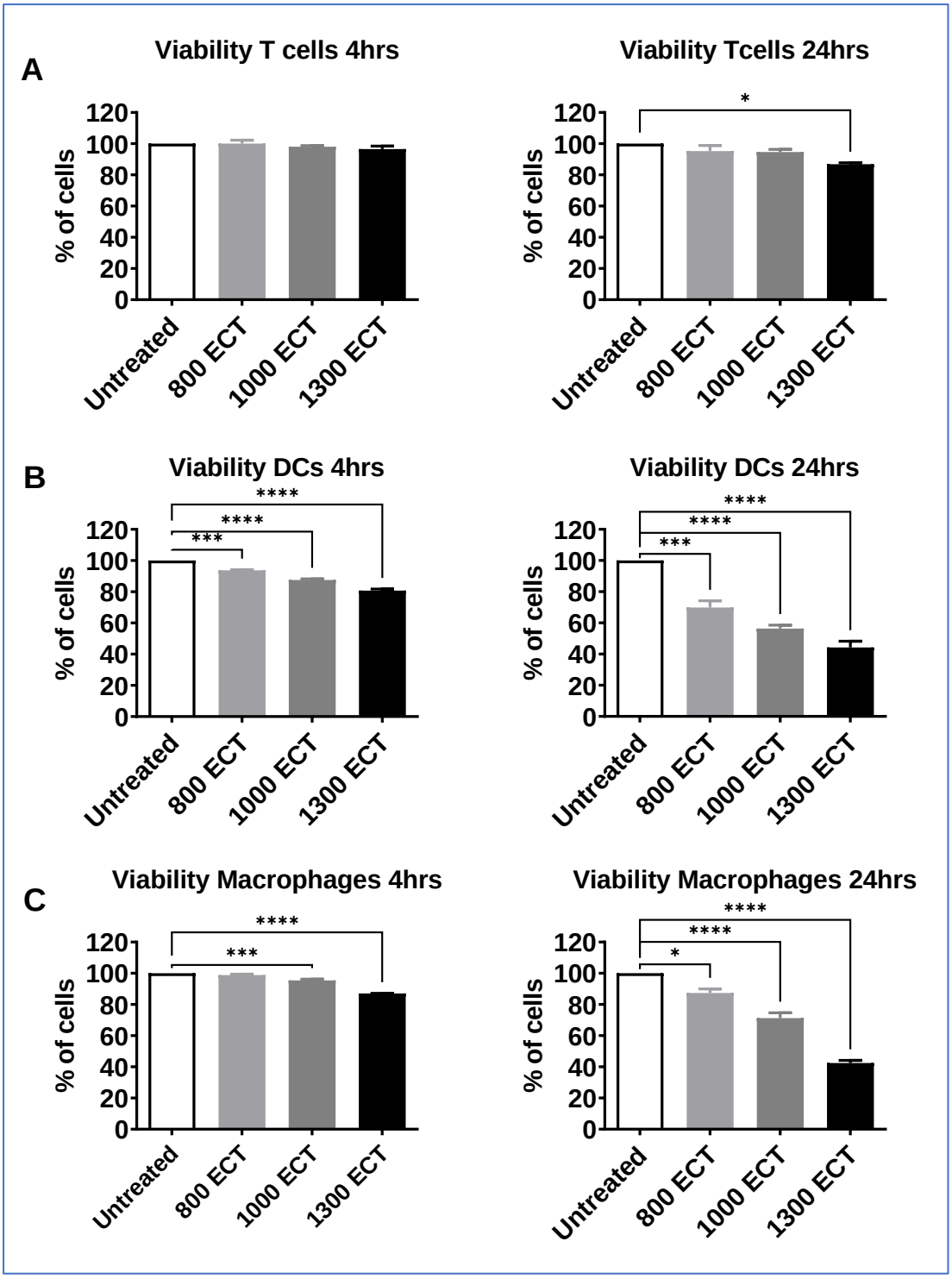


*Figure 4.6: Impact of ECT on Immune Cells. Viability was determined 4 respectively 24 hours post treatment either via PI-uptake (A) or Live-Dead marker staining (B and C) via flowcytometry. Viability is normalized per timepoint and cell type to the untreated condition. Data represents the mean ± SD from at least 3 separate experiments. *p ≤ 0.05, ***p ≤0.001, ****p ≤ 0.0001; compared to untreated.*

4.4.5 Various treated LLC conditioned media have no discernible impact on DC viability or activation status

In addition to elucidating the direct impact of EP on immune cells, the impact of EP and ECT-treated LLC cells on DCs was also investigated to determine if treated LLC cells differentially impact DCs to further elucidate the complex interplay of cancer and immune cells in the tumour microenvironment. ECT treatment of LLCs triggers the release of different DAMPs (Damage-associated molecular pattern) like calreticulin or heat-shock proteins, as well as tumour-associated antigens (TAAs)[13]. These DAMPs can induce maturation of the DCs which can then induce an adaptive immune response specific to the excreted TAAs[31]. Thus, the impact of the DAMPs and TAAs released by ECT-treated LLCs on the viability and phenotype of DCs was determined (Figure 4.7). 48 hours after LLC cells were treated with both EP and ECT at 800V/cm or 1300V/cm, DCs were incubated in the conditioned media from these treatments for another 24 hours prior to analysis. No significant impact on the viability, phenotype ($CD11c^+MHC\ II^+$) or activation status ($CD80^+$) of the DCs with any tested media was observed, although a slight downward trend in the viability of DCs with an increase in treatment strength was noted (Figure 4.7). This indicates that while there might be some impact from the treated LLCs on the DCs, the short timeframe investigated in this experiment may not be enough to clearly characterise this and thus further research is needed to elucidate the interactions between cancer and immune cells undergoing ECT treatment.

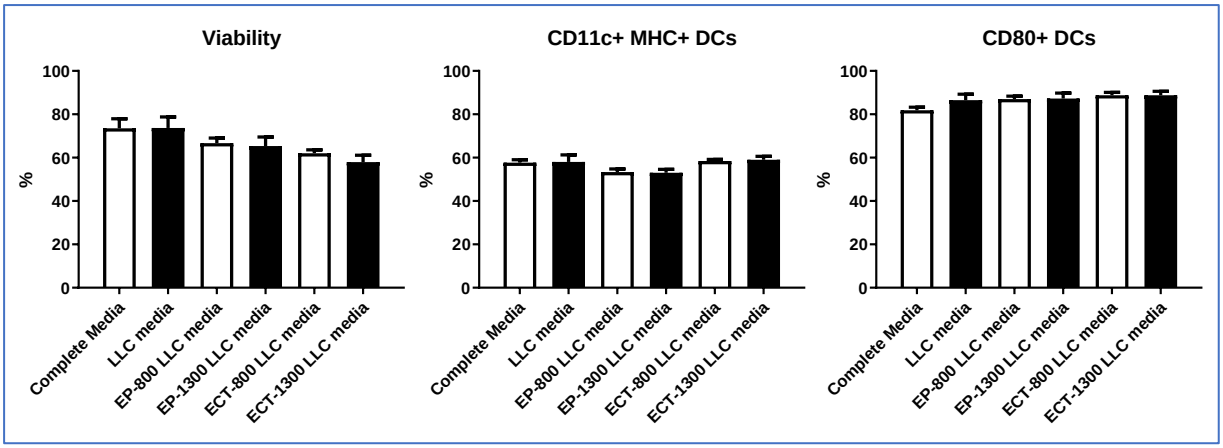


Figure 4.7: LLC conditioned media does not effect Dendritic cell viability, phenotype and activation status. 1x10^6 LLC cells were either left untreated or treated with EP at 800V/cm respectively 1300V/cm or ECT at 800V/cm respectively 1300V/cm and incubated in supplemented DMEM for 48 hours. DCS were then incubated in the thus developed conditioned media for another 24 hours and their viability as well as expression of the phenotypic marker CD11c and MHC II and the activation marker CD80 was determined by flow cytometry. Data represents the mean ± SD from at least 3 separate experiments.

4.4.6 Comparison of 800V/cm and 1300V/cm ECT with 11µM cisplatin in LLC cells

Electroporation of LLC cells had previously been optimised at 1300V/cm[23]. However, the findings shown in Figures 4.5 and 4.6 indicate that the optimal electric field strength for retaining viability and efficacy of APCs post ECT is 800V/cm. Thus, we next investigated the effect of ECT at 800V/cm with 11µM cisplatin on LLCs (Figure 4.8) to determine if ECT at 800V/cm could sufficiently reduce the tumour burden with the lowered electric field strength.

No significant difference was observed in metabolic activity between LLC cells treated with ECT at 800V/cm and 1300V/cm at any time point, whilst both treatments slightly increase the metabolic activity compared to the untreated condition at 72 and 120 hours post-treatment (Figure 4.8A). In contrast, similar to findings in Figure 4.2, the recovery (Figure 4.8B) of the treated cells was significantly impacted compared to untreated ($p \leq 0.001$). Whilst the effect on recovery was slightly more pronounced at 1300V/cm than at 800V/cm, there was a sizable and significant reduction in cell recovery at 800V/cm (Figure 4.8B). Metabolic activity could be less impacted than cell recovery potential, as cisplatin creates crosslinks in

the cell's DNA, which in turn inhibits mitosis[32]. Despite the inability of the cells to undergo mitosis, they are still alive and therefore metabolically active. This could indicate that the electric field strength could be lowered in ECT application such as to sufficiently reduce the local tumour burden while protecting the immune cell population in the tumour. This could possibly lead to an improved systemic immune response. To investigate this hypothesis, we next wished to translate these in vitro findings into an *in vivo* murine lung cancer model.

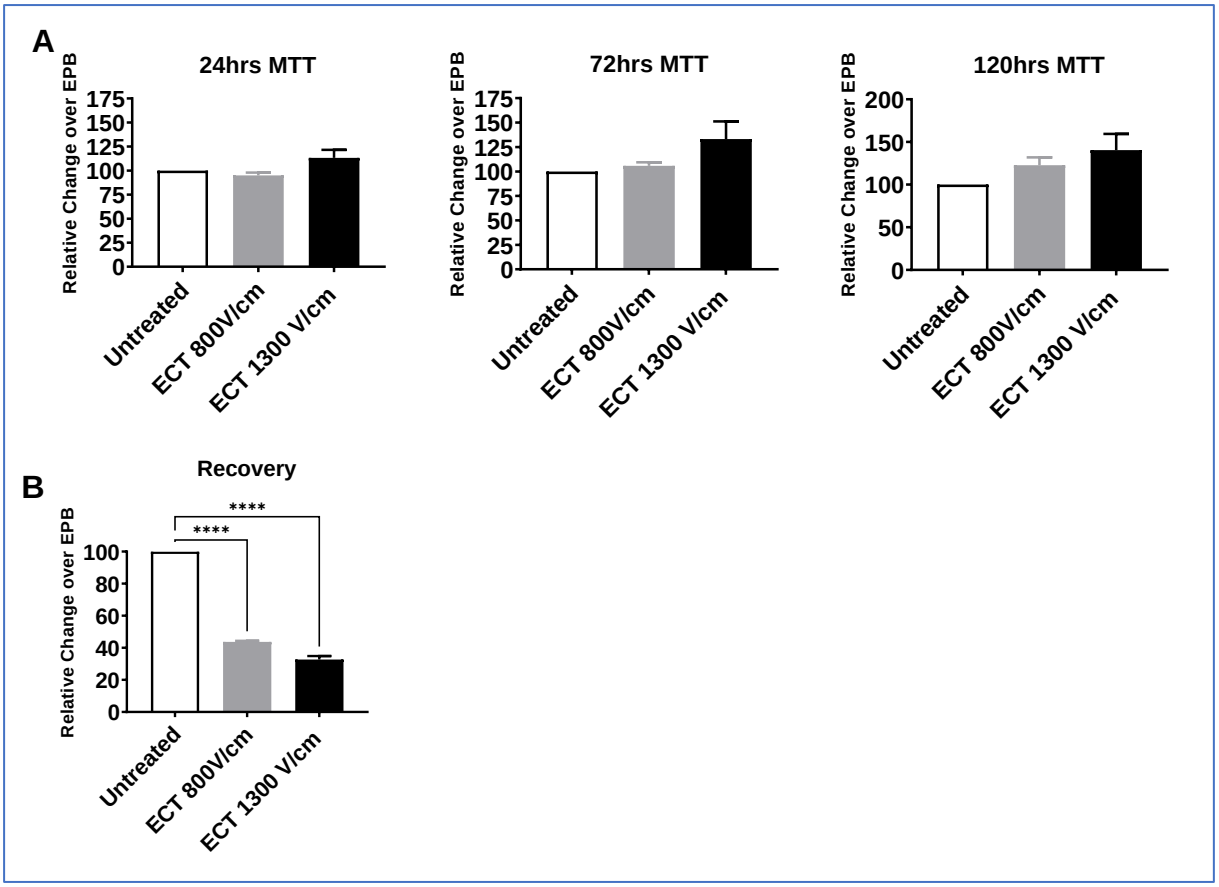


*Figure 4.8: Comparison of the impact of ECT at 800V/cm with ECT at 1300V/cm with 11µM cisplatin for LLCs on metabolic activity and recovery potential. Cells were subjected to electroporation at 800V/cm electric field strengths and 1300V/cm electric field strength in the presence of 11µM cisplatin. A) Metabolic activity was determined by MTT assay 24, 72 and 120 hours post-treatment. B) For recovery cells (400 cells/well) were plated for 10 days and formed colonies were fixed and stained, and the staining intensity was measured by the CLx imaging system. The signal intensities of the wells reflect the number and size of the formed colonies. The graph shows signalling intensity normalized per measurement to the untreated control. Data represents the mean ± SD from at least 3 separate experiments. ****p≤0.0001; compared to untreated.*

4.4.7 Evaluating impact of ECT at 800V/cm versus ECT at 1300V/cm in a murine lung cancer model

As our *in vitro* data had shown that ECT at 800V/cm can significantly impact LLC cells, we next wished to investigate the effectiveness of ECT at 800V/cm versus the effectiveness of ECT at 1300V/cm with respect to tumour reduction and to also investigate the impact of the treatments on the immune cells present at the treatment site in a murine lung cancer model. $5x10^5$ LLC cells were injected subcutaneously into syngeneic C57BL6 mice on their right flank. Tumour growth was monitored until the tumours reached a minimum size of 25mm². At this point, size-dependent, animals were treated either with cisplatin at 1mg/kg bodyweight, electroporation at either 800V/cm (800EP group) or 1300V/cm (1300EP group), or cisplatin ECT at 800V/cm (800ECT) or 1300V/cm (1300ECT group) (Figure 4.9). Tumours were then allowed to grow until they reached a maximum area of 625mm² or a humane endpoint was reached, whichever happened first. There were 5 animals each in the untreated group as well as in both ECT groups and the cisplatin group. There were 3 animals each in both of the EP groups.

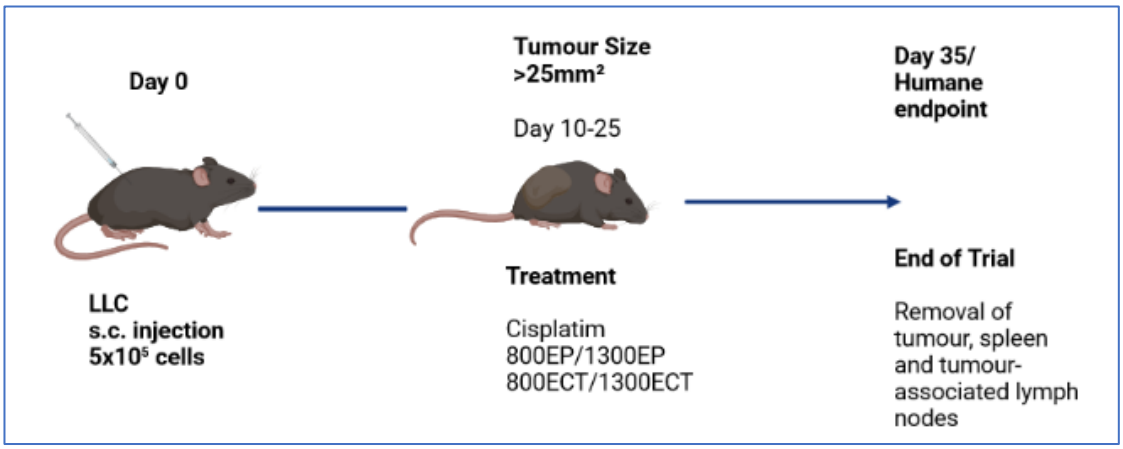


Figure 4.9: Timeline of murine lung cancer study to investigate the effectiveness of ECT at 800V/cm versus the effectiveness of ECT at 1300V/cm with respect to both tumour reduction and the impact on the immune cells present at the treatment side. Mice were treated with either cisplatin alone, or with EP at 800V/cm (800EP) respectively 1300V/cm (1300EP), or cisplatin ECT at 800V/cm (800ECT) respectively (1300ECT) once the tumour reached at least 25mm² in size. Graphic was created using Biorender.com.

Due to the size of the tumour being the relevant measurement for determining the treatment time-point, 4 animals were treated 10 days post-tumour cell injection, and 12 animals were treated 13 days post-tumour cell injection, with the final animal being treated 25 days post-tumour cell injection (Figure 4.10; arrows indicating when each animal was treated). Four animals (one each per ECT group and two in the EP 800V/cm group) did not grow any tumours, which equals a tumour-induction fail rate of 15%. There was no clear trend in any alteration of tumour growth with any tested treatment compared to the untreated condition (Figure 4.10; each growth curve line corresponds to a separate animal in each group) or between the treatment groups.

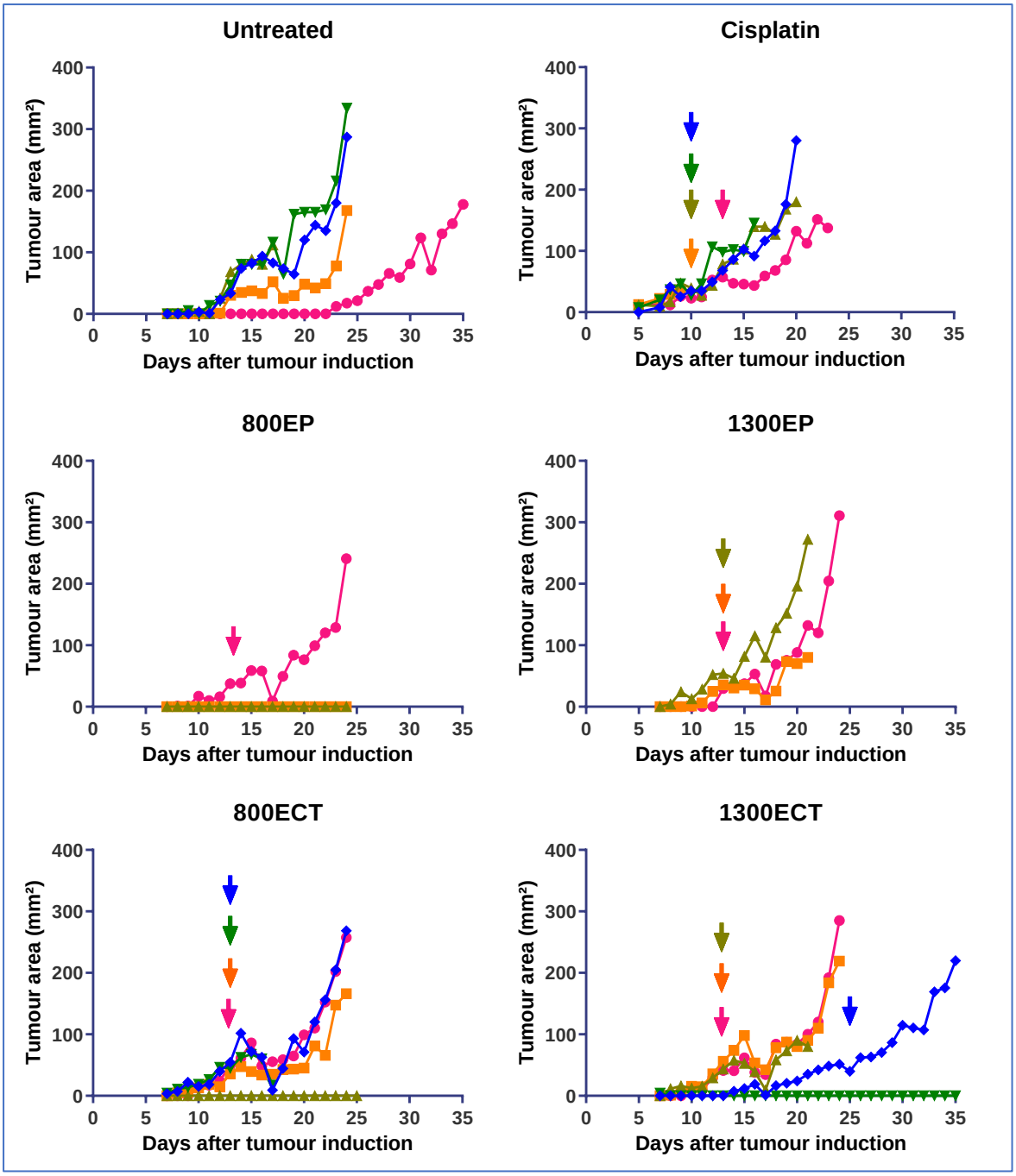


Figure 4.10: Development of tumour volume was not impacted by any tested treatment. LLC cells ($5x10^5$) were subcutaneously injected into female C57BL6J mice (3 animals in the EP groups and 5 animals in all other groups). Animals were either treated with Cisplatin (1mg/kg), EP at 800V/cm (EP800) respectively 1300V/cm (EP1300) or ECT (cisplatin at 1mg/kg) at 800V/cm (ECT800) respectively 1300V/cm (ECT1300) once the tumour reached 5mmx5mm (arrows indicate when an individual animal was treated). Tumour growth was followed by regular measurements of tumour length and width using an electrical calliper. Data points represent individual animals with line colour indicating individual animals per treatment group.

In addition to no observable difference in tumour growth, there was also no observable difference in the survival of the mice in the different treatment groups post tumour induction (Figure 4.11). Of interest, the untreated animals showed similar development of the tumour growth (Figure 4.10) and survival (Figure 4.11) compared to the animals undergoing treatments. Overall, the untreated animals belonged to the longest surviving animals in the study, with the final untreated animal being sacrificed on Day 35 together with one other animal from the 1300ECT group (Figure 4.11); all other animals that had developed tumours were sacrificed, with the latest occurring at day 25.

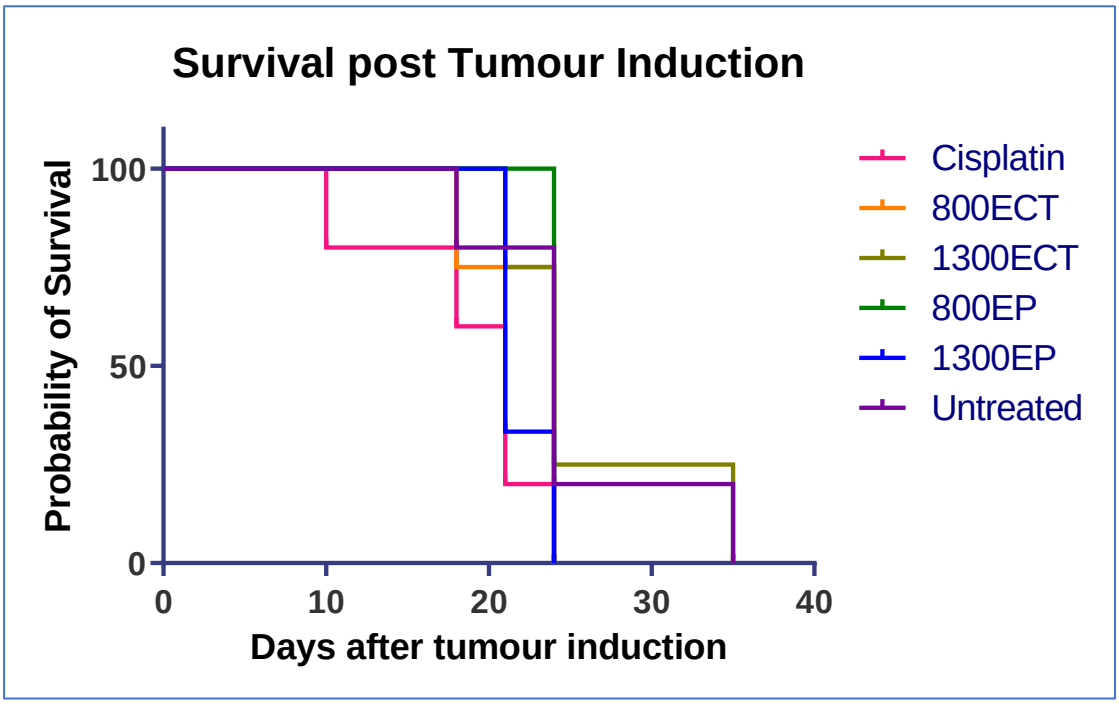


Figure 4.11: Survival was not impacted by any tested treatment. Mice were injected subcutaneously with 5x10^5 LLC cells on their right flank. Tumour growth was followed regularly by measuring with an electrical calliper. Animals were either treated with Cisplatin (1mg/kg; 5 animals), EP at 800V/cm (800EP; 3 animals) respectively 1300V/cm (1300EP; 3 animals) or ECT (cisplatin at 1mg/kg) at 800V/cm (800ECT; 5 animals) respectively 1300V/cm (1300ECT; 5 animals) once the tumour reached 5mmx5mm or left untreated (5 animals). Their survival was followed until they either reached humane or trial end point.

Findings shown in Figures 4.10 and 4.11 indicate that this *in vivo* experiment had not demonstrated the expected reduction in tumour growth and survival as has been previously observed and reported on by our group[22] and others[13,16,18] and as such we were unable to determine whether there was a difference between 800ECT and 1300ECT *in vivo*. One possible explanation for the lack of the expected outcome of this *in vivo* murine trial was that across all treatment groups, a sizable number of the animals developed severe ulcerating tumours (Figure 4.12). Of the 18 animals that developed a tumour in the experiment described in Figure 4.9, 10 animals developed ulcerations, which equals an ulceration rate of 56%. This high ulceration rate could be one major reason for the unexpectedly absent observable differences in tumour growth and survival between the treatment groups as the ulcerating tumours necessitated the removal of otherwise healthy animals with small tumours from the study, thereby reducing the number of mice in each treatment group which reached the study endpoint.

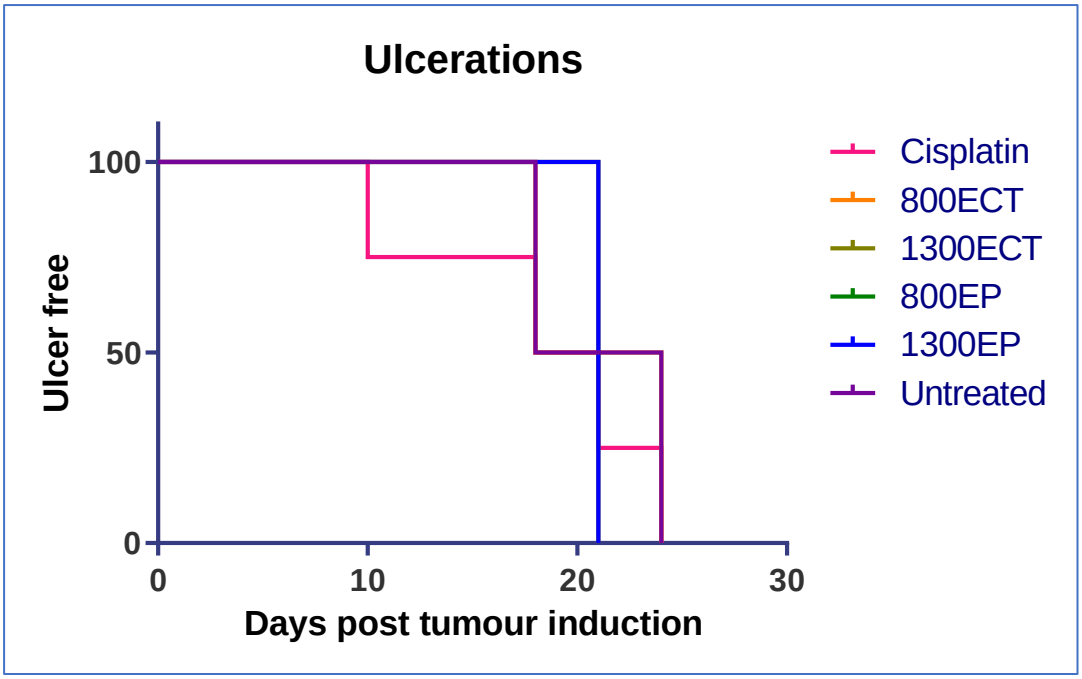


Figure 4.12: Developing of ulcerations was independent of any tested treatment. Mice were injected subcutaneously with 5x10^5 LLC cells on their right flank. Animals were either treated with Cisplatin (1mg/kg; 5 animals), EP at 800V/cm (800EP; 3 animals) respectively 1300V/cm (1300EP; 3 animals) or ECT (cisplatin at 1mg/kg) at 800V/cm (800ECT; 5 animals) respectively 1300V/cm (1300ECT; 5 animals) once the tumour reached 5mmx5mm or left untreated (5 animals). Ulcerations necessitated the cull of animals without additional clinical symptoms.

Despite the observed ulceration rate, tumours, spleens, and lymph nodes were assessed for the presence of immune cells to determine if there was any treatment-dependent effect. The presence of CD45, MHC II, CD4 and CD8 was analysed in the different tissues to gain an overview of the presence of leukocytes, APCs and T cells. CD45 is a general marker for leukocytes, MHC II is a marker for APCs while CD4 is a marker for CD4 positive T cells and CD8 is a marker for CD8 positive T cells. Analysis results are depicted separately on the same graph for non-ulcerating and ulcerating tumours per analysed cell marker and tissue type, to establish if changes in the presence of immune cells are ulceration dependent or also treatment dependent.

For the analysed tumour tissue, there was no change in the presence of CD45$^+$ cells (leukocytes) or MHC II$^+$ cells (APCs), thus neither treatment nor ulceration status changed the presence of leukocytes and APCs in the tumours (Figure 4.13 A+B). The presence of CD4$^+$ T cells was slightly increased in the ulcerating tumours with the

1300V/cm EP (1300EP) and 1300V/cm ECT (1300ECT) treatments compared to non-ulcerating tumours (Figure 4.13 C). The cisplatin treatment showed a slight decrease in $CD4^+$ T cells presence in the ulcerating tumours compared to the non-ulcerating tumours. No treatment by itself significantly changed the presence of $CD4^+$ T cells. Ulceration led to a very small increase in the presence of $CD8^+$ T cells (Figure 4.13D), while there was no treatment-dependent effect observed for the presence of $CD8^+$ T cells and overall $CD8^+$ T cells were present in very low percentages (Figure 4.13D).

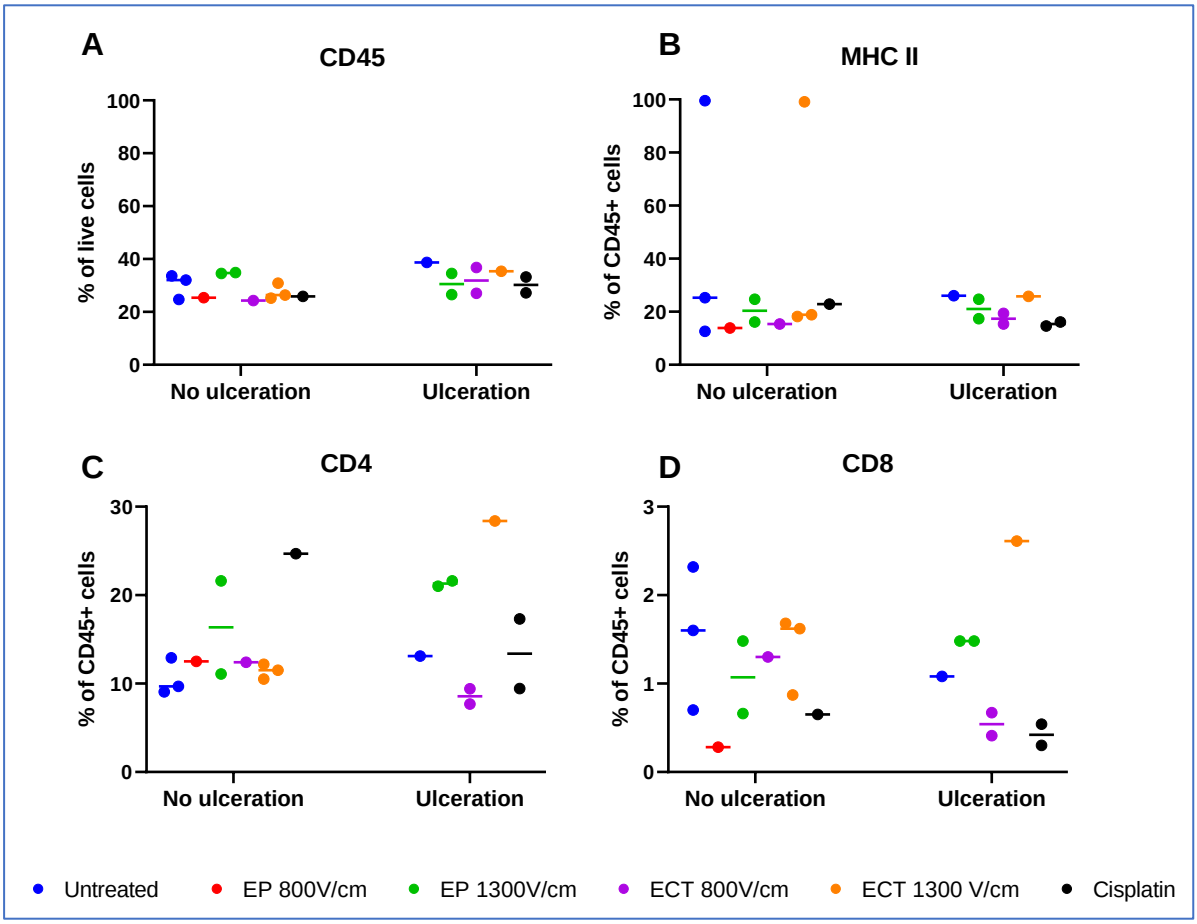


Figure 4.13: Neither treatment nor ulceration status impact the presence of $CD45^+$ (leukocytes), $CD45^+MHC\ II^+$ (APC), $CD45^+CD4^+$ ($CD4^+$ T cells), and $CD45^+CD8^+$ ($CD8^+$ T cells) cells in tumours. Mice were injected subcutaneously with $5x10^5$ LLC cells on their flank. Animals were either treated with Cisplatin (1mg/kg), EP at 800V/cm (EP800) respectively 1300V/cm (EP1300) or ECT (cisplatin at 1mg/kg) at 800V/cm (ECT800) respectively 1300V/cm (ECT1300) once the tumour reached 5mmx5mm or left untreated. Following the cull of animals due to either tumour size or humane endpoints, tumours were excised, processed and analysed by flow cytometry.

The percentage of CD45$^+$ cells (leukocytes) was increased in the spleen of treated animals compared to untreated animals in the absence of ulcerations (Figure 4.14A). Ulceration itself led to an increase in CD45$^+$ cells in the untreated condition thereby negating any treatment effects on the presence of CD45+ cells. There was no treatment or ulceration status impact on MHC II$^+$ cells (APCs), CD4$^+$ T cells, and CD8$^+$ T cells in all analysed spleen tissues (Figure 4.14 B-D).

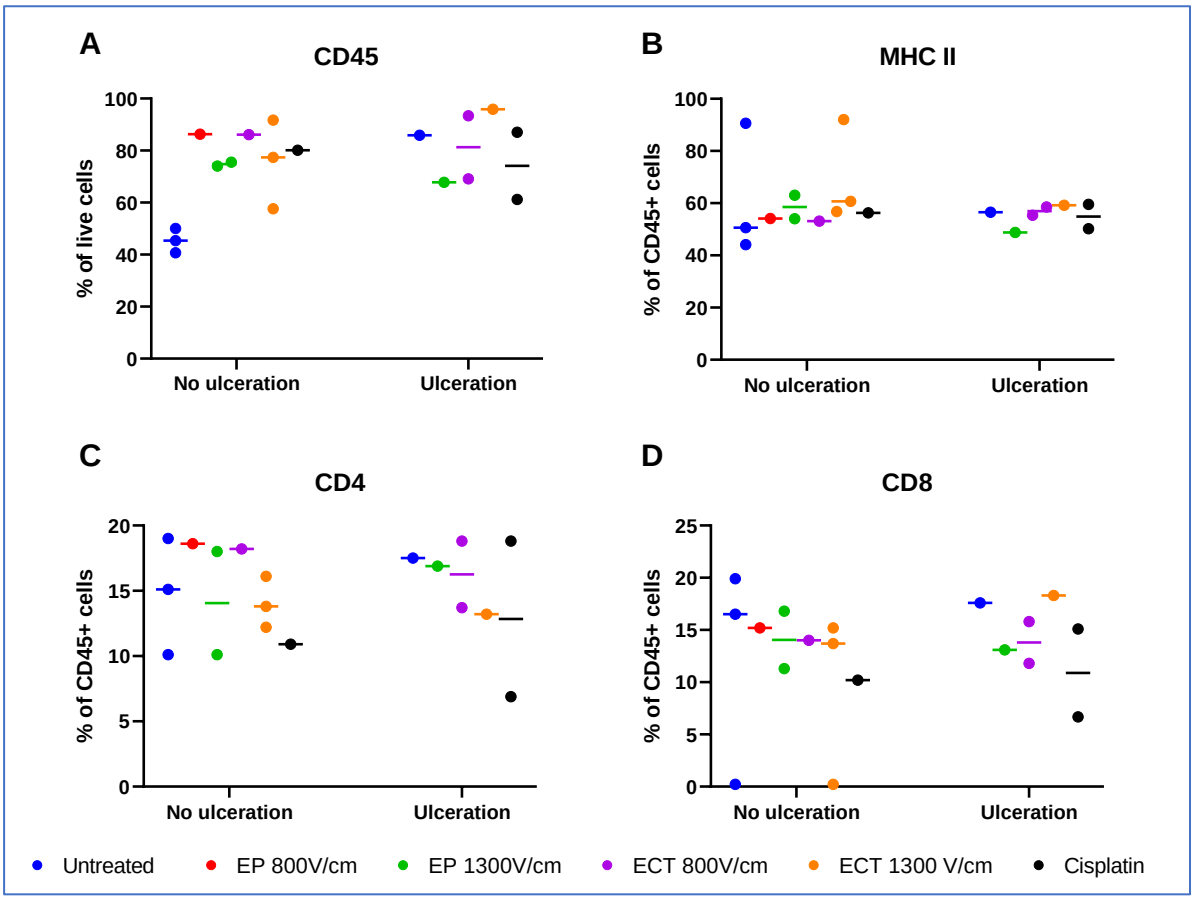


Figure 4.14: All treatments increased the presence of CD45+ (leukocytes) cells in spleens compared to untreated when the mice did not develop ulcerating tumours. Mice were injected subcutaneously with 5x105 LLC cells on their flank. Animals were either treated with Cisplatin (1mg/kg), EP at 800V/cm (EP800) respectively 1300V/cm (EP1300) or ECT (cisplatin at 1mg/kg) at 800V/cm (ECT800) respectively 1300V/cm (ECT1300) once the tumour reached 5mmx5mm or left untreated. Following the cull of animals due to either tumour size or humane endpoints, spleens were excised, processed and analysed by flow cytometry.

Presence of $CD45^+$ cells (leukocytes) in the lymph nodes was visibly decreased after 800ECT treatment and slightly decreased after 1300EP treatment compared to the control condition in the absence of ulceration (Figure 4.15A). In ulcerating tumours, all treatments, in varying degrees, decreased the presence of $CD45^+$ cells in the lymph nodes compared to the control condition (Figure 4.15A). No treatment-dependent effect was observed for the presence of MHC II^+ cells (APCs) in the lymph nodes in the non-ulceration group (Figure 4.15B), although ulceration itself led to a decrease in the presence of MHC II^+ cells for 1300EP, 1300ECT and cisplatin treatment (Figure 4.15B). The presence of $CD4^+$ T cells in the lymph node in the absence of ulcerations was only decreased in the 800ECT treatment group compared to untreated, while the other treatments did not impact the presence of $CD4^+$ T cells (Figure 4.15C). Ulceration itself lead to a slight decrease of $CD4^+$ T cells in the untreated group, whilst EP and ECT treatment at 1300V/cm did increase the percentage of $CD4^+$ T cells compared to the untreated control (Figure 4.15C). Similar to the observed results for the $CD4^+$ T cells, $CD8^+$ T cells (Figure 4.15D) in the lymph nodes was, in the absence of ulceration, only affected by 800ECT treatment, which decreased the presence of $CD8^+$ T cells (Figure 4.15D), again, unaffected of any treatment. Ulceration led to an increase in $CD8^+$ T cells in the 800ECT group, while overall the treatment impact was more diffuse on the presence of $CD8^+$ T cells (Figure 4.15D). Finally, ulceration led to a decrease, in combination with cisplatin treatment, in all tested cell markers in the lymph node (Figure 4.15 A-D).

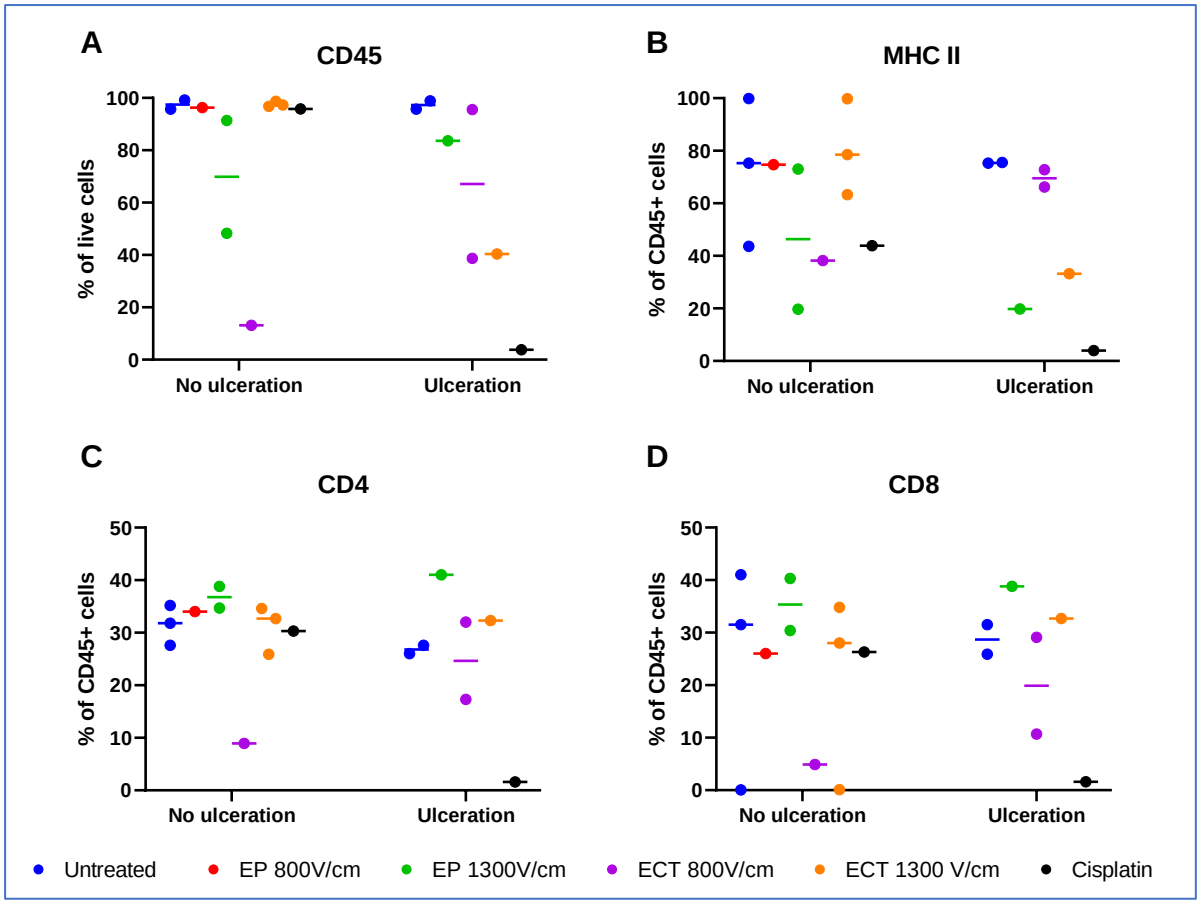


Figure 4.15: Cisplatin consistently lowers the expression of $CD45^+$ (leukocytes), $CD45^+MHC\ II^+$ (APC), CD45 $CD4^+$ (CD4+ T cells), and $CD45^+CD8^+$ ($CD8^+$ T cells) cells in tumour-associated lymph nodes when the mice developed ulcerations. Mice were injected subcutaneously with $5x10^5$ LLC cells on their flank. Animals were either treated with Cisplatin (1mg/kg), EP at 800V/cm (EP800) respectively 1300V/cm (EP1300) or ECT (cisplatin at 1mg/kg) at 800V/cm (ECT800) respectively 1300V/cm (ECT1300) once the tumour reached 5mmx5mm or left untreated. Following the cull of animals due to either tumour size or humane endpoints, tumour-associated lymph nodes were excised, processed and analysed by flow cytometry.

As the ulceration of the tumours interfered with the entire goal of discerning whether ECT at 800V/cm was as effective in terms of tumour reduction as compared to ECT at 1300V/cm, whilst being potentially beneficial for the immune response, we next investigated whether the cause of the unexpected high ulceration rate was cell line dependant. All previous usage of LLC cells in both this chapter and Chapter 3 relates to cells purchased in January 2019 (referred to as LLC-MB in Figure 4.16) and which had been passaged very few times since then. We also had cell aliquots frozen of a

previously brought in LLC cell line (referred to as LLC-LT), which in the past had successfully induced tumour growth without causing an unusual amount of ulcerated tumours[22]. Therefore, we tested both cell lines in this *in vivo* model to examine whether changing the cell line would resolve the ulceration issue (Figure 4.16). In addition, we increased the amount of tumour cells injected to $1x10^6$ cells, as this concentration seemed to be the more commonly used amount for inducing lung tumours in mice without creating metastatic disease. At $1x10^6$ subcutaneously injected cells, both cell lines induced tumours in all injected animals (Figure 4.16A+B). Tumour growth was a slightly delayed in the LLC-LT (Figure 4.16B) cell line compared to the LLC-MB (Figure 4.16A) cell line. Tumour growth was also slightly slower in the LLC-LT Figure (4.16B) cell line compared to the LLC-MB (Figure 4.16A) cell line. However, both cell lines induced ulcerating tumours in all tested animals within 15 days of tumour induction (Figure 4.16C).

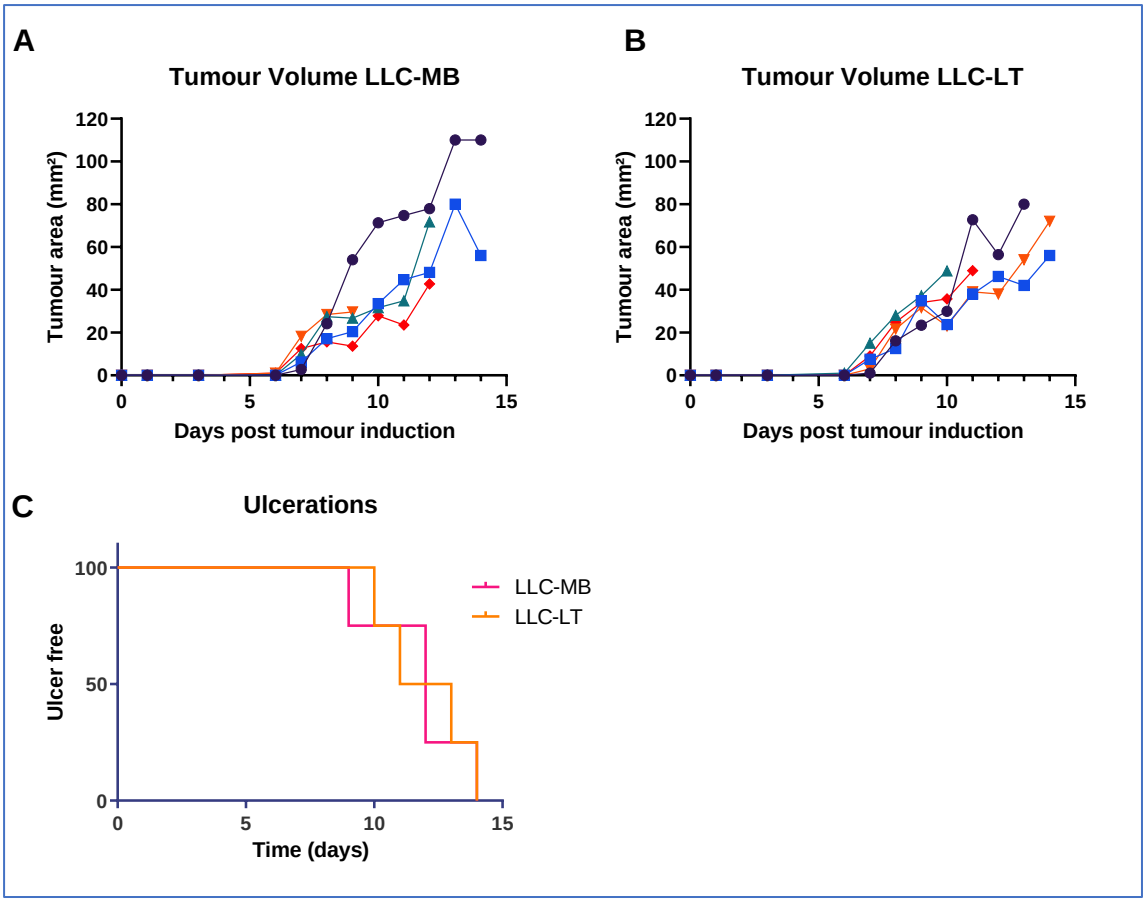


Figure 4.16: Subcutaneous injection of two different LLC cell lines resulted in similar levels of ulcerating tumours. 5 mice per group were injected subcutaneously with 1x10^6 LLC cells, either with the LLC-MB (A) or the LLC-LT (B) cell line, on their flank. Tumour growth was followed regularly by measuring with an electrical calliper. All animals were culled within 15 days due to ulcerating tumours (B).

This experiment demonstrated that the ulceration itself was not caused by the size of the tumour as all tumours were still comparably small (maximum of 110mm²; with 625mm² the maximum allowed tumour size under our ethical approval; Figure 4.17A+B) at the time of ulceration (Figure 16A+B). In addition, treatment itself did not cause the ulcerations as none of the animals underwent any treatment, thus showing that the ulceration was inherently caused by the tested LLC cell lines. The ulcers were observed to be very similar between the two tested cell lines (Figure 4.17A+B), but identically to the previous murine trial. Other than the ulcerating tumours, the animals showed again no other signs of distress and could have continued the study had ulceration not been designated as a humane endpoint.

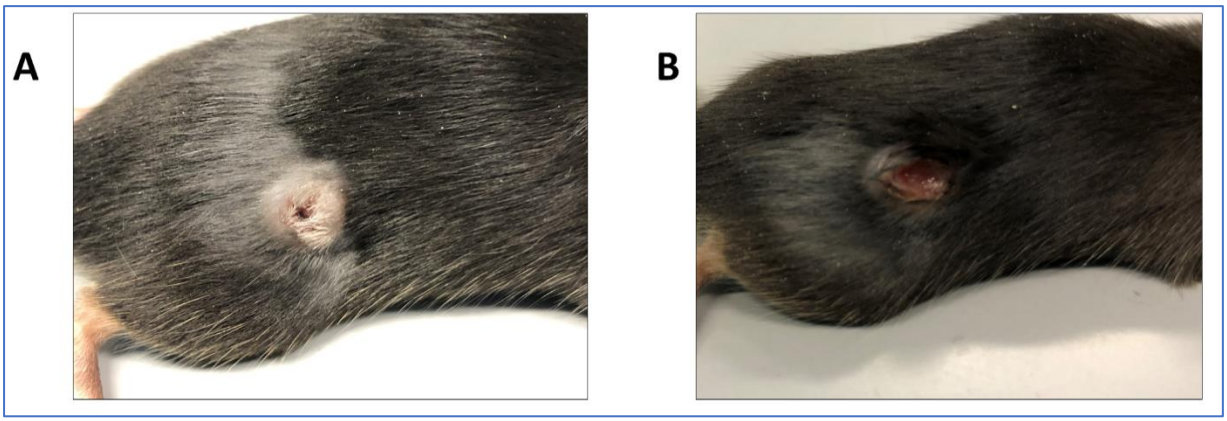


Figure 4.17: Both A) LLC-MB cell line and B) LLC-LT cell line led to similar ulcerating tumours. Pictures depict ulcerating tumours at the humane endpoint of the animal study.

Ulcerations can have a significant impact on the immune cell population present within a tumour and as it was a humane endpoint under our ethical approval, we decided to not continue with future murine trials as we could not resolve the ulceration issue. Thus, we were unfortunately unable to determine how effective 800ECT is compared to 1300ECT with respect to both tumour reduction and the impact on the immune cells present at the treatment side in an *in vivo* model. The impact of ECT on immune cells still needs to be evaluated in an *in vivo* model and depending on the outcome of this study, ECT protocols might need to be adapted for human application.

4.5 Discussion & Conclusion

ECT is successfully used in a wide range of malignancies such as melanoma[8], liver[33,34], and colorectal cancers[13,35], with ECT treatment for further malignancies currently under investigation. There is an unmet need in regard to lung cancer treatments[1] and ECT could potentially be a new treatment modality as ECT leads to robust local tumour reduction, while being able to preserve healthy tissue and also not impact blood vessels[36,37]. In this chapter, we have shown that cisplatin is the chemotherapy drug of choice for lung cancer cells within an ECT setting, and specifically that dosage of cisplatin is most effective at 11µM. Given the importance of the anti-tumour immune response in lung cancer, we have also investigated the effect of EP and ECT on several immune cell types and shown a clear difference in response between innate and adaptive immune cells to both EP and ECT, with these treatments having a clear impact on the viability and metabolism of two antigen presenting cell types, DCs and macrophages, while T cells are not impacted. These findings may, therefore, indicate that currently used ECT protocols might need to be adapted to preserve the antigen-presenting cell population within the treatment area to better facilitate a sustained immune response following ECT treatment.

In the previous chapter, 800V/cm was identified as the optimal EP setting *in vitro* for studying human lung cancer cell lines and 1300V/cm was identified as the optimal electroporation parameter for the murine LLC cell line[23]. Given that EP is always administered in combination with a chemotherapy drug (ECT) for cancer treatment, it is necessary to translate the EP findings relating to the lung cancer cells to include relevant clinical parameters. To this end, the effect of two commonly used lung cancer chemotherapy drugs, cisplatin and oxaliplatin, on cellular metabolic activity and recovery post-ECT was investigated. Our data indicates that, at equimolar concentrations, cisplatin reduces the metabolic activity and the recovery potential of all tested cell lines, to a greater extent than oxaliplatin. This is in agreement with previously published data for ECT with both drugs in a murine melanoma study[21]. This study found that ECT with oxaliplatin is as effective as ECT with cisplatin, when the oxaliplatin concentration is increased by 1.6-times compared to the cisplatin concentration[21]. Currently the understanding of the mechanism underlying this

difference between the effects of oxaliplatin and cisplatin is unclear. ECT with cisplatin at 11µM had the most impact on the recovery potential of all tested lung cancer cell lines. The tested drug concentration range (0.5-11µM) is towards the lower end of typically tested drug concentrations for ECT[21,28], thus effectiveness of oxaliplatin ECT, in a lung cancer context, could be tested in the future with higher oxaliplatin concentrations. While direct translation between *in vitro* used drug concentration and *in vivo* drug concentration is difficult, experiments employing ECT with cisplatin at 1mg/kg for murine melanoma and lung cancer treatment was successful[22], and in the ESOPE study cisplatin was administered successfully for ECT treatment to melanoma patients intratumorally at 0.5-2mg per cm^3 tumour size (tumour size dependent). Therefore, the exact dosage for cisplatin in *in vivo* human lung cancer treatment will need to be determined as part of a phase I clinical trial.

In addition to using electroporation to facilitate the uptake of chemotherapeutic drugs (ECT), electroporation can also be used to facilitate the uptake of calcium (CaEP). Calcium is tightly regulated at the cellular level and an excessive influx of calcium overwhelms the cells, causing mitochondrial dysfunction, leading to cell death[38]. This emerging treatment modality has a similar effect on tumour vasculature as ECT[38] and can induce a clear reduction in human cancer cell spheroids, similar to bleomycin ECT[28], whilst calcium is also hypothesised to have immunostimulatory effects[27]. However, in contrast to chemotherapeutic drugs, calcium is a non-toxic molecule that should be able to induce cell death in the treated cells, and thus has fewer side-effects than chemotherapeutic drugs[27]. Moreover, calcium is cheaper than chemotherapeutic drugs, and calcium, also does not lead to the immunosuppressive effects of chemotherapy[27]. As such, calcium is an attractive alternative to chemotherapeutic drugs in combination with EP. However, here we observed that CaEP with 5mM calcium did not have any significant impact on the metabolic activity or recovery potential of either A549 or LLC cells. It is possible that an increased dosage may have demonstrated more efficacy, as a higher calcium concentration of 9mM was used for *in vivo* CaEP treatment in one case of feline cutaneous malignant melanoma following disease re-occurrence after initial ECT treatment[39]. The treatment was well tolerated by the cat and the cat survived for 5

months post CaEP treatment, while a 2-month survival is typical for this type of feline cancer. This could indicate that higher calcium concentrations could be tested in the future for application in lung cancer treatment to see if the higher dosage would increase efficacy of the treatment. The effect of CaEP on immune populations has also been investigated. Tremble *et al.* investigated the impact of CaEP at different calcium concentrations on the phenotype and functionality of murine bone-marrow-derived melanoma conditioned macrophages *in vitro*[27]. This study showed that CaEP with 500µM calcium could protect the macrophages against EP-induced cell death, while the same was not observed with CaEP with 5mM calcium. Also, CaEP with 5mM calcium may inhibit anti-cancer functionality of murine bone-marrow-derived macrophages *in vitro* compared to CaEP with 0.5mM calcium. CaEP treated macrophages led to increased IL-10 secretion from co-cultured $CD4^+$ and $CD8^+$ T cells in a dose-dependent manner[27]. Thus, potential increases in killed tumour cells post CaEP at higher calcium concentrations might need to be weighed against the impact higher calcium dosage could have on immune cells to strike the right balance between killing of the tumour cells and protecting the immune cells to create a sustainable immune response. Therefore, in order to determine optimal calcium concentrations within a CaEP setting for lung cancer treatment, more research is required, which should also include the impact CaEP has on DCs.

Further to determining the right drug and drug concentration for electroporation-based lung cancer treatment, the right device for the delivery of the electric pulses to lung tumours needs to be developed. As lung tumours are in relatively close proximity to the heart, optimized treatment protocols will need to be employed to protect the heart's electric functions[40]. Therefore, the delivery of the electric pulse should not be delivered during the vulnerable period of the heart[6]. This added difficulty should not be overestimated though, as there is a case-report of a melanoma patient with a defibrillator/pace-maker being successfully treated with ECT without any reported side-effects, when the pace-maker was only 5cm from the treatment side[41]. Taken together our results indicate that ECT treatment for lung cancer patients is a possibility and that cisplatin is the drug of choice to be used for ECT for lung cancer treatment *in vitro* and *in vivo*.

Due to its heterogenic cell features and low immunogenicity, lung cancer is able to evade the patient's immune response. Moreover, despite the introduction of checkpoint inhibitor immunotherapy, disease prognosis for lung cancer patients overall remains low, although the treatment does increase long-term survival for some patients[3,12]. Therefore, the impact of ECT on the immune cells within the treated areas needs to be considered when designing the final treatment protocol for lung cancer patients. During the early stages of ECT development for cancer treatment, it was demonstrated that the treatment needed to be administered to immunocompetent mice to be effective. Specifically, T cells have been identified as a key mediator of the local immune response after ECT treatment, as no treatment effect was observed in T cell deficient mice[13,15–17,42]. Simultaneously, ECT itself can change the T cell subpopulation mix in treated melanoma lesions[19]. Therefore, we first examined the impact of electroporation and ECT on T cells. Our data indicates that T cells are not effected either by electroporation or by ECT with 11µM cisplatin. They have a high viability and metabolic activity at all tested conditions in the short- and long-term following treatment. Therefore, one of the simplest explanations as to why treatment results after ECT are T cell dependent is that T cells simply do not die from the treatment, and also that their functionality does not seem to be significantly impacted following treatment. One possible explanation as to why T cells are less impacted by EP and ECT is that they are smaller than cancer cells, and typically higher electric field strengths are needed to reach the same level of efficacy with a smaller cell compared to a bigger cell[5].

To sustain a long-lasting immune response following any treatment, antigen-presenting cells (APCs) are needed to activate the adaptive immune response. Therefore, we next examined the impact of electroporation and ECT on DCs and macrophages, as these APCs are known to be critical for activation of a systemic immune response in the context of tumorigenesis[43]. In contrast to T cells, APCs are significantly impacted by electroporation and ECT above 800V/cm, with the electric field strength being responsible for most of the reduced viability and metabolic activity. Of interest, Gerlini *et al*[19] showed that ECT induces a significant reduction in epidermal Langerin^{+} Langerhans cells (skin-specific subtype of DCs) 7 days post

treatment. As these cells co-expressed CCR7, needed for migration to the lymph nodes, and CD83, a maturation marker of DCs, Gerlini *et al* concluded that ECT induces the activation of the Langerhans cells and their migration out of the tumours, hence explaining their absence 7 days post ECT treatment. In light of our findings identifying the high level of APC death at higher electric field strengths, it is possible that instead of leading to activation of Langerhans cells, despite the relevant marker expression, ECT did kill a relevant proportion of the Langerhans cells present in the treated area, thus explaining the results from day 7 post-treatment.

Our *in vitro* data indicate that at standard ESOPE parameters of 1000V/cm, a significant percentage of APCs present at the site of local ECT will be impacted by the treatment. Whilst additional antigen presenting cells will likely be subsequently recruited to the treatment site, the direct damage caused to the intra-tumoral APCs may possibly delay, or reduce, the subsequent activation of a systemic immune response. Whether a similar effect will be observed on immune cells treated within tumour tissue will need to be determined in future studies, particularly considering that the immune cells present in the tumour microenvironment will differ per lung cancer patient[44]. Based on our results, it might therefore, be worthwhile to investigate the possibility of lowering the electric field strength for *in vivo* ECT treatments in order to preserve the APC population in the treatment side to enhance the systemic immune response. In addition, it would also be worthwhile to investigate which immune cells enter the tumour post-ECT treatment once the vascular lock has resolved itself.

In order to better understand the effect of ECT at 800V/cm compared to ECT at 1300V/cm, we next investigated these two conditions in a murine lung cancer model. Unfortunately, due to the inexplicable very high ulcerating tumour rates in our model, which forced us to sacrifice animals prematurely, we were unable to detect any differences in tumour growth, median survival time or immune cell composition post treatment. It is known that LLC-induced tumours can lead to ulceration in C57B6J mice, but it was challenging to identify papers reporting the ulceration rate[45–48]. Janker *et al.* showed in a comparison of subcutaneously injections of LLC cells, that

injection into the back did not lead to any ulcerations while injections into the neck lead to an ulceration rate of 40% within 15 days and 80% within 20 days when injecting $2.5x10^5$ cells[48]. Fitzgerald *et al.* reported that one out of eleven nude mice developed ulcerating tumours when injected with $5x10^5$ LLC cells genetically modified to express luciferase and green fluorescent proteins[47]. Therefore, whilst some authors have reported findings similar to those presented in this thesis, it is challenging to understand whether our observations of a high tumour ulceration rate are typical of the LLC cell line and generally go unreported, or whether this was an effect specific to the mice purchased for our study/the conditions in our animal unit. In addition, it was surprising to observe that the ulceration status had only a small impact on the immune cell population in the tumours, spleen and lymph nodes. Ulceration is typically liked with inflammation and with changes in the ulcerated lesions, like reduced $CD8^+$ lymphocyte infiltration, as it is a chronic wound, it would have been expected to observe some clear changes in the immune cell population at least in the tumour tissue[49,50]. Of interest, cisplatin was the treatment that most consistently reduced the presence of the tested immune cells in the ulcerated tumours, which could be linked to the immunosuppressive effects chemotherapy has in general[27]. The only change consistently induced by the tested treatments, and independent of the ulceration status, was the increase in the $CD45^+$ cell population in the spleens of treated mice. CD45 is the classical marker for leukocytes[51] and increased leukocyte infiltration is most often linked to infections and inflammatory processes[52]. Thus, the increased levels of $CD45^+$ cells post treatment in the spleen could indicate that the immune system was activated. As CD45 is only a very broad marker for all nucleated hemopoietic cells[51], more in depth analysis needs to be carried out in the future to further determine which type of processes got initiated by the tested treatments.

Alternative models for exploring the effectiveness of 800ECT compared to 1300ECT could be either the use of spheroid models or using different murine cancer models. Multicellular tumour spheroid models can predict *in vivo* efficacy of oncological drugs and they can also mimic several important key features of tumours *in vitro* like nutrients, oxygen and metabolic waste diffusive gradients, the presence of cell-to-

cell interactions and signalling, and chemoresistance[53]. Spheroid models are already used in pre-clinical ECT and CaEP experiments for different cancer types[28,54,55]. To examine the impact ECT has on immune cells in a tissue-like environment, LLC-immune cell spheroids could be included in any further studies employing spheroids to elucidate the impact ECT has on the immune populations. As the LLC murine lung cancer model resulted in a high rate of ulceration, it could be feasible to use other murine cancer cells lines, for example B16F10 or Pan02, to test the effectiveness of 800ECT compared to 1300ECT *in vivo* as a proof-of-concept study. B16F10 has previously been optimized to 700V/cm and Pan02 to 800V/cm[23] (Chapter 3). Both cell lines are less known for creating ulcerating tumours[56] and already only need a lowered electric field strength to induce 95% treatment efficacy[23].

Taken together, the findings of our experiments showed that cisplatin ECT is a potential treatment modality for lung cancer therapy. Before this can be implemented in clinical settings, some application questions need to be solved, but overall, it is potentially feasible. In addition, here we have demonstrated that the T cell response post ECT is not impacted, as T cells do not get highly permeabilised by electroporation, and that their viability and metabolic activity is not impacted following ECT treatment with ESOPE parameters. In contrast, DCs and macrophages both get highly permeabilised with electroporation with ESOPE parameters and their viability and metabolic activity is significantly impacted by ECT with ESOPE parameters. This could give an indication as to why long lasting and abscopal effects are not consistently observed in mice or patients following ECT treatment. Our experiment comparing the impact of ECT at 800V/cm with ECT at 1300V/cm for LLC cells showed that, at least for the *in vitro* setting, lowering the electric field strength to 800V/cm can still meaningfully reduce the recovery potential of the LLC cells. This potentially could translate into a sufficient local tumour reduction *in vivo* following ECT with a lower electric field strength. Due to the failure of our murine study, we were unable to show a translation from these *in vitro* findings into *in vivo* findings. Thus, further investigation into the impact of ECT on the immune cell population in treated lesions as well as testing the impact of ECT with lowered electric field

strength on local tumour burden reduction, immune cell populations, disease response and progression is required.

4.6 Bibliography

1. Bade, B. C. & Dela Cruz, C. S. Lung Cancer 2020: Epidemiology, Etiology, and Prevention. *Clin. Chest Med.* **41**, 1–24 (2020).

2. Janet Wangari-Talbot and Elizabeth Hopper-Borge. Drug Resistance Mechanisms in Non-Small Cell Lung Carcinoma. *J Can Res Updat.* **2**, 265–282 (2013).

3. Onoi, K. *et al.* Immune checkpoint inhibitors for lung cancer treatment: A review. *J. Clin. Med.* **9**, (2020).

4. Mir LM, Belehradek M, Domenge C, Orlowski S, Poddevin B, Belehradek J Jr, Schwaab G, Luboinski B, P. C. L. Electrochemotherapy, a novel antitumor treatment - 1st clinical-trial. *COMPTES RENDUS L Acad. DES Sci. Ser. III-SCIENCES LA VIE-LIFE Sci.* **313**, 613–618 (1991).

5. Yarmush, M. L., Golberg, A., Serša, G., Kotnik, T. & Miklavčič, D. Electroporation-Based Technologies for Medicine: Principles, Applications, and Challenges. *Annu. Rev. Biomed. Eng.* **16**, 295–320 (2014).

6. Miklavčič, D. *et al.* Electrochemotherapy: Technological advancements for efficient electroporation-based treatment of internal tumors. *Med. Biol. Eng. Comput.* **50**, 1213–1225 (2012).

7. Gehl, J. *et al.* Updated standard operating procedures for electrochemotherapy of cutaneous tumours and skin metastases. *Acta Oncol. (Madr).* **57**, 874–882 (2018).

8. Marty, M. *et al.* Electrochemotherapy - An easy, highly effective and safe treatment of cutaneous and subcutaneous metastases: Results of ESOPE (European Standard Operating Procedures of Electrochemotherapy) study. *Eur. J. Cancer, Suppl.* **4**, 3–13 (2006).

9. Campana, L. G. *et al.* Treatment efficacy with electrochemotherapy: A multi-institutional prospective observational study on 376 patients with superficial tumors. *Eur. J. Surg. Oncol.* **42**, 1914–1923 (2016).

10. Watson, R. A. *et al.* Development of a best-practice clinical guideline for the use of bleomycin in the treatment of germ cell tumours in the UK. *Br. J. Cancer* **119**, 1044–1051 (2018).

11. Farago, A. F. & Keane, F. K. Current standards for clinical management of small cell lung cancer. *Transl. Lung Cancer Res.* **7**, 69–79 (2018).

12. Domagala-Kulawik, J., Osinska, I. & Hoser, G. Mechanisms of immune response regulation in lung cancer. *Transl Lung Cancer Res* **3**, 15–22 (2014).

13. Calvet, C. Y., Famin, D., André, F. M. & Mir, L. M. Electrochemotherapy with bleomycin induces hallmarks of immunogenic cell death in murine colon cancer cells. *Oncoimmunology* **3**, 2–11 (2014).

14. Dudek, A. M., Garg, A. D., Krysko, D. V., De Ruysscher, D. & Agostinis, P. Inducers of immunogenic cancer cell death. *Cytokine Growth Factor Rev.* **24**, 319–333 (2013).

15. Serša, G. *et al.* Electrochemotherapy with CDDP on LPB sarcoma: Comparison of the anti- tumor effectiveness in immunocompetent and immunodeficient mice. *Bioelectrochemistry Bioenerg.* **43**, 279–283 (1997).

16. Roux, S. *et al.* Tumor destruction using electrochemotherapy followed by CpG oligodeoxynucleotide injection induces distant tumor responses. *Cancer Immunol. Immunother.* **57**, 1291–1300 (2008).

17. Sedlar, A. *et al.* Potentiation of electrochemotherapy by intramuscular IL-12 gene electrotransfer in murine sarcoma and carcinoma with different immunogenicity. *Radiol. Oncol.* **46**, 302–311 (2012).

18. Falk, H. *et al.* Calcium electroporation induces tumor eradication, long-lasting immunity and cytokine responses in the CT26 colon cancer mouse model. *Oncoimmunology* **6**, 1–8 (2017).

19. Gerlini, G. *et al.* Dendritic cells recruitment in melanoma metastasis treated by electrochemotherapy. *Clin. Exp. Metastasis* **30**, 37–45 (2013).

20. Di Gennaro, P. *et al.* CD4+FOXP3+ T regulatory cells decrease and CD3+CD8+ T cells recruitment in TILs from melanoma metastases after electrochemotherapy. *Clin. Exp. Metastasis* **33**, 787–798 (2016).

21. Ursic, K. *et al.* Comparable effectiveness and immunomodulatory actions of oxaliplatin and cisplatin in electrochemotherapy of murine melanoma. *Bioelectrochemistry* **119**, 161–171 (2018).

22. Tremble, L. F., O'Brien, M. A., Soden, D. M. & Forde, P. F. Electrochemotherapy with cisplatin increases survival and induces immunogenic responses in murine models of lung cancer and colorectal cancer. *Cancer Lett.* **442**, 475–482 (2019).

23. Bendix, M. B., Brint, E. & Forde, P. F. Electroporation of suspension cell lines – A proposed assay set for optimizations. *Bioelectrochemistry* **142**, 107891 (2021).

24. Szewczyk, A. *et al.* Calcium electroporation for treatment of sarcoma in preclinical studies. *Oncotarget* **9**, 11604–11618 (2018).

25. Duma, N., Santana-Davila, R. & Molina, J. R. Non–Small Cell Lung Cancer: Epidemiology, Screening, Diagnosis, and Treatment. *Mayo Clin. Proc.* **94**, 1623–1640 (2019).

26. Frandsen, S. K., Gissel, H., Hojman, P., Eriksen, J. & Gehl, J. Calcium electroporation in three cell lines: A comparison of bleomycin and calcium, calcium compounds, and pulsing conditions. *Biochim. Biophys. Acta - Gen. Subj.* **1840**, 1204–1208 (2014).

27. Tremble, L. F., Heffron, C. C. B. B. & Forde, P. F. The effect of calcium electroporation on viability, phenotype and function of melanoma conditioned macrophages. *Sci. Rep.* **10**, 1–12 (2020).

28. Frandsen, S. K., Gibot, L., Madi, M., Gehl, J. & Rols, M. P. Calcium electroporation: Evidence for differential effects in normal and malignant cell lines, evaluated in a 3D spheroid model. *PLoS One* **10**, 1–11 (2015).

29. Paardekooper, L. M. *et al.* Ethylene, an early marker of systemic inflammation in humans. *Sci. Rep.* **7**, 2–11 (2017).

30. Phothirath, P. *et al.* Generation of monocyte-derived dendritic cells in patients with hereditary hemochromatosis. *Clin. Immunol.* **105**, 93–103 (2002).

31. Cabeza-Cabrerizo, M., Cardoso, A., Minutti, C. M., Pereira Da Costa, M. & Reis E Sousa, C. Dendritic Cells Revisited. *Annu. Rev. Immunol.* **39**, 131–166 (2021).

32. Aldossary, S. A. Review on pharmacology of cisplatin: Clinical use, toxicity and mechanism of resistance of cisplatin. *Biomed. Pharmacol. J.* **12**, 7–15 (2019).

33. Edhemovic, I. *et al.* Intraoperative electrochemotherapy of colorectal liver metastases. *J. Surg. Oncol.* **110**, 320–327 (2014).

34. Tafuto, S. *et al.* Electrochemotherapy as a new approach on pancreatic cancer and on liver metastases. *Int. J. Surg.* **21**, S78–S82 (2015).

35. Bourke, M. *et al.* P80. Endoscopically targeted electrochemotherapy for the treatment of colorectal cancer. *Eur. J. Surg. Oncol.* **38**, 1127–1128 (2012).

36. Gasljevic, G. *et al.* Histopathological findings in colorectal liver metastases after electrochemotherapy. *PLoS One* **12**, 1–12 (2017).

37. Markelc, B., Sersa, G. & Cemazar, M. Differential Mechanisms Associated with Vascular Disrupting Action of Electrochemotherapy: Intravital Microscopy on the Level of Single Normal and Tumor Blood Vessels. *PLoS One* **8**, 1–11 (2013).

38. Staresinic, B. *et al.* Effect of calcium electroporation on tumour vasculature. *Sci. Rep.* **8**, 1–14 (2018).

39. Dos Anjos, D. S., Rodrigues, C. G., Silva, N. C., De Nardi, A. B. & Fonseca-Alves, C. E. Electrochemotherapy associated with calcium electroporation in metastatic feline cutaneous malignant melanoma. *Acta Sci. Vet.* **47**, 1–6 (2019).

40. Ziobrowski, Hannah N., Sonneville, Kendrin R. Eddy, Kamryn T., Crosby, Ross D., Micali, Nadia, Horton, Nicholas J., Field, A. E. Irreversible Electroporation Near the Heart: Ventricular Arrhythmias Can Be Prevented With ECG Synchronization. *AJR Am J Roentgenol. 2011* **65**, 139–148 (2011).

41. Marandola, M. *et al.* Electrochemotherapy and heart function: Treatment in a patient with implantable cardioverter defibrillator/pace-maker. *World J. Anesthesiol.* **2**, 14 (2013).

42. Falk, H. *et al.* Electrochemotherapy and calcium electroporation inducing a systemic immune response with local and distant remission of tumors in a patient with malignant melanoma–a case report. *Acta Oncol. (Madr).* **56**, 1126–1131 (2017).

43. Wculek, S. K. *et al.* Dendritic cells in cancer immunology and immunotherapy. *Nat. Rev. Immunol.* **20**, 7–24 (2020).

44. Schoenhals, J. E. *et al.* Uncovering the immune tumor microenvironment in non-small cell lung cancer to understand response rates to checkpoint blockade and radiation. *Transl. Lung Cancer Res.* **6**, 148–158 (2017).

45. Bugge, T. H., Kombrinck, K. W. & Xiao, Q. Growth and dissemination of lewis lung carcinoma in plasminogen-deficient mice. *Fibrinolysis and Proteolysis* **11**, 24 (1997).

46. Scott, K., Phan, T. T., West, A. P., Taniguchi, C. M. & Dantzer, R. Neutralizing interleukin-6 in tumor-bearing mice does not abrogate behavioral fatigue induced by Lewis lung carcinoma. *Behav. Brain Res.* **417**, 113607 (2022).

47. Fitzgerald, J. E. *et al.* Heterogeneity of circulating tumor cell dissemination and lung metastases in a subcutaneous Lewis lung carcinoma model. *Biomed. Opt. Express* **11**, 3633 (2020).

48. Janker, F., Weder, W., Jang, J. H. & Jungraithmayr, W. Preclinical, non-genetic models of lung adenocarcinoma: A comparative survey. *Oncotarget* **9**, 30527–30538 (2018).

49. Naseri, S. *et al.* Tumor ulceration, reduced infiltration of CD8-lymphocytes, high neutrophil-to-CD8-lymphocyte ratio and absence of MC virus are negative prognostic markers for patients with merkel cell carcinoma. *Cancers (Basel).* **12**, (2020).

50. Hua, Y. & Bergers, G. Tumors vs. Chronic Wounds: An Immune Cell's Perspective. *Front. Immunol.* **10**, 1–11 (2019).

51. Tchilian, E. Z. & Beverley, P. C. L. CD45 in memory and disease. *Arch. Immunol. Ther. Exp. (Warsz).* **50**, 85–93 (2002).

52. Bronte, V. & Pittet, M. J. The spleen in local and systemic regulation of immunity. *Immunity* vol. 39 806–818 (2013).

53. Lazzari, G. *et al.* Multicellular spheroid based on a triple co-culture: A novel 3D model to mimic pancreatic tumor complexity. *Acta Biomater.* **78**, 296–307 (2018).

54. Griseti, E. *et al.* Pulsed Electric Field Treatment Enhances the Cytotoxicity of Plasma-Activated Liquids in a Three-Dimensional Human Colorectal Cancer Cell Model. *Sci. Rep.* **9**, 1–15 (2019).

55. Bregigeon, P. *et al.* Integrated platform for culture, observation, and parallelized electroporation of spheroids. *Lab Chip* (2022) doi:10.1039/d2lc00074a.

56. Danciu, C. *et al.* Behaviour of four different B16 murine melanoma cell sublines: C57BL/6J skin. *Int. J. Exp. Pathol.* **96**, 73–80 (2015).

Chapter 5

An investigation into the effect of ECT on dendritic cell phenotype and function

5.1 Abstract

Dendritic cells (DCs) are central to the function of the innate and adaptive immune systems and also play a crucial role in the anti-tumour response. It was previously shown that DCs are significantly negatively impacted by electrochemotherapy (ECT) at electric field strengths surpassing 1000V/cm.

The impact of cisplatin ECT on murine DCs *in vitro* was examined at three different electric field strengths (800V/cm [800ECT], 1000V/cm [1000ECT] and 1300V/cm [1300ECT]). The type of cell death they undergo, phenotypic changes, global gene expression and functional responses were investigated post-treatment to examine if current ECT treatment effectiveness could be improved by modifying currently used ECT protocols. Our findings demonstrate that 800ECT and 1300ECT do induce different functional changes in treated DCs. It is also evident that the higher the electric field strength is for the treatment, the more cellular processes are impacted. ECT treatment seems to induce necrotic cell death with all treatment conditions. Cellular maturation makers were upregulated 24-hours post-treatment by both 1000ECT and 1300ECT, but not after 800ECT. 800ECT induced the upregulation of Toll-like Receptors (TLRs) 3, 1000ECT induced the upregulation of TLR3, TLR6 and TLR9, while 1300ECT induced the upregulation of TLR6 and TLR9. The gene expression profile induced in DCs post ECT treatment was also examined with distinctively different sets of genes upregulated 4-hours post 800ECT compared to 1000ECT and 1300ECT. In all three treatment groups the upregulated genes were connected to stress- and immune- responses. Finally, DCs remain partially functionally active following EP and ECT treatments as assessed by IFN-γ and TNF-α secretion, albeit with differential levels of these cytokines being secreted post treatment with the varying electric field strengths.

Future research is needed to investigate more specific questions in regard to the impact ECT at different electric field strengths has on DCs and how, depending on the outcome, ECT protocols for patient care might need to be updated to improve therapy results. Additionally, the observed changes presented here will need to be confirmed *in vivo* with DCs that have been exposed to the tumour-microenvironment.

5.2 Introduction

In the previous chapter we have shown that dendritic cells (DCs) and macrophages are significantly negatively impacted by electrochemotherapy (ECT) at electric field strengths exceeding 1000V/cm with respect to their metabolic activity and viability post-treatment, while T cells are not impacted[1]. DCs are professional antigen-presenting cells (APCs) that are central to link the innate and adaptive immune system. They originate in the bone-marrow and are found in virtually all mammalian tissues where they are maintained as resting DCs acting as sentinels of the immune system. Through changes in their environment, most likely the presence of damage-associated molecular patterns (DAMPs), but also through cytokine stimulation, these cells become activated, undergo phenotypic changes, and activate multiple additional immune cell types of the innate and adaptive immune system. DCs are able to prime naïve T cells, present antigens to B cells and also recruit Natural Killer (NK) cells[2–4]. In addition to their centrality in antigen-specific immunity and tolerance against pathogens, DCs are also vital for the anti-tumour response of the immune system[3]. To induce an anti-tumour response, activated DCs migrate to the draining lymph nodes of the tumours where they cross-present the tumour-associated antigens to cytotoxic T cells[5]. Whilst DCs generally have this anti-tumorigenic capacity, the suppressive environment of the tumour reduces the capacity of the activated DCs to elicit a potent immune response[4,5]. Thus, understanding how DCs are impacted by a new treatment modality is a key factor in optimizing treatment parameters.

Little attention has been paid towards the impact ECT has directly on immune cells both *in vitro,* but also within the tumour microenvironment (TME) *in vivo*. From murine[6–8] and human[9,10] studies it is known that ECT elicits changes in the immune cell composition in both the treated areas as well as at distant sites. Bleomycin ECT administered to mice for melanoma treatment increase the presence of DCs, T cells, NK cells and macrophages 3 days post treatment (see Table 1.1). In melanoma patients, bleomycin ECT increases the presence of $CD8^+$ T cells and plasmacytoid DCs while it decreases the presences of $CD4^+FOXP3^+$ Treg cells and Langerhans cells (skin-specific subtype of DCs)[11] (see Table 1.1). Additionally, Roux *et al.* showed that an

electroimmunotherapy consisting of ECT with CpG (TLR9 agonist) co-treatment can increase local and systemic (immune) responses in murine melanoma models and a murine fibrosarcoma model, as well as induce a specific immune memory that is T cell dependent[8]. Currently, the only study to date showing a direct impact of an electroporation-based cancer treatment on any type of immune cells found that calcium electroporation (CaEP) can increase the ability of melanoma-conditioned bone-marrow derived macrophages to stimulate cytotoxic $CD8^+$ T cells[12].

To determine the impact ECT has on DCs, we wished to examine the type of cell death they undergo and their global gene expression changes. In regard to the type of cell death immune cells undergo post ECT treatment, very little is currently known; even the way in which cancer cells are dying post ECT treatment is still under debate[13,14]. Immunogenic cell death (ICD) is defined as any form of regulated cell death causing activation of the adaptive immune system[13], and has been linked to ECT-induced tumour cell death *in vitro* and in rodent studies. The study of ICD following any kind of treatment so far has been limited to malignant cells and it is currently unknown whether immune cells can die via ICD.

Changes in gene expression could provide additional avenues to investigate with respect to designing suitable co-treatments for ECT, with the goal of increasing the effectiveness of the treatment. Similarly, improved understanding of the type of cell death DCs undergo post ECT treatment could be targeted to improve therapy outcome. A previous study has shown that electroporation itself does not change the expression profiles of major tumour suppressor genes, cell cycle oncogenes or the expression levels of genes relevant to DNA stability in malignant cells, making electroporation a safe method to manipulate cells that does not promote tumorigenesis[15]. Although EP, and thus ECT, is considered a non-thermal therapy, the same study showed an induction of Heat-shock-protein 70 stress responses[15].

In this chapter we wished to examine a range of cellular responses and processes associated with dendritic cells following ECT treatment at the various electric field strength parameters, in order to better understand what effect ECT has on these critical immune populations at these different electric field strengths, and therefore

be better able to both preserve their integrity, and also to tailor ECT treatments to enhance the antigen presenting efficacy of these cells. Therefore, we investigated DC cell death post ECT treatment, changes in DC phenotype and Toll-like receptor (TLR) expression by DCs post-treatment. In addition, UPX 3' Transcriptome Sequencing was performed to determine the effect of ECT on transcription across the genome. Finally, we assessed whether DCs remain functionally active post-treatment by determining their cytokine secretion post ECT at the various electric field strengths.

5.3 Materials & Methods

5.3.1 Murine Bone marrow-derived Dendritic cell derivation

Murine Bone marrow-derived cells were obtained from the back legs of healthy 8–20-week-old female C57BL6J mice (Envigo, Bicester, UK) by passing ice cold RPMI through the bones to obtain the bone marrow, which was then passed through 0.45µM cell strainer (BD, Falcon, Franklin Lakes, USA) to obtain the cells. Red cells were lysed with red cell lysis buffer for 3 minutes on ice (Biolegend, San Diego, USA). Bone marrow cells were diluted at $1x10^6$ cells/mL in RPMI with 10% heat inactivated FBS (heated for 30 minutes at 60°C; Sigma), 50 IU/mL penicillin and 50 µg/mL streptomycin supplemented with 10ng/mL GM-CSF (Peprotech, London, UK) and 10ng/mL IL-4 (Peprotech). Cells were cultured at 4mL/well in 6 well plates for a total of 6 days. Cells were split in half on day 2 and day 4. Non-adherent cells on day 6 were considered to be bone marrow-derived Dendritic cells (DCs).

5.3.2 In vitro ECT parameters

To test impact of ECT at different electric field strengths on Dcs, $1×10^6$ cells were suspended in 400 µL of electroporation buffer (EPB: 10mM HEPES, 250mM Sucrose and 1mM $MgCl_2$ in ddH20) with 11µM cisplatin. Cell suspensions were aliquoted into 4mm sterile EP cuvettes (VWR). Cuvettes were exposed to eight electric pulses at 800V/cm, 1000V/cm and 1300V/cm electric field intensities respectively, with pulse duration of 100 µs and 1 Hz frequency using a BTX ECM 2001 square wave electroporator (BTX, San Diego, USA). After the electroporation cells were rested for 20-30 minutes at 37°C and 5% CO_2 before various assays were set-up.

5.3.3 Flow cytometry

Single cell suspension from tissue or cell culture was prepared prior to the staining. 100,000 to 200,000 cells were diluted in 100µL FACS buffer (PBS supplemented with 5% heat-inactivated FBS and 2mM EDTA), cell surface receptors CD16/32 were blocked by incubating $1µg/1x10^6$ cells of TruStain FcX™ Antibody (Biolegend) for 10 minutes at 8°C in the dark. Following the blocking, without washing, the DC cell culture samples were stained for 30 minutes at 8°C in the dark with Fiaxable live-

death marker Near-infrared (Thermofisher Scientific), AF488 Anti-CD11c (Biolegend), PerCP-Cy5.5 Anti-CD80 (Biolegend) and APC Anti-MCH II (Biolegend). Samples were washed twice after the staining was completed and at least 10,000 events were collected per sample. Flow cytometry was conducted using an LSRII machine with a 5-laser (355 /405 /488 /561 /640nm) configuration (Table 2.2) (BD Biosciences) and the results analysed employing FlowJo V10 (BD Biosciences).

5.3.4 RNA Sequencing by Qiagen

For UPX 3' Transcriptome Sequencing $1x10^6$ cells were left untreated or treated with ECT at 800V/cm, 1000V/cm and 1300V/cm respectively and let to rest 4 hours prior to being pelleted and frozen down. All further processing steps as well as statistical analysis were done by Qiagen. In short, RNA was isolated using the RNeasy Plus Mini Universal (QIAGEN) according to manufacturer's instructions with an elution volume of 30 µL. The library preparation was done using the QIAseq UPX 3' Transcriptome Kit (QIAGEN). A total of 5 ng purified RNA was converted into cDNA NGS libraries, these were sequenced on a NextSeq®500 sequencing instrument according to the manufacturer instructions with 100 bp read length for read 1 and 27 bp for read 2. Raw data was demultiplexed and FASTQ files for each pool was generated using the bcl2fastq Conversion Software (Illumina® Inc.). The reads were then mapped to the mMouse genome GRCm38 v. 80 and annotated using the ENSEMBL GRCm38 v. 86 mRNA annotation. The 'Empirical analysis of DGE' algorithm of the CLC Genomics Workbench 21.0.4 was used for differential expression analysis with default settings. It is an implementation of the 'Exact Test' for two-group comparisons developed by Robinson and Smyth[16], and incorporated in the EdgeR Bioconductor package Robinson et al.[17].

Cytoscape 3.9.1 was used to perform Search Tool for the Retrieval of Interacting Genes/Proteins (STRING) and molecular complex detection (MCODE) analysis on the data provided by the UPX 3' Transcriptome Sequencing.

5.3.5 Morphology analysis

Morphology of treated cells were analysed 4 hours post-treatment by light microscopy. 50.000 cells per condition were cytospun onto glass slides and stained using Rapi-Diff (Braidwood Laboratories, London, UK). Presented images are representative of at least three independent experiments.

5.3.6 Cell Death Analysis

After 4 hours incubation post-treatment, cells were washed once in FACS buffer and stained with APC Annexin V and propidium iodine (Biolegend) for 15 minutes according to the manufacturer's protocol and analysed using the BD LSRII machine. The results were analysed employing FlowJo V10 (BD Biosciences).

5.3.7 Enzyme-Linked Immunosorbent Assays (ELISA)

Supernatants were either stored at -20°C or used directly to determine the concentration of murine IFN-γ and TNF-α using biolegend ELISA MAX Deluxe Kits according to manufacturer's manual (biolegend). Absorbance was directly read at 450nm with correction absorbance read at 570nmm on a FluoStar Omega (BMG Labtech; Aylesbury UK) machine. Difference between the 450nm and 570nm was calculated by the accompanying MARS software (BMG Labtech).

5.3.7.1 Stimulation protocol

DCs were left to rest for 30 minutes post-treatment before being stimulated for 24 hours by either 1µg/mL LPS (Invivogen, San Diego, USA), 1µM CpG (ODN2395; Invivogen), 10µg/mL polyI:C (Invivogen) or 1µg/mL R848 (Invivogen). After the 24-hour stimulation period supernatants were collected and analysed via ELISA.

5.3.8 qRT-PCR

RNA was isolated from treated cells 4 hours post-treatment utilizing the GenElute total mRNA kit (Sigma Aldrich) as per manufacturer's guidelines. cDNA synthesis was done by using the Bioline cDNA synthesis kit (Bioline, London, UK) according to the manufacturer's instructions. cDNA template was amplified on the LightCycler® 480 (Roche, Basel, Switzerland) in 10µl total reaction volume. All results were analysed

using the ΔΔct method and the gene of interest was normalized to the corresponding β-actin gene results. Fold-change values over the untreated condition are represented and at least 3 separate biological replicas were analysed.

5.3.9 Statistical analysis

In vitro experiments were repeated at least three times on different days and with different cell preparations. All treatment conditions were normalized to the untreated condition for viability, metabolic activity and recovery assays. First a one-way ANOVA with Gaussian distribution, determined by Shapiro-Wilk test, and equal standard deviations, was performed to determine overall significant changes followed by Dunnett's post-hoc test to determine difference between treatment conditions and untreated control groups. Grubb's Test was employed to identify outliers. GraphPad Prism Version 9.0 software was used for all statistical analysis. P-values of $p \leq 0.05$ were considered significant.

5.4 Results

5.4.1 DCs display a diffuse morphology post EP and ECT

As we have shown in the previous chapter that DCs undergo cell death at a significantly higher rate when treated with EP and ECT at 1000V/cm and 1300V/cm than with EP and ECT at 800V/cm, we next investigated which form of cell death DCs undergo post treatment. The type of cell death cells undergo can have an impact on subsequent immune system reactions and therefore can initiate different cellular responses. Thus, initially we analysed the morphology of DCs 4 hours post EP and ECT treatment. We analysed morphological changes that are associated with either apoptotic cell death or necrotic cell death. Apoptotic cells are characterized by several distinct morphological features like initial marginalization of its chromatin, fragmentation of the nucleus later during the apoptotic process, and finally membrane blebbing and release of apoptotic bodies. Necrotic cells, on the other hand, are characterized by an initial increase in cellular volume, possible condensation of the chromatin, while towards the end of the process necrotic cells lost membrane integrity[14].

Overall, the cells displayed a very mixed morphology post EP and ECT treatment (Figure 5.1), with some having horse-shoe shaped nuclei (Figure 5.1 across all treatment conditions), which are known to be typical for monocytes, and others displaying the more expected dendritic cell form with multiple dendrites (Figure 5.1 across all treatment conditions). The size of the cells also varied from very small to quite big, with no clear connection of size to any specific treatment modality. It was observed that as treatment intensity increases so does cellular clumping. Similarly, as the treatment intensity increases, so does the presence of cells filled with an abundance of vesicles (indicated by * in Figure 5.1), as well as the presence of cells with very translucent cytoplasm (indicate by * in Figure 5.1). The abundance of vesicles inside a cell can either point towards a stress response or could be a sign of autophagy, while translucent cytoplasm is most commonly found in necrotic cells[14]. Additionally, cells with condensed nuclear material (indicated by * in Figure 5.1) were present in all tested conditions. Taken together this data indicates that there is no

visibly identifiable form of cell death, but that the cells are undergoing a clear stress response, which seems to increase as treatment intensity increases.

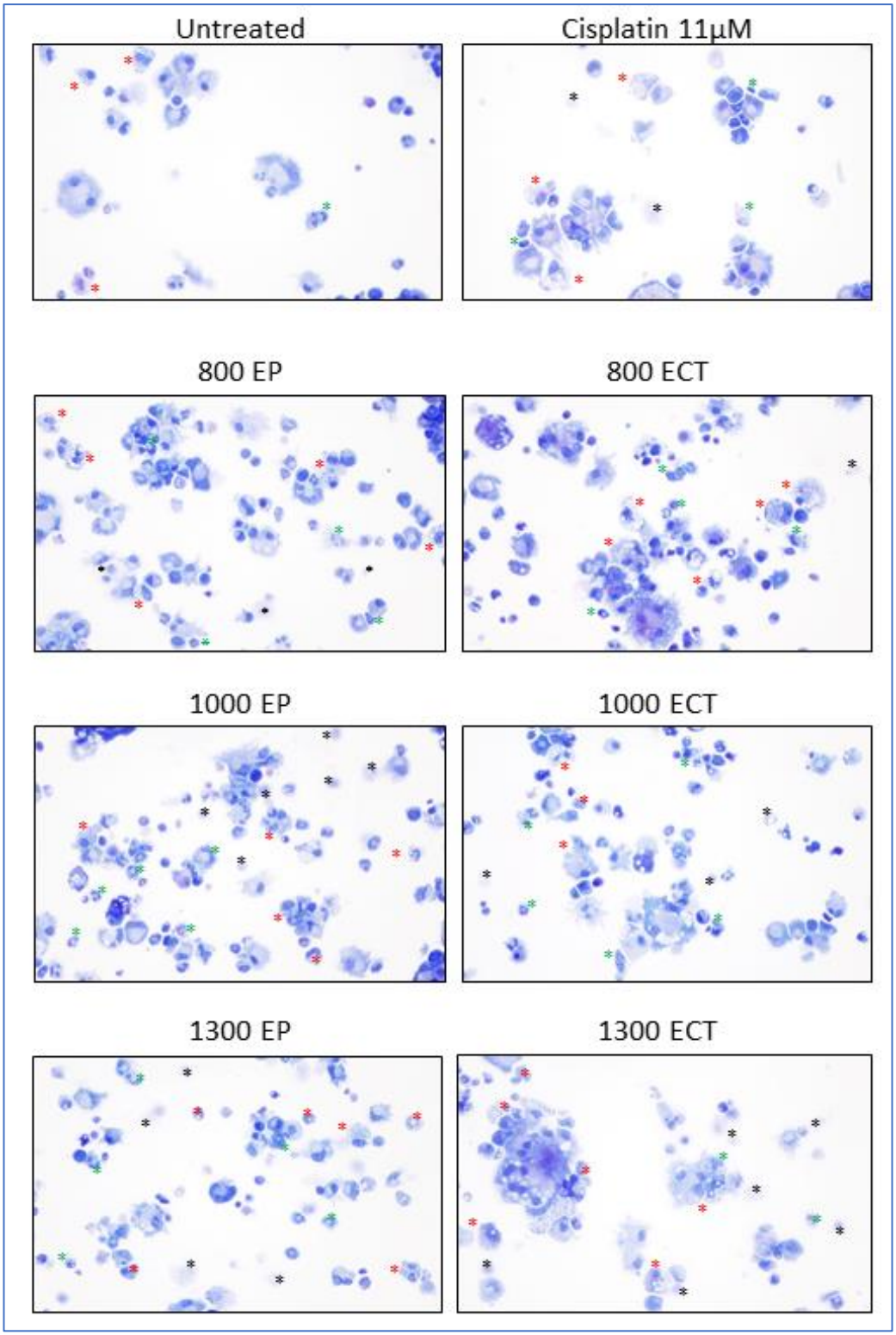


*Figure 5.1: Treatment with EP and ECT leads to mixed morphological responses. Morphology of murine DCs 4 hours post-treatment with EP respectively ECT at 800V/cm, 1000V/cm and 1300V/cm was assessed. Cells were harvested, cytospun and stained for morphological evaluation using light microscopy. Symbols denote cellular characteristics: *= condensed/fragmented nuclear material, *= vesicles, * = translucent cytoplasm. 400x magnification.*

5.4.2 Flow cytometry reveals that Dendritic cells undergo necrotic cell death post EP and ECT treatment

As morphology alone was not sufficient to determine the type of cell death DCs undergo following EP and ECT, we next analysed treated cells with an Annexin V-propidium iodine (PI) apoptosis assay. Annexin V binds to phosphatidylserine, which translocates to the outside of the cell membrane during apoptosis. As Annexin V is not sufficient to distinguish between apoptotic and necrotic cells, PI is used as a secondary marker to facilitate this distinction, as PI can bind to the DNA in the nucleus only due to loss of membrane integrity, and thus indicates typically dying cells. Therefore, cells which only stain positive for Annexin V are considered apoptotic cells, while cells staining double-positive for Annexin V and PI are considered late apoptotic cells, with PI-only positive cells considered to be necrotic cells. Cells which stain neither positive for Annexin V nor PI are viable cells[18].

This form of analysis revealed that all cells are dying via necrotic cell death rather than apoptotic cell death post EP and ECT treatment (Figure 5.2). With increasing electric field strengths, the percentage of cells dying increases, but no difference was observed between EP treatment alone and ECT at the same electric field strength. This may indicate that the loss in viability is caused mainly by the EP and that the addition of the drug has minimal additional effects. Cisplatin alone slightly, but not significantly, increased the proportion of cells dying via necrosis compared to untreated.

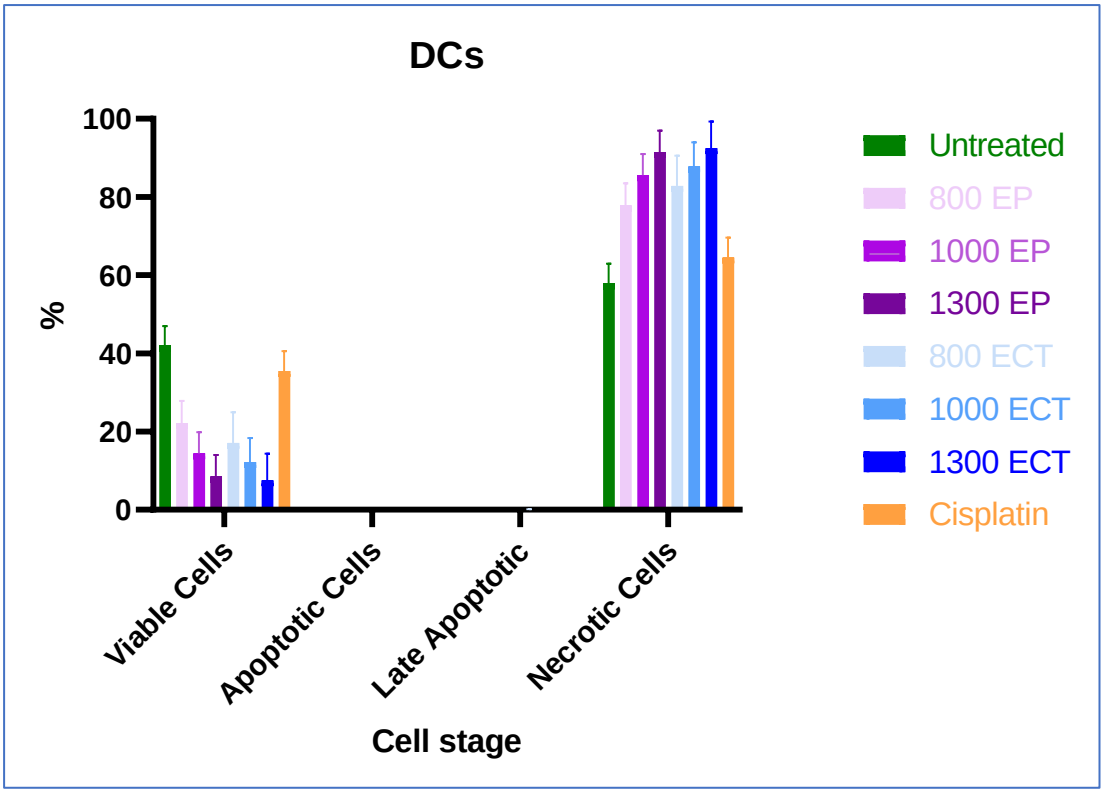


Figure 5.2: DCs undergo necrotic cell death independent of treatment type. DCs were treated either by EP or ECT with increasing electric field strength. 4 hours post-treatment the form of cell death was examined by AnnexinV and PI staining via flow cytometry.

5.4.3 1000ECT and 1300ECT induces maturation and activation of surviving DCs

In order to further examine the effect of different electric field strengths on dendritic cells, we initially investigated whether the differing voltages would alter any of the key cell surface expression markers of dendritic cells. CD11c, MHC II and CD80 were chosen as the markers for examination. MHC II expression increases as DCs mature and CD80 is a costimulatory molecule, also standardly considered a activation marker[2]. High levels of CD11c, which is not an exclusive DC phenotype marker, can be used in combination with MHC II expression to identify various subtypes of DCs[19]. DCs were treated with ECT at 800V/cm (800ECT), 1000V/cm (1000ECT) or 1300V/cm (1300ECT), rested for either 4 or 24 hours and then the expression of CD11c, MHC II and CD80 on the cell surface was analysed via flow cytometry.

4 hours post-treatment, the percentage of $MHCII^{+}CD11c^{+}$ DCs and the percentage of activated $CD80^{+}$ DCs within the $MHCII^{+}CD11c^{+}$ subpopulation was seen to be slightly, yet significantly, increased by 1300ECT ($p \leq 0.01$) (Figure 5.3A). 24 hours post-

treatment, the percentage of $MHCII^+CD11c^+$ DCs was increased following both 1000ECT ($p \leq 0.05$) and 1300ECT treatment ($p \leq 0.01$), with the percentage of activated $CD80^+$ DCs within the $MHCII^+CD11c^+$ subpopulation slightly, but significantly increased following 1300ECT treatment ($p \leq 0.01$) (Figure 5.3B). In contrast, 800ECT does not induce a significant change in the maturation or activation markers at either 4- or 24-hours post-treatment. Thus, whilst ECT decreases the viability of DCs post-treatment in a voltage-dependent manner, ECT also seems to activate the surviving cells at electric field strengths surpassing 1000V/cm.

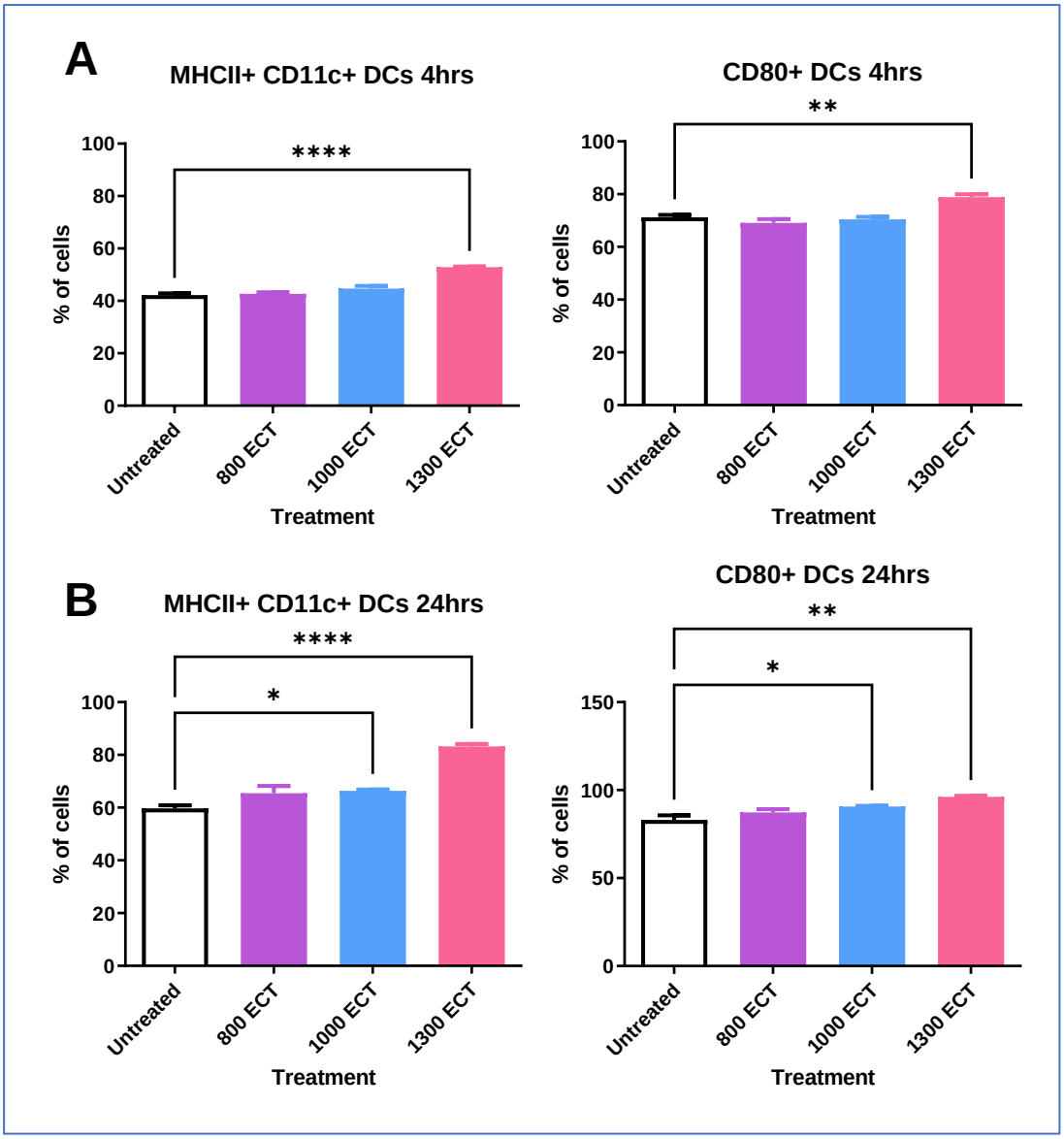


*Figure 5.3: 1000ECT and 1300ECT upregulate maturation and activation markers of treated DCs. DCs were treated with ECT at 800V/cm (800ECT), 1000V/cm (1000ECT) and 1300V/cm (1300ECT). Expression of MHC II, CD11c and CD80 was determined 4- and 24-hours post-treatment by flow cytometry. Expression of MHCII$^+$ CD11c$^+$ cells was determined of the viable population. CD80 expression was then analysed within the MHCII$^+$ CD11c$^+$ subpopulation. Data represents the mean ± SD from at least 3 separate experiments. *p≤0.05, **p≤0.01, ****p≤0.0001; compared to untreated.*

5.4.4 EP and ECT upregulate TLRs in a voltage dependent manner

As Roux *et al.* had shown that ECT can upregulate TLR9 expression within the TME in a murine melanoma model[8], we next investigated whether electroporation alone can induce upregulation of TLRs in DCs themselves, or whether the observed increased in TLR9 expression was predominately caused by infiltration of APCs into the treated lesions subsequent to the treatment. Furthermore, upon stimulation of TLRs by DAMPs, DCs mature and initiate innate and adaptive immune responses typically in a pathogen-specific manner. As DCs are important innate immune sensors and activators of the adaptive immune response, examining the effect of ECT on the TLR family of receptors, which are key proteins for dendritic cell function, was of particular interest, to determine whether DCs remain able to response to DAMPs, which can be tumour-associated antigens, following ECT treatment. DCs were treated with EP at 800V/cm (800EP), 1000V/cm (1000EP) and 1300V/cm (1300EP) as well as ECT at 800V/cm (800ECT), 1000V/cm (1000ECT) and 1300V/cm (1300ECT) and the expression levels of TLRs 1-9 determined 24 hours post-treatment by qRT-PCR.

Overall, the baseline expression of all 9 TLRs was high as expected for DCs. No change in the expression levels of TLR1, TLR4, TLR5 and TLR8 was detected following any EP treatment (Figure 5.4A). EP induced an up to 4-fold increase in the expression levels of TLR2, TLR3, TLR6 and TLR9, while slightly increasing the expression of TLR7 (Figure 5.4A). TLR2 and TLR3 had a greater than 2-fold increase in their expression levels after 800EP and 1000EP treatment while 1300EP did not increase gene expression (Figure 5.4A). The expression of TLR6 and TLR9 increased with increasing electric field strengths, with up to 4-fold increase seen following 1300EP treatment (Figure 5.4A). ECT treatments showed the same general pattern of increase in TLR gene expression for TLR3, TLR6 and TLR9 (Figure 5.4B) as observed following EP treatment. ECT treatment did not impact the expression levels of TLR2 as well as TLR7 and, as with the EP treatments, ECT did not induce any changes in the expression of TLR1, TLR4 and TLR8 (Figure 5.4B). ECT treatments induced a higher level of variability in the gene expression levels than EP treatments. Combined, this data supports the earlier findings that ECT can induce DC maturation, as it can also increase the expression of TLRs; activation of TLRs leads to induction of DC maturation[20]. Furthermore, the data also indicates that it was not only an increased APC presence in the treated tumour

lesions that lead to an increase in TLR9 expression in the analysed melanoma tissue, as Roux *et al.* had found[8], but that ECT itself leads to the upregulation of TLRs on cells that generally express TLRs.

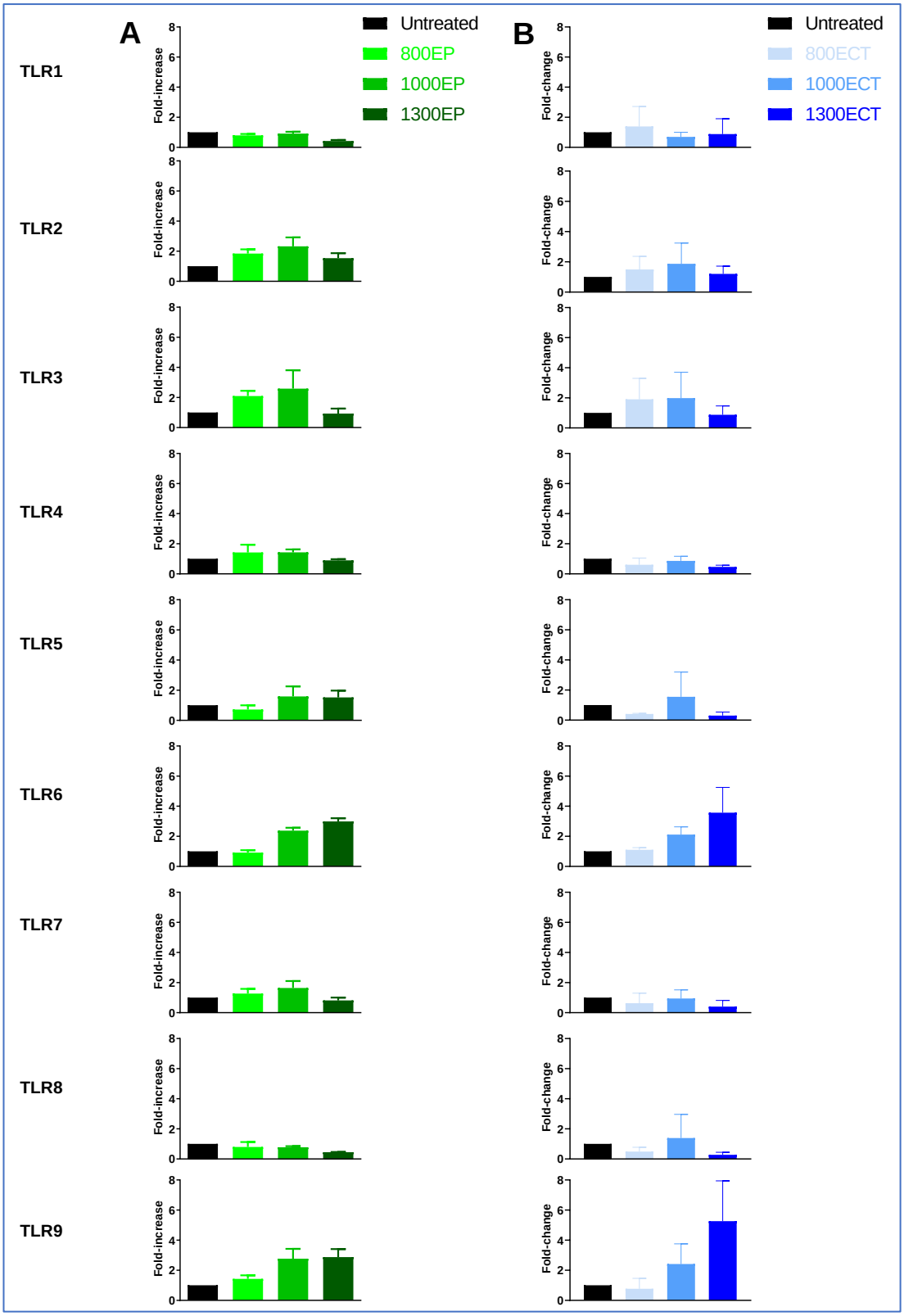


Figure 5.4: Effect of EP and ECT on TLR gene expression levels in DCs. DCs were treated with EP at 800V/cm (800EP), 1000V/cm (1000EP) and 1300V/cm (1300EP) as well as ECT at 800V/cm (800ECT), 1000V/cm (1000ECT) and 1300V/cm (1300ECT). TLR expression was determined by qRT-PCR 24 hours post-treatment. Data presented are representative for 3 independent experiments.

5.4.5 Analysis of gene transcription in DCs post ECT treatment

As we had observed certain alterations in the expression levels of phenotypic markers and TLRs post ECT, we wished to perform a comprehensive in-depth analysis of genome-wide changes that DCs exposed to ECT treatment at the different electric field strengths undergo. As dendritic cells present in the tumour microenvironment have the potential to phagocytose many of the key DAMPs released from the treated tumour cells, the aim of this component of the project was to perform an extensive characterisation of the genome following treatment in order to illuminate which cellular processes might be impacted by ECT. Knowing which processes are impacted will allow for a better understanding of the functional status of the DCs at the varying ECT electric field strengths following treatment, and ultimately therefore may assist in understanding whether there are better co-treatments to design/choose in order to improve the effectiveness of ECT and to increase the chance of systemic immune responses.

DCs were treated with ECT with electric field strengths at 800V/cm (800ECT), 1000V/cm (1000ECT) or 1300V/cm (1300ECT), rested for four hours and then were harvested and their gene expression levels were analysed using UPX 3' Transcriptome Sequencing (performed by Qiagen). On average, over 5.7 million paired-end reads were sequenced and assigned per sample, which is within the expected range for this type of sequencing. Between 75.0% and 91.6% of the reads per sample could be mapped to the murine reference genome, with the unmapped reads being discarded. After sequencing, each sample had a Phred score, a score to indicate the quality of DNA sequencing (Scale 0-40), assigned. All samples had Phred scores above 28, indicating a good quality for the sequencing and a sequencing accuracy exceeding 99%. After deduplication, the average number of reads per sample ranged from 1.23 to 1.32, values below 2 indicate a low amount of over-sequencing, thus indicating that the samples contained little polymerase chain reaction (PCR) amplification bias. The principal component analysis, a statistical analysis to quantitatively represent data on variation in gene expression between the samples, revealed that while there is overall little difference between the samples of each treatment group, the degree of differences increases as the treatment intensity

increases (Figure 5.5). This is exemplified by how physically close the samples of the 800ECT group (C88, C65 and C42) are compared to how dispersed the samples of the 1300ECT group (C89, C66 and C17) are on the graph (Figure 5.5).

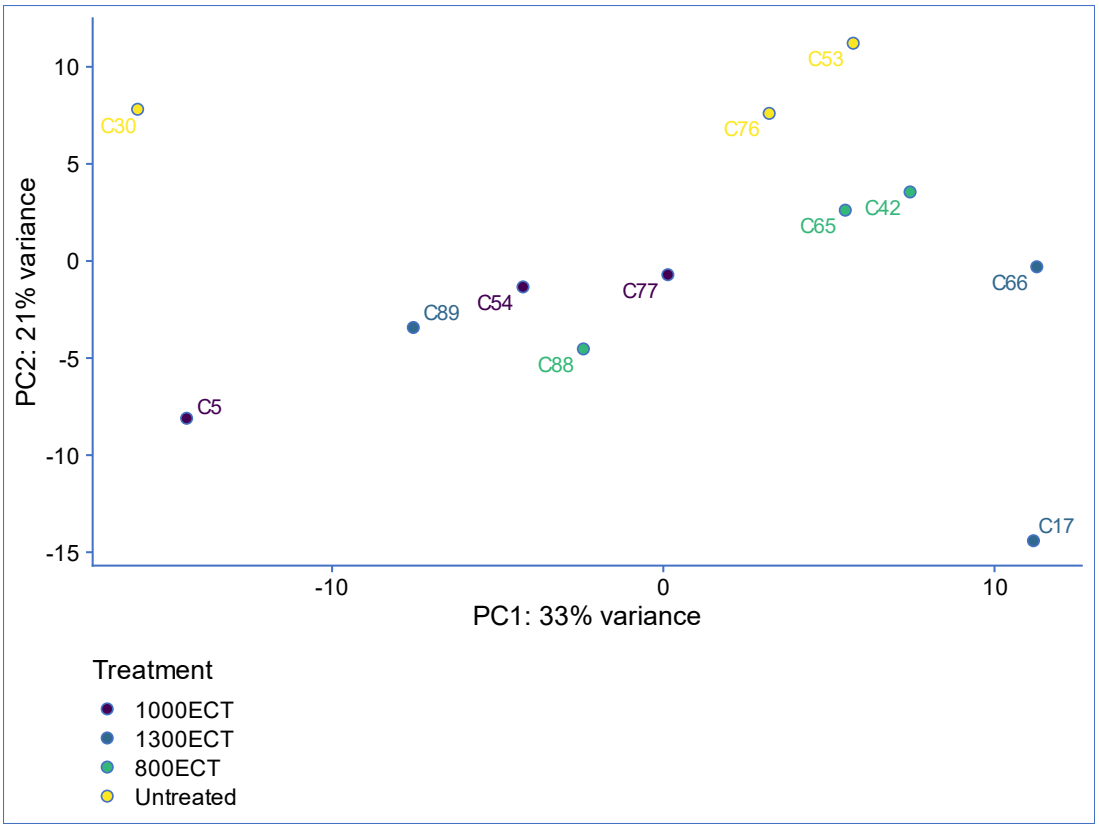


Figure 5.5: Principal component analysis of gene expression profiles of untreated (yellow) and treated DCs (ECT at 800V/cm green; ECT at 1000V/cm blue; ECT at 1300V/cm purple) shows that with increasing electric field strength the variance within the treatment groups increases. Numbers (e.g. C77) indicate in which well the samples were placed during processing and are used for individual identification of the samples.

There were significant differences in the gene expression between all treatment groups and the untreated control group. Of note is that there were no statistically significant changes observed in the genes induced between the three treatment groups. The 20 genes from each treatment group showing the highest fold change are listed in table 5.1 (p-value≤0.05, with 2 as threshold for fold change; full gene lists are in Appendix Tables A.1 to A.3). Fosb was the highest upregulated gene across all three treatment groups compared to the untreated condition, while Egr1 and Fndc7 were among the top 5 upregulated genes in all three treatment groups (Table 5.1).

Thereafter, the top 20 most upregulated genes start to vary slightly between the three treatment groups, but there is still a good overlap between the upregulated genes between the different treatment groups (Table 5.1). The expression changes (either up or down) in response to 800ECT were significant for 34 genes compared to untreated (Table A.1), while 1000ECT induced significant changes in 49 genes (Table A.2) and 1300ECT significantly changed 62 genes (Table A.3). Therefore, with increasing electric field strengths, the numbers of genes being differentially expressed increases (see Tables A.1 through A.3 for full differential expressed genes overview). Despite there being no significant differences between the treatment groups themselves, each treatment condition was observed to upregulate different gene clusters. Generally, ECT treatments leads to increases, rather than decreases, in gene expression as compared to untreated, as at least 33 genes were upregulated following ECT treatment compared to the untreated condition while only a maximum of 3 genes were downregulated following ECT treatment.

	ECT at 800V/cm (800ECT)		ECT at 1000V/cm (1000ECT)		ECT at 1300V/cm (1300ECT)	
#	Gene Name	Fold Change	Gene Name	Fold Change	Gene Name	Fold Change
1	Fosb	26.29	Fosb	34.55	Fosb	38.61
2	Egr1	17.47	Ptgs2	21.03	Egr1	17.87
3	Cxcl10	14.12	Egr1	16.38	Fndc7	15.88
4	Fndc7	11.54	Fndc7	13.22	Gm15922	15.50
5	Hist1h2ao	11.39	Wwc1	11.82	Hspa2	14.23
6	Rsad2	10.49	Hspa1b	10.78	Phlda1	11.51
7	Isg15	10.19	Isg15	10.40	Hist1h4i	11.24
8	Hist1h4i	8.17	Rsad2	10.35	Inhba	10.06
9	Ifit1	7.73	Gm13889	9.87	Hspa1a	8.41
10	Phlda1	7.72	Hist1h4i	9.53	Cd69	7.83
11	Inhba	7.36	Hspa1a	8.67	Cxcl2	7.37
12	Hspa1b	6.75	Tnfsf9	8.01	Emp1	6.14
13	Hspa1a	6.71	Phlda1	7.98	Dusp14	6.13
14	Tnfsf9	6.32	Cxcl2	7.61	Dusp1	5.85
15	Cd69	6.06	Inhba	7.53	Cd14	5.66
16	Rtp4	5.97	Socs3	6.26	Klf4	4.97
17	Cxcl2	5.73	Ralgds	5.69	Dqx1	4.90
18	A330069E16Rik	4.27	Cd69	5.66	Nr4a2	4.84
19	Dusp1	4.23	Cd14	5.34	A330069E16Rik	4.41
20	Cd14	4.03	Emp1	4.97	Socs3	4.35

Table 5.1: Overview of top 20 upregulated genes per treatment group compared to untreated control group with their fold change values.

To further illuminate the processes and pathways altered in DCs upon ECT treatment, we next employed both STRING (*Search Tool for the Retrieval of Interacting Genes/Proteins*) and Molecular complex detection (MCODE)[21] analyses via Cytoscape 3.9.1 per treatment on the differentially expressed genes (DEGs). STRING analysis is used to find known and predicted protein-protein interactions within a given dataset. MCODE is then utilised to identify the most highly interconnected regions (called clusters) in a given network. STRING enrichment was performed with Gene Ontology (GO) and Kyoto Encyclopedia of Genes and Genomes (KEGG) annotations on the whole STRING network, as well as separately on the clusters identified by MCODE. Therefore, the DEGs from the three ECT treatments groups (Table 5.1 and A.1-A.3) were used as the basis to explore which pathways or processes are activated post ECT treatment at the different electric field strengths.

STRING analysis of all genes differentially regulated at 800ECT compared to untreated (Figure 5.6) showed that a network could be retrieved for 33 genes of which 22 genes could be linked to each other. The 22 connected genes are concentrated within three groups, whilst the majority of the 22 genes could be linked to responses to chemical stimulation and immune system processes with GO analysis based on a whole genome background (Table A.4). KEGG enrichment analysis showed that mitogen-activated protein kinase (MAPK) and interleukin-17 (IL-17) signalling pathways are upregulated post 800ECT treatment compared to untreated, as well as the Legionellosis pathway. Legionellosis is an infectious disease caused by Legionella bacteria and upon closer inspection the genes causing the enrichment in the Legionellosis pathway (Cd14, Cxcl2, Hspa1a, Hspa1b; Table A.4) are generally all connected to inflammation.

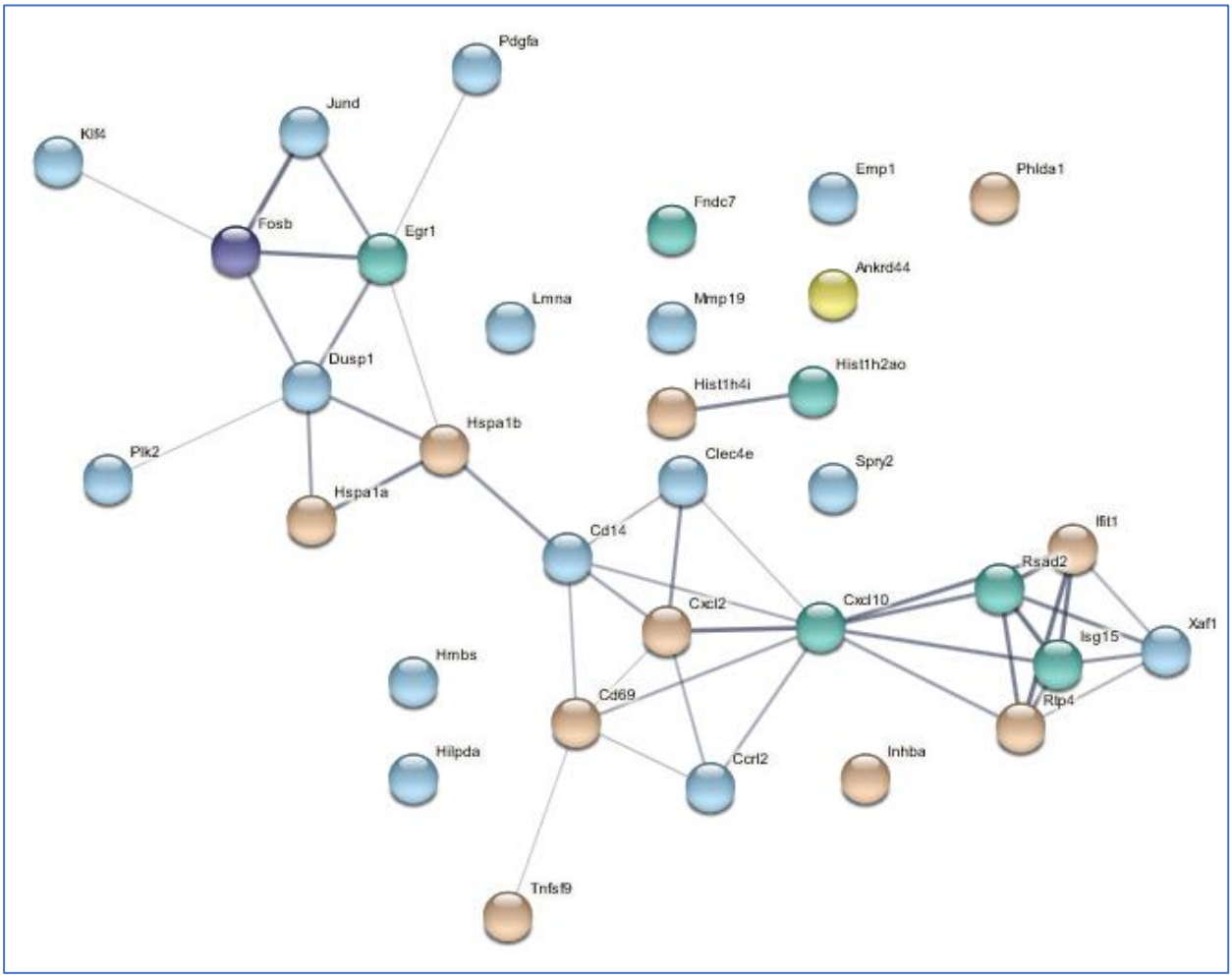


Figure 5.6: STRING analysis of interaction networks formed by proteins, unique for 800ECT group. Thickness of lines between the proteins indicate the confidence level (strength of data support) that the proteins linked will be interacting with each other. Yellow= downregulated gene; Purple = upregulated by Fold change (FC) >20; green= FC between 1 and 20; orange= FC between 5 and 10; blue= FC between 2 and 5.

To further tease out which genes are the most central after the 800ECT treatment, we next analysed the STRING network in Cytoscape with the MCODE analysis. The MCODE analysis of the upregulated genes in the 800ECT treatment revealed two clusters of interconnected genes (Figure 5.7). The Cxcl10 cluster (Cxcl10 being the most connected gene of this cluster; Figure 5.7A) included Cxcl10, Ifit1, Xaf1, Isg15, Rtp4 and Rsad2. While the Cxcl2 cluster (Cxcl2 being the most connected gene here; Figure 5.7B) included Cclr2, Cd14, Cd69 and Clec4e.

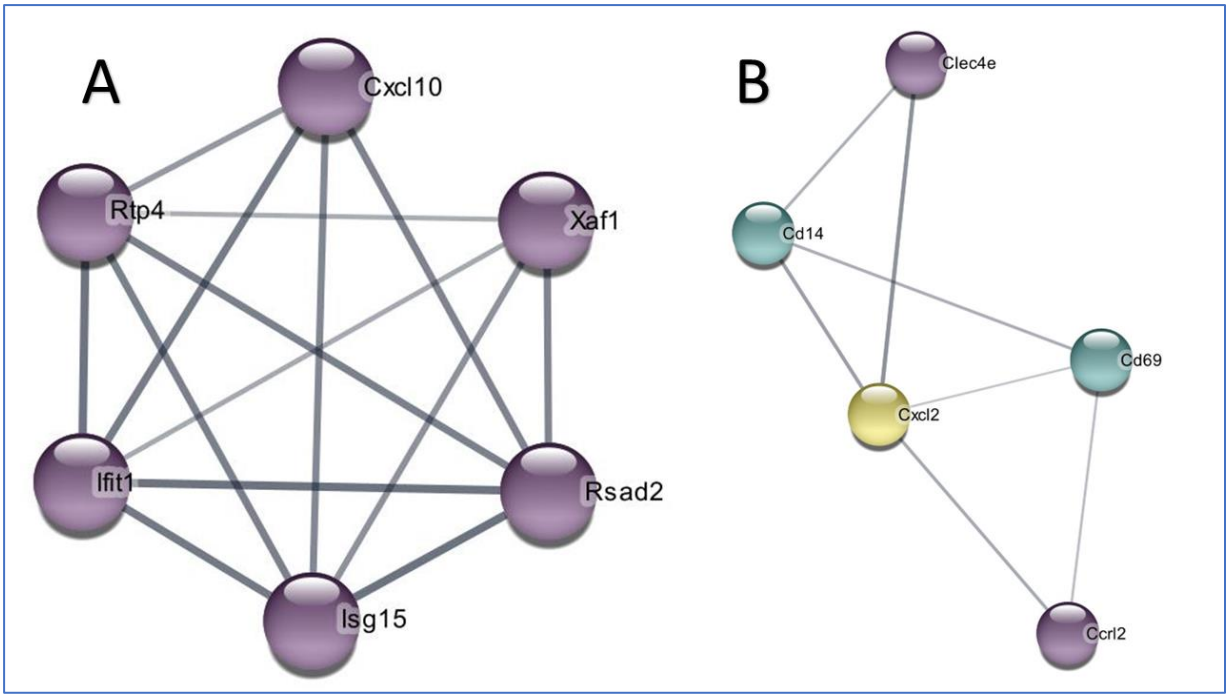


Figure 5.7: MCODE analysis revealed two central clusters within the 800ECT STRING network. A) shows the Cxcl10 cluster consisting of Cxcl10, Ifit1, Xaf1, Isg15, Rtp4 and Rsad2 and B) shows the Cxcl2 cluster consisting of Cclr2, Cd14, Cd69 and Clec4e.

The Cxcl10 cluster is based overall on genes relevant for a mixed response, as defined by STRING cluster analysis. The GO analysis revealed that the genes in this cluster found to be upregulated post 800ECT are otherwise typically found in defence responses to viruses and cytokine responses (Table 5.2). KEGG pathway enrichment analysis revealed enrichment in genes connected to Hepatitis C (viral infection) and the RIG-I-like receptor signalling pathway (key sensory pathway for viral infection[22]) (Table 5.2). The Cxcl2 cluster does not seem to be connected or enriched in any particular biological processes; its clustering seems to be based on the analysed cell type. KEGG pathway analysis of this cluster revealed an enrichment in NF-κB signalling pathway, which could indicate a stress-response, as well as enrichment in pathways typically connected to Legionellosis, Amoebiasis and Tuberculosis (Table 5.3), all infectious diseases caused by bacteria. Taken together this data indicates that 800ECT leads to activation of immune functions of the treated DCs while simultaneously the cells are also dealing with environmental stressors.

Description	FDR value	Connected Genes
Defense response to virus	2.28E-6	Rsad2, Rtp4, Cxcl10, Isg15, Ifit1
Response to cytokine	0.0317	Cxcl10, Isg15, Ifit1, Xaf1
Hepatitis C	0.0025	Rsad2, Cxcl10, Ifit1
RIG-I-like receptor signalling pathway	0.026	Cxcl10, Isg15

Table 5.2: Cxcl10 cluster within 800ECT STING network leads to upregulation of responses to viruses and cytokines (GO analysis blue shaded) as well as upregulation of Hepatitis C and RIG-I-like receptor signalling pathway (KEGG analysis green shaded). (FDR=false discovery rate). GO and KEGG enrichment analysis was performed on the Cxcl10 cluster identified by MCODE analysis with standard parameters and the removal of redundant terms.

Description	FDR value	Connected Genes
Legionellosis	0.0257	Cd14, Cxcl2
NF-kappa B signalling pathway	0.0342	Cd14, Cxcl2
Amoebiasis	0.0342	Cd14, Cxcl2
Tuberculosis	0.0494	Clec4e, Cd14

Table 5.3: Cxcl2 cluster within 800ECT STING network leads to upregulation of Legionellosis and NF-κB signalling pathway (KEGG analysis green shaded). (FDR=false discovery rate). GO and KEGG enrichment analysis was performed on the Cxcl2 cluster identified by MCODE analysis with standard parameters and the removal of redundant terms.

The STRING analysis of all genes differentially regulated at 1000ECT compared to untreated control, showed that a network could be retrieved for 49 genes of which 34 genes could be linked to each other (Figure 5.8). The 34 connected genes are concentrated around one main group, with the majority of genes linked to cellular responses to organic substances and response to different type of stressors based on a whole genome background for the analysis (Table A.5). KEGG enrichment analysis again revealed upregulation of NF-κB, IL-17, Legionellosis, MAPK and TLR signalling pathways (Table A.5). In contrast to the 800ECT treatment, the 1000ECT treatment leads to the unique upregulation of the TLR signalling pathway.

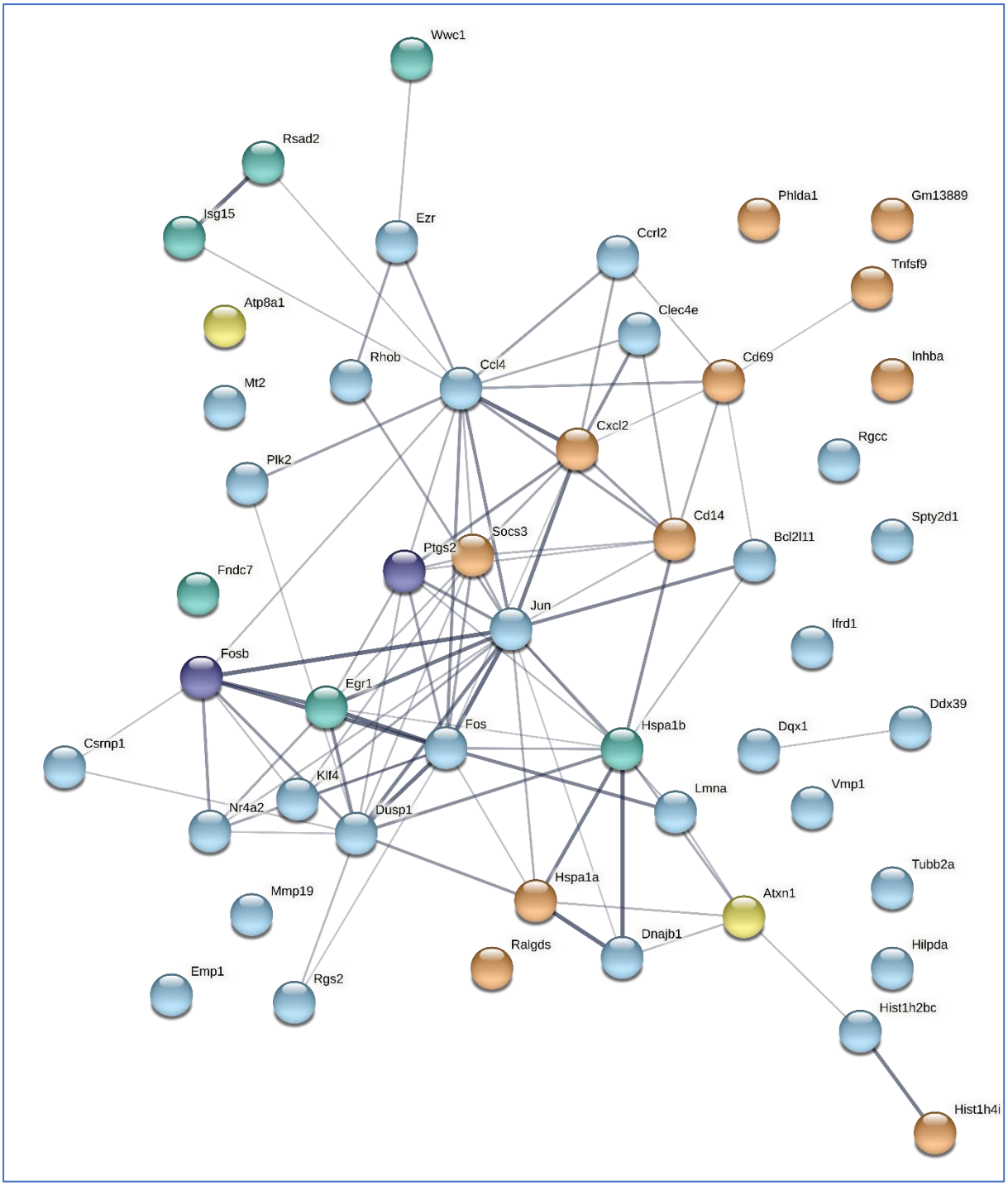


Figure 5.8: STRING analysis of interaction networks formed by proteins, unique for 1000ECT group. Thickness of lines between the proteins indicate the confidence level (strength of data support) that the proteins linked will be interacting with each other. Yellow= downregulated gene; Purple = upregulated by Fold change (FC) >20; green= FC between 1 and 20; orange= FC between 5 and 10; blue= FC between 2 and 5.

MCODE analysis of the DEGs in the 1000ECT treatment revealed one large cluster of interconnected genes containing 11 genes: Ccl4, Cd14, Cxcl2, Socs3, Ptgs2, Hspa1b, Jun, Fosb, Egr1, Dusp1 and Nr4a2 (Figure 5.9). The cluster overall is connected to a mixed response, with the main purpose of regulating cellular processes and molecular functions in addition to stress responses, including responses found in reaction to oxidative stress and gamma irradiation (Table 5.4). While based on KEGG pathway enrichment analysis, NF-κB, IL-17, Legionellosis, MAPK and TLR signalling pathways were enriched. Thus, the same pathways were enriched in the central cluster (Table 5.4) as were enriched in the overall STRING network (Table A.5) for 1000ECT treatment.

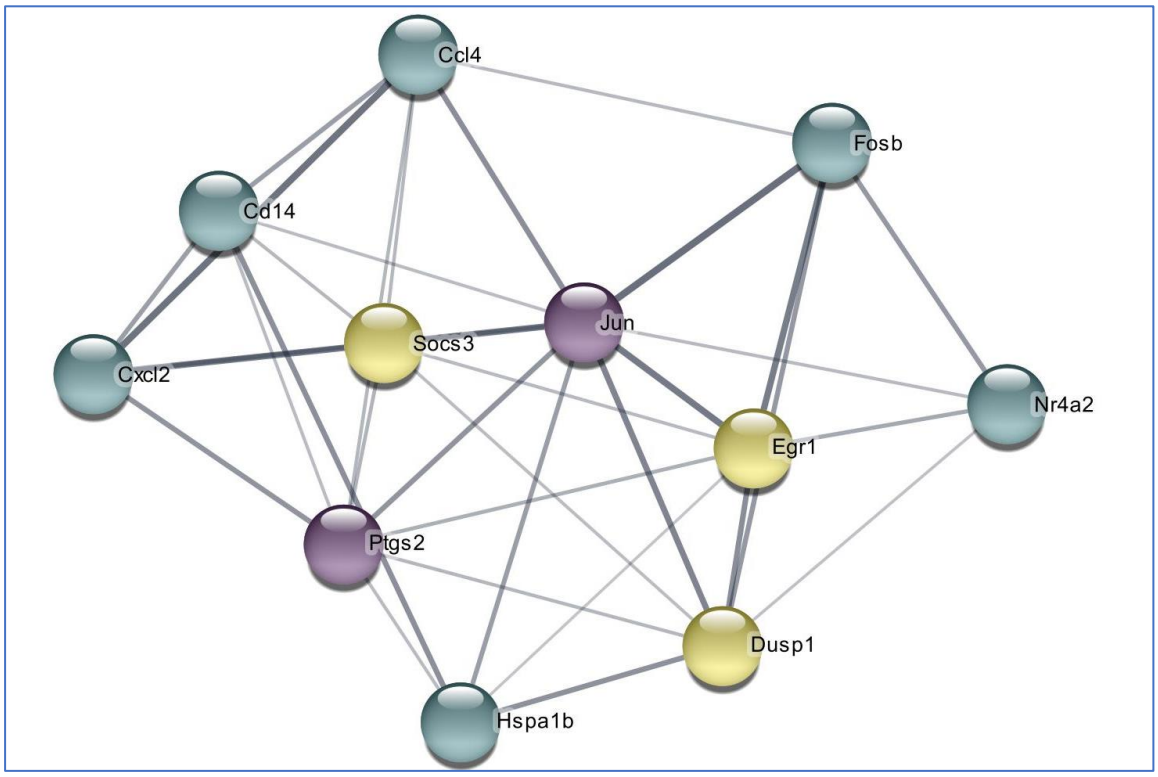


Figure 5.9: MCODE analysis revealed one central cluster within the 1000ECT STRING network. The cluster consists of Ccl4, Cd14, Cxcl2, Socs3, Ptgs2, Hspa1b, Jun, Fosb, Egr1, Dusp1 and Nr4a2.

Description	FDR value	Connected Genes
Cellular response to organic substance	4.23E-8	Fosb, Ccl4, Dusp1, Nr4a2, Ptgs2, Cd14, Socs3, Egr1, Cxcl2, Jun, Hspa1b
Cellular response to chemokine	0.0029	Ccl4, Dusp1, Cxcl2
Transcription, dna-templated	0.0052	Fosb, Nr4a2, Egr1, Jun
Positive regulation of smooth muscle cell proliferation	0.0052	Ptgs2, Egr1, Jun
Response to oxidative stress	0.0066	Dusp1, Nr4a2, Ptgs2, Jun
Response to toxic substance	0.0159	Ccl4, Nr4a2, Ptgs2
Response to amphetamine	0.017	Nr4a2, Cxcl2
Response to gamma radiation	0.0382	Egr1, Cxcl2
NF-kappa B signalling pathway	3.31E-5	Ccl4, Ptgs2, Cd14, Cxcl2
IL-17 signalling pathway	3.31E-5	Fosb, Ptgs2, Cxcl2, Jun
Legionellosis	3.0E-4	Cd14, Cxcl2, Hspa1b
MAPK signalling pathway	6.2E-4	Dusp1, Cd14, Jun, Hspa1b
Toll-like receptor signalling pathway	8.3E-4	Ccl4, Cd14, Jun

Table 5.4: Main cluster within 1000ECT STING network leads to upregulation of responses to various stressors (GO analysis blue shaded) as well as to upregulation of NF-κB, MAPK, TLR and IL-17 pathways (KEGG analysis green shaded). (FDR=false discovery rate). GO and KEGG enrichment analysis was performed on the Main cluster identified by MCODE analysis with standard parameters and the removal of redundant terms.

The STRING analysis of all genes differentially regulated after 1300ECT treatment compared to untreated showed that a network could be retrieved for 57 genes, of which 32 genes could be linked to each other (Figure 5.10). The 32 connected genes itself are concentrated around two interconnected groups. The majority of genes in the full 1300ECT cluster could be linked to cellular responses to chemical substances and a mixed cellular response including an early-growth response as well as modulation of the cell cycle and cell death pathways (Table A.6). KEGG enrichment analysis revealed upregulation of genes connected with MAPK, NF-κB, TLR and TNF signalling pathway as well as Legionellosis, Apoptosis, Fluid shear stress and atherosclerosis (Table A.6). This is the first time that ECT treatment led not only to upregulation of immune signalling pathways as well as legionellosis, but also to upregulation of stress-related and cell death pathways. In addition, the TNF-signalling pathway is uniquely upregulated after 1300ECT treatment.

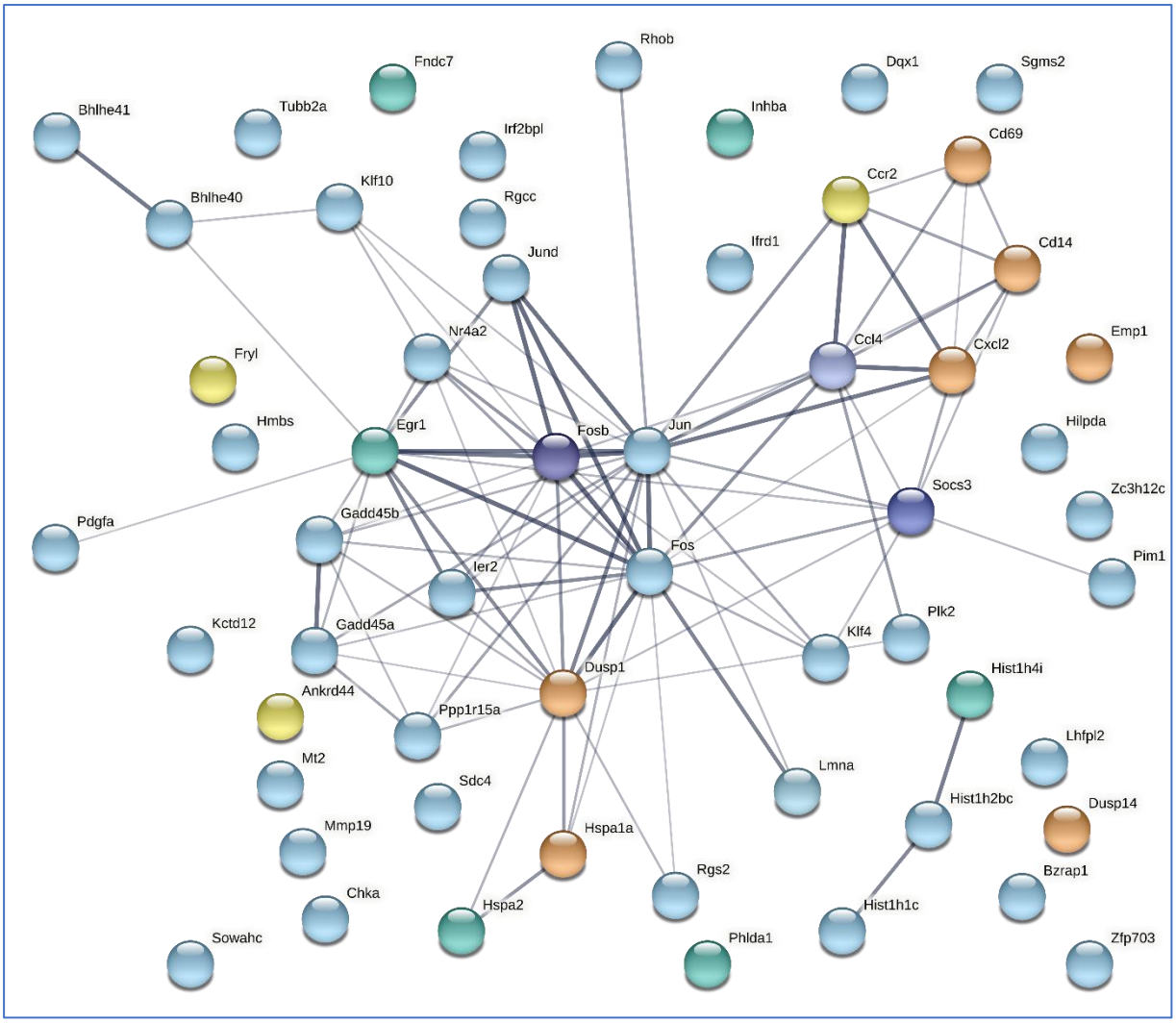


Figure 5.10: STRING analysis of interaction networks formed by proteins, unique for 1300ECT group. Thickness of lines between the proteins indicate the confidence level (strength of data support) that the proteins linked will be interacting with each other. Yellow= downregulated gene; Purple = upregulated by Fold change (FC) >20; green= FC between 1 and 20; orange= FC between 5 and 10; blue= FC between 2 and 5.

The MCODE analysis of the DEGs in the 1300ECT treatment revealed two clusters of interconnected genes containing 9 genes for the Dusp1 cluster (Figure 5.11A) and 6 genes for the Ccl4 (Figure 5.11B) cluster. The Dusp1 cluster (Figure 5.11A) contains Dusp1, Jun, Gadd45b, Gadd45a, Nr4a2, Egr1, Fos, Fosb and Ier2. It is overall connected to a mixed response, mainly with regulation of cellular processes and molecular functions (Table 5.5). The KEGG pathway analysis showed enrichment of the MAPK signalling pathway (Table 5.5). The Ccl4 cluster (Figure 5.11B) is made up of Ccl4, Cd14, Ccr2, Cxcl2, Cd69 and Socs3. This cluster is connected to responses and interactions with chemokines and cytokine based on STRING cluster analysis. It is also showing an enrichment of cellular responses to chemical stimuli and inflammatory responses. KEGG pathway analysis indicated an enrichment of viral protein interaction with cytokine and cytokine receptor, Legionellosis as well as TLR and tumour-necrosis factor (TNF) signalling pathways (Table 5.6).

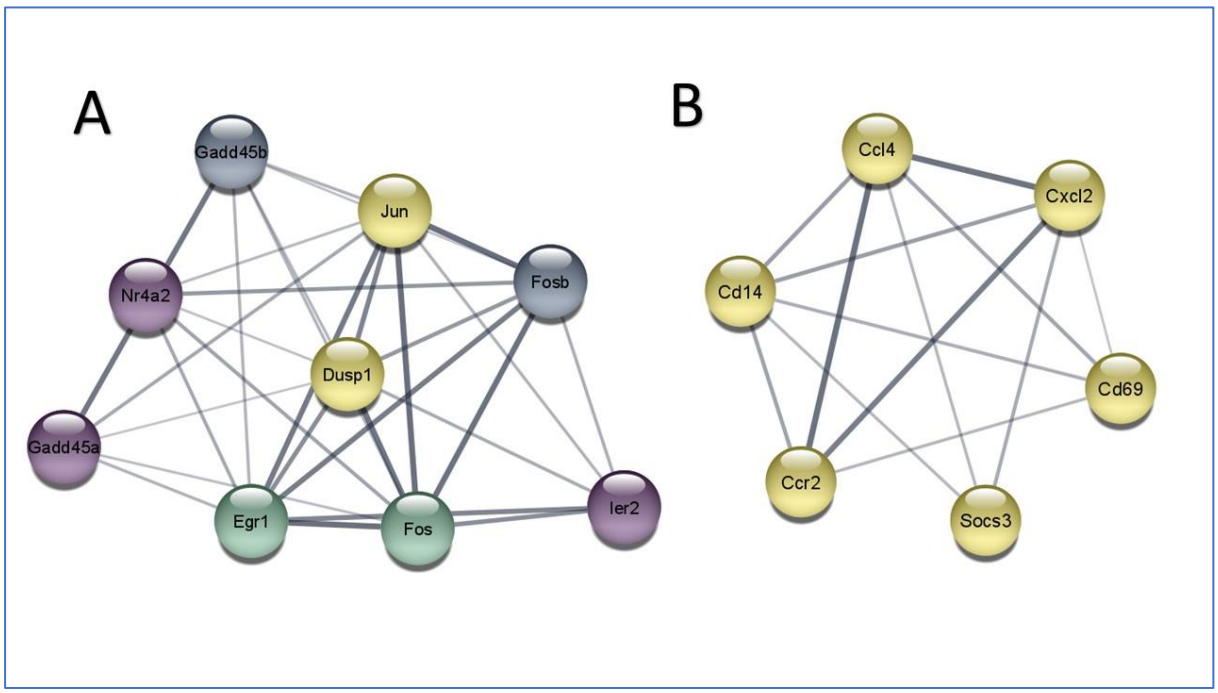


Figure 5.11: MCODE analysis revealed two central clusters within the 1300ECT STRING network. A) shows the Dusp14 cluster consisting of Dusp1, Jun, Gadd45b, Gadd45a, Nr4a2, Egr1, Fos, Fosb and Ier2 and B) shows the Cccl2 cluster consisting of Ccl4, Cd14, Ccr2, Socs3, Cd69 and Cxcl2.

Description	FDR value	Connected Genes
Response to endogenous stimulus	3.9E-4	Fosb, Fos, Dusp1, Nr4a2, Ier2, Egr1, Jun
Mitotic cell cycle arrest	0.0036	Dusp1, Gadd45a
Positive regulation of catalytic activity	0.011	Gadd45b, Nr4a2, Gadd45a, Egr1, Jun
Cellular response to ionizing radiation	0.0318	Gadd45a, Egr1
MAPK signalling pathway	1.17E-5	Gadd45b, Fos, Dusp1, Gadd45a, Jun

Table 5.5: Dusp1 cluster within 1300ECT STRING network leads to upregulation of responses to various stressors (GO analysis blue shaded) as well as to upregulation of MAPK pathway (KEGG analysis green shaded). (FDR=false discovery rate). GO and KEGG enrichment analysis was performed on the Main cluster identified by MCODE analysis with standard parameters and the removal of redundant terms.

Description	FDR value	Connected Genes
Viral protein interaction with cytokine and cytokine receptor	4.3E-4	Ccl4, Cxcl2, Ccr2
Legionellosis	0.0077	Cd14, Cxcl2
Toll-like receptor signalling pathway	0.0167	Ccl4, Cd14
TNF signalling pathway	0.0167	Socs3, Cxcl2

Table 5.6: Ccl4 cluster within 1300ECT STRING network leads to upregulation of TLR and TNF signalling pathways as well as Legionellosis pathway (KEGG analysis green shaded). (FDR=false discovery rate). GO and KEGG enrichment analysis was performed on the Main cluster identified by MCODE analysis with standard parameters and the removal of redundant terms

While ECT treatments generally lead to increases in gene expression, a few genes are downregulated post ECT treatment. 800ECT leads to a significant 3-fold (p=0.000020) decrease in expression of the Ankrd44 gene (Table A.1), whilst 1000ECT leads to a significant 5-fold decrease (p=0.000017) in Atp8a1 gene expression and a significant 3-fold decrease (p=0.0000017) in the Atxn1 gene expression (Table A.2). 1300ECT leads to a significant 4-fold decrease in Ankrd44 (p=0.000047), Ccr2 (p=0.000065) and Fryl (p=0.000064) gene expression (Table A.3). These downregulated genes collectively are not connected to any particular pathway or biological function, but

all genes seem to be connected to regulatory functions indicating that ECT could negatively impact cell homeostasis.

Taken together, the data from the UPX 3' Transcriptome Sequencing after the different ECT treatments showed that with increasing electric field strength the number of DEGs increases. This could indicate that higher electric field strengths more highly impact the treated cells, which might impact the ability of these cells to perform their cellular functions post-treatment. Overall, the majority of genes upregulated in the three distinct treatments can be linked to innate immune system pathways typically activated post pathogen infection (bacterial or viral for the most part). In addition, gene pathways upregulated after all three treatments show enrichment of the MAPK pathway, indicating that the cells are reacting to physiological stressors. Finally, only 1300ECT treatment led to an enrichment in upregulated genes connected to cell death processes.

Based on the different gene regulation clusters post ECT at different electric field strengths, several genes were selected for further validation using qRT-PCR, namely Cxcl10, Ptgs2, Dusp14, and Isg15. Cxcl10 is uniquely upregulated after the 800ECT treatment and seems to be central to the main cluster being responsible for antiviral responses (Figure 5.7 and Table 5.2). Ptgs2 (also known as COX2) is uniquely upregulated after 1000ECT and is connected to inflammatory responses (Table A.2) and is part of the main cluster of upregulated genes within the 1000ECT gene network (Figure 5.9). Dusp14 is uniquely upregulated (6-fold higher than untreated) after ECT at 1300V/cm and is part of the first main cluster of upregulated genes after 1300 ECT treatment (Figure 5.11A and Table A.3). It is an atypical DUSP (Dual specific protein phosphatase). Interestingly Dusp1, which is a typical DUSP, is similarly expressed after all 3 treatment conditions (Table A.1-3). Isg15 expression is similarly upregulated after 800ECT and 1000ECT treatment but was not significantly changed after 1300ECT treatment (Table A.1-3). It is part of the main Cxcl10 cluster within the 800ECT upregulated gene network (Figure 5.7A) but is not connected to the main cluster of 1000ECT upregulated genes. Finally, Isg15 is induced by type I interferon

and its expression level is increased about 10-fold in the 800ECT and 1000ECT groups compared to the untreated condition.

The unique expression of Cxcl10 in the 800ECT and the unique expression of Ptgs2 in 1000ECT as determined by UPX 3' Transcriptome Sequencing could not be validated by qRT-PCR (Figure 5.12), with no significant changes observed in either of these genes with any treatment. qRT-PCR analysis demonstrated a 9-fold upregulation of Dusp14 in the 1300ECT group but also showed a slight increase of Dusp14 in the 1000ECT group (Figure 5.12). While all ECT treatments increased Isg15 gene expression, this was most upregulated in the 1000ECT group with a 6-fold upregulation observed.

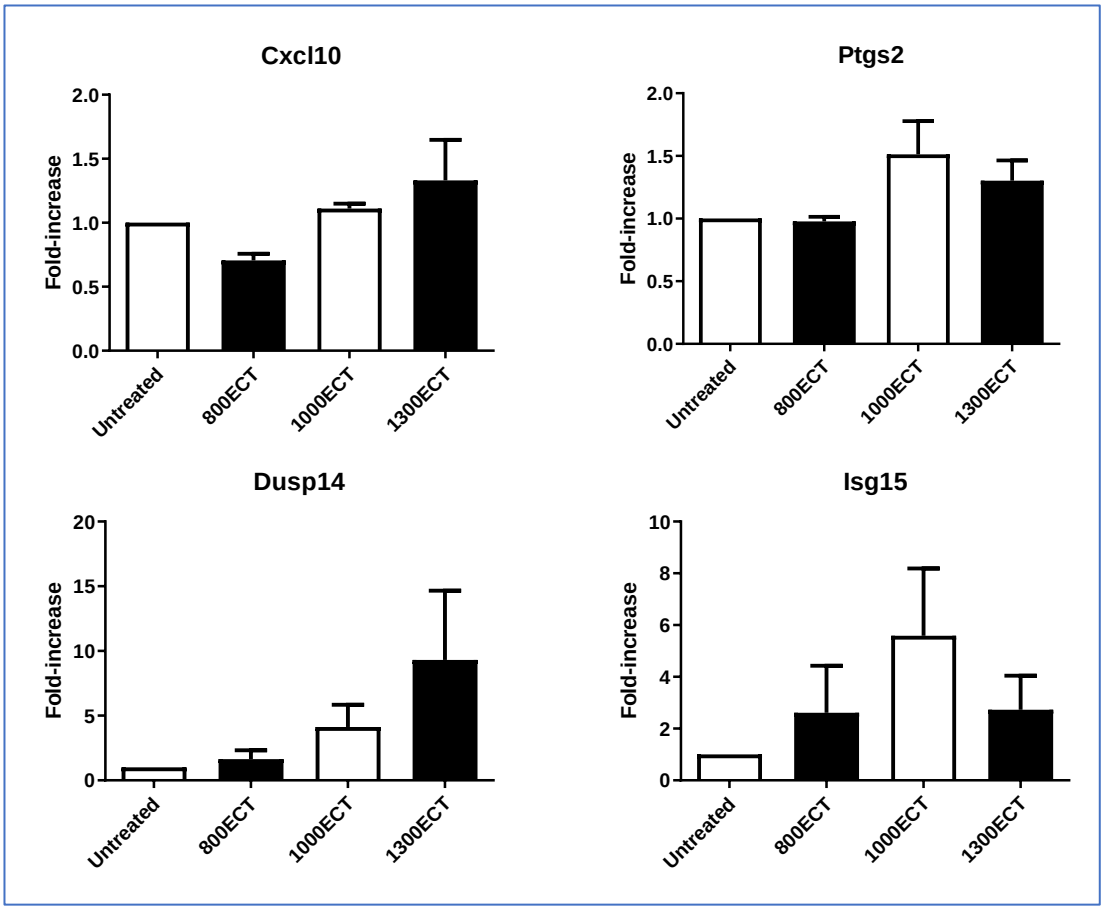


Figure 5.12: ECT treatment does not effect expression of Cxcl10 and Ptgs2 but does effect expression of Dusp14 and Isg15. DCs were treated with EP at 800V/cm, 1000V/cm respectively 1300V/cm. Cxcl10, Ptgs2, Dusp14 and Isg15 expression was determined by qRT-PCR 4 hours post-treatment. Data presents results from 3 combined independent experiments.

5.4.6 DCs remain in part functionally active after EP and ECT treatment

As we had observed clear gene changes associated with different stress responses, antiviral responses and upregulation of NF-κB, MAP Kinases (MAPK), as well as TLR signalling pathways at the different ECT settings, we wished to examine whether there was a difference in the ability of the dendritic cells to respond to stimulation once treated at the various settings. In order to determine this, we analysed the ability of EP/ECT treated DCs to secrete interferon gamma (IFN-γ) and tumour-necrosis factor alpha (TNF-α) in the first 24 hours post treatment. IFN-γ is an autocrine mediator for DC maturation and is linked to anti-cancer immunity[23,24]. TNF-α is a highly pro-inflammatory cytokine[25] linked to oedema formation[26], which is a positive biomarker for effectiveness of ECT in patients[27]. We analysed the ability of the treated DCs to respond to TLR agonist stimulation in terms of secretion of the above cytokines, in order to determine if, and how, functionally active they are post-treatment. DCs were stimulated with agonists of TLRs 3, 4, 7/8 and 9. polyI:C is a TLR3 agonist and TLR3 expression was increased following ECT treatment (Figure 5.4). LPS (TLR4 agonist) was chosen to test functionality of DCs post ECT as LPS induces significant upregulation of MAPK and NF-kB. R848 is a TLR7/8 agonist which is currently under investigation for adjuvant immunotherapy for lung cancer and as our overarching aim was to see if ECT treatments could be suitable for lung cancer treatment, we decided to determine the impact R848 stimulation would have on DCs that underwent ECT treatment. CpG (TLR9 agonist) was chosen as Roux *et al.* had shown, that ECT followed by CpG adjuvant therapy had a better treatment outcome than ECT alone in a murine melanoma model[8].

DCs were found to basally secrete significantly less ($p \leq 0.05$) IFN-γ with increasing field strength following EP treatments (Figure 5.13A), and ECT treatment ($p \leq 0.01$), (Figure 5.13B). Cisplatin alone had no impact on the amount of IFN-γ secreted (Figure 5.13B). Stimulation with CpG induced IFN-γ secretion in the untreated DCs, with EP found to have no impact on the ability of the cells to secrete IFN-γ in response to CpG stimulation (Figure 5.13C). In contrast, 800ECT treatment significantly ($p \leq 0.01$) impacted the ability of the cells to secrete IFN-γ in response to CpG stimulation (Figure 5.13D). The level of IFN-γ produced by DCs in response to CpG stimulation

slightly, yet significantly ($p \leq 0.05$), increased following 1000ECT treatment with no change observed following 1300ECT.

LPS stimulation increased IFN-γ secretion in the untreated DCs, but, in contrast to findings with CpG stimulation, the ability of the cells to respond to LPS was significantly reduced ($p \leq 0.01$) in both EP- and ECT treated cells (Figure 5.13 E+F). Similarly, polyI:C stimulation induced IFN-γ secretion in the untreated samples, but response to polyI:C was completely abrogated following all EP treatments (Figure 5.13G). In the case of the ECT treatments, no IFN-γ was detected following polyI:C stimulation for either the 800ECT and 1000ECT treatments, although IFN-γ was secreted at the same level as for untreated cells following 1300ECT treatment (Figure 5.13H). Finally, a similar effect was seen with R848 stimulation. R848 induced IFN-γ production in DCs, but the ability of the cells to produce IFN-γ in response to R848 was either very significantly ($p \leq 0.01$) reduced or completely abrogated following both EP (Figure 5.13I) and ECT (Figure 5.13J) treatments.

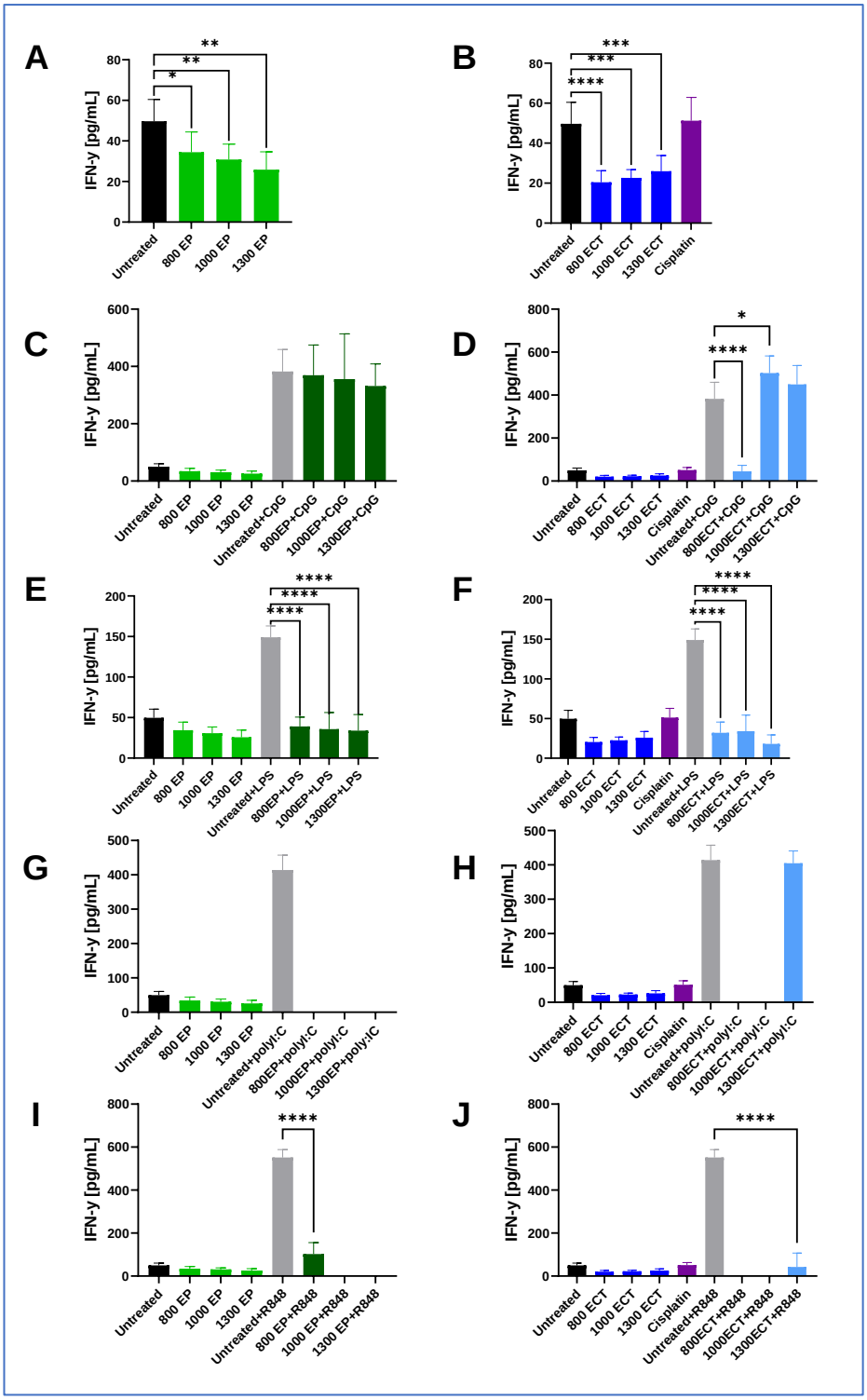


*Figure 5.13: Secretion of IFN-γ post ECT treatments was significantly impacted by 800ECT and 1000ECT, while treated cells were still able to respond to CpG stimulation but not LPS, R848, polyI:C stimulation. Cells were treated respectively with 800ECT, 1000ECT or 1300ECT and either left untreated or were stimulated with CpG, LPS, polyI:C or R848. 24 hours post-treatment and stimulation cell supernatant was collected and analysed by ELISA. Data represents the mean ± SD from at least 3 separate experiments. *p≤0.05, **p≤0.01, ***p≤0.001, ****p≤0.0001; compared to untreated.*

A somewhat different pattern of response was observed for TNF-α secretion of DCs stimulated with TLR ligands with either EP or ECT treatment. All EP treatments were found to have no effect on the basal level of secretion of TNF-α (Figure 5.14A). In contrast, 1000ECT and 1300ECT treatments significantly ($p \leq 0.01$) increase the basal level of TNF-α secretion, with the increase being most pronounced for the 1300ECT treatment (Figure 5.14B). Cisplatin had no effect on the basal levels of TNF-a secreted. CpG stimulation of untreated cells increased TNF-α secretion, with increasing electric field strengths seen to augment this effect (Figure 5.14C). CpG stimulation following ECT treatment, significantly ($p \leq 0.01$) increases the level of TNF-α secretion following 800ECT treatment. However, this increase was not sustained with higher electric field strengths with 1300ECT treatment seen to significantly ($p \leq 0.01$) impair the ability of the cells to produce TNF-α in response to CpG stimulation (Figure 5.14D). EP (Figure 5.14E) and ECT (Figure 5.14F) treatments significantly ($p \leq 0.01$) reduces the ability of the cells to respond to LPS stimulation in terms of TNF-α secretion, with the reduction increasing as the electric field strength increases. No significant difference in TNF-α secretion was observed between untreated and EP-treated cells following polyI:C stimulation (Figure 5.14G), with only a very marginal effect observed following ECT treatments (Figure 5.14H). Finally, a similar pattern was seen for R848 stimulation as for LPS stimulation. R848 stimulation following EP (Figure 5.14I) and ECT (Figure 5.14J) treatment significantly ($p \leq 0.01$) decreases the TNF-α secretion compared to untreated, with the decrease becoming more pronounced as the electric field strength increases.

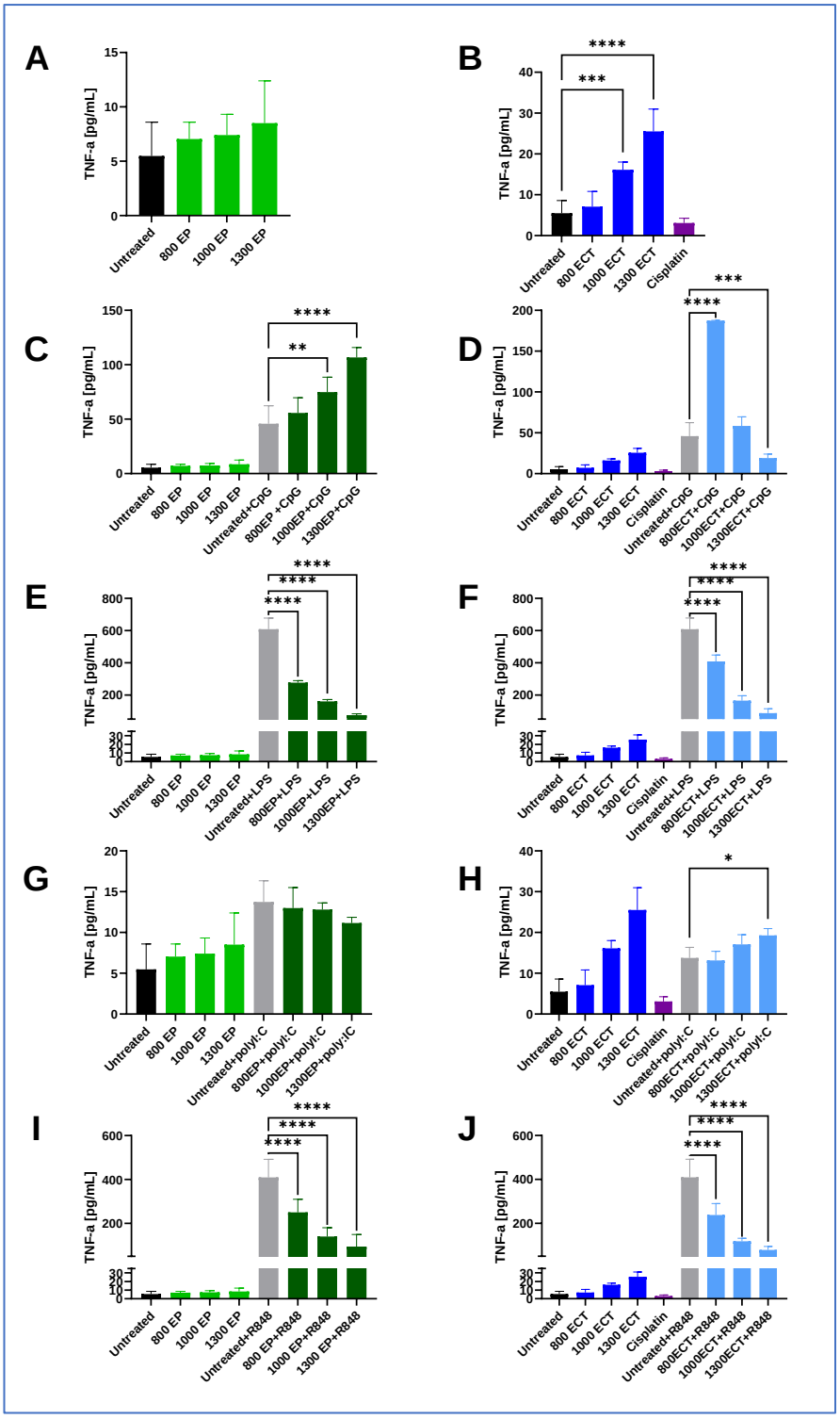


*Figure 5.14: Secretion of TNF-α post ECT treatments was significantly impacted by 800ECT and 1000ECT while treated cells were still able to respond to CpG stimulation but not LPS, R848 and polyI:C stimulation. Cells were treated respectively with 800ECT, 1000ECT or 1300ECT and either left untreated or were stimulated with CpG, LPS, polyI:C or R848. 24 hours post-treatment and stimulation cell supernatant was collected and analysed by ELISA. Data represents the mean ± SD from at least 3 separate experiments. *p≤0.05, **p≤0.01, ***p≤0.001, ****p≤0.0001; compared to untreated.*

Taken together these results indicate that EP and ECT treated cells remain partially functional in terms of their ability to respond to stimulation by TLR ligands.

5.5 Discussion & Conclusion

Dendritic cells are central to the innate and adaptive immune systems in general[2], and also play a key role in co-ordinating the immune response to cancer[3]. Thus, in this chapter we investigated the specific impact ECT has on this vital immune cell population. A better understanding of the cellular effects ECT induces in DCs may potentially facilitate the designing of ECT co-treatments to better support these immune cells or the re-designing of ECT treatments to better protect the DC population. Here we explored a range of cellular features post EP and ECT treatment, including cell death, cell surface phenotypic changes, gene expression and functionality, in order to fully describe the impact ECT has on DCs. In this chapter we have shown that ECT overall seems to activate DCs post-treatment, with increasing electric field strengths for the ECT treatment resulting in increasing cellular stress. In addition, data presented here show that DCs remain at least partially functionally active post-ECT with variability in their functional responses seen at the different electric field strengths. Overall, the higher the tested electric field strength, the more variable became the impact on the DCs and more cellular processes were impacted.

Cell death analysis via flow cytometry employing Annexin V as a marker for apoptotic cell death concluded that DCs undergo cell death by necrosis following EP and ECT treatment at all tested electric field strengths although this could not be confirmed by morphological analysis post-treatment. Annexin V[18] is a transient marker that may show up earlier/later in the cell death process of DCs dying from EP and ECT than the observed 4-hour timepoint. Thus, the right time point for Annexin V exposed on the cell surface might have been missed in these experiments, explaining the difference in results between the flow cytometry and the morphological analysis. Under homeostatic conditions *in vivo*, DCs die via programmed-cell death, most likely apoptosis, in order to prevent an accumulation of DCs in various tissue leading to autoimmunity, while formation of the immunological synapse between DCs and T cells inhibit DC apoptosis. The rate with which DCs die seems to be tissue dependent[28,29]. If the DCs are dying by any type of regulated cell death, their cell death should not lead to additional inflammation signalling while necrotic cell death may induce inflammatory responses[30], which in turn could impact the immune

response following ECT. If the observed necrosis via Annexin V and PI staining is indeed a form of unregulated cell death this could lead to an immune response polarized towards tissue repair due to the damage-associated molecular patterns (DAMPs) released during the necrotic process resulting in tumour repair and growth[31–33]. If on the other hand the observed necrosis is rather necroptosis, a form of regulated cell death resembling necrosis, or other necrosis-like regulated cell death forms[13], a lower level of DAMPs are released than with necrosis and the cytokines released during necroptosis are potentially able to induce an immune response that can lead to an anti-tumour microenvironment[31]. Which form of necrosis is present following ECT treatment would need to be evaluated further in the future.

DC maturation and activation needs to be induced before DCs can become functionally active and interact with other innate and adaptive immune cells to enhance the immune response[2]. Thus, it was investigated whether EP and/or ECT impact maturation and activation of DCs. While 1000ECT and 1300ECT lead to significant cell death[1], these treatments also led to increased expression of MHCII, CD11c and CD80 on treated DCs 24 hours post-treatment. Thus, the cells that survive the initial treatment seem to undergo maturation and activation processes. At the same time, 800ECT does not lead to significant cell death, but it also does not seem to initiate the same maturation and activation processes of the 800ECT treated DCs observed with treatments at higher electric field strengths. At the same time, if cancer cells die via ICD following treatment, the released DAMPs by themselves are able to induce activation of DCs leading to maturation[3] and thus, it might not be physiologically significant *in vivo* that ECT by itself does not induce DC maturation. A higher percentage of viable cells following treatment should ultimately result in an increase in the number of activated cells. In addition, the tumour-microenvironment itself can modulate the phenotype and functionality of immune cells[34–36] and thus the impact of ECT on these already altered DCs might be different than the changes invoked by ECT on naïve DCs in an *in vitro* context. Also, MHCII, CD11c and CD80 are only very broad markers to phenotype DCs[2,19] and thus in the future additional markers, like B220 (plasmacytoid DC marker)[3,5], CD8α (classical DC type 1 marker)[3,5],

CD172a (classical DC type 2 marker)[3,5], and CD86 (activation marker)[3,37], should be investigated to better understand any phenotype changes induced by ECT. Ideally, DCs from patients undergoing ECT treatment at different electric field strengths would also be analysed to encompass phenotype changes DCs in the tumour-microenvironment are undergoing following treatment.

Interestingly, both EP and ECT induced a voltage-dependent upregulation of some, but not all, TLRs. TLR3, TLR6 and TLR9 were induced by EP and ECT, whilst TLR1, TLR2, TLR4, TLR5, TLR7 and TLR8 were not induced post-treatment. This is at least partially in agreement with the TLR expression pattern Roux *et al.* observed following ECT in treated melanoma lesions[8]. They observed a strong enhancement of TLR9 expression, a slight enhancement of TLR7 expression and no change in the expression of TLR3 and TLR4 expression[8]; they did not analyse the expression of the other murine TLRs. There are no particular functional or location differences between the upregulated and non-upregulated TLRs observable. Both groups contain TLRs that are expressed on the cell surface (TLR1, TLR2, TLR4, TLR5, TLR6)[38] as well as TLRs that are located on the endosome (TLR3, TLR7, TLR8, TLR9)[38]. Also, the types of stimuli activating the respective TLRs are distributed across the two groups. TLR1, TLR2 are reactive to gram-positive bacteria, while TLR 4 and TLR6 are reactive to gram-negative bacteria[39]. TLR3, TLR7 and TLR8 are activated by single- stranded RNA with TLR3 also getting activated by double-stranded DNA[39]. TLR5 is uniquely stimulated by bacterial flagellin while TLR9 is uniquely stimulated by unmethylated CpG DNA[39], which is commonly found in bacterial DNA[40]. Considering the great overlap in TLR expression pattern between the EP and ECT treatments, it could be concluded that the electroporation is causing the upregulation of the specific TLRs while the addition of the cytotoxic drug only seems to augment the effect without inducing any additional effects. It can be further concluded that electroporation induces more structural changes in the cells than simply creating pores in their cell membrane for microseconds to facilitate component uptake, as IFN-γ secretion without additional stimulation was decreasing significantly with increasing electric field strength, whilst TNF-α secretion was unchanged following EP treatment. It is possible, that the structural changes could be caused by the short-term disturbance of cell homeostasis

following the creation of the pores by electroporation and the influx and efflux of molecules. The observed upregulation of the TLR3, TLR6 and TLR9 creates the possibility to test further TLR agonists, other than CpG, in combination with ECT to improve therapy outcome, once the upregulation is confirmed to be functional.

As the previously described experiments in this chapter had indicated that ECT exerts certain effects on DC cellular processes, in order to further understand this analysis, UPX 3' Transcriptome Sequencing was employed to identify global gene changes that could illuminate upregulated pathways, including cell death pathways, following ECT treatment, and potentially expand on the observed phenotypic changes. 800ECT did induce upregulation of a discreet set of genes that was distinctively different to the set of genes upregulated after 1000ECT and 1300ECT. Despite the difference in the upregulated genes, these genes were, in all three treatments, connected to similar pathways. The majority of the pathways are connected to immune responses to pathogen recognition with an emphasis on responses to bacterial and viral infections. Considering that DCs are an immune cell type, this might explain why the majority of the impacted pathways are connected to immune functions rather than other physiological functions, even though several different stress responses to different substances (toxins, chemicals and irradiation) were also observed across the three treatment conditions. The MAPK and NF-κB signalling pathways were upregulated in all 3 treatment conditions. The IL-17 signalling pathway was only upregulated after 800ECT and 1000ECT, while the TLR signalling pathway was only upregulated after 1000ECT and 1300ECT, with the TNF signalling pathway only being upregulated after 1300ECT.

Both the MAPK[41,42] and the NF-κB[43–46] pathways are central to the cellular responses to extracellular stimuli (particular stressors like cytokines or heat-shock), regulating diverse aspects such as cell proliferation and differentiation, cell survival, apoptosis, but also cytokine production and innate and adaptive immune responses. Both pathways were impacted across the three treatments which likely indicates that these cells are stressed by the treatment and are trying to maintain or restore cellular homeostasis rather than these cells responding to pathogens and therefore activating immune responses.

IL-17 as a pro-inflammatory cytokine plays a central role in the control of infections, specifically extracellular fungi, and is typically secreted by T cells (Th17 cells)[47]. It can also stimulate the MAPK and NF-κB pathways[48]. In addition, gram-positive bacteria can induce upregulation of IL-17 by activating TLR2 on DCs[47]. We had shown that TLR2 is indeed upregulated post EP at 800V/cm and 1000V/cm, but not after ECT, which is in agreement with the upregulated IL-17 pathway in 800ECT and 1000ECT but not 1300ECT. Thus, it is possible that the upregulation of TLR2 caused by electroporation itself is responsible for the upregulation of the IL-17 signalling pathway following ECT treatment.

The TLR signalling pathway is critical for the innate immune response to invading pathogens. Given that the TLR signalling pathway was upregulated following ECT treatment, it is unlikely that it was indeed some type of a pathogen causing the upregulation, but it seems possible that the electroporation aspect of the ECT treatment caused the upregulation, as was observed for the TLR expression pattern itself particularly given the different stimuli activating the upregulated TLRs. Unless the samples were infected simultaneously with viral, bacterial and fungal pathogens, the electric field strength seems to have induced the upregulation of TLRs electro-mechanically. A closer look at the upregulated genes causing the enrichment in the TLR signalling pathway (Ccl4, Fox, Cd14 and Jun) reveals that all these genes are also more commonly connected with immune cells (Ccl4 being a chemoattractant[49] and Cd14 being a main surface marker for monocytes/ macrophages[50]) and with modification of gene transcription (both Jun[51] and Fos[52] are transcription factors) than with TLR signalling specifically. The genes might play a role in the TLR signalling pathway, but they are not exclusively enriched in the TLR signalling pathway.

The TNF signalling pathway regulates diverse physiological functions like modulation of immune and inflammatory responses, apoptosis and cell survival[53]. It is an upstream regulator of the NF-kB and MAPK pathways[54]; which were both upregulated independently of the TNF signalling pathway in all three treatment conditions. Interestingly, despite the TNF signalling pathway being upregulated only in the 1300ECT group, TNF-α secretion was not found to be upregulated following TLR stimulation in our EP and ECT treated DCs except following CpG stimulation in the 800ECT group. Ankrd44, also known as PP6-ARS-B, is one of three ankyrin repeat

proteins that plays an important role in determining the specificity and regulation of PP6 phosphatase[55]. PP6 itself is a member of type 2A protein phosphatase family and impacts DNA damage repair, cell cycle regulation, inflammatory signalling and lymphocyte development[55,56]. Additionally, ANKRD44 is overexpressed in patients showing only partial response to Trastuzumab in Her2-Like Breast Cancer[57]. Why ECT800 and ECT1300 cause a downregulation of Ankrd44 and what impact this has on the DC functionality is currently unknown. The Atxn1 gene encodes Ataxin-1 which is a DNA-binding protein and seems to be involved in gene expression regulation, even though its full function is not yet understood. Furthermore, aberrant Ataxin-1 proteins are known to cause several neurodegenerative diseases[58–60]. How and why only ECT1000 is causing a downregulation of Atxn1 will need to be investigated in future studies. The Ccr2 chemokine receptor is extensively expressed in haematopoietic cells and upon binding of CCL2, it mediates chemotaxis and migration of monocytes and macrophages as well as regulates T-cell inflammatory processes. Ccr2 has been functionally implicated in several diseases among which are rheumatoid arthritis, multiple sclerosis and atherosclerosis[61,62]. The Fryl gene, also known as AF4p12, is an evolutionary well conserved gene and may regulate the actin cytoskeleton[63]. This downregulation of Fryl by 1300ECT could indicate that DCs undergoing ECT at 1300V/cm may be losing cell integrity.

Combined, the pattern of DEGs illustrates that the cellular responses not only shift from immune responses to stress responses, but also that the experienced stress is higher with the higher the electric field strengths, and thus, more genes are differentially impacted. Of interest, only the highest treatment with 1300ECT led to the induction of cell-death pathways, while we originally had already observed that DCs undergo cell death at a significantly higher rate at 1000ECT[1]. Therefore, it might be of interest to further explore the possibility to reduce the electric field strength of the ECT treatment *in vivo*, to protect the crucially important dendritic cell population during the treatment, so that the DCs can then induce immune response able to respond to the treated tumours.

We were unable to confirm the observed expression patterns of Cxcl10 and Isg15 by UPX 3’ Transcriptome Sequencing via qRT-PCR, indicating that further in-depth and targeted analysis of the gene changes upon ECT treatment is required. Future

targeted research could further illuminate relevant changes in regards to the experienced cell death or immune function of DCs post-treatment. The presented data is merely a first overview of which processes might be impacted by ECT in DCs. More specific questions, such as what component of the NF-κB pathway is impacted by ECT, will allow investigation of a particular pathway in much more detail and with a more targeted approach, potentially even allowing to functionally access the pathway by inhibiting specific key components of that pathway. In addition, further research is needed to understand how the observed gene changes might correlate with any changes in the functionality of DCs post-treatment and the impact this has on treatment results. Better understanding of the changes in gene expression may mean that adjuvant therapies could be designed to increase tumour reduction and disease-free survival post-treatment. Collectively, this is the first time that UPX 3' Transcriptome Sequencing was performed on immune cells undergoing ECT treatment with various electric field strengths in order to illuminate the impact ECT has on DCs.

In addition to examining the above phenotypic and genome wide changes in DCs post EP and ECT treatment, the functional capacity of the cells was also examined in terms of their ability to respond to stimulation by cytokine secretion. TLR agonist stimulation was analysed by ELISA to determine whether treated DCs remain functionally active and thus, would be able to process and respond to the DAMPs and tumour-associated antigens secreted from ECT-treated cancer cells[11]. Stimulation with CpG, LPS, polyI:C and R848 led to a stimulation and treatment dependent impact on the cytokine secretion. Treated cells were unable to respond to LPS, polyI:C and R848 in terms of IFN-γ production, whilst still being able to respond to CpG stimulation. In contrast, treated cells were able to respond to CpG, LPS and R848 stimulation in terms of TNF-α secretion, but were unable to respond to polyI:C. These observed differences in ability to respond to TLR stimuli cannot be explained by the expression patterns of TLRs following EP and ECT treatment. Further research would be required to elucidate how EP and ECT treatment at the different electric field strengths is impacting TLR signalling pathways. Signalling specificity of the TLR family members are controlled by different downstream signalling pathways, for example

the MyD88- and TRIF-pathways[38], and it is possible that EP and ECT impact one or more proteins in the different signalling pathways, potentially in a field strength dependent manner. Overall, whilst there is some observable difference between the response in relation to the analysed cytokine secreted and used TLR agonists, the overall trend is that EP and ECT reduce the ability of the treated cells to respond to stimulation. Moreover, the higher the used electric field strength is the higher the impact on the ability of the treated cells to respond to TLR stimuli, while the reduced responsiveness cannot be explained purely by decreased viability of the cells. As TLR6 were also upregulated following EP and ECT treatment, it would be of interest to test the combination of ECT treatments with TLR6 agonist in the future. TLR6 agonists are currently not under clinical trials investigation for any type of cancer treatment.

TNF-α is a key factor in inflammation and cancer[54] with an anti-vascular effect[64], thus the increased TNF-α secretion following 800ECT could create a more pronounced inflammatory reaction which in turn could increase the immune response to the tumour, thereby increasing effectiveness of the treatment. Mature immunogenic DCs produce, among other cytokines, huge amounts of TNF-α[65], so despite the absence of increased maturation marker of the DCs following 800ECT treatment, based on their TNF-α secretion they seem to be functionally mature. While TNF-α secretion can induce an anti-tumour immune response by T cell stimulation[4], in the context of the TME, TNF-α can induce a phenotypic subtype of $CD4^+$ T cells, which promote tumour growth, via its effects on the DCs[66]. The anti-vascular properties of TNF-α could also potentially facilitate the tumour vessel destruction, which could either improve the therapy outcome as reduced blood flow to the tumour makes necrosis more likely or decrease the therapy outcome as immune cells would be less able to access the tumour. Some evidence of a role for TNF-α in ECT has already been shown as adjuvant TNF-α therapy with cisplatin ECT in a murine sarcoma model showed a synergistic effect of the two treatments if the TNF-α was administered prior to the ECT treatment. However, when the TNF-α was administered after the ECT treatment it resulted in significant shorter tumour growth delay and decreased tumour cure rate than when the TNF-α was administered prior to the ECT treatment[67]. It would need to be tested if endogenous produced TNF-α at the

produced levels following ECT treatment would have the same effect as intratumoral injection of recombinant TNF-α post ECT treatment.

Taken together our results indicate that ECT has an electric field strength-dependent effect on a variety of cellular processes of DCs. It is currently unclear why ECT is causing such differential effects on DCs and how these effects could be targeted to improve therapy outcome. There is some indication that the majority of the impacts exhibited by ECT are caused by the electroporation component of the treatment, with the drug component, at least in the case of cisplatin, only augmenting any impact. Whether calcium, or other cytostatic drugs such as bleomycin, also only lead to the augmentation of the EP impact would need to be investigated in the future. There is a possibility that calcium could induce additional effects following ECT treatment, that are independent of the EP effect, as calcium by itself already has immunostimulatory functions[12,68].

As this study was completely performed with naïve DCs *in vitro*, the results also need to be confirmed in the *in vivo* setting, either via murine or patient trials. Whilst employing *in vitro* models allowed the assessment of a wide range of cellular features following treatment, it is impossible to replicate all conditions that would be present in the *in vivo* situation. The tumour microenvironment, in which the DCs reside prior to treatment, already induces cellular and metabolic changes in immune cells[36], often leading to a regulatory phenotype of the immune cells, which finally supports the tumour to avoid immune detection. It is reasonable to assume, that the phenotype and/or gene changes following ECT treatment might be different for DCs *in vivo*, which are already altered by the tumour microenvironment, compared to naïve DCs *in vitro*.

Data presented here indicates that, at least in terms of immune cells, ECT treatment at the different electric field strengths has the potential to differentially affect cells in terms of phenotypic maturation, gene expression and responses to stimulation. Thus, to improve therapy outcome following ECT, it would be worthwhile to test ECT with 800V/cm *in vivo* alone to protect DCs during treatment, potentially allowing for

an improved immune response following treatment, thus leading to increased tumour eradication. In addition, the combination of 800ECT with TLR ligands, to not only initially protect the DCs, but to also to support immune activation following treatment should be further examined. Currently tested immune co-treatments using checkpoint-inhibitor therapy with ECT are leading to mixed results[69,70], thus it might be of interest to not only test removal of immune response inhibitors, but to use immune co-treatments supporting immune activation.

5.6 Bibliography

1. Bendix, M. B., Houston, A., Forde, P. F. & Brint, E. Defining optimal parameters to maximize the effect of electrochemotherapy on lung cancer cells whilst preserving the integrity of immune cells. *Bioelectrochemistry* **148**, 108257 (2022).

2. Cabeza-Cabrerizo, M., Cardoso, A., Minutti, C. M., Pereira Da Costa, M. & Reis E Sousa, C. Dendritic Cells Revisited. *Annu. Rev. Immunol.* **39**, 131–166 (2021).

3. Wculek, S. K. *et al.* Dendritic cells in cancer immunology and immunotherapy. *Nat. Rev. Immunol.* **20**, 7–24 (2020).

4. Veglia, F. & Gabrilovich, D. I. Dendritic cells in cancer: the role revisited. *Curr. Opin. Immunol.* **45**, 43–51 (2017).

5. Gardner, A. & Ruffell, B. Dendritic Cells and Cancer Immunity. *Trends Immunol.* **37**, 855–865 (2016).

6. Tremble, L. F., O'Brien, M. A., Forde, P. F. & Soden, D. M. ICOS activation in combination with electrochemotherapy generates effective anti-cancer immunological responses in murine models of primary, secondary and metastatic disease. *Cancer Lett.* **420**, 109–115 (2018).

7. Tremble, L. F., O'Brien, M. A., Soden, D. M. & Forde, P. F. Electrochemotherapy with cisplatin increases survival and induces immunogenic responses in murine models of lung cancer and colorectal cancer. *Cancer Lett.* **442**, 475–482 (2019).

8. Roux, S. *et al.* Tumor destruction using electrochemotherapy followed by CpG oligodeoxynucleotide injection induces distant tumor responses. *Cancer Immunol. Immunother.* **57**, 1291–1300 (2008).

9. Gerlini, G. *et al.* Dendritic cells recruitment in melanoma metastasis treated by electrochemotherapy. *Clin. Exp. Metastasis* **30**, 37–45 (2013).

10. Di Gennaro, P. *et al.* CD4+FOXP3+ T regulatory cells decrease and CD3+CD8+

T cells recruitment in TILs from melanoma metastases after electrochemotherapy. *Clin. Exp. Metastasis* **33**, 787–798 (2016).

11. Bendix, M. B., Houston, A., Forde, P. F. & Brint, E. Electrochemotherapy and immune interactions; A boost to the system? *Eur. J. Surg. Oncol.* **48**, (2022).

12. Tremble, L. F., Heffron, C. C. B. B. & Forde, P. F. The effect of calcium electroporation on viability, phenotype and function of melanoma conditioned macrophages. *Sci. Rep.* **10**, 1–12 (2020).

13. Galluzzi, L. *et al.* Molecular mechanisms of cell death: Recommendations of the Nomenclature Committee on Cell Death 2018. *Cell Death Differ.* **25**, 486–541 (2018).

14. Fernandes, P., O'Donovan, T. R., McKenna, S. L. & Forde, P. F. Electrochemotherapy causes caspase-independent necrotic-like death in pancreatic cancer cells. *Cancers (Basel).* **11**, (2019).

15. Mlakar, V., Todorovic, V., Cemazar, M., Glavac, D. & Sersa, G. Electric pulses used in electrochemotherapy and electrogene therapy do not significantly change the expression profile of genes involved in the development of cancer in malignant melanoma cells. *BMC Cancer* **9**, 299 (2009).

16. Robinson, M. D. & Smyth, G. K. Small-sample estimation of negative binomial dispersion, with applications to SAGE data. *Biostatistics* **9**, 321–332 (2008).

17. Robinson, M. D., McCarthy, D. J. & Smyth, G. K. edgeR: A Bioconductor package for differential expression analysis of digital gene expression data. *Bioinformatics* **26**, 139–140 (2009).

18. Engeland, M. Van, Nieland, L. J. W., Ramaekers, F. C. S., Schutte, B. & Reutelingsperger, C. P. M. Cytometry - 1998 - van Engeland - Annexin V-Affinity assay A review on an apoptosis detection system based on. *Cytometry* **31**, 1–9 (1998).

19. Steinman, R. M. Decisions about dendritic cells: Past, present, and future. *Annu. Rev. Immunol.* **30**, 1–22 (2012).

20. Krawczyk, C. M. *et al.* Toll-like receptor-induced changes in glycolytic metabolism regulate dendritic cell activation. *Blood* **115**, 4742–4749 (2010).

21. Hogue, C. W. & Groll, M. An automated method for finding molecular complexes in large protein interaction networks. *BMC Bioinformatics* **29**, 137–140 (2001).

22. Rehwinkel, J. & Gack, M. U. RIG-I-like receptors: their regulation and roles in RNA sensing. *Nat. Rev. Immunol.* **20**, 537–551 (2020).

23. Jorgovanovic, D., Song, M., Wang, L. & Zhang, Y. Roles of IFN-γin tumor progression and regression: A review. *Biomark. Res.* **8**, 1–16 (2020).

24. Pan, J. *et al.* Interferon-γ is an autocrine mediator for dendritic cell maturation. *Immunol. Lett.* **94**, 141–151 (2004).

25. Mercogliano, M. F., Bruni, S., Mauro, F., Elizalde, P. V. & Schillaci, R. Harnessing tumor necrosis factor alpha to achieve effective cancer immunotherapy. *Cancers (Basel).* **13**, 1–33 (2021).

26. Page, M. J., Bester, J. & Pretorius, E. The inflammatory effects of TNF-α and complement component 3 on coagulation. *Sci. Rep.* **8**, 1–9 (2018).

27. Gehl, J. *et al.* Electrochemotherapy in the treatment of metastatic malignant melanoma : a prospective cohort study by InspECT. *Br. J. Dermatol.* **176**, 1475–1485 (2017).

28. Chen, M. & Wang, J. Programmed Cell Death of Dendritic Cells in Immune Regulation. (2010) doi:10.1111/j.1600-065X.2010.00916.x.

29. Chen, M. & Wang, J. Regulation of Immune Responses by Spontaneous and T cell- mediated Dendritic Cell Death. *J Clin Cell Immunol.* (2011) doi:10.4172/2155-9899.S3-005.

30. Fink, S. L. & Cookson, B. T. Apoptosis, pyroptosis, and necrosis: Mechanistic description of dead and dying eukaryotic cells. *Infect. Immun.* **73**, 1907–1916 (2005).

31. Brock, R. M., Beitel-White, N., Davalos, R. V. & Allen, I. C. Starting a Fire

Without Flame: The Induction of Cell Death and Inflammation in Electroporation-Based Tumor Ablation Strategies. *Front. Oncol.* **10**, 1–9 (2020).

32. Jacobson, L. S. *et al.* Cathepsin-mediated necrosis controls the adaptive immune response by Th2 (T helper type 2)-associated adjuvants. *J. Biol. Chem.* **288**, 7481–7491 (2013).

33. Vakkila, J. & Lotze, M. T. Inflammation and necrosis promote tumour growth. *Immunology* **4**, 1–8 (2004).

34. Gallois, A. & Bhardwaj, N. Dendritic cell-targeted approaches to modulate immune dysfunction in the tumor microenvironment. *Front. Immunol.* **4**, 1–8 (2013).

35. Pitt, J. M. *et al.* Targeting the tumor microenvironment: Removing obstruction to anticancer immune responses and immunotherapy. *Ann. Oncol.* **27**, 1482–1492 (2016).

36. Netea-Maier, R. T., Smit, J. W. A. & Netea, M. G. Metabolic changes in tumor cells and tumor-associated macrophages: A mutual relationship. *Cancer Lett.* **413**, 102–109 (2018).

37. Wang, W., Li, J., Wu, K., Azhati, B. & Rexiati, M. Culture and identification of mouse bone marrow-derived dendritic cells and their capability to induce T lymphocyte proliferation. *Med. Sci. Monit.* **22**, 244–250 (2016).

38. Kawasaki, Takumi ; Kawai, T. Toll-like receptor signaling pathways. *Front. Immunol.* **5**, (2014).

39. Vidya, M. K. *et al.* Toll-like receptors: Significance, ligands, signaling pathways, and functions in mammals. *Int. Rev. Immunol.* **37**, 20–36 (2018).

40. Hemmi, H. *et al.* A Toll-like receptor recognizes bacterial DNA. *Nature* **408**, 740–745 (2000).

41. Wei, Z. & Liu, H. T. MAPK signal pathways in the regulation of cell proliferation in mammalian cells. *Cell Res.* **12**, 9–18 (2002).

42. Whitmarsh, A. J. Regulation of gene transcription by mitogen-activated protein kinase signaling pathways. *Biochim. Biophys. Acta - Mol. Cell Res.* **1773**, 1285–1298 (2007).

43. Liu, T., Zhang, L., Joo, D. & Sun, S. C. NF-κB signaling in inflammation. *Signal Transduct. Target. Ther.* **2**, (2017).

44. Perkins, N. D. Integrating cell-signalling pathways with NF-κB and IKK function. *Nat. Rev. Mol. Cell Biol.* **8**, 49–62 (2007).

45. Brasier, A. R. The NF-κB regulatory network. *Cardiovasc. Toxicol.* **6**, 111–130 (2006).

46. Li, Q. & Verma, I. M. NF-kappaB regulation in the immune system. *Nat. Rev. Immunol.* **2**, 725–34 (2002).

47. Ge, Y., Huang, M. & Yao, Y. M. Biology of Interleukin-17 and Its Pathophysiological Significance in Sepsis. *Front. Immunol.* **11**, 1–13 (2020).

48. Karanika, S., Karantanos, T., Li, L., Corn, P. G. & Timothy, C. Interleukin 17 Family Cytokines: Signaling Mechanisms, Biological Activities, and Therapeutic Implications. *Cold Spring Harb Perspect Biol* **34**, 2815–2822 (2015).

49. Bystry, R. S., Aluvihare, V., Welch, K. A., Kallikourdis, M. & Betz, A. G. B cells and professional APCs recruit regulatory T cells via CCL4. *Nat. Immunol.* **2**, 1126–1132 (2001).

50. Heidenreich, S. Monocyte CD14: A multifunctional receptor engaged in apoptosis from both sides. *J. Leukoc. Biol.* **65**, 737–743 (1999).

51. Wisdom, R., Johnson, R. S. & Moore, C. c-Jun regulates cell cycle progression and apoptosis by distinct mechanisms. *EMBO J.* **18**, 188–197 (1999).

52. Kovács, K. J. c-Fos as a transcription factor: A stressful (re)view from a functional map. *Neurochem. Int.* **33**, 287–297 (1998).

53. Aggarwal, B. B. Signalling pathways of the TNF superfamily: A double-edged sword. *Nat. Rev. Immunol.* **3**, 745–756 (2003).

54. Sabio, G. & Davis, R. J. TNF and MAP kinase signalling pathways. *Semin. Immunol.* **26**, 237–245 (2014).

55. Stefansson, B., Ohama, T., Daugherty, A. E. & Brautigan, D. L. Protein phosphatase 6 regulatory subunits composed of ankyrin repeat domains. *Biochemistry* **47**, 1442–1451 (2008).

56. Ohama, T. The multiple functions of protein phosphatase 6. *Biochim. Biophys. Acta - Mol. Cell Res.* **1866**, 74–82 (2019).

57. Ferla, M. La *et al.* ANKRd44 gene silencing: A putative role in trastuzumab resistance in HER2-like breast cancer. *Front. Oncol.* **9**, 1–15 (2019).

58. Kim, E., Lee, Y., Choi, S. & Song, J. J. Structural basis of the phosphorylation dependent complex formation of neurodegenerative disease protein Ataxin-1 and RBM17. *Biochem. Biophys. Res. Commun.* **449**, 399–404 (2014).

59. Lam, Y. C. *et al.* ATAXIN-1 Interacts with the Repressor Capicua in Its Native Complex to Cause SCA1 Neuropathology. *Cell* **127**, 1335–1347 (2006).

60. Orr, H. T. *et al.* Expansion of an unstable trinucleotide CAG repeat in spinocerebellar ataxia type 1. *Nat. Genet.* **4**, 221–226 (1993).

61. Feria, M. & Díaz-González, F. The CCR2 receptor as a therapeutic target. *Expert Opin. Ther. Pat.* **16**, 49–57 (2006).

62. Charo, I. F. *et al.* Molecular cloning and functional expression of two monocyte chemoattractant protein 1 receptors reveals alternative splicing of the carboxyl-terminal tails. *Proc. Natl. Acad. Sci. U. S. A.* **91**, 2752–2756 (1994).

63. Hayette, S. *et al.* AF4p12, a human homologue to the furry gene of Drosophila, as a novel MLL fusion partner. *Cancer Res.* **65**, 6521–6525 (2005).

64. Mocellin, S., Rossi, C. R., Pilati, P. & Nitti, D. Tumor necrosis factor, cancer and anticancer therapy. *Cytokine Growth Factor Rev.* **16**, 35–53 (2005).

65. Ma, Y., Shurin, G. V., Peiyuan, Z. & Shurin, M. R. Dendritic cells in the cancer microenvironment. *J. Cancer* **4**, 36–44 (2013).

66. Laha, D., Grant, R., Mishra, P. & Nilubol, N. The Role of Tumor Necrosis Factor in Manipulating the Immunological Response of Tumor Microenvironment. *Front. Immunol.* **12**, 1–12 (2021).

67. Cemazar, M. *et al.* Adjuvant TNF-α therapy to electrochemotherapy with intravenous cisplatin in murine sarcoma exerts synergistic antitumor effectiveness. *Radiol. Oncol.* **49**, 32–40 (2015).

68. Hoejholt, K. L. *et al.* Calcium electroporation and electrochemotherapy for cancer treatment: Importance of cell membrane composition investigated by lipidomics, calorimetry and in vitro efficacy. *Sci. Rep.* **9**, 1–12 (2019).

69. Karaca, B., Yayla, G., Erdem, M. & Gürler, T. Electrochemotherapy with anti-PD-1 treatment induced durable complete response in heavily pretreated Metastatic melanoma patient. *Anticancer. Drugs* **29**, 190–196 (2018).

70. Mozzillo, N. *et al.* Assessing a novel immuno-oncology-based combination therapy: Ipilimumab plus electrochemotherapy. *Oncoimmunology* **4**, (2015).

Chapter 6

Final Discussion and Future Directions

6.1 Final Discussion and future directions

Lung cancer is an increasing burden on healthcare systems worldwide. It is still, despite recent advances in developing new treatment options, the leading cause of cancer-related death[1,2]. Therefore, more effective treatment options are needed for lung cancer treatment. ECT has become an established therapy option for the treatment of melanoma and is currently under investigation for the treatment of internal organ cancers like prostate and colon cancer[3–5]. I have shown in this thesis that it would be worthwhile to further investigate ECT as an additional treatment modality for lung cancer patients. While ECT is a powerful local treatment, with reduction of local tumour burden of up to 85%[6], its systemic effects are more varied. My results show that up to 60% of DCs and 90% of macrophages, which together are responsible for activating systemic immune responses, get killed with ESOPE-based field strengths *in vitro*[7], whilst T cells, responsible for the local immune response, do not get killed at significant levels *in vitro*[7]. Thus explaining the potent effect of ECT on the local tumour burden and the absence of a consistent systemic immune response. A better understanding of the impact EP and ECT have both on cancer cells and immune cells could open up avenues to increase systemic immune effects and thus the effectiveness of the treatment as well as open the possibility of effective immune co-treatments.

6.2 ESOPE equivalent parameters for treatment of internal organ tumours

The landmark ESOPE study, in 2006, allowed for the unification of ECT-based cancer treatments, making comparing results between different cancer centres and countries easier[6]. ESOPE standardized the ECT treatment modalities to 8 pulses, with 100µs pulse length, at 1Hz frequency with an electric field strength of 1000V/cm for type II electrodes[6]. These parameters have been unchanged since then for ECT-application for cancer patients, even as additional different cancer types were identified as treatable with ECT and also when calcium, instead of cytotoxic drugs, is used (then called CaEP)[3,8–12]. One major drawback of the ESOPE study, as well as the following Updated standard operating procedures for electrochemotherapy of cutaneous tumours and skin metastases[13] and the InspECT[14] studies was the main

focus of these studies on a single tumour type, namely melanoma. The Updated protocol[13], while giving guidelines for which type of electrode to use, when to use systemic versus local drug administration, and defining exclusion criteria for ECT treatment, did not include guidelines for adapting the electric pulse parameters in a tumour-type dependent manner. This could be explained as the updated protocol was written when ECT was still considered mainly as a melanoma treatment. With the recent advances exploring usage of ECT for treatment of internal organ cancers[3,15–17], it is clearly time to not only assess and optimize the chosen drugs for ECT treatments, but also to assess and optimize the applied electric field parameters, in a cancer-type dependent manner. Several groups[7,18–21] in recent years have optimized different electric field strength *in vitro*, while keeping all other pulse parameters identical to the ESOPE parameters, for different cell lines. For example Tremble *et al.*[18] optimized 700V/cm for B16F10 cells (murine melanoma cell line) and 1300V/cm for LLC cells (murine lung cancer cell line) and Frandsen *et al.*[20] optimized 250V/cm for HCC1419 cells (human breast cancer cell line). As this kind of optimization has not yet been carried out for *in vivo* applications of ECT and electric field distributions are impacted by the properties of the specific tumour, with different conductivity leading to different therapeutic yields[22], it remains to be seen whether the optimised parameters translate to the *in vivo* setting or whether further optimization will be required. Employing patient trials to optimize the electric pulse parameters is not practical or desirable, but early work on the translation of *in vitro* ECT findings to *in vivo* application has shown that optimized *in vitro* parameters are applicable also for *in vitro* work[23]. Thus, optimizing parameters for a specific cancer type, for example a lung adenocarcinoma, with a representable cell line *in vitro*, like A549 for the lung adenocarcinoma, could be utilized to pre-optimize the electric pulse parameters for application in patients. Furthermore, it would be of interest to illuminate and understand any differences in the cell type, contents and/or membrane composition that directly impacts the needed electric field strengths to sufficiently electroporate a given cell type. So far different studies have shown that the lipid composition and heat capacity of the cell membrane might directly influence the permeability of cells[24,25]. In addition, the cell intrinsic repair capacity was also shown to impact the sensitivity of a given cell line to electroporation, with non-

malignant cells being generally less sensitive than their malignant counterparts[26]. If these currently known parameters are enough to explain the observed differences between primary immune cells and cancer cell lines would need to be investigated in the future.

Finally, in the published work as well as this thesis, electric field strength was chosen as the parameter to optimize[7,18–21], which does not exclude that optimization of another parameter (for example number of pulses, pulse lengths, frequency) or a combination of different optimized parameters could be even more suited for the goal.

6.3 Optimizing ECT parameters for abscopal effects

In addition to optimizing electric field treatment parameters in a tumour-type dependent manner, it is also important to consider the effects ECT has on the treated immune cells in order to optimize treatment outcomes as it was previously shown that ECT needs to be administered to immunocompetent mice to be effective[4,11,27]. Results from this thesis have shown that DCs and macrophages, both antigen-presenting cells (APCs), die at a high rate if exposed to ESOPE-based electric pulse conditions[7]. The abscopal effect, the regression of untreated metastasis following localized treatment, is not only T cell dependent[28], but also APCs need to be sufficiently alive to induce a systemic immune response[29]. Abscopal effects are a particularly wished-for treatment result for any cancer type that frequently metastasizes or only gets diagnosed once it already has metastasized, like lung cancer[2]. Therefore, further studies need to be conducted to evaluate the possibility to either preserve the antigen-presenting immune population by lowering the applied electric field strength or by increasing the presence of APCs prior to the ECT treatment. Lowering the applied electric field strength to preserve the APC population needs to be balanced with the need to reduce the local tumour burden sufficiently. Therefore, the optimization of the ECT parameters for a given tumour-type ideally would be carried in tandem with evaluating the impact ECT has on the immune cells in the same tumour-type. Different level of tumour tissue

conductivity[22] and structures would most likely also have an impact on the immune cells in the given tumour.

One option that seems to increase the presence of immune cells in the tumour prior to ECT treatment, leading to an augmented immune response, is the use of IL-12 GET, which is currently already under investigation. Further elucidation of the exact impact IL-12 GET, or GETs with different gene constructs, has on the immune cell population in a given tumour could help to fine-tune the effectiveness of this GET-ECT co-treatment.

6.4 Understanding molecular mechanisms of actions of ECT in a cell-type dependent manner

It is also important to understand how ECT impacts both cancer cells and immune cells at the molecular level in order to optimize treatment results. Data from this thesis showed that EP and ECT treatments can change gene expression and induce phenotypic changes in DCs. Understanding how such changes impact treatment results would greatly aid in either optimizing treatment conditions as needed and/or designing immune co-treatments to increase the effectiveness of the ECT treatment. A relatively new field of investigation, immunometabolism, interrogates the interplay between metabolic and immunological changes in a given organism[30]. In the context of immune cells, the metabolic regulation of immune function is of particular interest. It has been recently understood that cell-intrinsic metabolic processes in immune cells can influence the functioning of these cells, for example stimulation of Toll-like receptors (TLRs) shifts the DC cellular metabolism to a glycolytic metabolism, and that the extracellular environment can also impact cell metabolism[30,31]. EP and ECT treatments both showed an ability to increase TLR expression in a voltage-dependent manner in DCs (Chapter 5) and ECT treatments *in vivo* also change the tumour microenvironment[32,33], thus these treatments will likely impact on the metabolism of treated immune cells. In addition, activated immune cells have an increased need for glucose, thus leading to increased level of glycolysis[34], with results presented here showed that ECT lead to activation of immune cells in a field strength dependent manner (Chapter 5). Thus, studies designed to examine metabolic

changes post treatment will further illuminate certain immune processes that are impacted post ECT. Once these impacts are better understood metabolic changes in the immune cells can be taken into account when designing ECT treatment plans with the best fitting co-treatments.

Currently there are no published study results from prospective studies combining ECT treatments with immune co-treatments in patients. There are some retrospective studies[35–37] and case reports[38,39] published that give conflicting information about the effectiveness of combining ECT with checkpoint inhibitor therapy (CPI). While these studies and case reports are an important tool to further design potent co-treatments for ECT, the missing controls and reports from heavily pre-treated patients[38] make it difficult to gain a clear understanding of the interplay of the ECT treatment with the immune co-treatment. Therefore, by understanding and deciphering the impact ECT has on different molecular processes in the cancer cells and immune cells, (immune) co-treatments could be designed to either explore vulnerabilities in the cancer cells or be designed to boost the immune cells. One potentially interesting co-treatment option, particularly for the application in the lung cancer context, that could be further investigated would be to combine ECT with TLR agonist stimulation. Roux *et al.* showed that a combination of ECT with TLR9 ligand administration on day 2 and 9 post ECT treatment lead to the induction of a systemic immune response in three murine tumour models (fibrosarcoma, two melanoma)[27]. Data presented here also showed that TLR expression is upregulated in a field strength dependent manner following EP and ECT treatments on DCs (Chapter 5), making it worthily to further investigate the ECT-TLR co-treatment modality in general. Inhalable TLR agonists are under consideration for the treatment of pneumonia[40] and could also be an interesting delivery option for lung cancer patients, as it would allow for targeted delivery of the TLR agonists to the lung.

Further research on the molecular processes impacted by ECT is needed, as thus far very few studies have been published that have described phenotypic and molecular changes on immune cells following ECT treatment and those studies were both *in vitro* studies[7,41]. The use of *in vivo* mouse models to examine molecular changes in

both cancer and immune cells following ECT treatment should allow for a better understanding of the complex effects ECT has in a tumour environment.

6.5 Considerations of use of ECT in the context of affordable cancer care

With increasing life expectancy in middle- and lower income countries the rate of cancer occurrence is rising as well, making affordable cancer care necessary to limit the number of unnecessary deaths and suffering. The prediction of the WHO is that by 2040 67% of all new cancer diagnosis will happen in middle- and low-income countries[1]. Also, over the past 25 years cancer treatments in the developed world has also become more expensive as more and more cancer therapeutics and therapies have been developed. Current predictions are that 20% of humanity will face a cancer diagnosis at one point in their life[1], whilst health care systems are already taxed by Covid, vascular diseases and an overall aging population in high-income countries[42] and by Covid and communicable diseases in low- and middle-income countries[43]. Therefore, it is critical to take the financial implications of cancer treatments, both medical and non-medical costs, into account when designing novel cancer treatments as well as policies.

One approach to reduce overall cancer care costs would be to reduce the price of the treatment. This is not only necessary to make cancer care more accessible in low- and middle-income countries. Also, patients in high income countries are unable to access all available cancer treatment options due to costs, either because they have to pay for the treatments themselves like in the USA or because the overall costs are too high for the health care system in general. Based on a 2019 study, the Norwegian health care system, a solidarity-based health care system in one of the richest countries in the world, was unable to pay for up to 22% of newly developed cancer treatments[44]. High costs for new treatments are, partially, caused by increasingly more complex research needed to develop these new treatment options, because more specialized medical personnel are required for some of the procedures and new medication also being protected by patent-rights. Thus, one way to reduce some of the direct costs causing high overall cancer treatment costs, would be to utilize

already proven cancer treatments for new cancer types or tweaking older treatment options to be suitable for different cancer types. One promising candidate for this approach would be ECT treatments. Initially designed and optimized for melanoma treatment, ECT treatments and the related CaEP and GET treatments have been under investigation for application to cancer types as varied as melanoma[6], colon[4,45] and head-and-neck cancers[17] over the past 15 years. By employing a technique that is already approved for clinical use and usage of comparatively old cytotoxic drugs like bleomycin and cisplatin, resulting in lower drug price compared to newly approved drugs, ECT could become a preferred treatment option for various cancer types across the world.

An early cost-comparison of different ECT modalities (bleomycin or cisplatin as used drug in combination with local or general anaesthetic; ESOPE protocol, using the Cliniporator; 2008 in Italy) came to an average price per treatment of about 1,410€ per treatment for melanoma patients[46]. In comparison radiotherapy for the same cohort would have costs 1,130€ and isolated limb perfusion 18,530€. Radiotherapy was cheaper in the tested cohort, but with a treatment effectiveness of just 56% for radiotherapy compared to 74% for ECT, ECT at a slightly higher price delivered the better treatment outcome[46], thus was more cost-effective. A small study (23 patients) from 2020 came to the result that the mean cost of a single ECT treatment is 2757€ for advanced-stage melanoma patients in Slovenia[47]. In comparison, the cost of immunotherapy, which would be an alternative treatment option to ECT in the analysed patient cohort, would be approximately 60,000€ per year. Furthermore, the study, despite the limited patient numbers enrolled, came to the conclusion that the cost-effectiveness is mainly influenced by the disease-stage and age of the patient, with early-stage disease and lower patient age leading to lower costs, thus making ECT more cost-effective. In addition, the majority of the total cost of the ECT treatment is caused by the costs of the single-use electrodes[47]. Therefore, reductions in the cost of the needed electrodes will have the biggest impact in the future to drive down costs of the overall treatment. Finally, while the costs might be higher for internal organ tumours, as general anaesthetic is always required, it still stands to reason that the cost-advantages would be largely sustained for these tumour types

as well compared to alternative treatments, including current standard of care treatments.

Finally, while direct medical cost can be more exactly quantified and therefore savings can also be made visible easier, non-medical costs associated with a cancer diagnosis should not be forgotten[1,48], such as additional child-care costs or loss of work. The less time-consuming the treatment is (single treatment versus multiple treatments; length of recovery time post-treatment) and the higher effectiveness at the same time, the more these non-medical costs can also be reduced. Objective response of 85% were achieved with ECT treatment for melanoma after a single-treatment, with little side effects being reported (all mild)[6,14]. Longer-lasting periods of pain, up to one week[49], following ECT was reported for soft tissue sarcomas and breast cancer, but could be managed on an out-patient basis[45,49]. Thus, the recovery time following the ECT treatment, at least for skin-based tumours, will be minimal, reducing the time in which childcare is needed and where the patient is unable to work. While a majority of patients had the ECT treatment performed under general anaesthesia, it is possible to perform ECT under local anaesthesia, depending on the tumour burden, which allows for ECT do be done on an outpatient-basis[45]. This reduces the cost associated with spending time in a hospital.

The potential is there for ECT to become a standard-of-care treatment for a variety of cancers in different health-care systems. However, for the full potential of ECT to be realised further work is required to understand the impact ECT has on cancer and immune cells and to properly optimize the ECT parameters in a tumour-type dependent manner.

6.6 References

1. *WHO report on cancer: setting priorities, investing wisely and providing care for all.* (2020). doi:10.1007/978-3-662-11496-4_24.

2. Bade, B. C. & Dela Cruz, C. S. Lung Cancer 2020: Epidemiology, Etiology, and Prevention. *Clin. Chest Med.* **41**, 1–24 (2020).

3. Kiełbik, A., Szlasa, W., Saczko, J. & Kulbacka, J. Electroporation-based treatments in urology. *Cancers (Basel).* **12**, 1–26 (2020).

4. Calvet, C. Y. & Mir, L. M. The promising alliance of anti-cancer electrochemotherapy with immunotherapy. *Cancer Metastasis Rev.* **35**, 165–177 (2016).

5. Calvet, C. Y., Famin, D., André, F. M. & Mir, L. M. Electrochemotherapy with bleomycin induces hallmarks of immunogenic cell death in murine colon cancer cells. *Oncoimmunology* **3**, 2–11 (2014).

6. Marty, M. *et al.* Electrochemotherapy - An easy, highly effective and safe treatment of cutaneous and subcutaneous metastases: Results of ESOPE (European Standard Operating Procedures of Electrochemotherapy) study. *Eur. J. Cancer, Suppl.* **4**, 3–13 (2006).

7. Bendix, M. B., Houston, A., Forde, P. F. & Brint, E. Defining optimal parameters to maximize the effect of electrochemotherapy on lung cancer cells whilst preserving the integrity of immune cells. *Bioelectrochemistry* **148**, 108257 (2022).

8. Dos Anjos, D. S., Rodrigues, C. G., Silva, N. C., De Nardi, A. B. & Fonseca-Alves, C. E. Electrochemotherapy associated with calcium electroporation in metastatic feline cutaneous malignant melanoma. *Acta Sci. Vet.* **47**, 1–6 (2019).

9. Granata, V. *et al.* Electrochemotherapy in locally advanced pancreatic cancer: Preliminary results. *Int. J. Surg.* **18**, 230–236 (2015).

10. Broholm, M. *et al.* Calcium electroporation for the treatment of colorectal

cancer calcium endove – preliminary results. *Eur. J. Surg. Oncol.* **45**, e119 (2019).

11. Falk, H. *et al.* Calcium electroporation induces tumor eradication, long-lasting immunity and cytokine responses in the CT26 colon cancer mouse model. *Oncoimmunology* **6**, 1–8 (2017).

12. Tellado, M. N., Maglietti, F. H., Michinski, S. D., Marshall, G. R. & Signori, E. Electrochemotherapy in treatment of canine oral malignant melanoma and factors influencing treatment outcome. *Radiol. Oncol.* **54**, 68–78 (2020).

13. Gehl, J. *et al.* Updated standard operating procedures for electrochemotherapy of cutaneous tumours and skin metastases. *Acta Oncol. (Madr).* **57**, 874–882 (2018).

14. Gehl, J. *et al.* Electrochemotherapy in the treatment of metastatic malignant melanoma : a prospective cohort study by InspECT. *Br. J. Dermatol.* **176**, 1475–1485 (2017).

15. Miklavčič, D. *et al.* Electrochemotherapy: Technological advancements for efficient electroporation-based treatment of internal tumors. *Med. Biol. Eng. Comput.* **50**, 1213–1225 (2012).

16. Edhemovic, I. *et al.* Intraoperative electrochemotherapy of colorectal liver metastases. *J. Surg. Oncol.* **110**, 320–327 (2014).

17. Plaschke, C. C. *et al.* European Research on Electrochemotherapy in Head and Neck Cancer (EURECA) project: Results from the treatment of mucosal cancers. *Eur. J. Cancer* **87**, 172–181 (2017).

18. Tremble, L. F., O'Brien, M. A., Soden, D. M. & Forde, P. F. Electrochemotherapy with cisplatin increases survival and induces immunogenic responses in murine models of lung cancer and colorectal cancer. *Cancer Lett.* **442**, 475–482 (2019).

19. Bendix, M. B., Brint, E. & Forde, P. F. Electroporation of suspension cell lines – A proposed assay set for optimizations. *Bioelectrochemistry* **142**, 107891

(2021).

20. Frandsen, S. K., Gissel, H., Hojman, P., Eriksen, J. & Gehl, J. Calcium electroporation in three cell lines: A comparison of bleomycin and calcium, calcium compounds, and pulsing conditions. *Biochim. Biophys. Acta - Gen. Subj.* **1840**, 1204–1208 (2014).

21. Vera-Tizatl, C. E. *et al.* Cell morphology impact on the set-up of electroporation protocols for in-suspension and adhered breast cancer cells. *Electromagn. Biol. Med.* **39**, 323–339 (2020).

22. Ongaro, A. *et al.* Identification of in vitro electropermeabilization equivalent pulse protocols. *Technol. Cancer Res. Treat.* **10**, 465–473 (2011).

23. Larkin, J. O. *et al.* Electrochemotherapy: Aspects of preclinical development and early clinical experience. *Ann. Surg.* **245**, 469–479 (2007).

24. Kotnik, T., Rems, L., Tarek, M. & Miklavcic, D. Membrane Electroporation and Electropermeabilization: Mechanisms and Models. *Annu. Rev. Biophys.* **48**, 63–91 (2019).

25. Hoejholt, K. L. *et al.* Calcium electroporation and electrochemotherapy for cancer treatment: Importance of cell membrane composition investigated by lipidomics, calorimetry and in vitro efficacy. *Sci. Rep.* **9**, 1–12 (2019).

26. Frandsen, S. K., McNeil, A. K., Novak, I., McNeil, P. L. & Gehl, J. Difference in Membrane Repair Capacity Between Cancer Cell Lines and a Normal Cell Line. *J. Membr. Biol.* **249**, 569–576 (2016).

27. Roux, S. *et al.* Tumor destruction using electrochemotherapy followed by CpG oligodeoxynucleotide injection induces distant tumor responses. *Cancer Immunol. Immunother.* **57**, 1291–1300 (2008).

28. Rodriguez-Ruiz, M. E. *et al.* Abscopal effects of radiotherapy are enhanced by combined immunostimulatory mAbs and are dependent on CD8 T cells and crosspriming. *Cancer Res.* **76**, 5994–6005 (2016).

29. Brix, N., Tiefenthaller, A., Anders, H., Belka, C. & Lauber, K. Abscopal,

immunological effects of radiotherapy: Narrowing the gap between clinical and preclinical experiences. *Immunol. Rev.* **280**, 249–279 (2017).

30. Mathis, D. & Shoelson, S. E. Immunometabolism: An emerging frontier. *Nat. Rev. Immunol.* **11**, 81–83 (2011).

31. Møller, S. H., Wang, L. & Ho, P. C. Metabolic programming in dendritic cells tailors immune responses and homeostasis. *Cell. Mol. Immunol.* **19**, 370–383 (2022).

32. Sersa, G. *et al.* Biological factors of the tumour response to electrochemotherapy: Review of the evidence and a research roadmap. *Eur. J. Surg. Oncol.* **47**, 1836–1846 (2021).

33. Longo, F. *et al.* Boosting the immune response with the combination of electrochemotherapy and immunotherapy: A new weapon for squamous cell carcinoma of the head and neck? *Cancers (Basel).* **12**, 1–11 (2020).

34. O'Neill, L. A. J., Kishton, R. J. & Rathmell, J. A guide to immunometabolism for immunologists. *Nat. Rev. Immunol.* **16**, 553–565 (2016).

35. Mozzillo, N. *et al.* Assessing a novel immuno-oncology-based combination therapy: Ipilimumab plus electrochemotherapy. *Oncoimmunology* **4**, (2015).

36. Heppt, M. V. *et al.* Immune checkpoint blockade with concurrent electrochemotherapy in advanced melanoma: a retrospective multicenter analysis. *Cancer Immunol. Immunother.* **65**, 951–959 (2016).

37. Campana, L. G. *et al.* Combination of pembrolizumab with electrochemotherapy in cutaneous metastases from melanoma: A comparative retrospective study from the inspect and slovenian cancer registry. *Cancers (Basel).* **13**, (2021).

38. Karaca, B., Yayla, G., Erdem, M. & Gürler, T. Electrochemotherapy with anti-PD-1 treatment induced durable complete response in heavily pretreated Metastatic melanoma patient. *Anticancer. Drugs* **29**, 190–196 (2018).

39. Quaresmini, D. *et al.* Electrochemotherapy as a Trigger to Overcome Primary

Resistance to Anti-PD-1 Treatment: A Case Report of Melanoma of the Scalp. *Front. Oncol.* **11**, 1–7 (2021).

40. Evans, S. E. *et al.* Inhaled innate immune ligands to prevent pneumonia. *Br. J. Pharmacol.* **163**, 195–206 (2011).

41. Tremble, L. F., Heffron, C. C. B. B. & Forde, P. F. The effect of calcium electroporation on viability, phenotype and function of melanoma conditioned macrophages. *Sci. Rep.* **10**, 1–12 (2020).

42. O'Reilly, P., Perret, S. & Van Dender, K. Tax and Fiscal Policy in Response to the Coronavirus Crisis: Strengthening Confidence and Resilience. *Intertax* **48**, 736–742 (2020).

43. Yadav, U. N., Rayamajhee, B., Mistry, S. K., Parsekar, S. S. & Mishra, S. K. A Syndemic Perspective on the Management of Non-communicable Diseases Amid the COVID-19 Pandemic in Low- and Middle-Income Countries. *Front. Public Heal.* **8**, (2020).

44. Vogler, S. Can we achieve affordable cancer medicine prices? Developing a pathway for change. *Expert Rev. Pharmacoeconomics Outcomes Res.* **21**, 321–325 (2021).

45. Miklavčič, D., Mali, B., Kos, B., Heller, R. & Serša, G. Electrochemotherapy: From the drawing board into medical practice. *Biomed. Eng. Online* **13**, 1–20 (2014).

46. Colombo, G. L., Di Matteo, S. & Mir, L. M. Cost-effectiveness analysis of electrochemotherapy with the Cliniporator™ vs other methods for the control and treatment of cutaneous and subcutaneous tumors. *Ther. Clin. Risk Manag.* **4**, 541–548 (2008).

47. Pirc, E. *et al.* Early Cost-effectiveness Analysis of Electrochemotherapy as a Prospect Treatment Modality for Skin Melanoma. *Clin. Ther.* **42**, 1535-1548.e2 (2020).

48. Héquet, D. *et al.* Direct medical and non-medical costs of a one-year care

pathway for early operable breast cancer: Results of a French multicenter prospective study. *PLoS One* **14**, 1–12 (2019).

49. Campana, L. G. *et al.* Electrochemotherapy treatment of locally advanced and metastatic soft tissue sarcomas: Results of a non-comparative phase II study. *World J. Surg.* **38**, 813–822 (2014).

Appendix

Name	max_group_mean	FC	Pvalue
A330069E16Rik	29.75	4.27	0.0000099
Ankrd44	28.27	-3.36	0.000020
Ccrl2	20.49	3.41	0.000014
Cd14	50.82	4.03	0.0000085
Cd69	24.32	6.06	2.8e-8
Clec4e	26.36	3.67	0.0000043
Cxcl10	18.34	14.12	0.000019
Cxcl2	39.02	5.73	0.0000044
Dusp1	78.16	4.23	2.1e-10
Egr1	60.60	17.47	8.9e-18
Emp1	19.73	3.67	0.000013
Fndc7	14.65	11.54	0.0000013
Fosb	20.80	26.29	1.6e-8
Hilpda	86.87	3.01	0.0000044
Hist1h2ao	16.42	11.39	0.000025
Hist1h4i	11.93	8.17	0.000017
Hmbs	32.00	3.66	0.0000038
Hspa1a	24.48	6.71	1.8e-7
Hspa1b	11.13	6.75	0.000038
Ifit1	45.55	7.73	0.0000059
Inhba	46.18	7.36	8.8e-11
Isg15	41.43	10.19	5.9e-8
Jund	319.37	2.55	0.000013
Klf4	85.05	3.51	5.2e-9
Lmna	130.93	3.87	5.6e-7
Mmp19	91.78	2.93	5.4e-7
Pdgfa	42.11	3.40	0.0000010
Phlda1	58.45	7.72	5.8e-15
Plk2	106.13	2.43	0.000011

Rsad2	53.64	10.49	4.8e-7
Rtp4	12.25	5.97	0.000028
Spry2	46.08	3.49	0.000034
Tnfsf9	17.44	6.32	0.000015
Xaf1	28.03	3.59	0.000020

Table A. 1: Genes differentially regulated between untreated DCs and DCs treated with ECT at 800V/cm represented in Figure 5.6. FC=Fold Change

Name	max_group_mean	FC	Pvalue
Atp8a1	22.49	-5.19	0.000017
Atxn1	96.35	-2.81	0.0000017
Bcl2l11	71.73	2.31	0.000037
Ccl4	76.14	3.65	0.000037
Ccrl2	26.78	4.16	2.8e-7
Cd14	70.68	5.34	6.8e-8
Cd69	22.45	5.66	1.1e-7
Clec4e	28.27	3.69	0.0000039
Csrnp1	18.38	3.89	0.000033
Cxcl2	52.46	7.61	7.7e-8
Ddx39	42.00	2.56	0.000039
Dnajb1	52.59	2.77	0.000047
Dqx1	33.33	4.95	0.0000018
Dusp1	83.15	4.27	1.6e-10
Egr1	58.17	16.38	5.3e-17
Emp1	26.91	4.97	3.5e-8
Ezr	85.51	2.78	0.000032
Fndc7	17.70	13.22	2.9e-7
Fos	33.86	3.44	0.0000096
Fosb	29.39	34.55	7.7e-10
Gm13889	10.87	9.87	0.000032

Hilpda	95.22	3.14	0.0000017
Hist1h2bc	492.52	2.97	0.0000017
Hist1h4i	14.80	9.53	0.0000034
Hspa1a	32.18	8.67	2.1e-9
Hspa1b	19.45	10.78	1.5e-7
Ifrd1	41.31	3.65	4.4e-7
Inhba	49.75	7.53	5.2e-11
Isg15	42.26	10.40	4.4e-8
Jun	139.38	2.52	0.000027
Klf4	97.24	3.89	2.1e-10
Lmna	145.16	4.08	1.9e-7
Mmp19	90.48	2.81	0.0000015
Mt2	346.06	2.56	0.000014
Nr4a2	22.12	3.81	0.0000058
Phlda1	62.76	7.98	2.0e-15
Plk2	127.17	2.78	3.4e-7
Ptgs2	17.31	21.03	0.0000027
Ralgds	11.72	5.69	0.000022
Rgcc	102.16	2.71	0.000034
Rgs2	79.26	3.56	0.0000037
Rhob	52.10	2.66	0.0000057
Rsad2	52.45	10.35	5.5e-7
Socs3	24.81	6.26	4.5e-8
Spty2d1	24.28	3.19	0.000036
Tnfsf9	22.79	8.01	7.8e-7
Tubb2a	20.61	3.39	0.000039
Vmp1	106.52	2.54	0.000016
Wwc1	9.65	11.82	0.000036

Table A. 2: Genes differentially regulated between untreated DCs and DCs treated with ECT at 1000V/cm represented in Figure 5.8. FC=Fold Change

Name	max_group_mean	FC	Pvalue
A330069E16Rik	26.74	4.41	0.000011
Ankrd44	28.27	-4.38	0.000047
Bhlhe40	143.67	2.27	0.000039
Bhlhe41	208.27	2.53	0.000051
Bzrap1	28.84	3.29	0.000027
Ccl4	74.09	4.00	0.000012
Ccr2	62.28	-3.86	0.000065
Cd14	64.39	5.66	3.5e-8
Cd69	25.57	7.83	4.3e-10
Chka	27.41	3.72	0.000013
Cxcl2	42.42	7.37	1.9e-7
Dqx1	28.20	4.90	0.0000038
Dusp1	95.21	5.85	1.0e-14
Dusp14	10.31	6.13	0.000028
Egr1	53.72	17.87	1.4e-17
Emp1	27.82	6.14	9.3e-10
Fndc7	17.30	15.88	5.6e-8
Fos	33.46	3.99	0.0000012
Fosb	27.36	38.61	3.0e-10
Fryl	37.06	-3.41	0.000064
Gadd45a	28.96	3.01	0.000038
Gadd45b	91.89	2.37	0.000068
Gm12374	28.41	3.58	0.000020
Gm15922	10.17	15.50	0.000011
Gm26735	32.99	3.02	0.000045
Gm26917	59.95	3.17	0.0000047
Hilpda	75.21	2.96	0.0000095
Hist1h1c	123.55	2.47	0.000014
Hist1h2bc	439.50	3.08	8.2e-7

Hist1h4i	14.91	11.24	9.2e-7
Hmbs	25.89	3.31	0.000046
Hspa1a	26.92	8.41	8.4e-9
Hspa2	19.13	14.23	3.5e-8
Ier2	67.09	3.31	1.9e-7
Ifrd1	41.29	4.28	2.7e-8
Inhba	56.54	10.06	9.0e-14
Irf2bpl	49.27	3.25	0.000052
Jun	145.25	3.11	2.9e-7
Jund	369.91	3.38	1.4e-8
Kctd12	73.09	2.35	0.000033
Klf10	38.51	2.65	0.000037
Klf4	105.99	4.97	1.1e-13
Lhfpl2	12.60	4.19	0.000050
Lmna	120.23	4.08	2.6e-7
Mmp19	69.50	2.62	0.000013
Mt2	303.61	2.65	0.0000080
Nr4a2	23.91	4.84	1.6e-7
Pdgfa	34.89	3.19	0.0000095
Phlda1	77.19	11.51	1.3e-20
Pim1	1,103.92	3.25	0.000030
Plk2	146.03	3.77	4.9e-11
Ppp1r15a	44.85	2.64	0.000026
Rgcc	84.03	2.64	0.000073
Rgs2	71.43	3.86	0.0000012
Rhob	67.40	4.19	3.4e-11
Sdc4	152.41	3.64	6.3e-7
Sgms2	53.84	2.99	0.000014
Socs3	14.59	4.35	0.000044
Sowahc	30.99	3.28	0.000037
Tubb2a	21.67	4.31	0.0000014

Zc3h12c	32.34	3.07	0.000068
Zfp703	25.50	2.88	0.000039

Table A. 3: Genes differentially regulated between untreated DCs and DCs treated with ECT at 1300V/cm represented in Figure 5.10. FC=Fold Change

Description	FDR value	Connected Genes
Response to chemical	3.77E-6	Fosb, Spry2, Dusp1, Mmp19, Lmna, Cd69, Rtp4, Cxcl10, Inhba, Cd14, Hilpda, Egr1, Cxcl2, Pdgfa, Isg15, Hspa1a, Jund, Ifit1, Klf4, Ccrl2, Xaf1, Hspa1b
Immune system process	0.0016	Rsad2, Clec4e, Tnfsf9, Rtp4, Cxcl10, Inhba, Cd14, Egr1, Cxcl2, Isg15, Ifit1, Klf4, Ccrl2
Positive regulation of multicellular organismal process	0.0021	Rsad2, Plk2, Lmna, Clec4e, Tnfsf9, Inhba, Cd14, Hilpda, Egr1, Pdgfa, Isg15, Jund, Klf4
Regulation of cell population proliferation	0.003	Spry2, Dusp1, Lmna, Tnfsf9, Cxcl10, Inhba, Hilpda, Egr1, Pdgfa, Hspa1a, Jund, Klf4
Response to abiotic stimulus	0.0042	Fosb, Dusp1, Lmna, Cd14, Hilpda, Egr1, Cxcl2, Hspa1a, Jund, Hspa1b
Defense response to virus	0.0058	Rsad2, Rtp4, Cxcl10, Isg15, Ifit1
Cellular response to cytokine stimulus	0.0066	Spry2, Dusp1, Cxcl10, Egr1, Cxcl2, Ifit1, Klf4, Ccrl2
Response to camp	0.009	Fosb, Dusp1, Mmp19, Jund
Negative regulation of angiogenesis	0.0165	Plk2, Spry2, Cxcl10, Klf4
Positive regulation of cytokine production	0.0171	Rsad2, Clec4e, Tnfsf9, Cd14, Hilpda, Egr1
Response to bacterium	0.0171	Clec4e, Cxcl10, Cd14, Cxcl2, Isg15, Jund, Ifit1
Regulation of apoptotic process	0.0171	Plk2, Spry2, Dusp1, Lmna, Cxcl10, Inhba, Egr1, Klf4, Phlda1, Hspa1b
Response to oxygen-containing compound	0.0205	Fosb, Dusp1, Mmp19, Cxcl10, Inhba, Cd14, Egr1, Cxcl2, Jund, Klf4
Chemokine-mediated signalling pathway	0.0394	Cxcl10, Cxcl2, Ccrl2
Negative regulation of erk1 and erk2 cascade	0.0463	Spry2, Dusp1, Klf4
Transcription by rna polymerase ii	0.0465	Fosb, Egr1, Jund, Klf4

MAPK signalling pathway	8.2E-4	Dusp1, Cd14, Pdgfa, Hspa1a, Jund, Hspa1b
Legionellosis	8.2E-4	Cd14, Cxcl2, Hspa1a, Hspa1b
IL-17 signalling pathway	0.0013	Fosb, Cxcl10, Cxcl2, Jund

Table A. 4: 800ECT leads to upregulation of responses to chemical stimulation as well as immune system responses (GO analysis blue shaded) as well as upregulation of MAPK and IL-17 signalling pathways (KEGG analysis green shaded). (FDR=false discovery rate). GO and KEGG enrichment analysis was performed on the derived STRING network for the DEGs in the 800ECT group with standard parameters and the removal of redundant terms.

Description	FDR value	Connected Genes
Cellular response to organic substance	4.23E-8	Fosb, Ccl4, Dusp1, Nr4a2, Ptgs2, Cd14, Socs3, Egr1, Cxcl2, Jun, Hspa1b
Cellular response to chemokine	0.0029	Ccl4, Dusp1, Cxcl2
Transcription, dna-templated	0.0052	Fosb, Nr4a2, Egr1, Jun
Positive regulation of smooth muscle cell proliferation	0.0052	Ptgs2, Egr1, Jun
Response to oxidative stress	0.0066	Dusp1, Nr4a2, Ptgs2, Jun
Response to toxic substance	0.0159	Ccl4, Nr4a2, Ptgs2
Response to amphetamine	0.017	Nr4a2, Cxcl2
Response to gamma radiation	0.0382	Egr1, Cxcl2
NF-kappa B signalling pathway	3.31E-5	Ccl4, Ptgs2, Cd14, Cxcl2
IL-17 signalling pathway	3.31E-5	Fosb, Ptgs2, Cxcl2, Jun
Legionellosis	3.0E-4	Cd14, Cxcl2, Hspa1b
MAPK signalling pathway	6.2E-4	Dusp1, Cd14, Jun, Hspa1b
Toll-like receptor signalling pathway	8.3E-4	Ccl4, Cd14, Jun

Table A. 5: 1000ECT leads to upregulation of responses to various stressors (GO analysis blue shaded) as well as upregulation of NF-κB, MAPK, TLR and IL-17 signalling pathways (KEGG analysis green shaded). (FDR=false discovery rate). GO and KEGG enrichment analysis was performed on the derived STRING network for the DEGs in the 1000ECT group with standard parameters and the removal of redundant terms.

Description	FDR value	Connected Genes
Response to chemical	1.72E-6	Fosb, Ccl4, Fos, Rgcc, Pim1, Dusp1, Mmp19, Nr4a2, Lmna, Cd69, Mt2, Inhba, Ppp1r15a, Cd14, Socs3, Ier2, Hilpda, Rhob, Egr1, Chka, Klf10, Cxcl2, Pdgfa, Hspa2, Hspa1a, Jund, Jun, Klf4, Rgs2, Zfp703, Ccr2
Response to abiotic stimulus	1.01E-5	Fosb, Fos, Rgcc, Dusp1, Nr4a2, Lmna, Bhlhe40, Gadd45a, Cd14, Hilpda, Rhob, Egr1, Cxcl2, Hspa2, Hspa1a, Jund, Jun
Positive regulation of nitrogen compound metabolic process	6.82E-5	Ifrd1, Fosb, Gadd45b, Sdc4, Ccl4, Fos, Plk2, Rgcc, Pim1, Nr4a2, Lmna, Irf2bpl, Gadd45a, Hist1h1c, Inhba, Ppp1r15a, Ier2, Egr1, Klf10, Pdgfa, Hspa2, Hspa1a, Jund, Jun, Klf4
Regulation of cell migration	6.87E-5	Sdc4, Ccl4, Plk2, Rgcc, Dusp1, Lmna, Gadd45a, Rhob, Egr1, Pdgfa, Jun, Klf4, Zfp703, Ccr2
Regulation of protein phosphorylation	7.78E-5	Gadd45b, Sdc4, Ccl4, Rgcc, Pim1, Dusp1, Gadd45a, Inhba, Ppp1r15a, Socs3, Egr1, Pdgfa, Hspa2, Dusp14, Jun, Klf4, Rgs2
Response to organic cyclic compound	7.78E-5	Fosb, Fos, Pim1, Dusp1, Mmp19, Nr4a2, Inhba, Egr1, Chka, Cxcl2, Jund, Jun, Klf4, Zfp703
Negative regulation of cellular biosynthetic process	7.78E-5	Dusp1, Nr4a2, Bhlhe40, Bhlhe41, Irf2bpl, Gadd45a, Hist1h1c, Ppp1r15a, Egr1, Klf10, Pdgfa, Hspa1a, Jund, Jun, Klf4, Rgs2, Zfp703
Regulation of multicellular organismal development	9.53E-5	Ifrd1, Fos, Plk2, Rgcc, Pim1, Lmna, Bhlhe40, Bhlhe41, Gadd45a, Inhba, Rhob, Egr1, Klf10, Pdgfa, Sgms2, Jun, Klf4, Rgs2, Zfp703, Ccr2
Response to camp	9.89E-5	Fosb, Fos, Dusp1, Mmp19, Jund, Jun
Regulation of cell cycle	9.89E-5	Gadd45b, Plk2, Rgcc, Pim1, Dusp1, Gadd45a, Inhba, Rhob, Hspa2, Hspa1a, Jund, Jun, Klf4, Zfp703
Rhythmic process	3.9E-4	Mmp19, Bhlhe40, Bhlhe41, Inhba, Egr1, Klf10, Jund, Jun
Response to inorganic substance	4.4E-4	Fosb, Fos, Dusp1, Nr4a2, Mt2, Cd14, Rhob, Jund, Jun, Klf4
Response to cytokine	0.001	Ccl4, Fos, Dusp1, Cd14, Socs3, Egr1, Cxcl2, Jund, Jun, Klf4, Ccr2
Negative regulation of transcription from rna polymerase ii promoter in response to stress	0.0014	Ppp1r15a, Hspa1a, Jun
Mitotic cell cycle arrest	0.0016	Rgcc, Dusp1, Gadd45a

Response to toxic substance	0.0017	Ccl4, Fos, Pim1, Nr4a2, Mt2, Chka
Positive regulation of cell death	0.0017	Gadd45b, Fos, Rgcc, Dusp1, Gadd45a, Inhba, Rhob, Egr1, Jun, Phlda1
Negative regulation of angiogenesis	0.002	Plk2, Rgcc, Gadd45a, Klf4, Ccr2
Cell differentiation	0.0022	Ifrd1, Gadd45b, Sdc4, Fos, Plk2, Mmp19, Nr4a2, Lmna, Bhlhe40, Bhlhe41, Inhba, Socs3, Tubb2a, Ier2, Rhob, Egr1, Hspa2, Jund, Jun, Klf4, Rgs2, Zfp703, Ccr2
Positive regulation of cell differentiation	0.0023	Fos, Rgcc, Pim1, Lmna, Inhba, Socs3, Klf10, Jund, Jun, Rgs2, Zfp703, Ccr2
Regulation of protein serine/threonine kinase activity	0.0032	Gadd45b, Rgcc, Pim1, Dusp1, Gadd45a, Pdgfa, Dusp14, Rgs2
Cellular response to chemokine	0.0063	Ccl4, Dusp1, Cxcl2, Ccr2
Tissue development	0.0082	Ifrd1, Sdc4, Fos, Dusp1, Lmna, Inhba, Socs3, Rhob, Egr1, Klf10, Pdgfa, Jun, Klf4, Zfp703
Cellular response to external stimulus	0.0108	Fos, Pim1, Nr4a2, Gadd45a, Klf10, Jun
Response to drug	0.0164	Ccl4, Fos, Cd69, Inhba, Jund, Jun
Positive regulation of transferase activity	0.0178	Gadd45b, Sdc4, Rgcc, Pim1, Gadd45a, Egr1, Pdgfa, Klf4
Cellular response to lipid	0.0229	Pim1, Nr4a2, Inhba, Cd14, Cxcl2, Klf4, Zfp703
Cellular response to hypoxia	0.023	Rgcc, Lmna, Hilpda, Egr1
Negative regulation of cell population proliferation	0.0239	Sdc4, Rgcc, Dusp1, Lmna, Inhba, Hspa1a, Jun, Klf4
Response to external stimulus	0.024	Fosb, Ccl4, Fos, Pim1, Nr4a2, Bhlhe40, Mt2, Gadd45a, Cd14, Klf10, Cxcl2, Pdgfa, Jund, Jun, Ccr2
Response to hydrogen peroxide	0.0243	Dusp1, Rhob, Jun, Klf4
Blood vessel development	0.0289	Mmp19, Socs3, Rhob, Egr1, Pdgfa, Jun, Ccr2
Cell death	0.0317	Gadd45b, Pim1, Inhba, Ppp1r15a, Rhob, Cxcl2, Jun, Emp1, Phlda1
Negative regulation of response to stimulus	0.0359	Plk2, Dusp1, Nr4a2, Lmna, Ppp1r15a, Socs3, Egr1, Pdgfa, Dusp14, Klf4, Rgs2, Ccr2

Negative regulation of growth	0.0369	Ifrd1, Mt2, Inhba, Hspa1a, Rgs2
Peptidyl-serine dephosphorylation	0.0392	Dusp1, Ppp1r15a
Response to ionizing radiation	0.0393	Gadd45a, Rhob, Egr1, Cxcl2
Negative regulation of cell adhesion	0.0466	Sdc4, Rgcc, Dusp1, Klf4, Zfp703
Response to glucocorticoid	0.047	Fosb, Fos, Dusp1, Cxcl2
Negative regulation of map kinase activity	0.0485	Dusp1, Dusp14, Rgs2
Positive regulation of cytokine production	0.0492	Ccl4, Rgcc, Cd14, Hilpda, Egr1, Ccr2
MAPK signalling pathway	1.44E-6	Gadd45b, Fos, Dusp1, Gadd45a, Cd14, Pdgfa, Hspa2, Hspa1a, Jund, Jun
NF-kappa B signalling pathway	8.0E-4	Gadd45b, Ccl4, Gadd45a, Cd14, Cxcl2
Legionellosis	0.0015	Cd14, Cxcl2, Hspa2, Hspa1a
Apoptosis	0.0017	Gadd45b, Fos, Lmna, Gadd45a, Jun
Fluid shear stress and atherosclerosis	0.0018	Sdc4, Fos, Dusp1, Pdgfa, Jun
Toll-like receptor signalling pathway	0.005	Ccl4, Fos, Cd14, Jun
TNF signalling pathway	0.0063	Fos, Socs3, Cxcl2, Jun

Table A. 6: 1300ECT leads to upregulation of responses connected to various homeostasis mechanisms, responses to various stressors and cell death processes (GO analysis blue shaded). It also upregulates NF-κB, MAPK, TLR and TNF signalling pathways (KEGG analysis green shaded). (FDR=false discovery rate). GO and KEGG enrichment analysis was performed on the derived STRING network for the DEGs in the 1000ECT group with standard parameters and the removal of redundant terms.